1 INTRODUCTION

1.1 The world-wide status of magnetic fusion in 2000

During the year 2000, no major decisions were taken concerning the construction of ITER-FEAT, which is being submitted to the different parties for assessment as the New Year starts. The design itself has matured to the required state for a decision to construct to be taken. The year 2001 will therefore see the ITER-FEAT project leave the technical arena and enter the political arena. One of the major questions is the potential site, since no party has formally proposed a site yet. In Europe the assessment of Cadarache (France) is well advanced technically. Canada and Japan also intend to propose a site. The programmatic impact of the decision to build ITER will be discussed in 2001. During 2000 CRPP contributed to different aspects of the ITER-FEAT project, as described in this annual report.

The JET tokamak sited in the UK operated successfully during 2000 under the auspices of the European Fusion Development Agreement. Different teams from European Associations contributed to the scientific and technical programmes, with the operation itself delegated to the UK Association. This new method has proven to be very productive scientifically. The CRPP contributed significantly to JET this year.

The plan to enhance JET (JET-EP) for operation beyond the present 5th Framework Programme has advanced to the engineering design phase and has passed a series of scientific and technical assessments. The enhancements foreseen include an increase to the heating power, with among other methods the inclusion of a significant electron cyclotron power for the stabilisation of "neoclassical tearing modes" and for heating a new divertor and refurbishment of many technical subsystems. Some diagnostics will be added, especially those which would be most relevant to ITER in a DT campaign. Again, the CRPP is heavily involved with the JET-EP project.

In Japan, the future of the JT-60U tokamak is being discussed with options being considered for continuing or upgrading this large tokamak. Any ITER decision would certainly influence this choice.

In the US, no decisions have been made concerning a future advanced experiment, although the question continues to be hotly debated. Regarding ITER, US officials have repeatedly mentioned that US will seek to join ITER when a decision on its construction is taken.

The progress towards the goal of fusion, using the approach of magnetic confinement, has lasted about 40 years. Although measuring this progress accurately is fraught with difficulties, the so-called triple product, the product of the ion density, the ion temperature and the time for which the energy is confined, is a useful indicator. Figure 1.1 illustrates the rapid progress of fusion over several decades, comparing favourably with two undeniable progress-leaders, namely transistor numbers per chip in the semi-conductor industry and particle accelerators in physics research. Fusion researchers are ready to make the Next Step to a large fusion power device as a natural extension to this progress already made.

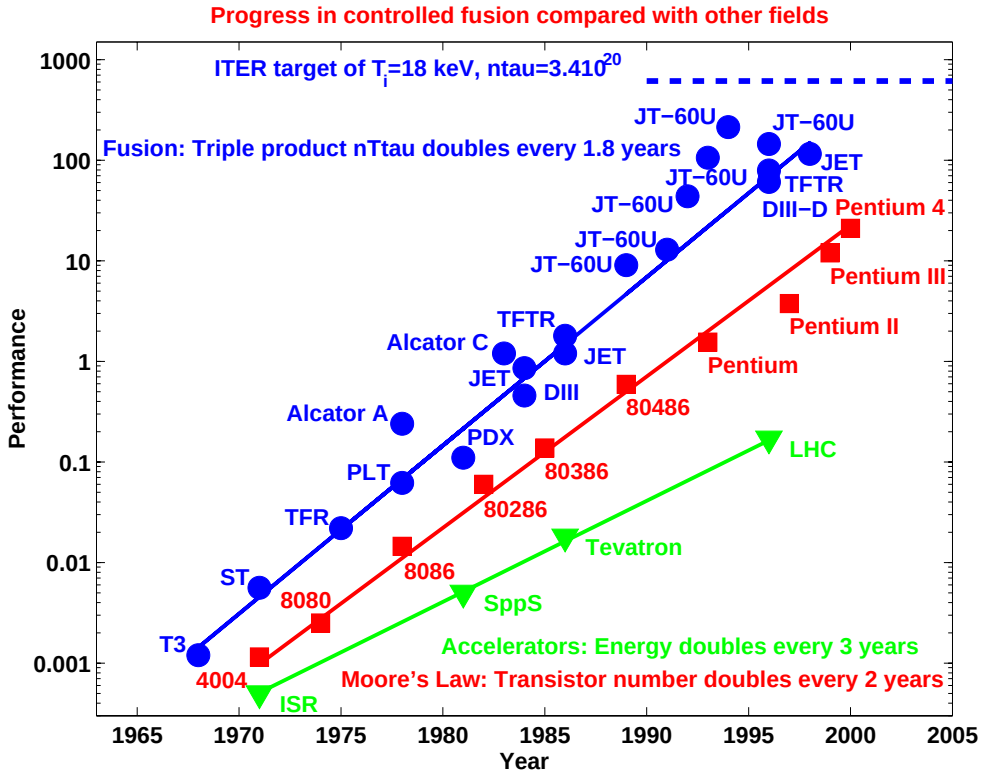

Fig. 1.1 Progress made in controlled fusion over the years shows the same impressive advance as other fields recognised as world leaders.

1.2 The CRPP in 2000

The long-standing strategy of the CRPP aims at excellence in certain carefully selected areas, based either on existing facilities capable of making a unique contribution to the field, or on solid scientific experience and expertise in the field. In the area of the physics of fusion plasmas, research at the CRPP has concentrated in 2000 on the following fields, maintaining our historical mixture:

- the exploitation of the TCV tokamak, which has a unique flexibility for producing and studying strongly shaped plasmas;
- the study of electron cyclotron heating and current drive, combining a high power and versatile additional heating scheme with the shape flexibility of TCV;
- the theoretical and numerical simulation of the equilibrium, stability and confinement of magnetically confined plasma, including the tokamak, stellarator and novel configurations;
- the development of high power high frequency sources for plasma heating and diagnostics;
- supporting the JET experiments and the ITER Engineering Design Activity.

In the field of technology, the CRPP continues its long standing work in superconductors and low activation material R&D. Applications of plasma in industrial processes remain an important activity of the CRPP.

Although it is difficult to present the highlights of such a diversified programme, the following advances are indicative of the progress made at the CRPP during 2000.

The TCV tokamak achieved an impressive demonstration of non-inductive current drive using electron cyclotron waves, maintaining a plasma current of 210kA for over 2 seconds without any transformer action. The range of plasma equilibria accessible has been increased using the electron cyclotron waves to widen the radial profile of the plasma current, allowing higher elongations to be created for a given applied field configuration. At the same time, the vertical elongation of the plasma was increased to 2.8.

Theory and numerical simulations have had a main emphasis on the first principle based analysis of micro-instabilities related to anomalous transport. In this context, the stabilising role of radial electric fields has been brought out in global gyro-kinetic computations for both tokamak and stellarator geometries. Also, the influence of magnetic topology has been studied in 3D configurations, including magnetic perturbations generating islands and stochastic regions. In particular, we have shown the creation of a transport barrier against particle transport in the presence of resonant magnetic perturbations at the position in the plasma where shear reversal occurs.

Materials studies have both a modelling and experimental aspect. For the first time, multi-scale simulation methods were successfully used to describe defect cluster accumulation during irradiation and the resulting tensile properties, in particular, the nucleation and scaling of the dislocation channelling phenomena, described in an article in Nature. Procedures to simulate images from molecular dynamics results were developed and applied to pure metals and alloys. The properties of the Titanium alloy "alpha phase" were shown to have a low level of hardening after irradiation and also maintain good ductility. These properties are also found in the irradiated pure Titanium. Bonded Cr_2O_3 plasma sprayed coatings were proven experimentally to be efficient hydrogen barriers.

In the research on superconductivity, the SeCRETS experiment in SULTAN represents the focus of the main efforts. In an unprecedented way it demonstrated the extremely high stability of the cable in conduit conductors against electromagnetic field transients of the type which would occur during a tokamak disruption. This was found to be the case even in cables built with segregated copper as proposed by CRPP for reducing conductor costs for ITER. Other relevant results on stability dependence on coolant flow are still under investigation by long-running numerical simulation models. The development of High critical temperature current leads has made significant progress, reaching the 20kA level. As an emergency action, a classical full copper 80kA current lead was developed as a fallback solution for the Toroidal Field Model Coil Test in preparation for ITER.

The highlights of the research and development of plasmas for industrial uses were an increased understanding of large area Radio Frequency reactors and a so-called multiple root attachment in the plasma torch, which has been seen for the first time. These industrial activities are encountering an increasing level of interest from various Swiss industries and other institutions for the work performed at the CRPP, translated into an increase of small project proposals and mandates from industry.

Most of the research activities in the CRPP were performed within the framework of the Association Euratom-Confédération Suisse and have benefited from collaboration with all the Associations of the European Fusion Program. Bilateral collaborations with Eastern European institutions, Japan and the US in physics and diagnostic development include the exchange of personnel and equipment. Such scientific relationships are extremely beneficial to the CRPP, especially in view of our tight personnel situation.

1.3 Impact outside the fusion community

The most direct contribution of the CRPP to industry is based on its knowledge of the plasma state. A CRPP research group is actively pursuing the transfer of plasma physics skills and knowledge to industries which already use plasma processing techniques in their production. Many examples of these activities are illustrated in this report.

As in other high-technology fields, spin-off of the techniques and knowledge acquired in the fusion research of the CRPP is important and takes several distinct forms.

A first spin-off is collaborative research carried out together with industry on fusion related research. Specific examples are the development of high-power gyrotrons, of large magnet superconductors and of new materials. This work is funded by the fusion programme and benefits particular industries linked to the specific needs of the programme. It is documented in detail in this report.

Another easily identified spin-off of the CRPP is the transfer of know-how to fields outside fusion (industry, education, services) through the hiring of young physicists or engineers after spending time as doctoral students or as post-doctoral researchers. Typically 5% of the personnel turns over annually in this way.

A final, normally undocumented transfer to industry is collaboration on techniques and methods for achieving the rather stringent requirements of our own purchases, enabling the industrial partner to enhance the quality of his product line.

2 RESEARCH ACHIEVEMENTS OF THE CRPP IN 2000

The main experimental device at the CRPP is the tokamak TCV (Tokamak à Configuration Variable). TCV is being progressively equipped with a powerful electron cyclotron heating scheme. In 1999 1.5MW of ECH power was available. During 2000 this power was doubled to 3MW at 82.7GHz, and a further 0.5MW were made available at 118GHz. The study of the confinement of particles and energy as the plasma shape is modified remains the primary goal of the TCV tokamak.

The theoretical studies of magnetic confinement systems still concentrate on exploring new configurations in the 3D geometry of the stellarator family. Both tokamaks and stellarators are experimentally found to exhibit enhanced transport losses and modelling the potential causes of these additional losses is the second pillar of the CRPP theory group. Understanding these losses might lead to ideas for reducing them, which could have an enormous impact on all magnetic confinement devices.

The CRPP continues to participate in the design and development of high power gyrotons as tools for fusion research, not only for experiments at the CRPP but also elsewhere in Europe. These systems are regularly increasing the pulse lengths at their nominal power of the order of 1MW per tube.

Any controlled fusion reactor will require two major technical developments, namely improving the materials for constructing the innermost part of the reactor and enhancing the field properties and reducing the cost of the superconducting magnet systems. These activities are both pursued at the CRPP in its Villigen laboratories.

Plasmas are more and more recognised as a useful and economically interesting tool in various areas of industrial production. The underlying knowledge and experience of plasma physics at the CRPP is being put to good use in a series of industrial partnerships to promote plasma processing in industry and to help industry with specific problems related to their plasma systems. These activities are expanding at present, still limited by the available personnel rather than the possible scope of activities and are performed outside the frame of the Association EURATOM-Confédération Suisse.

This very broad scope of activities range from long calculations on the world's fastest super-computers for the rather exotic field of magnetic confinement of high temperature plasmas to the quest for better and faster preparation of machine tool surfaces or packaging surfaces. This variety of activities makes the CRPP an excellent example of the importance of studying, understanding and mastering the 4^{th} state of matter, namely the plasma state. The rest of this section presents some of the detailed results obtained as a result of these studies during 2000.

2.1 The TCV tokamak

2.1.1 Recent Advances

The TCV (Tokamak à Configuration Variable, R=0.88m, a<0.25m, B_T<1.54T) with a vessel elongation of 3, was designed from the outset to be a highly versatile facility dedicated to the investigation of the effects of plasma shaping on confinement and stability. Following the installation of a flexible electron cyclotron heating (ECH) and

current drive (ECCD) system, totalling, in 2000, 2.8MW of power available to the plasma at the second cyclotron harmonic (82.7GHz), TCV has delivered significant achievements to the fusion community. One of these is the first demonstration of steady state, fully non-inductive ECCD operation for 2s at plasma currents of up to 210kA, a significant advance from 1999, when a 123kA full ECCD discharge was first obtained in TCV. These experiments also established the necessity of tailoring the driven current profile by suitably distributing the six available sources over the plasma cross section in order to avoid disruptive MHD instabilities and have provided a first validation of theoretical predictions for ECCD efficiencies in steady-state conditions.

ECH and ECCD have also proven to be powerful tools for current profile modification for the purpose of establishing and controlling improved core electron confinement (ICEC) modes and for improving vertical stability at high elongation. Reversed or weak central shear discharges at moderate elongation ($\kappa \sim 1.7$), produced by central counter-current drive (CNTR-ECCD) in combination with pure ECH deposited off-axis for improving MHD stability, have led to stable electron confinement enhancements $H_{RLW}=3.5$ over Rebut-Lallia-Watkins scaling, limited in duration by the length of the RF pulse. With Ohmic heating alone, the most elongated plasmas can only be vertically stabilised at high plasma current and hence low internal inductance and the highest elongation achieved so far is 2.8 with an edge safety factor $q_{95}=2.5$. The addition of a moderate level of off-axis ECH power (0.5-1MW) has allowed the minimum stable plasma current for $\kappa_a=2.4$ to be reduced to $q_{95}=8.2$, a three-fold reduction in equivalent current. These experiments open up a wide and promising operational domain for future investigation of improved confinement modes at high elongation.

Studies of the scaling of sawtooth inversion radii and profile shapes have revealed that these depend solely on the parameter $<j>/q_0 j_0$ in Ohmic plasmas and both on this parameter and the deposition profile with ECH or ECCD. The results show that, due to the significant effect of the central elongation, current profile width and inversion radii do not become excessive at high elongation. A study of sawtooth behaviour as a function of elongation revealed a progressive decrease of sawtooth periods and crash amplitudes with increasing elongation, both with ECH and in purely Ohmic plasmas, attributed to a reduced internal kink stability margin.

The first of three 118GHz gyrotrons, destined for operation at the third harmonic X-mode, has been brought into service for physics investigations of the role of target plasma conditions on wave absorption. These experiments have already demonstrated that absorption of X3 power is vastly enhanced when a suprathermal electron population produced by X2-ECCD is present in the plasma. Total absorption (within 10% error bars) was achieved for the 470kW of injected X3 power with as little as 350kW of X2-ECCD for target plasma conditioning, as compared to 25% absorption with the same power of X2-ECH.

Although Ohmic H-modes are easy to obtain in TCV, even with the ion ∇B drift direction away from the X-point, transitions to steady-state ELMy H-modes are only obtained in a narrow region of the operational domain. Remarkably, after such a transition this attractive confinement mode has been shown in TCV to be very resilient to subsequent changes of elongation and density.

Detachment in open divertor geometries and pure deuterium is found to be easier than expected from simulations, suggesting important contributions from recombination pathways other than three-body and radiative processes.

TCV has also been used as a test-bench for the non-linear evolution code DINA with the purpose of validating it for ITER poloidal field coil feedback controller design.

2.1.2 Fully Non-Inductive Operation with ECCD

The six ECH launchers in TCV allow independent steering of the heating sources in both the poloidal and toroidal directions; this high flexibility matches that of the TCV control system, permitting the entire vast range of shapes that can be created to be heated in an accurately localised manner. The six sources can be employed to tailor the current profile in a stationary state, as will be required in a prospective reactor for MHD stabilisation and optimisation of performance. Crucial to the stationarity requirement is the ECH pulse length capability which substantially exceeds the current redistribution time from Ohmic to non-inductively driven profiles (typically < 0.5s).

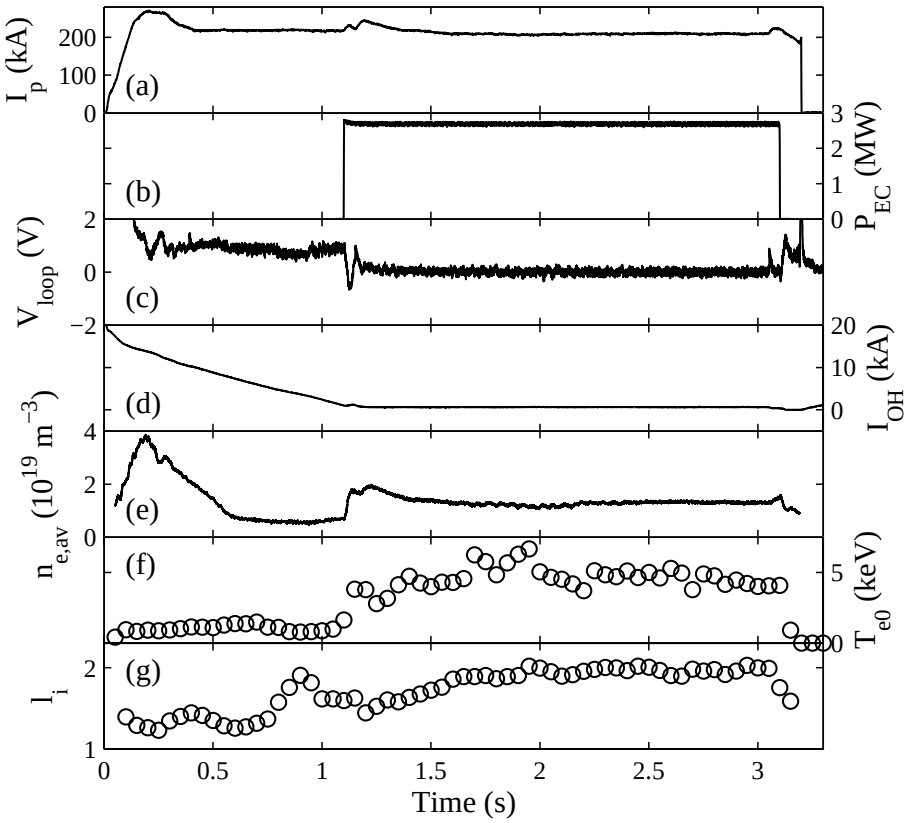

Fig. 2.1.1 Steady-state, fully non-inductive 210kA discharge in a single-null diverted plasma with 2.8MW of distributed ECCD: time histories of (a) plasma current, (b) EC power, (c) edge loop voltage, (d) current in the Ohmic transformer primary, (e) line-averaged density, (f) peak electron temperature, (g) internal inductance

Studies have been carried out over the past year in TCV aimed at increasing power levels to demonstrate stable, steady state current profile control and to validate ECCD physics. After the first demonstration of fully non-inductive operation in steady state with ECCD in a tokamak was performed in TCV in 1999, work has progressed to a present record non-inductively driven current of 210kA, shown in Fig. 2.1.1. The current is sustained non-inductively for 2s, while plasma conditions relax over a time scale of less than 0.5s. The current in the Ohmic transformer primary is kept constant by feedback throughout the ECCD pulse; thus, in the stationary phase during which the currents in all the shaping coils are also constant, no magnetic flux is supplied to the plasma. The bootstrap current fraction is calculated to be 8% in this discharge. The ECCD efficiency is defined as $\eta = I_{ec}/P_{ec}$, where I_{ec} is the driven current and P_{ec} the power. A common figure of merit is the product $n_e R_0 \eta$, where n_e is the line averaged density, which for the discharge

in Fig. 2.1.1 corresponds to 0.0073 [10^{20}A/W/m^2]. Higher figures of merit, up to 0.016 in the same units, have been obtained by concentrating all sources in the centre, but such discharges quickly become MHD unstable and disrupt. It was experimentally found that at each power level there is a minimum stable driven current profile width, below which such MHD instabilities develop and lead to disruption. As these instabilities are driven by current or pressure gradients, which increase with power for constant profile shape, the deposition width must be increased with increasing power. This results in an effective degradation of the maximum global ECCD efficiency with power. By way of illustration of this effect, Fig. 2.1.2 shows the power and current deposition profiles calculated by the linear ray tracing code TORAY for the case of Fig. 2.1.1 and for a case with similar plasma conditions but only three sources (1.35MW) and a steady-state non-inductive current of 160kA. Each case corresponds to the narrowest stable deposition profile identified over a series of discharges at each power level.

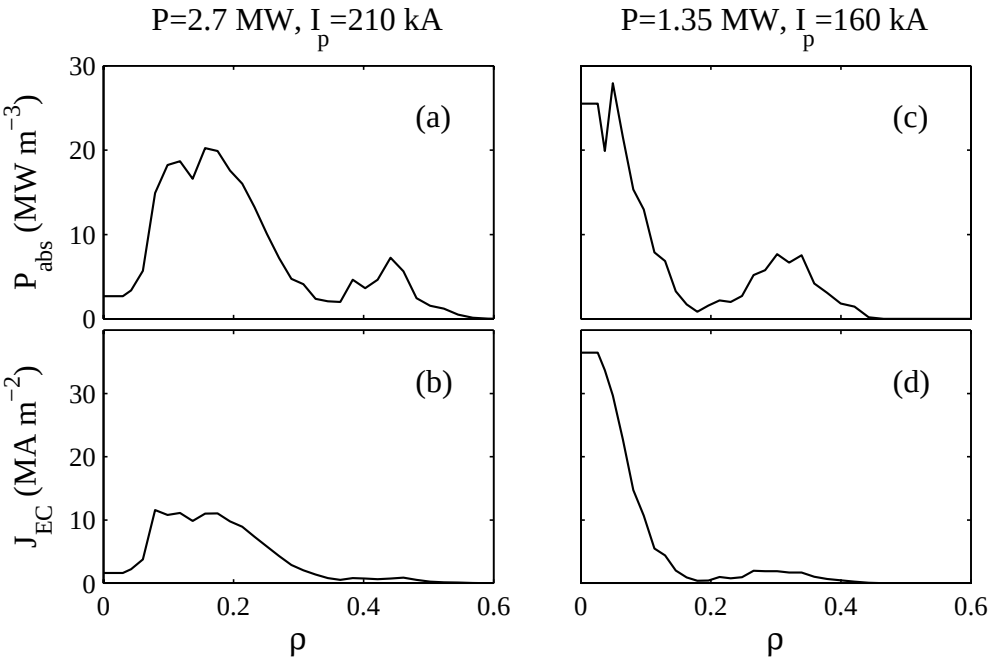

Fig. 2.1.2 Flux-surface-averaged (a)-(c) absorbed power and (b)-(d) driven current density as functions of a normalized radial coordinate proportional to the square root of the plasma volume, for two different discharges. All profiles are calculated by TORAY. Line-averaged density $1x10^{19}$m^{-3} (a-b) and $1.2x10^{19}$m^{-3} (c-d), central electron temperature 3.1keV (a-b) and 3.7keV (c-d).

The fundamental principles of ECCD have been known for some twenty years, but a thorough experimental validation is still missing. One of the principal aims of the ongoing experiments on TCV is to provide that validation, particularly through exhaustive measurements of the efficiency η. In linear theory the efficiency has the theoretical dependence, $\eta=T_e\eta_T'/[Rn_e(Z_{eff}+5)]$ where T_e is the electron temperature, R is the major radius, n_e is the density, Z_{eff} is the effective ion charge and η_T' is a function of the trapped particle fraction and of the parallel wave number. The average efficiencies measured on TCV in a series of fully non-inductive discharges with varying deposition profile widths have shown a dependence on the minor radius of the magnitude predicted by theory, supporting the existence of trapped particle effects. Furthermore, the absolute value of η_T' agrees with predictions by the linear TORAY code to within 30%, over a range of profiles resulting in a variation in η_T' of a factor of 3.5. Non-linear effects thus do not appear to be significant in the present conditions. This observation is in conflict with theoretical predictions

indicating that efficiency should be enhanced in TCV conditions owing to quasi-linear modification of the electron distribution function. This discrepancy may be due in part to the radial diffusion of fast electrons, an effect not considered in the theoretical analysis.

2.1.3 Quasi-Stationary Improved Core Electron Confinement by Shear Optimisation

An Improved Core Electron Confinement (ICEC) regime has been obtained by current profile tailoring with ECH and ECCD in quasi steady state conditions. The intense central counter current drive (CNTR-ECCD) produced in the ICEC regime and related equilibrium modelling suggest the presence of a strong reverse shear profile in the plasma core. In many tokamak experiments reversed shear profiles are obtained only transiently by heating during the ramp up phase of the plasma current. Taking advantage of the very localised power deposition, which is typical of ECH and ECCD, and making use of the flexibility of the beam launching system on TCV, an optimised current density profile could be established and maintained for the duration of the heating pulse, corresponding to 200 energy confinement times and several current redistribution times. For this purpose a combination of 4-5 X2 heating beams was used to deliver a total power in the range 1.8-2.3MW to the plasma. The optimised scenario begins with off-axis heating just outside the q=1 surface using two or three X2 beams followed 300ms later by central power deposition with a strong counter current drive (CNTR-ECCD) component using two beams. The discharge evolution is shown in Fig. 2.1.3 for two examples with central CNTR-ECCD and for central ECH. Typical plasma parameters were $\delta_{95}\approx 0.2$, $\kappa_{95}\approx 1.6$, $q_{95}\approx 6$, $I_p\approx 200$kA and $\langle n_e\rangle \approx 1.5\cdot 10^{19} m^{-3}$.

Central CNTR-ECCD leads to significantly higher peak electron temperatures (8-12keV) than central ECH (~4keV) and better global plasma performance. The delay between the beginning of the off-axis ECH and the on-axis CNTR-ECCD, which is of the order of the current redistribution time, is necessary to establish a suitably broad and MHD stable target current profile for the central CNTR-ECCD pulse. If the delay is reduced to zero, or if the off-axis ECH is altogether omitted, high temperatures (~10keV) and high confinement can also be obtained, albeit transiently, frequently terminating with violent sawtooth-like MHD collapses. Unlike discharges with central CNTR-ECCD only, the ICEC plasmas shown in Figs 2.1.3 & 2.1.4 are MHD quiescent, like #18639 and #18518, or else only exhibit benign levels of sawtooth activity, like #18635, with crash amplitudes of ~3keV and periods of ~20ms, which far exceed the global energy confinement time of ~5ms.

The electron energy confinement times achieved exceed that predicted by the Rebut-Lallia-Watkins (RLW) global electron confinement scaling law by a factor of ~3.5, as seen in Fig. 2.1.3b. The enhancement over the ITER-89P global confinement law (which includes the ion energy) during the CNTR-ECCD phase is a factor of 1.5. It should however be noted that, while RLW scaling agrees with the measured confinement during the Ohmic phase, ITER-89P overestimates the Ohmic confinement by a factor of two. Owing to the low densities necessary in TCV for application of efficient ECCD, electrons and ions are decoupled, resulting in core ion temperatures of only a few hundred eV, measured using a neutral particle analyser. This, together with the main ion dilution by carbon impurities, leads to the ion contribution to the stored energy being negligible (<10%) and is the likely reason for falling short of ITER-89P predictions in ordinary L-modes at low density.

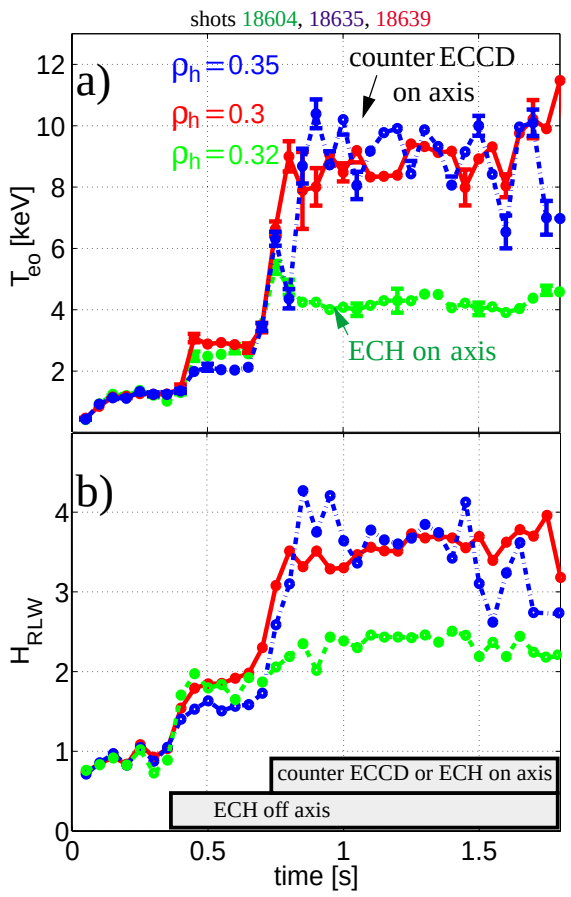

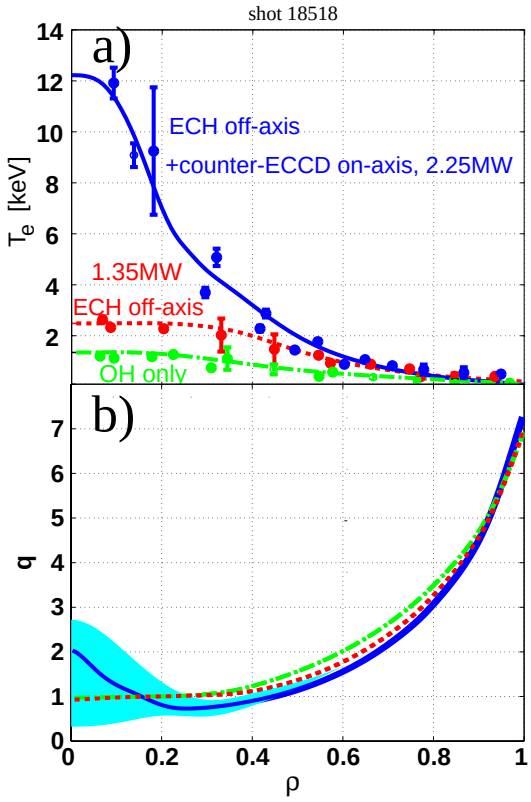

FIG 4.Pietrzyk.PRL (color)

Fig. 2.1.3 a) Evolution of the central electron temperature from Thomson scattering and b) enhancement factor over RLW energy confinement time for different ECH/CNTR-ECCD scenarios combining off-axis ECH (0.9MW) at different locations ρ_h with delayed central ECH or CNTR-ECCD. green: with 0.9MW central ECH blue and red: with 0.9MW central CNTR-ECCD

Fig. 2.1.4 a) Electron temperature profiles as simulated using the RLW transport model for 3 phases of an ICC shot, together with the measurements. green: OH phase, red: 1.35MW off-axis ECH, blue: combination off-axis ECH and 0.9MW central CNTR-ECCD. b) Corresponding calculated safety factor profiles with uncertainties (shaded) related to location of central CNTR-ECCD sources.

In the absence of direct measurements of the current density profile, the evolution of the q-profile and its relation to the reduction in transport coefficients is inferred from time dependent simulations using the PRETOR code and the RLW local transport model. The RLW transport parameters depend strongly on the magnitude of the magnetic shear, but are assumed not to depend on its sign. An example is presented in Fig. 2.1.4a, with simulated temperature profiles for the Ohmic, off-axis ECH and high performance ICEC phases, together with the experimental data from Thomson scattering, showing good agreement. Within the framework of the local RLW heat diffusivity model, used in these calculations, the negative shear zone near the centre is essential for the confinement enhancement. The corresponding q-profile in Fig. 2.1.4b show reversed shear during the central counter ECCD phase. The central CNTR-ECCD current is calculated to be 125kA. The range of plausible q-profiles has been computed by PRETOR used as a fixed-boundary equilibrium

solver (without a transport model) constrained by the experimental density and temperature profiles, the effective ion charge, the edge loop voltage, and reflects the high sensitivity of the calculation to the location of the CNTR-ECCD source taken from TORAY calculations. This sensitivity to the ECCD source location has motivated an experimental scan of the position of the CNTR-ECCD component which has shown that an outward displacement of only 10% of the minor radius caused a 40% reduction in the central plasma temperature, which is also borne out by the PRETOR simulations.

2.1.4 Full Absorption of ECH Power at the Third EC Harmonic in X-Mode

Plasmas in the TCV Tokamak have, for the first time, been heated using the first of three 0.5MW gyrotrons to be deployed at a frequency of 118GHz, corresponding to the third EC harmonic. One of the motivations for X3 ECH in TCV is the possibility of heating at densities which are inaccessible with the X2 ECH system. The experiments reported here were aimed at establishing the importance of the plasma conditions, mainly electron temperature and suprathermal tail electron distributions, for the absorption of X3 ECH power. For this purpose the plasmas were preheated with different power levels of X2 ECH and ECCD. The X3 wave was launched from the low field side via one of the upper lateral launching mirrors normally used for X2 heating.

The target plasmas used in these experiments have the parameters R=0.88m, a=0.25m, κ=1.31, B_0 = 1.42T, $n_e(0)= 2.5\cdot10^{19}m^{-3}$. The launching geometry and time traces of relevant parameters are shown in Fig. 2.1.5 for a typical discharge. The top trace shows the timing of the X2 ECCD and the X3 ECH. In all experiments the X2 power was kept constant from 0.3s to 1.3s whereas the X3 power was applied from 0.5s to 1.2s and included a phase with 100% modulation at 237Hz (0.8s to 1s).

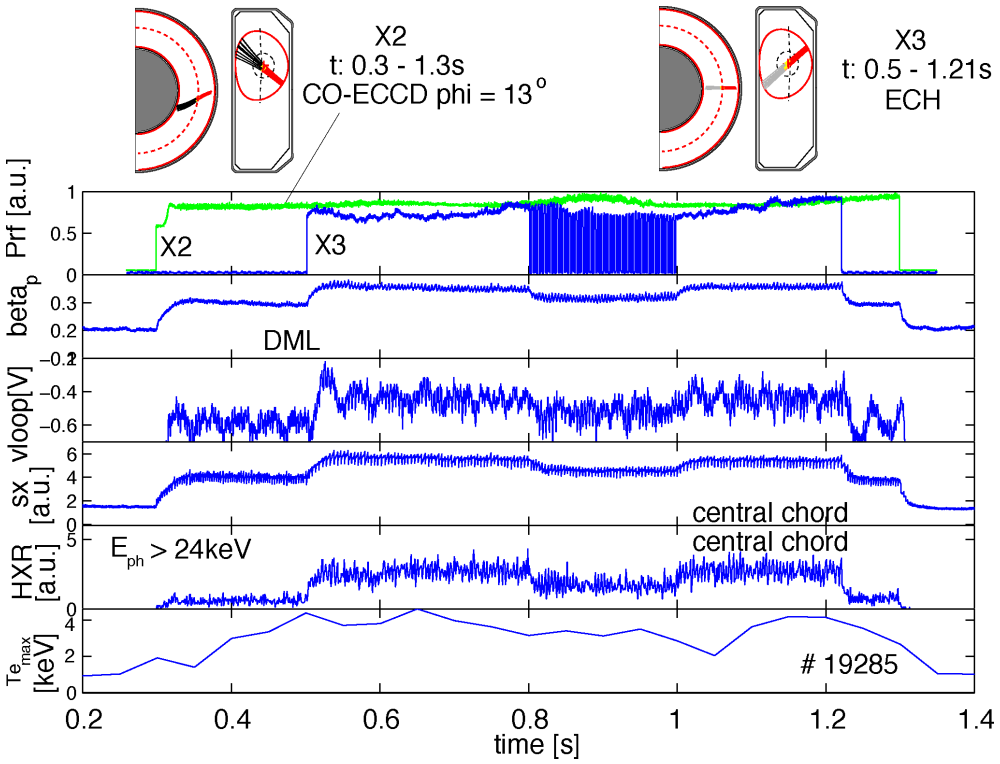

Fig. 2.1.5 Launching geometry and typical time traces for the X2 and X3 ECH. Top to bottom: RF power, poloidal beta, loop voltage, soft X-ray signal, hard X-ray signal, peak electron temperature. $P_{X2}=P_{X3}$=0.47MW, I_p=200kA.

The total stored energy variation was measured during the modulated part of the X3 RF pulse using the diamagnetic loop response. The modulation frequency of f_m=237Hz was chosen such that $1/2\pi f<\tau_e$~5ms, where τ_e is the electron energy confinement time. While the 0.47MW X3 power and launching geometry, aimed at the plasma centre, were kept constant, different X2 conditions were investigated, including variations of the toroidal launch angle ϕ, the power deposition radius, the total X2 power and the plasma current. A toroidal injection angle scan of the X2 launch, with P_{X2} P_{X3}=0.47MW, has revealed a clear asymmetry. X3 absorption is highest on target plasmas with X2 injected with ϕ=+13^0, corresponding to CO-ECCD. Figure 2.1.6 shows the X3 absorbed power fraction, versus X2 preheat power for three X2 launching angles corresponding to CO-ECCD (ϕ=13^0), ECH (ϕ=0^0) and CNTR-ECCD (ϕ=-13^0). For CO-ECCD target plasmas, within the experimental error bars, nearly 100% single pass absorption is obtained. The interpretation of the measured absorption as being due to single pass absorption is supported by a polarisation scan of the X3 RF beams, from X-mode to O-mode, as well as by a poloidal scan of the launch angle, from central to off-axis deposition. These unfavourable conditions lead to a strong reduction of the measured X3 power absorption, which is not consistent with a picture attributing absorption to a multi-pass effect involving many internal reflections in the vacuum vessel.

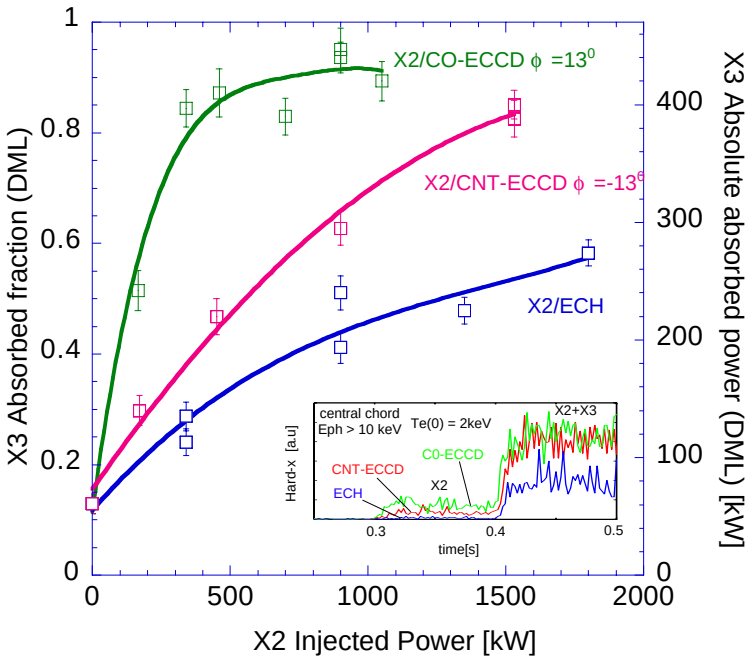

Fig. 2.1.6 Measured X3 absorption using the DML versus X2 preheat power for three different X2 launching configurations: - CO-ECCD (green, ϕ=13º), - CNTR-ECCD (red, ϕ=-13º), - and ECH (blue, ϕ=0º). 3rd harmonic ECH (ϕ=0^0) is kept constant at 0.47MW with central deposition. Insert shows hard X-ray (>10keV) signals for X2 Co- (green) and CNTR-ECCD (red) as well as X2 ECH (blue) cases. X3 ECH is applied from 0.4s when the large rise in hard X-ray emission is observed.

Calculations of the theoretical absorption with the TORAY ray tracing code, which makes the assumption of an isotropic, Maxwellian velocity distribution, are in fair agreement with the experimental results corresponding to ECH preheating. However, the measured X3 absorption exceeds that predicted by TORAY by a factor of up to 3 for the CNTR- and CO-ECCD cases. The only explanation of this discrepancy is that a large fraction of the X3 power is absorbed by energetic tail electrons created by X2 ECCD. The presence of these is confirmed by the

measurement of photon spectra using an energy resolving hard X-ray camera and a high field side ECE radiometer. The ECE radiometer detects supra-thermal radiation levels exceeding the thermal level by up to a factor of 5, while effective X-ray photon temperatures in the range 12-30keV, depending on the ECCD injection angle, are measured in the presence of ECCD and X3 ECH. The insert in Fig. 2.1.6 shows that hard X-ray (>10keV) emission is highest with X2 CO-ECCD and lowest with X2 ECH in all phases of the experiment.

2.1.5 Particle Transport with High Power ECH and ECCD

A coupled heat and particle transport phenomenon, leading to particle depletion from the plasma core, is observed in a variety of plasma conditions with centrally deposited ECH and ECCD in TCV. This phenomenon, known as “density pumpout”, causes inverted density sawteeth in the core of sawtoothing discharges and leads to stationary hollow profiles in the absence of sawteeth. The density pumpout has been linked to the presence of (n,m)=(1,1) MHD modes and can be suppressed by stabilising the mode by means of operation at high triangularity. The correlation of pumpout with loss of axisymmetry suggests that neoclassical transport processes involving locally trapped particles other than those arising from the toroidal field ripple and analogous to those in heliacs, may account for the phenomenon in tokamaks as well.

Figure 2.1.7 shows the difference in sawtooth behaviour at low and high heating power at low triangularity. For P_{ECH}>0.5 MW density sawteeth are inverted. The situation is different at high triangularity (δ_a>0.3) when both X-ray traces and central densities have “normal”, triangular sawteeth. The essential difference appears to be that at low triangularity a (1,1) magnetic island is present during the sawtooth ramp phase, whereas the plasma is MHD-quiescent during the ramp phase at high triangularity.

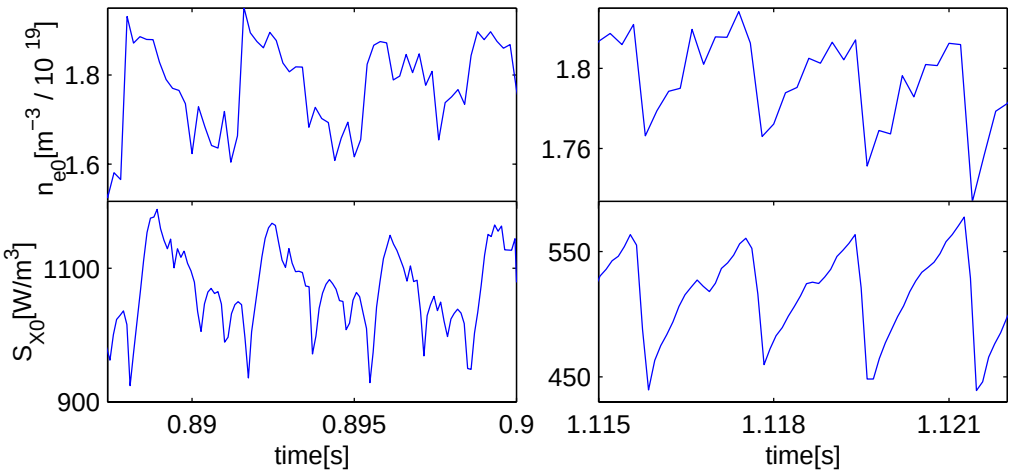

Fig. 2.1.7 Sawteeth on central Abel-inverted density (top) and raw X-ray signal (bottom) for Ohmic heating (left) and *ECH* (right) with δ_a=0.22 and P_{ECH}= 1.45MW.

The convective heat flux associated with the “pumped-out” particles is a small fraction, estimated to be less than 10%, of the power lost from the core. In sawtoothing plasmas strongly hollow density profiles cannot develop because the sawtooth crashes regularly flatten density and temperature profiles. However with ECCD many situations arise when sawteeth are stabilised for long enough (typically

10 ms or more) for the hollowness to become significant enough to be measured by the Thomson scattering system, as shown in Fig. 2.1.8.

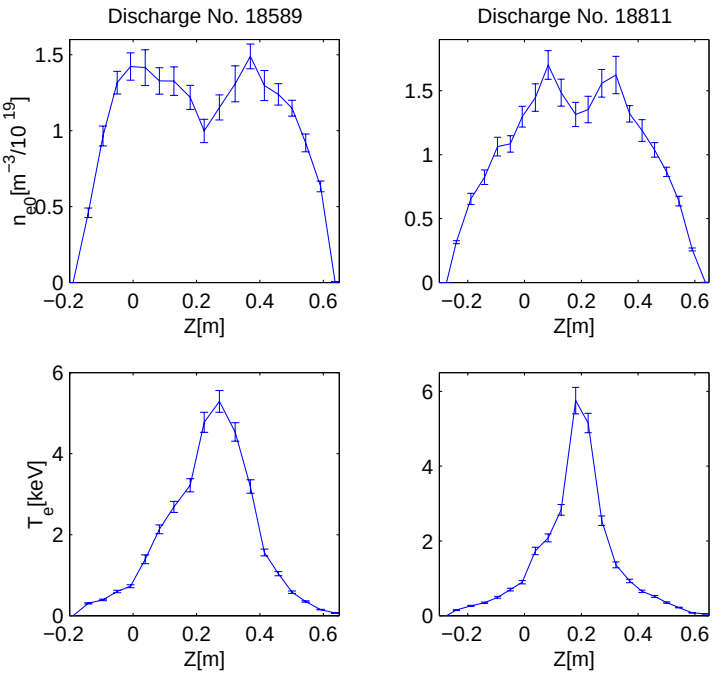

Fig. 2.1.8 Examples of electron density (top) and temperature (bottom) profiles in a CO-ECCD (left) and a CNTR-ECCD discharge (right).

We propose that a loss of axisymmetry provides the crucial physics for this phenomenon by allowing the existence locally trapped particles, which are not confined in the core region. The presence of an (n,m)=(1,1) island causes the core to be helically displaced. The vicinity of the displaced core acquires stellarator-like features. As a result trapped particle orbits exist even at the magnetic axis, just as in a heliac configuration. This region may act as a sink from where locally trapped particles are lost to beyond the non-axisymmetrical region (typically outside q=1). The coexistence of locally and toroidally trapped particles within the q=1 surface can also be expected to give rise to competing transport phenomena, including pumpout, since the neoclassical off-diagonal terms associated with these two classes of particles have opposite signs. In steady state the resulting profiles should be characterised by $\nabla n_e/n_e = d_{12eff} \times \nabla T_e/T_e$, where d_{12eff} is the effective normalised non-diagonal term resulting from all relevant transport processes. Near the displaced axis the effect of locally trapped particles dominates (d_{12}~1 in the long mean-free path regime), giving rise to an outward flux after a sawtooth crash, such as to set up a hollow density profile, while further away toroidally trapped particles (d_{12}=-1/2), or an anomalous mechanism, are most important, giving rise to an inward pinch.

2.1.6 Dependence of Inversion Radii and Peaking Factors on Plasma Shape

When considering highly elongated tokamak designs, a frequently expressed concern is that as a result of the high current carrying capacity of elongated plasmas, sawtooth inversion radii and consequently crash amplitudes may become excessive. In Ohmic plasmas we observe that the normalised sawtooth inversion radius ρ_{inv} and the profile inverse peaking factors (normalised widths) $\langle p_e \rangle / p_{e0}$, $\langle T_e \rangle / T_{e0}$ and $\langle n_e \rangle / n_{e0}$ for electron pressure, temperature and density, depend on the current profile peaking via the parameter $\langle j \rangle / (q_0 j_0)$, where $\langle j \rangle$ is the cross-

section averaged current density, irrespective of plasma shape and electron density. This parameter can be evaluated without knowledge of the still somewhat controversial value of the axial safety factor since $q_0 j_0 = B_0(\kappa_0 + 1/\kappa_0)/(\mu_0 R_0)$, where κ_0 is the axial elongation. The core elongation is generally in good agreement with the elongation of emmissivity contours from X-ray tomography. In order to reduce the large scatter of the Thomson scattering measurements at random times in the sawtooth cycle we define "clipped" profile widths as $\langle \underline{T}_e \rangle / T_{e1}$ where T_{e1} is the electron temperature at the sawtooth inversion radius and $\underline{T}_e = T_{e1}$ for $\rho < \rho_{inv}$ and $\underline{T}_e = T_e$ for $\rho \geq \rho_{inv}$. These widths are sensitive to the profile in the confinement zone ($q>1$) and are shown in Fig. 2.1.9 for a wide variety of Ohmic and ECH L-mode plasmas. The Ohmic data show a remarkably narrow distribution as a function of $\langle j \rangle / (q_0 j_0)$ and are in good agreement with an Ohmic relaxation model based on the assumption that the magnetic entropy is stationary in time. The parameter $\langle j \rangle / (q_0 j_0)$ performs better than safety factor based scalings such as $1/q_{95}$, for which the dispersion is larger, and is related to the popular database variables q_{95}, κ_{95} and δ_{95}. With ECH heating, $\langle j \rangle / (q_0 j_0)$ remains the primary scaling parameter, but now the profiles are modified by the ECH heat deposition profiles, the widths of which are not matched in the experiments to $\langle j \rangle / (q_0 j_0)$.

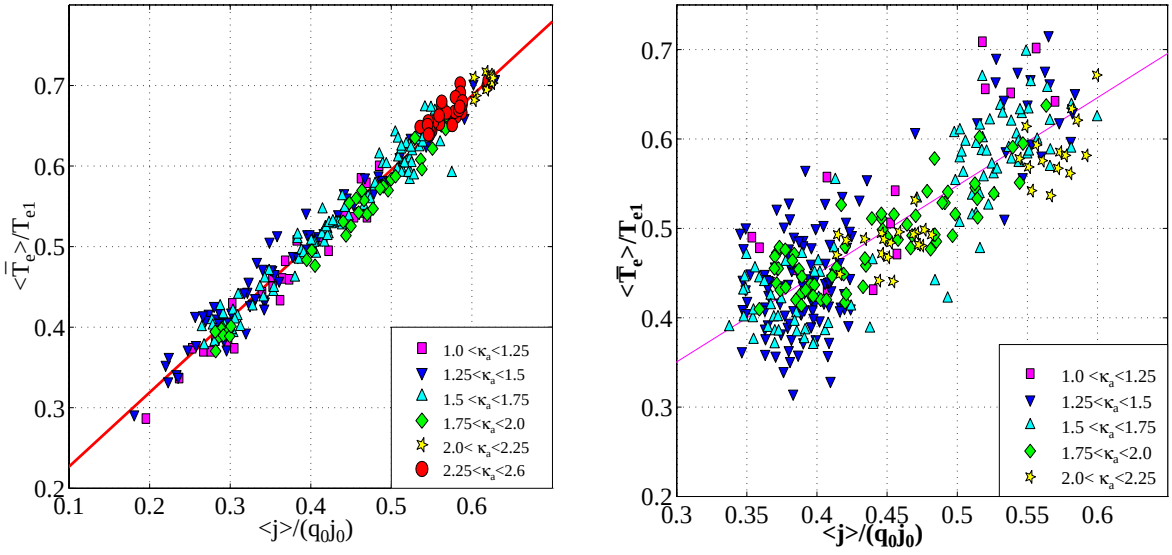

Fig. 2.1.9 Electron temperature inverse peaking factors in Ohmic (left) and ECH (right) plasmas.

One of the benefits of high elongation in a large future fusion experiment is the ability to raise the plasma current for a given value of the edge safety factor. There is therefore a concern that the high plasma currents sustainable at high elongation may lead to excessively large inversion radii and sawtooth amplitudes, susceptible of producing seed islands that may trigger neoclassical tearing modes (NTM's) which degrade confinement and limit β. From the observed scaling for the inversion radius, $\rho_{inv} \approx \langle j \rangle / (q_0 j_0)$, we can express the total current as

$$I_p \cong \rho_{inv} \cdot \frac{\pi a^2 B_0}{\mu_0 R_0} \cdot \kappa_a \left(\kappa_0 + 1/\kappa_0 \right)$$

This relation is similar to that obtained when scaling I_p at fixed edge safety factor, where $I_p \propto \kappa_a(\kappa_a + 1/\kappa_a)$. The above results show that if sawtooth inversion radii per se are a concern, the design plasma current and elongation can be scaled at fixed inversion radius instead of fixed safety factor. This results in a small penalty in plasma current (compared to fixed safety factor scaling), given by the ratio $(\kappa_0 + 1/\kappa_0)(\kappa_a + 1/\kappa_a)$. For typical plasma parameters this ratio is still as high as 0.9 for

κ_a=2. Moreover, as shown in the next section, sawtooth amplitudes are seen to decrease strongly for κ_a>2 both in Ohmic and in ECH heated discharges. These observations suggest that operation at high elongation may be of specific interest for the avoidance of NTM's.

2.1.7 Shape dependence of sawtooth periods and crash amplitudes

In Ohmic plasmas, increasing triangularity with constant ρ_{inv} and moderate elongation (κ_a~1.6) leads to increased sawtooth periods and crash amplitudes. The increase in amplitude with triangularity can be explained by the combined effect of longer sawtooth periods and a higher Ohmic heating power density. The dependence of the sawtooth period on elongation is opposite, with shorter sawtooth periods and smaller crash amplitudes at higher elongation. The example of a discharge which reached κ_a=2.8 is shown in Fig. 2.1.10. Beyond κ=2 the sawteeth are reduced. Beyond κ_a~2.4, sawteeth disappear altogether despite the low edge safety factor (q_{95}~2.5) and large inversion radius (ρ_{inv}~0.6) in this discharge.

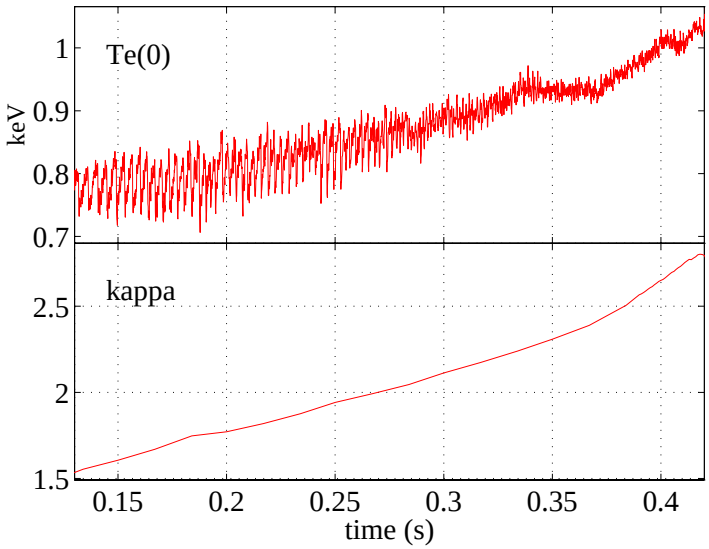

Fig. 2.1.10 Sawtooth behaviour in the high elongation discharge shown in Fig. 2.1.12. top: electron temperature from X-ray foil measurements. bottom: evolution of plasma elongation.

Central ECH deposition strongly enhances the effect of shape already apparent in Ohmic plasmas. For high positive triangularity, central ECH increases the sawtooth period even further. Small and negative triangularity result in further shortening of the period. Similarly for low/high elongation, the additional heating further increases/decreases the sawtooth period.

The observed response of sawteeth to heating is compared with a model in which the ideal internal kink is destabilised when the plasma pressure inside q=1 exceeds a critical value, depending on plasma shape, by a sufficient margin. Thus additional heating, by increasing the plasma pressure, increases the drive, leading to a decrease in the sawtooth period. For plasma shapes which are stable with respect to the ideal mode however, resistivity becomes important. The resistive growth rate (in the ion-kinetic regime), depends on the magnetic shear at the q=1 surface, whereas the stabilising electron diamagnetic rotation increases with pressure. ECH has the effect of increasing pressure as well as influencing the evolution of magnetic shear during the sawtooth cycle, leading to different dynamics, compared to the ideal mode. Therefore, the response of sawteeth to auxiliary heating is

expected to depend on whether ideal or resistive MHD determines the mode dynamics.

A necessary condition for ideal MHD stability is the Mercier criterion. In Fig. 2.1.11 the marginal stability domain, according to the Mercier criterion, is shown for two values of $\beta_{p,1} = (< p > - p_1)/B_{p,1}^2$, where <p> relates to the average pressure within the q=1 surface and the subscript 1 to values at the q=1 surface. The normalised shear at the q=1 surface, s_1=0.1 and q=1 radius ρ_1=0.5 are assumed constant. A comparison of the sawtooth response to ECH with the Mercier stability boundary shows that the critical $\beta_{p,1}$ is particularly low for discharges where additional heating decreased the sawtooth period (and hence stability), consistently with the above trigger model. These are shown as filled triangles and correspond to low triangularity or high elongation. Earlier numerical calculations had already suggested that the shape dependence of the ideal internal kink stability is essentially as expected from the ideal Mercier criterion. This has now been confirmed both experimentally and by calculations using the linear full ideal MHD code KINX and the experimental equilibria.

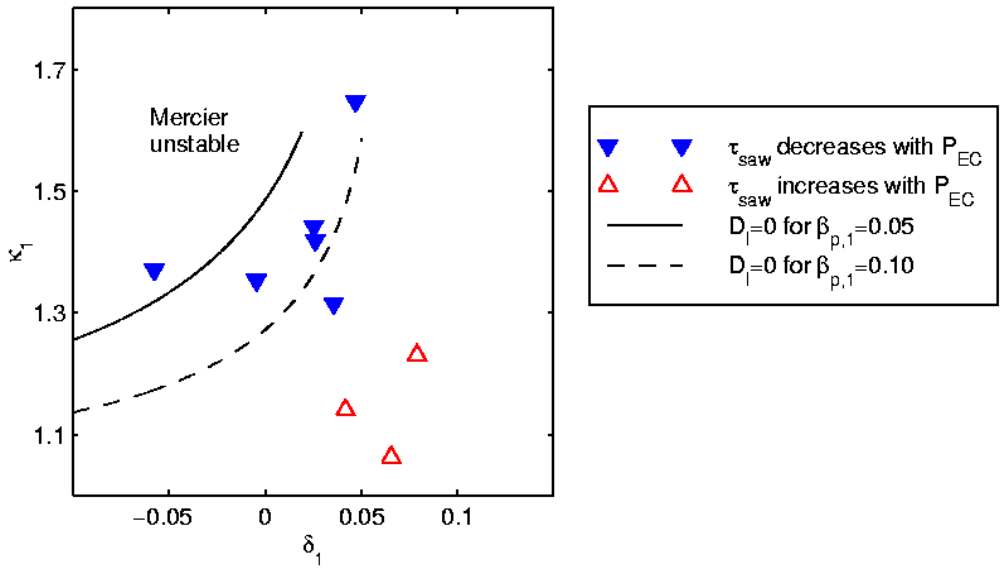

Fig. 2.1.11 Sawtooth stability in κ–δ space. The discharges where τ_{saw} decreases or increases are shown as a function of shaping parameters on the q=1 surface. The plasma shapes are compared to the marginal stability according to the Mercier criterion for two different values of $\beta_{p,1}$ and assuming constant shear s_1=0.1 and inversion radius ρ_1=0.5.

2.1.8 Development of Highly Elongated Discharges

One of the main aims of the TCV tokamak is the creation and study of highly elongated plasmas. Part of the motivation for this comes from the fact that the maximum plasma current increases with elongation and according to Troyon scaling, the beta limit is proportional to the normalised current, $I_N = I/(aB_T)$. This favourable trend has been verified experimentally up to elongations of κ=2.3 in the DIII-D tokamak, but it is not known whether it continues to be valid at higher elongation. The creation of elongated plasmas with κ>2.5 in a tokamak with conventional aspect ratio is an extremely difficult task since the stability margin of vertical control becomes very small. In Ohmic plasmas, axisymmetric stability imposes a lower limit to the normalised plasma current, which is necessary to produce a sufficiently broad current profile, and simultaneously, the non-

axisymmetric modes impose an upper limit to the current. The stable operating window between these two limits therefore decreases as the elongation increases.

Axisymmetric stability can be improved in several different ways. First, the passive stability can be improved by adapting the plasma shape as closely as possible to the shape of the vacuum vessel. Second, the vertical position control system can be optimised such that operation at very low stability margins becomes possible. Third, the current profile can be widened either by operating at the maximum possible plasma current, by using a fast ramp-up scenario or by applying off-axis ECH/ECCD. Non-axisymmetric stability, on the other hand, can be improved by operating at low beta or at low current, since at high elongation, the current limit increases as beta decreases. Clearly, the requirements for axisymmetric and non-axisymmetric stability are partially contradictory. As a result, beyond a certain elongation, the stable operating window shrinks to zero. Using the above methods in Ohmic plasmas, a maximum elongation κ=2.8 with I_p/aB_T=3.6MAm^{-1}T^{-1} has been achieved in TCV (Fig. 2.1.12).

With Ohmic heating alone, vertically stable plasmas with such extreme elongations have only been obtained at high values of normalised average current density, $\langle j\rangle^* = \mu_0 R_0 \langle j\rangle / B_T \sim 1.7$. With 1-2MW of ECH power deposited near or outside mid-radius, it is possible to create highly elongated plasmas with much lower values of $\langle j\rangle^*$. In the example of Fig. 2.1.13, the plasma elongation was raised from $\kappa_a \approx 1.75$ to $\kappa_a = 2.4$ corresponding to $\langle j\rangle^* = 0.46$ and $\langle j\rangle / q_0 j_0 = 0.2$, just by applying the ECH power at fixed quadrupole field. The resulting broadening of the current profile leads to vastly improved vertical stability. The example presented has a temperature profile width $\langle T_e\rangle / T_{e0} \approx 0.4$, which is a factor ~1.5 times broader than obtained in Ohmic plasmas at the same value of $\langle j\rangle / q_0 j_0$. These experiments open up a wide operational domain for the investigation of confinement at high elongation.

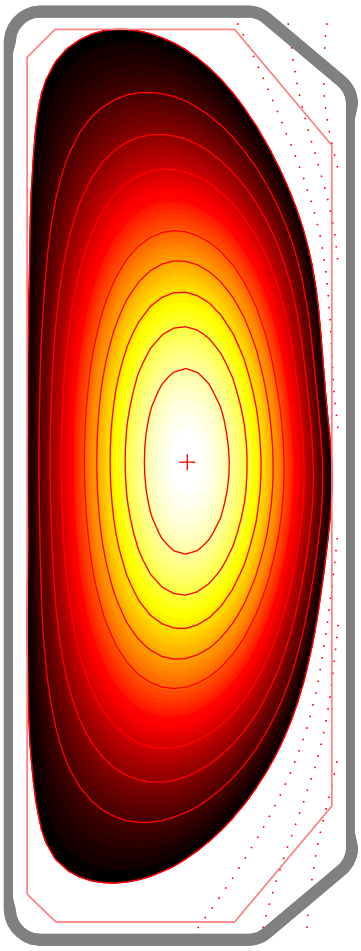

Fig. 2.1.12 (left)
Record elongation in TCV (#19373). I_p=755kA, B_T=0.8T, κ_a=2.8, k_0=2.15, δ_a=0.4, q_{95}=2.5, $\langle j\rangle^*$=1.74

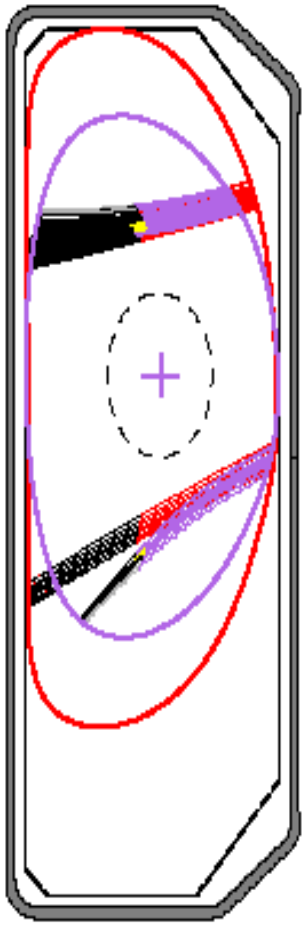

Fig. 2.1.13 (right)
ECH-assisted, highly elongated plasma (#19533).
Magenta: LCFS of initial configuration.
Red: LCFS of final elongated plasma with I_p=300kA, B_T=1.43T, κ_a=2.4, q_{95}=8.3, $\langle j\rangle^*$=0.46.
ECH ray trajectories from TORAY are also shown, parts beyond the X2 resonance are in black.

2.1.9 Ohmic ELMy H-mode accessibility

Ohmic H-modes are easily obtained in TCV, even with the ∇B driftaway from the X-point. In most conditions these are ELM-free and terminate in a high density disruption. Transitions from L-mode to stationary ELMy H-modes for SN configurations with reversed ion ∇B are only observed (at the nominal field B_T=1.43T) in a narrow range of discharge parameters: 0.35MA≤Ip≤0.43MA, $4.5\cdot10^{19}$m^{-3}≤<n_e>≤$6\cdot10^{19}$m^{-3}, 1.6≤κ_a≤1.7, 0.5≤δ_a≤0.6. Moreover the gap width between the inner wall and the plasma last closed flux surface must be between 1 and 3cm. Outside this domain either L-modes or ELM-free H-modes are obtained. This would be very restrictive, were it not for the high robustness of the ELMy H-mode, once it is established. After the transition, both the plasma elongation (together with the plasma current) and the plasma density can be varied over a wide range as shown in Fig. 2.1.14.

For improved vertical control in ELMy H-modes, an ELM-insensitive magnetic position estimator has been developed, which prevents an undesirable vertical controller response during the ELM events.

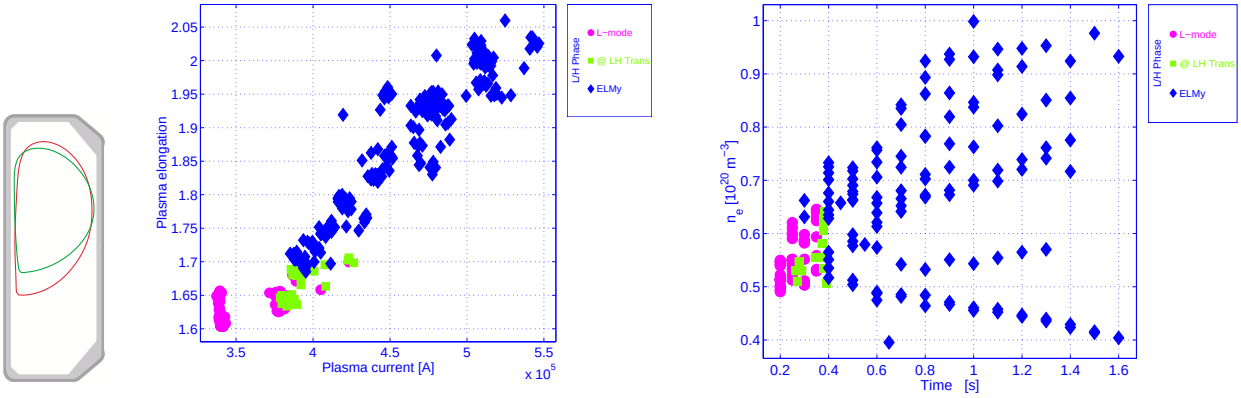

Fig. 2.1.14 Operational domain for ELMy SN H-modes. a) Accessible elongations and currents, b) Accessible density (time evolutions). All discharges transited through a “gate” in the operational domain indicated by the green symbols. Central insert: LCFS at transition and at highest elongation.

The behaviour of the ELMs is being investigated from the point of view of determining the underlying dynamics which define the inter-ELM time series. The presence of a chaotic behaviour signature has been confirmed, as on JT-60U, and work is ongoing on determining the statistical significance of these observations.

2.1.10 Detachment in Variable Divertor Geometry

Although the requirement of shape flexibility precludes the use of fixed baffle or optimised divertor target structures, it does allow the investigation of diverted equilibria not achievable in more conventional tokamaks. One such configuration, shown in Fig. 2.1.15, has been extensively used for studies of divertor detachment in Ohmic conditions and unfavourable ∇B drift direction with deuterium fuelling only. The equilibrium is simultaneously characterised by a very short inboard poloidal depth from X-point to strike point on a vertical target and an extremely long poloidal depth to a horizontal target on the outboard side. Density ramp discharges, invariably terminated by an X-point MARFE, leave the inboard target plasma attached even at the highest densities, while clear partial detachment is observed at the outboard target. Extensive modelling of this configuration using the

B2-EIRENE coupled package shows in fact that the outboard divertor achieves high recycling at very low densities, with the rollover to detachment occurring near the outer strike point very soon after the density ramp begins. The differences in detachment threshold at the two targets can be ascribed to a large extent to divertor magnetic geometry.

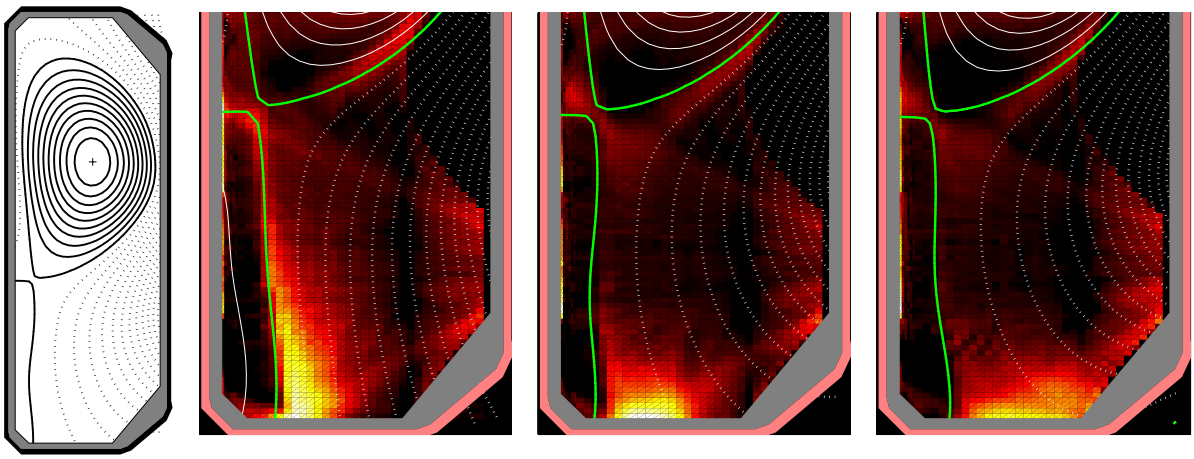

Fig. 2.1.15 Distributions of D_α emissivity for varying outer target flux expansion with the same degree of detachment.

While there is little latitude for changing the inboard geometry, a series of experiments has recently concentrated on studying the effect of outer target flux expansion, f_e, on the detachment behaviour. Figure 2.1.15 (b,c,d) show inverted tangential CCD camera images of D_α emissivity from the divertor volume for the same absolute degree of detachment (DOD) as f_e increases. The DOD describes the extent to which the target ion flux obeys the scaling, $\Gamma \propto \bar{n}_e^2$ predicted by the basic Two-Point Model of the divertor for the high recycling regime. By comparing D_α emissivities for the same degree of particle flux detachment, any differences due to magnetic geometry can be isolated. The distributions in Fig. 2.1.15 clearly show the effect of plasma plugging by the expanded flux surfaces and can be qualitatively reproduced by code simulations. Interestingly, however, the latter find the maximum in the emissivity to be located at the strike point, in evident disagreement with experimental observation.

Moreover, if the absolute level of detachment is to be quantitatively matched by the code using the three-body and radiative recombination processes commonly accepted to be responsible for detachment in most tokamak divertors, then the rate coefficients for these processes must be artificially increased by factors of 5 or more. This is a strong indication that other effects dominate in the relatively low density plasma characterising the TCV outer divertor. Such pathways may include molecularly assisted recombination processes involving the deuterium molecule (for example, inelastic charge exchange, $D^+ + D^0 \rightarrow D + (D_2)^+$ followed by immediate dissociative recombination, $e + (D_2)^+ \rightarrow D + D$) or as recently proposed, a source of increased volume recombination involving proton charge exchange with hydro-carbon molecules. Such pathways are currently under further study.

2.1.11 Non-linear simulations using the DINA code

The full TCV control system has been implemented in the non-linear evolution code DINA, with the aim of cross-validating the code for use on ITER. The first results have been extremely encouraging, allowing the DINA code to simulate the effects of coil-voltage perturbations onto the Poloidal Field coil system. Although to first order

such experiments are also quite well modelled using locally linearised models, one particular feature, Fig. 2.1.16, cannot be modelled so simply. In this example, the perturbation itself modifies the vertical field decay index sufficiently to drive the closed loop system unstable, briefly and with a small unstable growth rate. After the control system has counteracted the perturbation, the closed loop becomes stable once more. This sequence of events is almost perfectly reproduced by the DINA simulation.

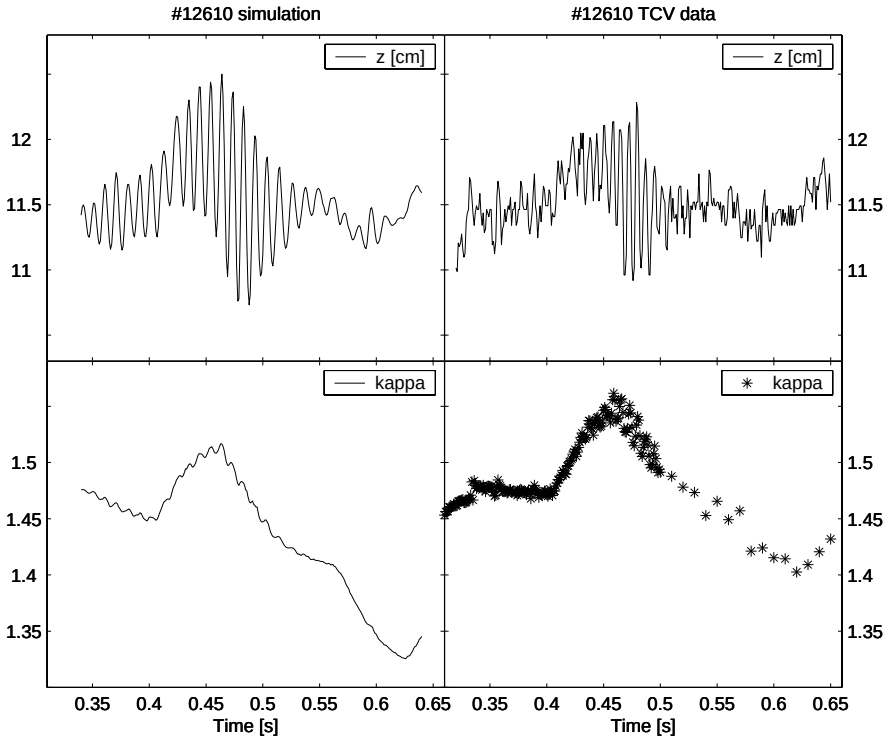

Fig. 2.1.16 Comparison between TCV (left) and the DINA simulation (right) for a large excursion due to a square voltage pulse OH1 stimulation. The vertical position becomes closed loop unstable and returns to closed loop stable once the elongation is reduced to its initial value.

2.2 Theory and numerical simulation

2.2.1 Transport-related instabilities

The so-called anomalous transport observed in tokamaks is generally accepted to result from the presence of drift wave instabilities such as the Ion Temperature Gradient (ITG) mode and the Trapped Electron Mode (TEM) that are referred to under the generic term of microinstabilities. When gradients of equilibrium profiles exceed a certain critical value microinstabilities can develop. After an initial phase of exponential growth, nonlinear saturation mechanisms enter into play and the system establishes a new turbulent equilibrium state. It is the heat flux due to this turbulence that is responsible for the observed anomalous transport.

There is therefore a strong motivation to understand these microinstabilities and to determine how they depend on the physical parameters and geometry of the magnetic confinement configuration.

2.2.1.1 Pivotal role of radial electric fields

The present understanding of the saturation mechanism involves the self-generation of radial electric fields (so-called "zonal flows") that in turn reduce the turbulence level. Several observations point to the correlation between improved confinement, the reduction of turbulence and the increase of radial electric fields, in particular in some "transport barriers" within which anomalous transport is suppressed. Theories predict that turbulence is suppressed when the shearing rate of the ExB flow exceeds the decorrelation rate. Very often, for reasons of practical use, this decorrelation rate is taken as the maximum linear growth rate in the absence of ExB flow.

In order to test these ideas we have studied the stabilisation of ITG modes by ExB flows in tokamak and, for the first time, stellarator configurations, by means of our global gyrokinetic codes.

In a circular tokamak we have analysed the effect of various radial electric field profiles on the toroidal ITG mode, Fig. 2.2.1.

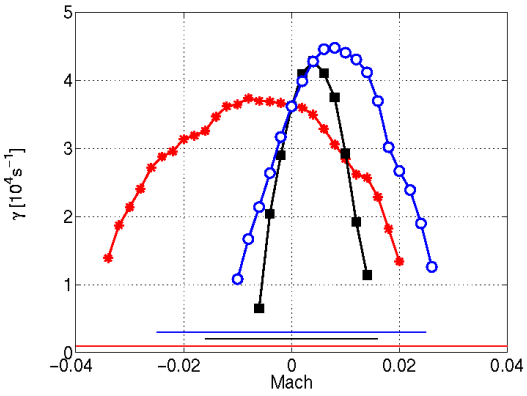

Fig. 2.2.1 Growth rates of the most unstable toroidal ITG mode vs Mach number for a linear profile of $u=ExB/B^2$ (open symbols), a constant profile of u/ρ (filled symbols) and a constant profile of $d\phi_0/d\psi$ (stars). ρ is the minor radius.

We note that the expression for the ExB shearing rate that should be used contains a combination of the magnetic shear and the shear of the ExB flow: $\Omega_{ExB}=r/q\ d(qu/r)/dr$. For profiles having a non-zero shearing rate (open circles and filled squares in Fig. 2.2.1), we have found that the shearing rate stabilisation criterion $\Omega_{ExB}=\gamma_{max}$ gives the correct answer to an accuracy of about 30% when compared to the global computation, and that the effect of such ExB profiles is indeed to shear the mode structure. But for profiles having zero shearing rate (stars) we found that another stabilising mechanism is at work: the ExB flow indeed does not shear the mode structure but pushes the maximum mode amplitude poloidally away from the unfavourable magnetic field gradient region, thus reducing the drive of the toroidal ITG mode.

We then considered a heliac stellarator. We have found that radial electric field profiles possessing a finite shearing rate do stabilise both helical-ITG and slab-ITG modes, while profiles with zero shearing rate can only stabilize helical-ITG (Fig. 2.2.2).

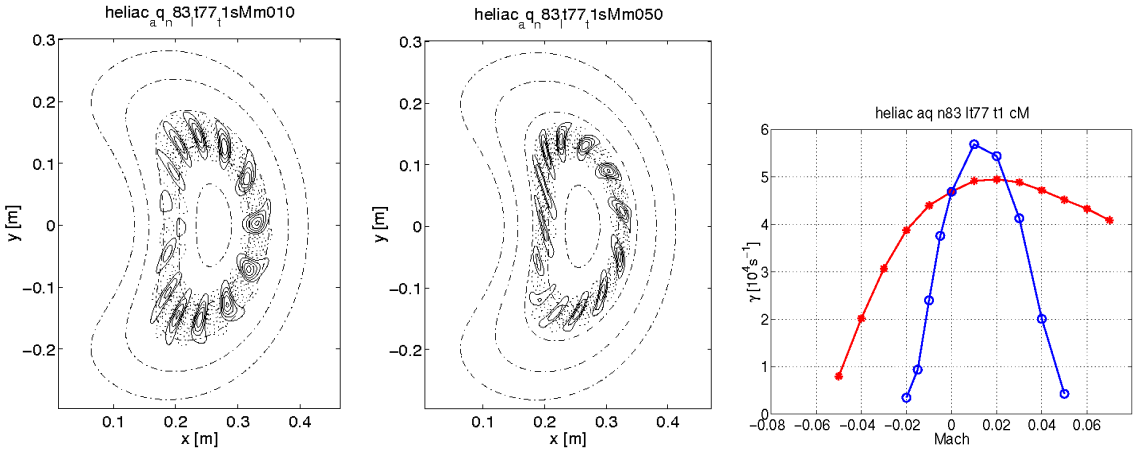

Fig. 2.2.2 Helical-ITG mode structure in a heliac without ExB flow (left), with sheared ExB flow (middle). Right: Growth rates of helical-ITG modes vs Mach number for a linear profile of $d\phi_0/d\psi$ (circles) and a constant profile of $d\phi_0/d\psi$ (stars) but not the slab-ITG modes. Our results show that the shearing rate stabilisation criterion can be written in a unified form for tokamaks and heliacs using either the poloidal flux or the helical flux as a radial variable.

We have analysed an improved confinement case from the ASDEX-Upgrade tokamak. We have shown that three necessary factors must be included to find agreement between the theoretical calculation and the experimental observations: the destabilising influence of trapped electron dynamics; the large (favourable) T_i/T_e ratio; the presence of a radial electric field that is sufficiently stabilising. These studies have been performed with the global spectral code GLOGYSTO that is restricted to the large aspect ratio, circular cross-section approximation. A more quantitative comparison with experiment requires new developments: the introduction of radial electric fields into a global, Particle-In-Cell, finite element gyrokinetic code including trapped electron dynamics that is able to treat arbitrary axisymmetric magnetic configurations. A new code, implementing these developments, is now under benchmarking and will hopefully be a powerful tool for studying the interplay between the sheared ExB flow and the magnetic shear in stabilising microinstabilities.

2.2.1.2 Electromagnetic effects

The study of electromagnetic effects on ITG driven instabilities, by means of the electromagnetic extension of the global gyrokinetic spectral code, GLOGYSTO, has been continued. Electron dynamics, including trapped electrons, have been implemented using the drift-kinetic approximation. Our results show that electromagnetic effects strongly stabilise ITG modes even when trapped electrons are taken into account, Fig. 2.2.3.

The study has been extended to Trapped Electron Modes (TEMs), drift waves propagating in the electron diamagnetic direction, showing that finite beta effects are minimal, which is unsurprising given the electrostatic character of these instabilities.

Finally, a family of magnetic shear profiles, ranging from positive to negative, have been analysed to study the combined effects of finite beta and magnetic shear. Results are in good agreement with electrostatic cases: negative magnetic shear reduces but does not completely stabilise ITG modes, while it does stabilise the TEM.

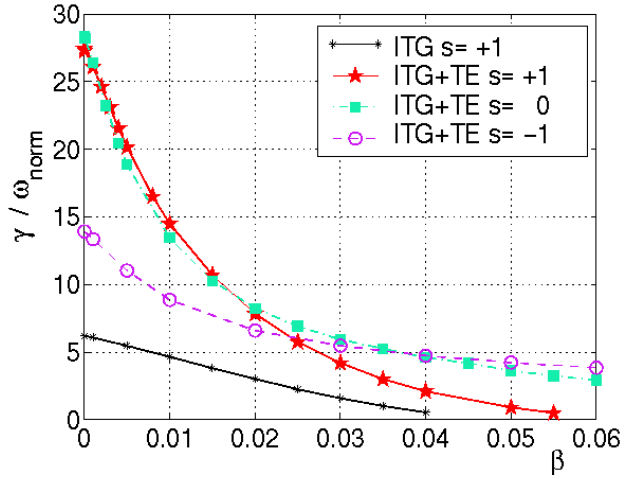

Fig. 2.2.3 Growth rate of ITG modes vs β with and without Trapped Electrons (TE) and for positive, zero and negative magnetic shear.

2.2.1.3 Microinstabilities down to the ion Larmor radius scale

During the past years, the CRPP theory group has developed several Particle In Cell (PIC) codes in 2D and 3D configurations in order to study low frequency electrostatic microinstabilities. All those codes contain finite Larmor radius (FLR) effects only to second order. This imposes a restriction on the possibility of making reliable comparisons between numerical results and experiments, in particular for the TEM that can have wavelengths comparable to the ion Larmor radius.

A more sophisticated quasi-neutrality equation has been implemented in order to include higher order FLR effects. This has been applied to the linear gyrokinetic global code L-ORB5 that also contains trapped electron dynamics. The new code has been successfully benchmarked against the global spectral code GLOGYSTO that is valid to all orders in Larmor radius. This has been done in circular, large aspect ratio tokamak plasmas for which the spectral code had been written. We have then studied the transition from ITG modes to TEMs for small wavelength perturbations.

2.2.1.4 Microinstabilities in stellarators

While previous generations of stellarators have been dominated by strong neo-classical transport, current advanced designs aim to reduce this to the smaller levels found in tokamaks. The Wendelstein VII-X (W VII-X) stellarator, presently under construction by the Max-Planck-Institut für Plasmaphysik (IPP), has been optimised against neo-classical transport in this way. The question then naturally arises as to whether these optimised configurations will be subject to turbulence-driven anomalous transport in the same way as tokamak configurations are. There is thus a great deal of interest in understanding what the drift wave dynamics of W VII-X will be.

The 3D, global, gyrokinetic code EUTERPE has been used to simulate the linear evolution of ITG modes using the parameters of the W VII-X design. In a tokamak the dominant poloidal harmonics of the magnetic field result in a corresponding coupling of the poloidal harmonics of the instability. EUTERPE has previously shown analogous effects for 3D configurations. In contrast, the results of the W VII-X simulations have shown that here the instabilities are characterised by a single mode. Motivated by this observation it was shown that in terms of growth rates the

results from W VII-X could be well approximated using an appropriately chosen straight cylindrical configuration, in which no coupling is implied. In moving from the cylinder to the stellarator geometry the radial mode structure remained conformal to the same magnetic surface, Fig. 2.2.4.

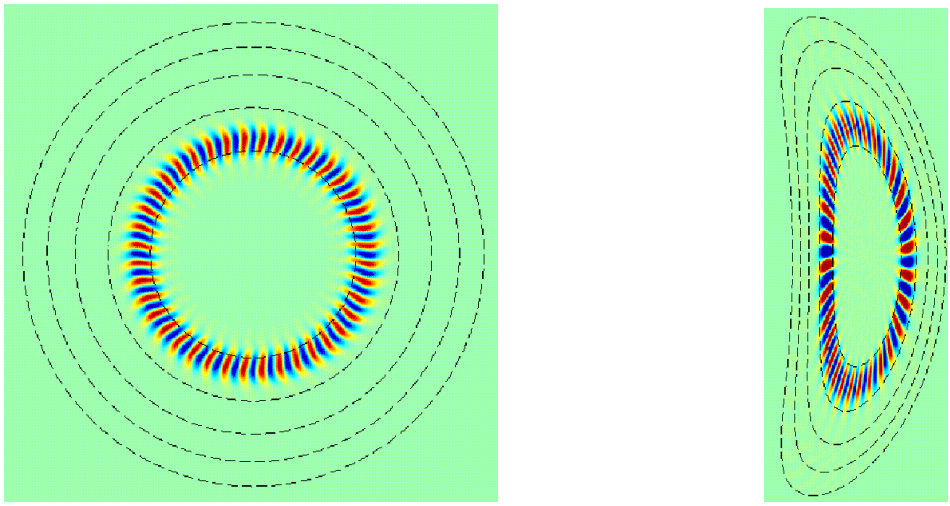

Fig. 2.2.4 ITG mode structure in stellarator W7-X (right) and in a straight cylinder having the same rotational transform and average minor radius (left).

Such results encourage speculation that simulations in cylindrical magnetic geometry of the non-linear phase of such instabilities may be indicative of the full 3D non-linear behaviour in such configurations.

2.2.1.5 A Semi-Lagrangian method for a drift-kinetic model resolution

This work deals with the nonlinear study of electrostatic instabilities caused by the ion temperature gradient. As a first step, we consider a cylindrical geometry (r,θ,z) with a uniform magnetic field, constant in time. We neglect the Larmor radius and thus the particles precisely follow their guiding centres. The resulting drift-kinetic model is then described by a non-linear Vlasov equation, where the ion distribution function is a 4-dimensional function (3 spatial dimensions and the parallel velocity). This system is closed by a quasi-neutrality equation where the electron response is assumed adiabatic. In this case the Liouville theorem is valid so we can use a time-splitting method to transform the resolution of the 4D equation into the resolution of 3 simpler successive equations (two 1D equations for the z and the velocity directions and one 2D equation in the (r,θ) directions). The specific purpose of this work is to try to solve the non-linear system obtained by a semi-Lagrangian method. This consists in solving the equations on a regular fixed grid in phase space and thus to avoid the problem of numerical noise and slow convergence with number of particles inherent to the particle-in-cell (PIC) schemes. This non-linear semi-Lagrangian code is still under construction.

2.2.2 Optimisation of 3D magnetic configurations

2.2.2.1 Sphellamak reactor stability

The local ideal MHD stability properties of a Sphellamak reactor system (Fig. 2.2.5, bottom) with a peaked toroidal plasma current of 30MA that generates a

configuration which approaches isodynamic conditions in the plasma core has been investigated at a fixed volume average β=7.3%. A sequence of configurations has been explored where the current in the helical Furth-Hartman type coils is varied from 42MA to 122MA, resulting in plasma volumes that vary from 700m^3 to 480m^3, respectively.

Ideal ballooning and Mercier stability are satisfied in this sequence except on locally isolated magnetic flux surfaces. Marginal conditions for ballooning stability in the outer half of the plasma volume are achieved when the helical coil current reaches 122MA. The configuration sequence analysed, however, is unstable to global n=1 kink modes in which the m=1 component is dominant. Marginal stability with respect to this type of structure is predicted with a helical coil current of 138MA.

2.2.2.2 Toroidal plasma current effect on quasiaxisymmetric local stability

Finite toroidal plasma current decreases the normal magnetic field line curvature near midvolume in a quasiaxisymmetric stellarator to improve ballooning stability properties. Near the edge of the plasma, a hollow current profile deteriorates the ballooning stability conditions through enhanced normal curvature while a parabolic current profile has the opposite effect. When the normal curvatures are comparable, the magnetic field line bending stabilisation plays a critical role. The local magnetic shear and the geodesic curvature vanish in the region where the normal curvature destabilises ballooning modes.

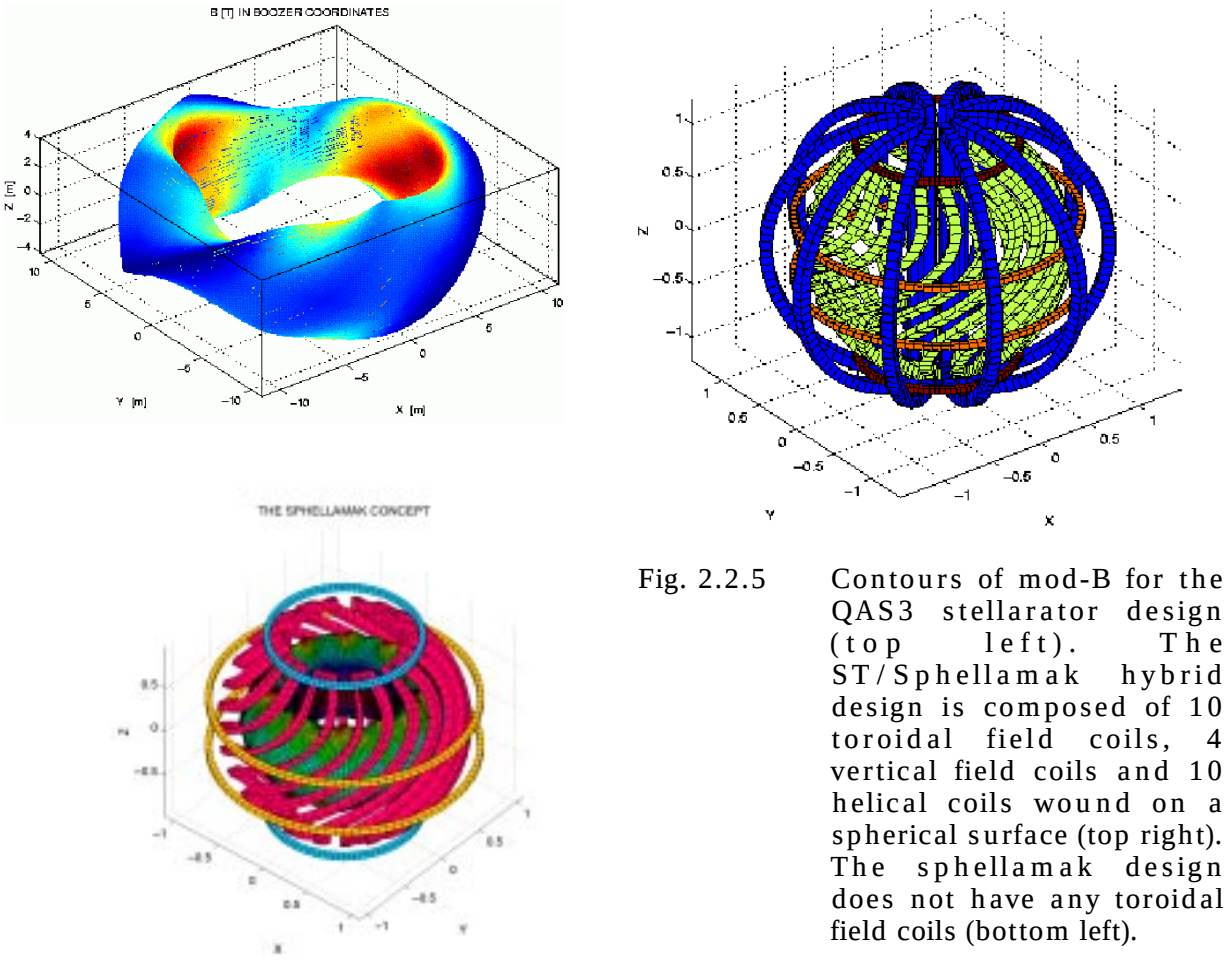

Fig. 2.2.5 Contours of mod-B for the QAS3 stellarator design (top left). The ST/Sphellamak hybrid design is composed of 10 toroidal field coils, 4 vertical field coils and 10 helical coils wound on a spherical surface (top right). The sphellamak design does not have any toroidal field coils (bottom left).

2.2.2.3 Electric field effects on the bootstrap current destabilisation of external kinks in LHD

The effect of the electrostatic potential on the bootstrap current has been calculated and its impact on the global MHD stability of a LHD configuration with a temperature T=2.5keV has been evaluated. The bootstrap current can trigger an external m/n=2/3 kink mode when it causes the edge rotational transform to approach 1.5. For vanishing potential, the unstable m/n=2/3 structure is strongly coupled to a m/n=9/13 component. Negative potential reduces the edge transform below 1.4 which causes the m/n=2/3 mode to couple with a m/n=5/7 term. Positive potential displaces the edge transform closer to the critical value 1.5 weakening the contribution of the m/n=9/13 toroidal sideband but deteriorating the stability conditions.

2.2.3 Behaviour of magnetic field lines and particle confinement in 3D configurations

The confinement of particles in 3D magnetic fields is of particular concern because, unless special care is taken to optimise the configuration, the particles will leave the plasma very quickly even if the magnetic field lines themselves are confined. We have studied the behaviour of fusion α–particles in the absence of collisions, and the transport of thermal particles in the presence of collisions (neoclassical transport) in various 3D configurations. The numerical tools developed for this purpose are a magnetic field line integrator, including the possibility of perturbations creating stochastic field lines in some regions of the plasma, and a particle motion integrator with a Monte-Carlo operator for collisions.

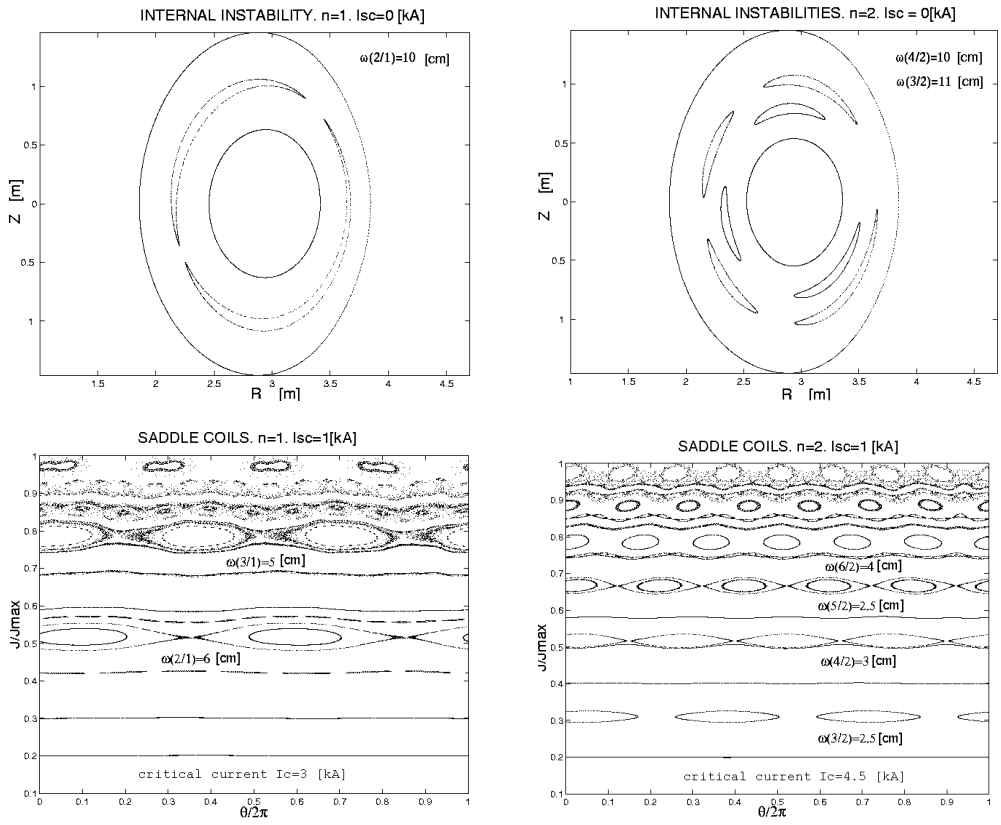

Fig. 2.2.6 a) Tearing mode instabilities for n=1 (top left) and b) n=2 (top right) in the JET tokamak. c) Poincaré cross-section of the magnetic structure in the presence of Saddle Coils for n=1 (bottom left) and d) n=2 (bottom right).

The perturbed magnetic field generated by saddle coils in the JET tokamak has been studied, in relation to the possibility of controlling the spontaneous formation of magnetic island chains that may occur on certain magnetic surfaces inside the plasma, the so-called tearing modes or neoclassical tearing modes, Fig. 2.2.6. We have shown that by applying a coil current of a few kA it is possible to substantially reduce the island width. We have been able to find the optimum value of coil current beyond which the perturbation induced by the coil creates its own island chains and eventually stochastic regions as well.

Various stellarator configurations have been studied. The QAS3 design (Fig. 2.2.5, top left) under study at PPPL is a 3 field period approaching quasiaxisymmetric features. We have shown that unfortunately the non-quasiaxisymmetry is strong enough to cause the loss of nearly all α-particles. Moreover, the neoclassical transport of thermal ions is found to be described by a diffusion coefficient proportional to $1/n$, which is an indication that the helical component of the magnetic field strength dominates the process. The same type of behaviour has been calculated for the Spherical Tokamak / Sphellamak hybrid configuration (Fig. 2.2.5, top right).

In the sphellamak concept, on the other hand (Fig. 2.2.5 bottom left) we have found excellent confinement properties: collisionless α-particles are well confined, and the neoclassical diffusion coefficient is close to that of an equivalent tokamak, Fig. 2.2.7.

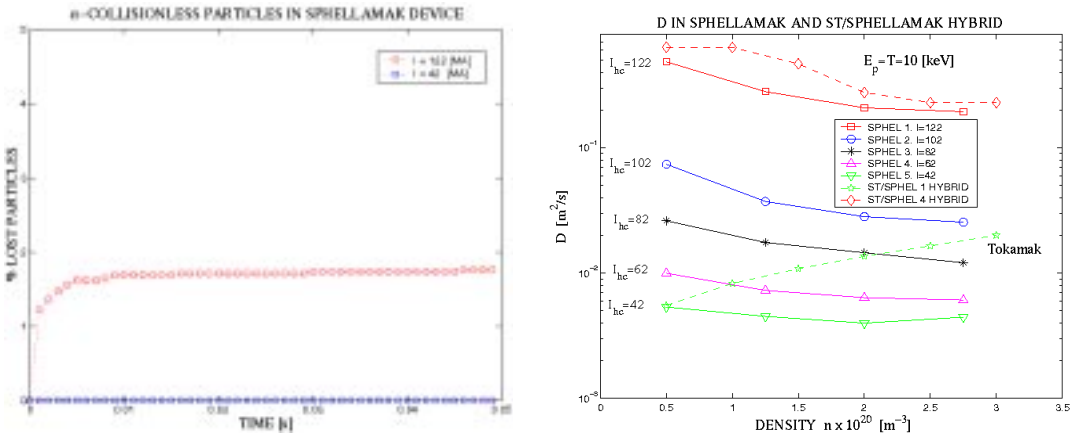

Fig. 2.2.7 Percentage of lost collisionless α-particles (left) and neoclassical diffusion coefficient of thermal Deuterium ions in sphellamak configurations with varying helical coil currents (right). The neoclassical diffusion coefficient of an equivalent tokamak is shown for the sake of comparison (stars).

We interpret these very favourable results to the fact that the magnetic structure in a sphellamak approaches quasi-isodynamic properties: the lines of constant second adiabatic invariant form closed contours.

2.2.4 Macroscopic stability of tokamaks

MHD stability studies of tokamak plasmas with a magnetic separatrix have been performed, with emphasis on low aspect ratio configurations. The series of numerical codes developed in the past few years (CAXE for equilibrium and KINX for stability) have been further augmented.

Free-boundary equilibria related to the spherical tokamak (ST) power plant and burning ST configuration designs have been investigated and optimised. One of the key requirements is to have a large bootstrap current fraction so as to minimise the transformer flux in the central column. For this reason, an improved bootstrap current calculation, taking collisionality into account, has been implemented into the CAXE free-boundary equilibrium code. We could obtain nearly 100% bootstrap current fraction cases with high normalised β of up to 8 which are ballooning stable. We have shown that this can be achieved by appropriate plasma shaping, e.g. a high elongation of 3.4 and a small negative outboard squareness.

Resistive wall modes have been studied with a newly developed version of the KINX stability code that has been optimised for computer memory use, thereby making it practical for runs on a workstation or a PC. The stabilisation of resistive wall modes with rigid plasma rotation was considered. The mechanism used so far, namely a simplified model for sound wave damping, is not very robust and a feedback stabilisation scheme looks more promising.

The ideal MHD internal kink mode is one of possible triggers of sawtooth oscillations and it is important to determine its stability so as to be able to predict the behaviour of sawteeth. Experiments on TCV show that the sawtooth activity depends on the plasma elongation and triangularity. We have undertaken the study of the dependence of the internal kink stability on plasma shape and current in a wide range of parameters. This has allowed us to propose semi-empirical analytical formulae giving a better description in particular of the dependence on triangularity. This will allow us to improve the sawtooth crash model used for sawteeth simulations and to compare with TCV experimental data.

2.2.5 Radiofrequency waves

2.2.5.1 Electron Cyclotron Current Drive

A study of electron cyclotron driven current in TCV plasmas with a small or vanishing toroidal electric field, has been made. The current drive efficiency, defined as the ratio of driven plasma current per unit RF power input, has been evaluated for different toroidal launching angles using both experimental and theoretical methods. Also, a comparison between a linear model for the EC current calculation (TORAY code) and values obtained from the loop voltage, corrected by the bulk plasma temperature to compensate different plasma conductivities, was performed. It was found that the theoretical values are close to the experimental values with small and moderate launching angles but with large parallel wave numbers the code underestimates the efficiency. This may be explained by the interplay between the toroidal electric field and the hot electron tail created by the EC waves because, in the case of vanishing electric field, the results were consistent, even with a large toroidal launching angle (35 degrees). Experimentally the conductivity was found to be greater than the neoclassical value. Again, this observation can probably be attributed to the conductivity due to the hot electron tail.

2.2.5.2 Alfvén and ICRF frequencies

We have started a study of electromagnetic wave propagation in three-dimensional plasma configurations. One of the possible applications of this work is the optimisation of low-frequency plasma heating systems in stellarators. The aim is to develop a 3D code that will allow the calculation of perturbed electromagnetic potentials, fields, and energy deposition in a plasma at low frequencies (Alfvén, ion-cyclotron frequency) when the wavelength becomes comparable to the plasma

dimensions. At these frequencies, a homogeneous plasma approximation is not applicable, so a solution of a full wave equation, with an inhomogeneous dielectric tensor, is necessary. The equation is to be solved numerically, applying Fourier decomposition in the poloidal and toroidal angles and finite elements discretisation in the radial direction. We are presently expanding the equations in a Boozer magnetic coordinate frame applying the transformation algorithms employed in the TERPSICHORE code to treat 3D equilibria produced with the VMEC code. We have tested this procedure for large aspect ratio tokamak configurations.

In the field of Alfvén waves and their possible destabilisation by fast ions in tokamak plasmas we have developed an improved gyrokinetic model in which parallel wavenumbers are consistently evaluated. It is now being implemented in the global wave code PENN. The intent is to explore advanced scenarios and low aspect ratio cases for which the Alfvén eigenfrequencies are comparable to the drift frequency range.

2.3 Materials for fusion

The main objective of the Fusion Technology Materials (FTM) group is to investigate the effects of the damage produced by radiation in metals and alloys, especially in candidate materials for structural components of the future fusion reactors. This group uses the high energy (590MeV) proton beam of the PSI accelerator, through the Proton Irradiation Experiment (PIREX) facility, to simulate experimentally the effects of the 14MeV neutrons that are the product of the fusion reactions between deuterium and tritium nuclei.

Like 14MeV neutrons, 590MeV protons produce atomic displacement cascades and transmutation nuclear reactions inside the irradiated material. From the point of view of materials science, atomic displacement cascades induce the formation of point defects, such as vacancies and interstitial atoms, while nuclear transmutation reactions produce radioactive impurities, such as helium or hydrogen atoms. The final microstructure of the irradiated material results from reactions between these different defects, including dislocation loops, dislocation networks, stacking fault tetrahedra, gas bubbles and/or voids resulting from the accumulation of point defects. This microstructure has an important effect on the physical and mechanical properties of the material. It can lead to significant hardening, loss of ductility and fracture toughness, as well as macroscopic swelling of the material. These effects are the main factors limiting the candidate materials. The residual radioactivity of a large amount of exposed material is also a concern and will govern the handling methods, dictate the storage periods and the overall waste management and recycling scenarios. The development strategy that takes into account these limitations has led to the development of the so-called low activation materials.

The design of materials with properties adequate for use in an irradiation environment requires an understanding of the effects of irradiation on their physical and mechanical properties. The FTM group has been active in that field for 17 years within the framework of the European Fusion Technology Program and collaborates with many research institutes and industries in Switzerland as well as abroad. For some specific experiments, neutron irradiations are carried out in reactors in Denmark, Hungary, Sweden and the Netherlands. The actual research program of the FTM group includes basic research on radiation damage in metals and alloys (paragraph 2.3.1), development of low activation materials for fusion applications (paragraphs 2.3.2 and 2.3.3) and development of new techniques for the investigation of the structure/mechanics relationships in radioactive materials (paragraphs 2.3.4). The main experimental tools include macroscopic mechanical testing and transmission electron microscopy (TEM) measurements.

2.3.1 The early stages of damage

Nickel-aluminium intermetallics constitute interesting systems for the study of irradiation-induced phase transformations (order-disorder, amorphisation) and defect production. Their irradiation may induce disorder or amorphisation depending on the projectile characteristics, irradiation conditions and physical characteristics of the target. In previous investigations by the FTM Group, the evolution of displacement cascades has been investigated using molecular dynamics (MD) simulations. It was shown that under certain conditions, the development of a cascade can lead to the formation of an amorphous region in NiAl, but under no conditions does this amorphisation take place in Ni_3Al.

In order to investigate these MD results further, image simulation techniques were first applied to the MD results. To properly analyze the results, calibration images were produced of both disordered and amorphous regions embedded in a perfect crystal. These images were used as a comparison basis to the actual images obtained from the MD files. Examples of the results of the simulation of conventional transmission electron microscopy (CTEM) images are shown in Fig. 2.3.1 for both NiAl and Ni_3Al. A disordered region is identified in NiAl under dark field (DF) using the superlattice reflection g=(100), see Fig. 2.3.1a. The weak beam WBDF g(3,1g) image is simulated to identify the defects present, which are shown to be formed inside the disordered region, Fig. 2.3.1b. Furthermore, as indicated in Fig. 2.3.1c, partial amorphisation has taken place in the irradiated specimen.

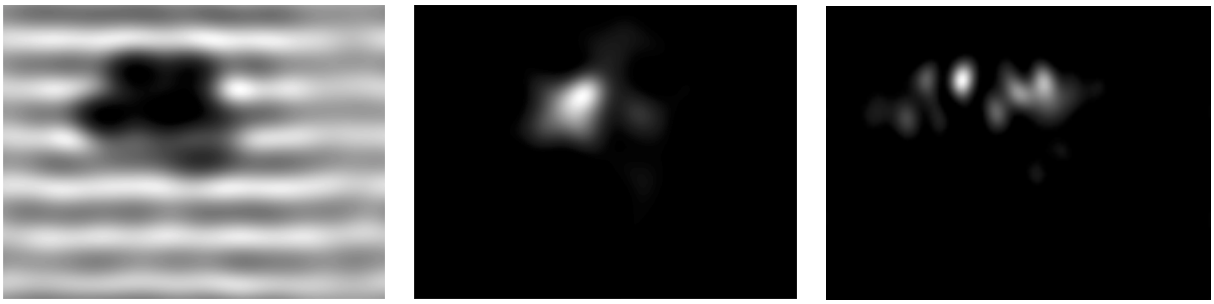

a b c

Fig. 2.3.1 Simulated images of irradiated NiAl : (a) dark field image of a disordered region, (b) weak beam image of a disordered region, (c) weak beam image of a partially amorphised region.

Transmission electron microscopy observations have been performed on single crystals of NiAl and Ni_3Al irradiated with Ni ions of 700keV and 6MeV at 300K. In NiAl, an increase of fluence from 10^{14} to 10^{15} ions.cm^{-2} of 700keV ions increases the defect cluster density ρ_c from $7x10^{22}$ to $1.1x10^{23}$m^{-3} with mean diameters between 2.5 and 3.5nm. A comparable increase is observed on increasing the energy from 700keV to 6MeV ($7x10^{22}$ to $1.4x10^{23}$m^{-3}). The density of disordered zones ρ_d is of the order of $7x10^{22}$m^{-3} at 10^{14} ions.cm^{-2}, independently of the ion energy. The ratio ρ_d/ρ_c is a measure of the radiation-induced disordering efficiency and it decreases with increasing primary ion energy. No amorphisation has been observed under the irradiation conditions used in the present research, indicating that most probably the amorphisation results from defect accumulation (dose, dose rate) rather than from cascade formation and evolution.

2.3.2 The low activation ferritic/martensitic steels

The low activation ferritic-martensitic steels known as OPTIMAX steels were developed by the group as candidate structural materials for the first wall of future fusion reactors. They contain about 9 wt%Cr and their detailed composition is based on that of MANET steels where Ni, Mo and Nb have been replaced by the W, V and Ta low activation elements. A series of casts with different contents of W, Mn and N have been produced from high purity components under clean processing conditions. The main difference between the different casts is that the steel designated as OPTIMAX A contains 0.56 wt% Mn and 0.0007 wt% N, while the conditions are reversed in alloy B that contains 0.037 wt% Mn and 0.003 wt% N. In OPTIMAX C and D, the W content was raised to 2 wt%, with a higher N content in the alloy D. A fine carbide structure has been obtained in all cases by normalising the steels at 1370K before austenization for 30 minutes at 1230-1250K (depending on the steel composition) for obtaining a final preaustenite grain size of 16-20μm. After tempering at 1020K (which was used as tempering temperature for all steel compositions) for 2 hours, the carbide volume fraction in both OPTIMAX A and B steels is about 4%. The main difference between the two steels is due to the presence of a higher density of small carbides (<40nm) in the higher nitrogen containing steel B.

The F82H ferritic/martensitic steel was developed in Japan. It is investigated as part of the IEA (International Energy Agency) Fusion Materials Internationally Coordinated Program on ferritic/martensitic steels. The F82H steel is based on the Fe-8Cr-2W-V-Ta composition. It was heat treated by normalizing at 1313K for 0.5 hours and tempering at 1013K for 2 hours.

Mechanical behavior of the OPTIMAX steels

The irradiation matrix of OPTIMAX steels, which already includes specimens irradiated at 320K or 523K to a dose of 0.3 or 1dpa, has been complemented. Specimens of OPTIMAX A, B, C, and D have been proton-irradiated at 320K to a dose of about 2dpa, and specimens of OPTIMAX A, B, C, and D have been proton-irradiated at 623K to a dose of about 1dpa. These specimens are still too radioactive to be mechanically tested and/or observed with transmission electron microscopy.

Mechanical behavior of the F82H steel

It was already shown that the strain-hardening of the F82H steel, measured in tension tests, follows a Voce type of law at deformations larger than 1% of plastic strain. In order to reconstruct the entire tensile curve, further investigations in the low plastic strain, namely between the yield stress at 0.2% plastic strain and 1%, were undertaken. Empirically, it was found that the most convenient way of describing the initial part of the curves is to use the simple relationship:

$$\sigma_{pl} = \sigma_{0.01}\left(\frac{\varepsilon_p - 0.002}{0.008}\right)^n \qquad 0.002 \le \varepsilon_p \le 0.01$$

This relation yields a good fit over the range of temperatures investigated (123K – 300K). Thus, the curves can be recalculated by connecting two fits corresponding to two strain-hardening stages. As an example, Fig. 2.3.2 shows the two fits obtained for the hardening component of the flow stress at T=173K.

The first fit corresponds to the power law described above while the second one refers to the Voce law. A temperature dependence of σ_{pl} was found via that of the two parameters $\sigma_{0.01}$ and n. Similarly, a slight temperature dependence was evidenced for the Voce curve. Even if a weak temperature dependence exists for the strain-hardening, the reversibility of the flow stress was tested with Cottrell-Stokes

experiments. This type of experiment is performed in two steps. First, a specimen is deformed up to a given strain at a fixed temperature T_1 and unloaded. Then the test temperature is changed to T_2 and the deformation is continued. Usually T_2 is chosen lower than T_1 in order to avoid irreversible annealing processes. The flow stress required to deform plastically the specimen at T_2 can be compared to that obtained for a specimen tested only at T_2. This technique can quantify the influence of the temperature on the development of the microstructure and to assess the reversibility of the flow stress for a given strain-hardened state. An example of a Cottrell-Stokes experiment is shown in Fig. 2.3.3 for which a specimen was deformed at 293K up to about 0.02 plastic strain and then deformed at 173K up to fracture. The second deformation curve is compared to that obtained for a single reference specimen tested only at 173K. It can be seen that pre-deformation at 293K up to 0.02 plastic strain does not influence the flow stress and/or the strain-hardening obtained for the subsequent deformation at 173K. Similar experiments performed between the temperatures T_1-T_2 equal to 293-223K and 223-123K showed no influence of pre-deformation. Thus, while the strain-hardening rate was found to be slightly temperature sensitive, the flow stress appears to depend only on the amount of deformation. This observation provides additional support to the conclusion that the temperature dependence of the strain-hardening is weak.

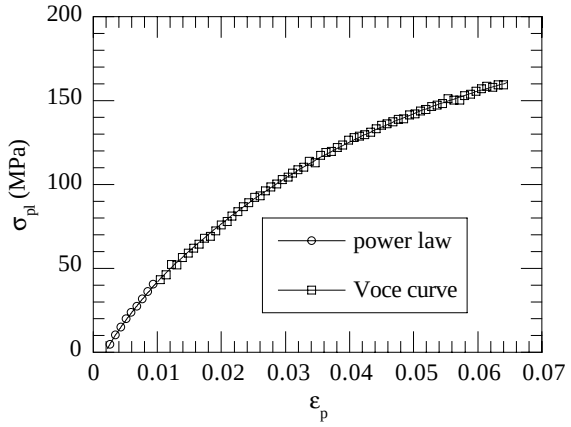

Fig. 2.3.2 Plastic stress-plastic strain deformation curve calculated by connecting two fits corresponding to two strain-hardening stages.

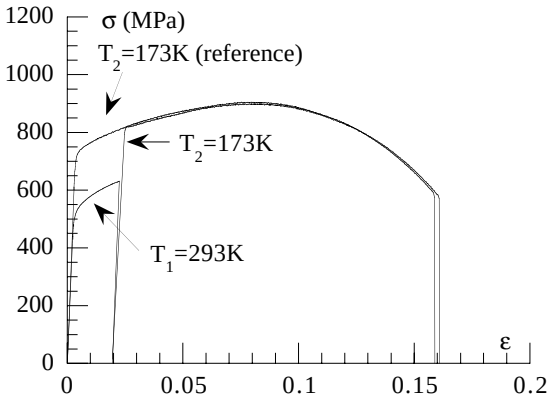

Fig. 2.3.3 Example of a Cottrell-Stokes experiment.

2.3.3 The Titanium-based alloys

Titanium alloys exhibit a number of properties that make them attractive candidates as structural materials for fusion reactors, including: high strength-to-weight ratio, plasticity, good fatigue and creep rupture properties, small modulus of elasticity, high electrical resistivity, heat capacity, small coefficient of thermal expansion, low long-term (> 10 years after shutdown) residual radioactivity (after V and Cr, Ti exhibits the fastest decay rate), compatibility with coolants such as lithium, helium and water, corrosion resistance, high workability and good weldability, commercial availability with established mine and mill capacity, together with good resistance to void swelling under a wide variety of irradiation conditions. Titanium alloys are basically low temperature alloys with a maximum useable temperature in the neighbourhood of 500°C. In addition, titanium and its alloys have a high chemical affinity with hydrogen which, in the fusion environment, leads to hydrogen embrittlement and tritium inventory. Therefore, in order to make practical use of titanium alloys for fusion applications, hydrogen barrier coatings are required to prevent hydrogen intake and subsequent hydrogen isotope induced deterioration of the material.

Titanium alloys can be divided into three major classes determined by phase constituency that are referred to as α, β and α/β, where the α phase is hcp (hexagonal compact) and the β phase is bcc (body centred cubic). The alloying elements used in the titanium system can be divided into two classes upon the basis of which phase the element stabilises. The α stabilisers are Al, Zr and Sn, while the β stabilisers are V, Cr, Mn, Fe, Co, Ni and Mo.

The amount of hydrogen that can enter titanium alloys depends upon a variety of factors that include the partial pressure of hydrogen, temperature, surface conditions, microstructure and alloy content (type and amount of phase present). In general, the alloys that consist primarily of α phase have a lower solubility for hydrogen than alloys that are primarily β phase. In the case of α/β alloys, the solubility increases with increasing amounts of β phase. The influence of alloying elements on the solubility of hydrogen relates essentially to the type or amount of phase, either α or β, that alloying elements promote.

Titanium-base alloys for ITER

An assessment of the tensile, fatigue and fracture toughness performance under irradiation of two titanium alloys for the ITER-FEAT modules is under progress. The two candidate alloys considered are: a classical α/β alloy, Ti-6Al-4V, and an α alloy, Ti-5Al-2.5Sn.

It was found that the resistance to tensile deformation of both alloys is very similar. The critical stress measured at 0.2% plastic strain, $\sigma_{0.2}$, has a mean value of about 800MPa at ambient temperature (that is about 40% higher than that exhibited by a 9Cr-1Mo low activation ferritic/martensitic steel) and 450MPa at 500°C (about the same as that obtained for a 9Cr-1Mo ferritic/martensitic steel). Both alloys exhibit a good ductility. The total elongation of the α/β alloy, between 15 and 20%, is slightly higher than that of the α alloy, for a test temperature between 20 and 500°C. Irradiation with 590MeV protons (mean dose rate: 3×10^{-6} dpa.s^{-1}, mean He production rate: 50appm/dpa) leads to hardening and loss of ductility for both alloys. However, these phenomena are much stronger for the α/β alloy than for the α alloy. Irradiation at 350°C affects both the critical and the ultimate stresses, while irradiation at 40°C affects mainly the critical stress. Whatever the irradiation temperature, 40 or 350°C, the hardening values are independent of the test temperature between 20 and 350°C, which indicates that irradiation-induced hardening is a non-thermal and long range mechanism. TEM investigation revealed a very fine precipitation in the primary and secondary α grains of the two-phase alloy. The irradiation-induced precipitates appear as elongated particles of sizes up

to 15nm, with different orientations and distributions. This precipitation phenomenon could be the cause of the strong radiation hardening shown up for the α/β alloy. It is thought that these particles relate to the strong segregation of V, a β stabiliser, in the two-phase alloy.

Fatigue tests were performed, under total strain range control, on the Ti-5Al-2.5Sn and Ti-6Al-4V alloys. Since titanium alloys are very elastic (E=120000MPa) and very strong, the elastic contribution of the total strain is much larger than the plastic contribution. As low cycle fatigue requires plastic deformation, the testing of titanium alloys demands very high total strain ranges, typically between 1 and 2%. Fatigue tests were performed only at 350°C, since preliminary experiments conducted at ambient temperature on Ti-5Al-2.5Sn led to sudden failure of the specimens, due to local instabilities resulting from stress concentration effects. Fatigue resistance at 350°C was found to be slightly better for Ti-5Al-2.5Sn than for Ti-6Al-4V. The behaviour of the fatigue cyclic stress as a function of the number of fatigue cycles could be divided into two regimes. At low imposed strain and for both alloys, a regime of cyclic softening takes place during the first period of life. It is followed by a regime of cyclic hardening that could result from interactions of dislocations with cyclic strain-induced dislocation debris. At high imposed strain, softening is almost absent for Ti-6Al-4V and very weak for Ti-5Al-2.5Sn. The main effect of irradiation with 590MeV protons at 350°C lead to 0.3dpa is the disappearance of the hardening cyclic stress regime for both alloys. No significant degradation of the fatigue resistance of Ti-5Al-2.5Sn has been observed, while the life of Ti-6Al-4V appears clearly reduced for an imposed strain above 1.2%. Fractography performed in scanning electron microscopy revealed a pseudo-brittle fracture mode for both materials. The strain appears to be localised in some grains, well oriented with respect to the applied stress and next to them brittle fracture occurs. The anisotropy of the materials induces many small intra- and trans-granular cracks. The crack nucleation mechanism is the same in both materials, explaining their similar fatigue behaviour.

Both alloys have been loaded with different amounts of hydrogen, namely 150ppm and 400ppm and irradiated with neutrons at the RisØ Laboratory (Denmark). At low concentrations, the damage due to hydrogen is not important and appears as a loss of ductility. When the hydrogen concentration exceeds the solubility limit, a new phase segregates in the hcp lattice in the form of hydrides, namely TiH_2. Precipitation of hydrides is very detrimental for the mechanical properties of the alloys, especially for the fracture toughness properties. Irradiation could have the effect of re-dissolving the hydrides, thus improving the fracture behaviour. The situation should be better in the two-phase alloy, because the solubility of hydrogen in the β phase is much higher than in the α phase, e.g. 50wppm of H in a 90% α/10% β alloy results in 200-300wppm of H in the β phase. However, assuming that titanium does not form hydrides does not mean that tritium will not accumulate. The synergistic effect of hydrogen + irradiation will be studied by measuring fracture toughness properties. The fracture behaviour of titanium alloys is such that an initiated crack grows in a stable and slow manner. For this reason, the fracture toughness can be evaluated using the J1C concept, at crack initiation. For this purpose a special 3-point bend fixture has been developed. The critical experimental parameter to measure is the crack length. This can be done using the potential drop method and the elastic compliance method. Testing is under progress.

Development of new titanium-base alloys

It is believed that the resistance to radiation damage is superior for an α alloy compared with a more complex α/β alloy. The new results reported seem to confirm this idea. Our efforts are therefore concentrated in the development of new α titanium alloys. Radiation resistance is an important issue but reduced activation is a prime requirement for use in a nuclear system. To achieve this goal it is first

necessary to understand the influence of particular chemical elements on the structure and properties of these alloys. Having chosen the promising alloy Ti-5Al-2.5Sn as a reference, a series of 5 alloys has been prepared in which first the substitution of Al and Sn has been tested and also where an attempt was made to vary the associated impurities (O, N, Fe) to detect their influence on the properties. Al has been substituted with Zr, to create a Ti-5Zr-2.5Sn alloy, then Sn was removed and two binary alloys were developed, containing 5%Zr and 22%Zr respectively.

The first results indicate that Al is a stronger strengthener of the α phase than Zr. The role of Sn is not yet completely understood, but it seems to be a solid solution strengthener. Sn also forms intermetallic precipitates, which in fact could generate difficulties after high dose irradiation. Another very important strengthener is oxygen, was found from β annealing experiments. It seems that Fe is also contributing to the strengthening of the solid solution, but it also forms bcc precipitates, due to its very low solubility in the α phase.

Some of the alloys have been irradiated with protons in the PIREX facility and with neutrons in Hungary, but the specimens are not yet tested.

In parallel, attempts were made to get results on the particular elements that should be used for an alloy with good low activation properties. A calculation has been made at JET using a fusion neutron spectrum and the normal impurities of titanium as input, and a list of possible elements in allowable quantities was obtained. These data should serve as a base for the selection of new compositions.

Coatings for Titanium-based alloys

A duplex coating has been plasma sprayed using the SULZER Metco F4 gun onto a set of specimens of an α titanium alloy, namely Ti-5Al-2.5Sn. The selected duplex coating system consisted of a 0.1-0.2mm thick bond layer of pure tantalum and a chromium oxide top layer doped with 3 wt% titanium oxide to increase the coating ductility. The achieved thickness of the top layer was about 0.6mm. The coated specimens have been subsequently tested for structural integrity, via bond strength and hardness measurements and microstructure observations, and for hydrogen permeation, via experiments performed in a Sievert's apparatus. The results appear encouraging concerning the barrier efficiency of plasma sprayed deposits against hydrogen intake.

Irradiation effects on pure Titanium

A number of investigations of radiation damage effects in fcc (face centered cubic) and bcc pure metals have already been reported. They revealed significant differences in the defect accumulation rate and the dose dependence of the hardening between these two structure types. In order to complement such investigations, a study of the irradiation effects on the mechanical behaviour and microstructure of hcp pure titanium has been undertaken.

Tensile flat specimens of 8mm in gauge length and 0.3mm in thickness have been prepared from thin polycrystalline foils of pure titanium (99.999%) and annealed at 1023K for 5 hours. The specimens were irradiated with 590MeV protons in the PIREX facility. These irradiations were performed at ambient temperature (300–320 K) and 523K to doses ranging between 10^{-3} and 1dpa. The damage rate was approximately 10^{-7} dpa.s^{-1}. The simply annealed and the irradiated tensile specimens were deformed at ambient temperature up to fracture. Figure 2.3.4 shows typical stress-strain curves. The defects associated with deformation and/or irradiation were imaged in TEM by using the bright/dark field and weak beam techniques.

As previously observed for fcc and bcc pure metals, proton-irradiation at ambient temperature of hcp pure titanium produces a hardening of the material, found to be proportional to the fifth root of the irradiation dose, a behaviour similar to that of bcc pure iron. The radiation hardening of pure titanium is low, however. The yield strength increases by about 30MPa, compared with the unirradiated case, while the elongation is still of the order of 20-25%. These results confirm those obtained for the α titanium alloy (see above), indicating that the hexagonal phase is more resistant to the effects of irradiation compared with the fcc or bcc structures.

For doses ranging between 10^{-3} and $3x10^{-2}$dpa, plastic deformation of irradiated titanium is homogeneous. It occurs by propagation of dislocations through a cloud of irradiation-induced defect clusters, leading to their annihilation and the formation of a cellular dislocation structure together with twins. This mechanical behaviour is similar to what was previously observed for pure fcc metals, the formation of twins being intrinsic to the deformation of hcp titanium, however.

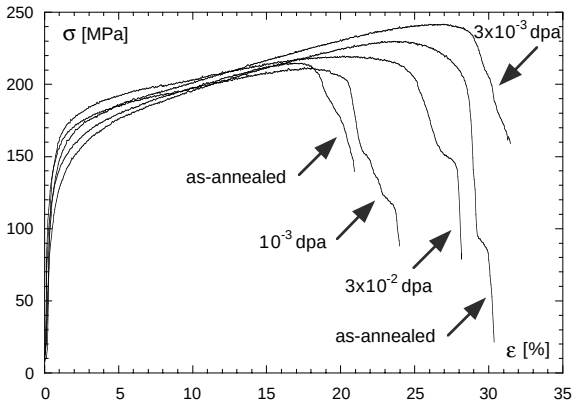

Fig. 2.3.4 Stress-strain deformation curves obtained at ambient temperature for unirradiated specimens of pure Titanium and for specimens of pure Titanium irradiated to different doses.

New materials sample deformation setup

A new deformation setup has been developed and installed on a computer-controlled Zwick deformation machine. It allows conventional tensile/compression tests that can be complemented with transient tests (load relaxation experiments, strain rate jumps, changes of temperature), and also small punch tests. Specimens to be used are tensile flat specimens ($0.3x2.5x20mm^3$) and punch specimens ($Ø3x0.2mm^3$). Deformation experiments can be performed in a secondary vacuum or in a flow of inert gas (helium, argon), at any temperature between -196°C and 1000°C. The maximal allowable load is 10kN. The length of the specimens is measured continuously by means of electronic extensometers with a range of ±5mm. A lead shielding has been installed around the setup, that allows for mechanical testing of radioactive materials.

In a first step, this new setup will be dedicated to tensile mechanical testing of unirradiated and proton-iradiated specimens of ferritic/martensitic steels and pure nickel, at intermediate (up to 500-600°C) and low (LN_2) temperatures.

2.3.4 Development of new investigation techniques

Small specimen technology

Further development of small specimen techniques was undertaken to use ultra-small specimens to investigate the irradiation effects on the fracture properties of the tempered martensitic steels. The goal is not only to investigate the irradiation effects on the degradation of the fracture properties but also to determine how the helium content affects the fracture behaviour. Since one of the main characteristics of our PIREX irradiation facility is to produce a large He appm/dpa ratio, ultra-small fracture specimens were designed to be irradiated in PIREX. The geometry of these specimens is Charpy type, whose dimensions are 1mm x 1mm x 12mm. New specimen holders were also designed and a first irradiation was performed to test the cooling capability of the helium loop. The results were quite promising, since cooling of the specimens was found to be sufficient with a beam intensity of 15μA and a beam shape given by $4\sigma_x = 4\sigma_y = 4$mm. This constitutes the best compromise between the beam size and beam intensity, which provides a dose of about 0.2dpa in 72 irradiation hours. It is planned to irradiate about 20 specimens at 250°C in 2001 to characterise the fracture toughness behavior as a function of temperature. This study is done in collaboration with the University of California Santa Barbara.

Status of the Master Curve Experiment

In the frame of the collaboration with the University of California Santa Barbara on fracture properties of tempered martensitic steels, two sets of specimens were prepared to be neutron-irradiated in Petten (Netherlands). The specimens of the irradiation matrix were cut from the modified F82H steel. The first irradiation, at 80°C and to 2dpa, was performed in 2000 while the second one, at 250°C and to 2dpa, will be done in 2001. Different specimen sizes/geometries were included in the irradiation matrix, in order to investigate the irradiation effects on the fracture toughness-temperature curve while assessing the constraint loss effect. All the fracture specimens were fatigue pre-cracked before irradiation. A neutron-irradiation is currently taking place in Budapest at 250°C and to 0.5dpa, expected to be completed in Spring 2001. Along with fracture specimens, a set of tensile specimens were also included in the irradiation matrix to characterise the post-irradiation constitutive behaviour of the F82H steel.

New transmission electron microscopy technique for ferritic/martensitic steels

It is proposed to use weak beam imaging under electron illumination that is slightly convergent. This was shown by image simulation to be a benefit for investigating of the dislocation dissociation distance measurement by weak beam imaging, as the convergence averages the contrast of the defect over depth. The approach has successfully applied experimentally in the past to the case of Ni_3Al. The use of convergence in weak beam imaging should be useful for the investigation of three-dimensional defects such as those induced by irradiation. Their nanometric sizes make them difficult to identify, to size and to count in a reliable way because of the oscillation of their contrast with depth. The use of a moderate convergence should allow to homogenise their contrast over the thickness of the thin foil.

The weak beam condition was carefully selected to be about g(4g), with g = (110), as it provides the best contrast. It is useless to use weak beam conditions that are higher than g(5g) because the contrast is overwhelmed by surface feature contrasts, such as the ones arising from the oxide particles or layer. In addition, the diffraction contrast of crystalline defects, such as dislocations, becomes too faint and narrow.

Convergent weak beam imaging was performed by selecting the appropriate diffraction condition and by condensing the illumination over the region of interest. The convergence angle is estimated from the diameter of the diffraction spots. The convergence angle is limited by the objective aperture size about 4mrad radius. This results in a homogeneously illuminated area that is about 300nm wide.

It is also important to preserve the resolution of the image as much as possible, particularly when contrast features are to be carefully investigated in order to identify the type of defects. Convergent weak beam imaging will be used for the identification of defects by matching their contrast to image simulations of candidate defects. The approach was applied to the case of the ferritic/martensitic steel F82H irradiated with protons at room temperature to a dose of 1.7dpa. Convergent weak beam imaging proved successful in improving the visibility of radiation-induced damage.

2.4 Superconductivity

In superconductivity the SeCRETS experiment in SULTAN represented the focus of the main effort. In an unprecedented way, it demonstrated the extremely high stability of the cable in conduit conductors against electromagnetic field transients of the type which will be incurred during a plasma disruption. This will even be the case in cables built with segregated copper, as proposed by the CRPP, to reduce the conductor costs for ITER. Other relevant results such as the stability dependence on coolant flow are still under investigation using rather heavy numerical simulation models. For the forthcoming Conductor Optimisation program awarded to the CRPP, the preparation of prototype short samples has already started.

The development of High Tc Current Leads has made significant progress, reaching the 20kA level. As an emergency action, a classical full copper 80kA Current Lead was developed as a fallback solution for the Toroidal Field Model Coil Test in preparation at the Forschungszentrum Karlsruhe .

2.4.1 Superconductivity studies

2.4.1.1 Thermal hydraulic analysis with the code Gandalf

The Gandalf code by CryoSoft is the numerical implementation of a 1D thermal hydraulic model for the simulation of quench initiation, quench propagation and transient stability in cable-in-conduit conductors (CICC) with multiple cooling channels. The code has been used for the predictive analysis of one ITER Model Coil and for the interpretation of the SeCRETS experiment in SULTAN.

Current sharing temperature analysis in the TFMC

The Toroidal Field Model Coil (TFMC) is being constructed, in the frame of the ITER program, by the European industry consortium AGAN under the responsibility of the European Fusion Development Agreement. The TFMC uses a new type of winding designed to withstand the large electromagnetic forces typical of the ITER full size coils. The objective of the TFMC, which will be tested in the TOSKA facility of the Forschungszentrum Karlsruhe in 2001, is to demonstrate the feasibility of Nb_3Sn superconducting coils wound in pancakes, using a dual channel CICC. The TFMC is a racetrack coil consisting of 5 double pancakes. The connection between adjacent pancakes is provided by two joints at the inner and outer sides of the coil. One double pancake is equipped with external heaters which will be used for the

current sharing temperature (T_{cs}) test. Since all the available sensors are outside the coil, T_{cs} in the conductor must be measured indirectly and this requires sophisticated analysis tools because of the complexity of the system. The main goal of this study, performed in parallel with other European laboratories, is to define the heating procedures so that the heat front will generate a normal zone initiation in the high field region of the conductor without quench propagation out of the inlet joint.

The main components of the model are the heated pancake, which includes the resistive heater, the connecting pipe, the joint and the conductor, as well as the cryogenic system, which also includes the unheated pancakes. Two values of the total mass flow rates are used: 180g/s (nominal) and 108g/s (reduced using an artificial friction in the parallel pipe). This analysis shows that one condition that must be satisfied to initiate a quench in the conductor rather than in the joint is that the flow instability between heated and unheated pancakes, referred to as helium choking, must be minimised. The T_{cs} test should be performed by heating using procedures leading to a thermal front with low gradient, such as linear ramps whereas heating pulses (square in time and space) are not possible, and by cooling with high helium mass flow rates in the heated pancake. With the same mass flow rates of 18g/s in heated and unheated pancakes, the resulting load is just within the operational limits of the refrigerator when testing one pancake (DP12) (350W for 60s), but is clearly above these limits when testing the other pancake (DP11) (450W for 250s). If throttling the mass flow in the unheated pancakes is possible, for example using external valves, the heating times and the refrigerator loads tend to decrease. With 10g/s flow the loads are still above the refrigerator limits when testing the pancake DP11. The more favourable behaviour of the pancake DP12 is due to the lower critical magnetic field at the joint inlet with respect to DP11 (the difference is 0.26T), where the effect of helium choking happens to be maximum. At this stage of the project, hardware modifications such as the installation of valves to throttle the flow in the unheated pancakes are not possible. Although they could be included after the end of the first testing phase, their use is not justified by the results of this analysis.

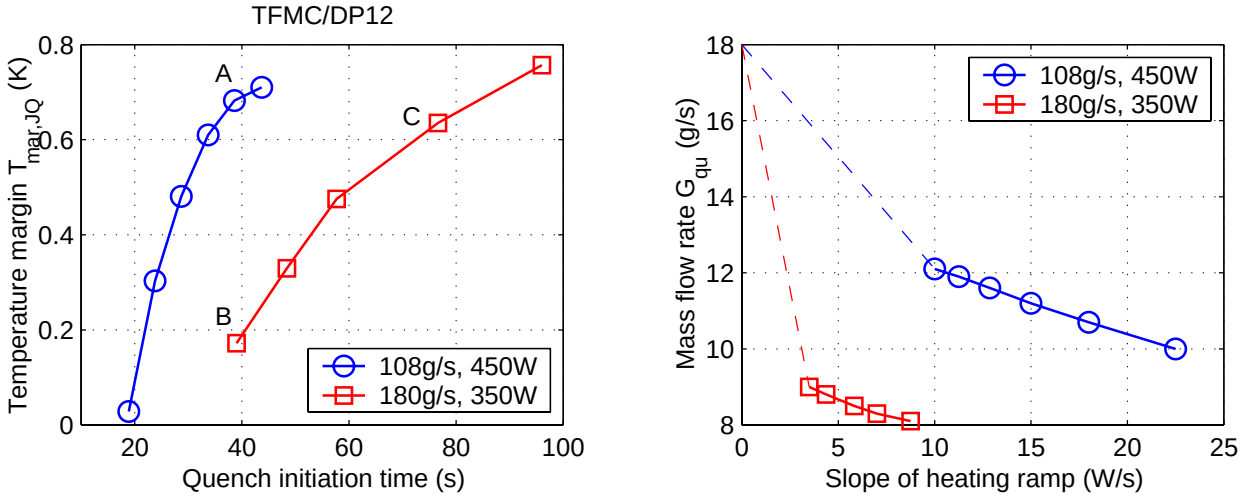

Fig. 2.4.1 Results in the pancake DP12. Left: Temperature margin in the joint at the time when a quench is initiated in the conductor. For example, a safe margin of 0.5K in the joint is achieved when heating with 350W for ~60s and cooling with 180g/s. Right: Helium mass flow rate at the joint inlet at the time when the quench is initiated in the conductor. For an infinitely slow heating ramp the effect of helium choking vanishes, i.e. steady state and quench mass flow rates are the same.

Stability analysis in SeCRETS

SeCRETS, the stability experiment on copper segregation for Nb_3Sn CICC, has been successfully completed in SULTAN (see Section 2.4.3). A detailed thermal hydraulic stability analysis has been performed in support of the interpretation of the experimental results. The study, applied to the conductors with and without segregated copper (conductor A and B, respectively), has focused on the dependence of the transient stability on the temperature margin, helium mass flow rate and operating current, inside and outside the experimental range. The simulations have also been used for the calorimetric energy calibration of the stability runs. The 1D model includes three components: the superconducting strands, the helium and the conductor jacket. The simulation of conductor B fully neglects the segregated copper, i.e. the energy is deposited in the strands, only the wetted perimeter of the strands is accounted for in the heat transfer to helium, and only the copper embedded in the strands participates in the current sharing. The simulated conductor is 2m long and its centre coincides with the centre of the heated zone where the heat is deposited homogeneously in the strand cross section. A sinusoidal modulation of the magnetic field is superimposed onto the constant background field during the heating for a 65ms duration for full wave and 32ms for half wave heating. The heat deposited in the strand along the 0.3m heated zone is modulated by a waveform proportional to $\cos^2(\omega t)$. The Summer coefficients are used in the standard ITER routines to determine the Nb_3Sn properties and the calculated values of the current sharing temperature and longitudinal strain match the experimental results. The Joule heat contribution is obtained through the critical field in the superconductor, defined by $E=E_0(I_{sc}/I_c)^n$, where E_0 is the electrical field used for the definition of the critical current I_c, I_{sc} is the current in the superconductor and n is the power law exponent. The values assumed in the simulations are $E_0=10^{-4}V/m$ and n=15. The standard heat transfer coefficient implemented in Gandalf is used.

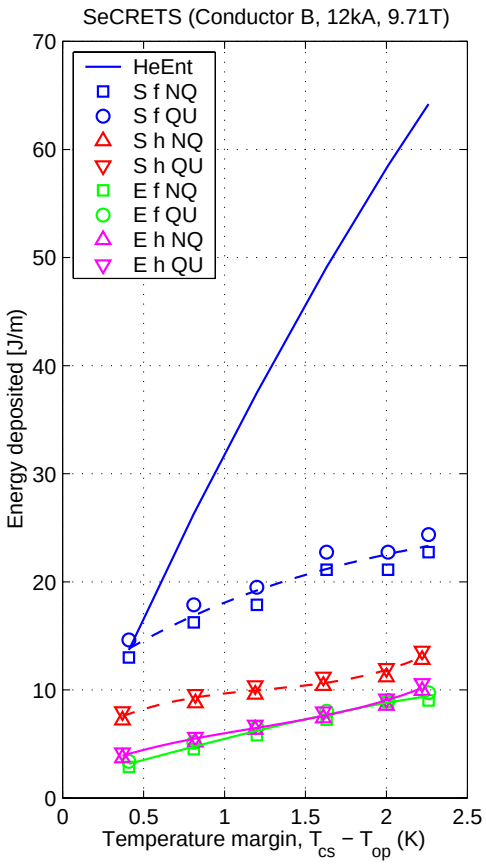

Fig. 2.4.2 Comparison of the Gandalf simulation (S, dotted lines) and the experimental results (E, solid lines) for transient stability as a function of temperature margin, for conductor B with segregated copper. The threshold between quench (QU) and no quench (NQ) is shown. Results are for full wave (f) and for half wave (h) heating. The helium enthalpy (HeEnt) is also shown as an upper limiting case.

A comparison of the transient stability, i.e. energy margin per conductor length is shown in Fig. 2.4.2 as a function of the temperature margin for conductor B at the operating current of 12kA. In both conductors the simulation results indicate higher stability for full wave pulses. This result, which does not fully support the experimental evidence (i.e. the stability seems to be identical for full and half waves), is strongly influenced by the assumption of power modulation and by the selection of the heat transfer coefficient model. In both conductors the stability is below the helium enthalpy, which is the upper limiting value in case of ideal heat exchange between strands and helium. The energy modulation has a negative impact on stability since it reduces the energy margin by ~30% compared to the case of non modulated power during the transient.

Simulations of the transient stability as a function of operating current I_{op} at constant operating temperature were performed in the range of I_{op}/I_c from 0.4 to ~1, i.e. broader than the experimental one. For conductor B, the start of the expected limiting current inflection occurs at I_{op}/I_c=0.95, whereas no inflection occurs in conductor A. The latter result is in agreement with the unexpected experimental result and is probably due to a conservative assumption of the heat transfer coefficient. The stability as a function of the helium mass flow rate is investigated at a constant temperature margin (1K) using a full wave heating. The simulated results are plotted in Fig. 2.4.3 together with the experimental results and the helium enthalpy margin. The helium enthalpy is higher for conductor B because of the higher operating temperature (5.95K instead of 5.53K for conductor A) necessary to obtain the same temperature margin. The improvement of the transient stability with higher mass flow rate is due to the enhanced steady state heat transfer coefficient. No evidence of induced flow could be observed either in the experimental or in the simulated results.

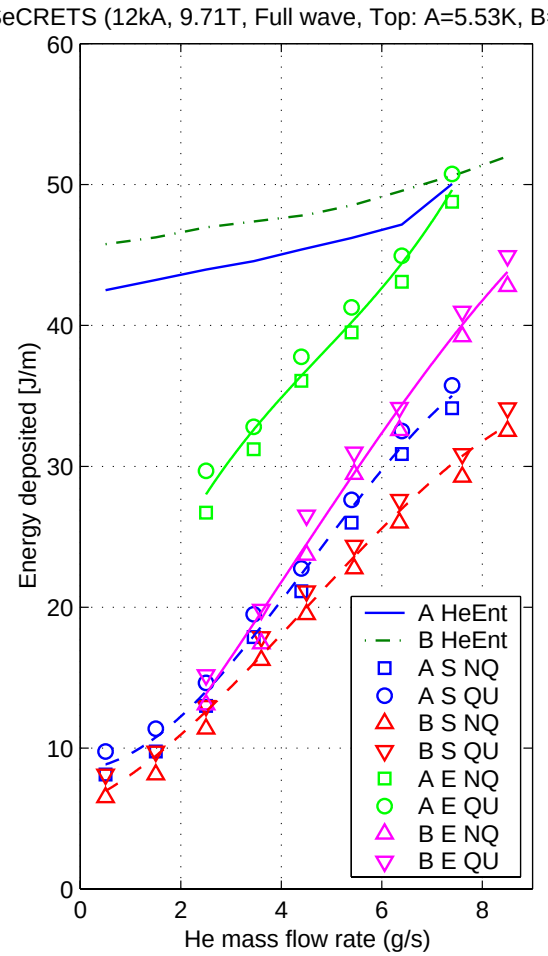

Fig. 2.4.3 Comparison of the Gandalf simulation (S, dotted lines) and the experimental results (E, solid lines) for transient stability as a function of helium mass flow rate. The threshold between quench (QU) and no quench (NQ) is shown. Conductor A is without segregated copper and conductor B with segregated copper. The helium enthalpy (HeEnt) is also shown as an upper limiting case.

2.4.1.2 Self-Field Effects in Large Superconducting Cables for ITER

The full-size Cable In Conduit Conductors (CICC) for ITER are currently investigated at the SULTAN facility in Villigen.

The CICC are made of a great number (N_s~10^3) of superconducting strands (NbTi, Nb_3Sn or Nb_3Al) packed in a steel conduit, which also encloses the supercritical helium used as the coolant. In order to reduce the AC losses and to improve the mechanical stability, the strands are twisted in multiple stages according to a predefined scheme. A typical example is a cable with the scheme 3x4x4x4x6. At the lowest stage the basic unit is the triplet, consisting of three strands twisted with a twist-pitch of p_1=45mm. The second stage consists of a quadruple of triplets, twisted with a larger twist-pitch of p_2=85mm. The third stage is a quadruple of quadruples with a twist-pitch of p_3=125mm. This process continues up to the last stage (the 5^{th} in this case) where a cable is finally formed consisting of six groups of 3x4x4x4 strands each. The last stage has the largest twist-pitch of typically p_5=400mm. The internal structure of a typical CICC is illustrated in Fig. 2.4.4 where both a transverse and longitudinal section are shown.

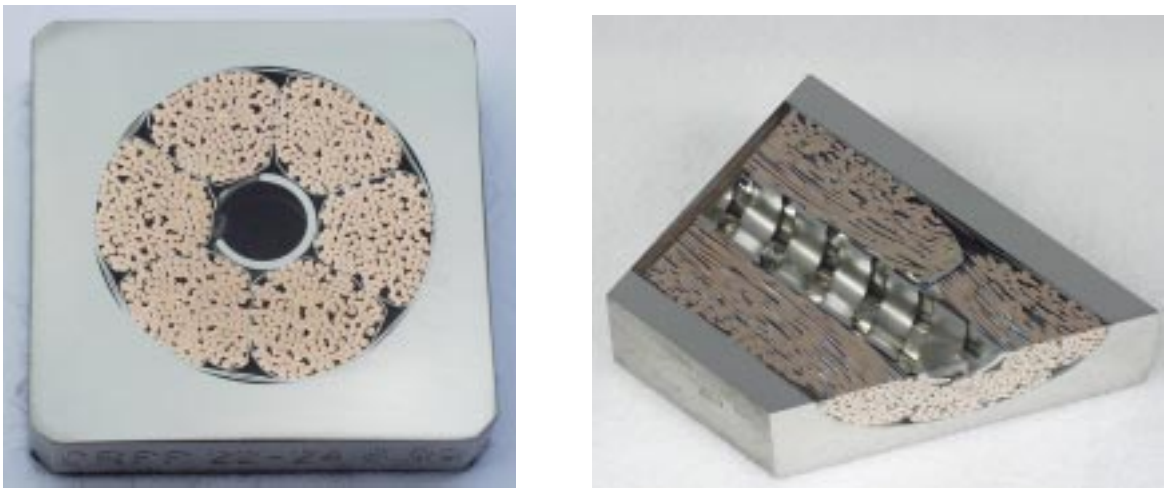

Fig. 2.4.4 Transverse and longitudinal cross-section through a typical CICC

This illustration shows another important characteristic of a CICC i.e. the possibility to have a hole in the central section. This hole, also called the central channel, is essential for large magnets in which the total length of the cable is as large as several hundred meters. Without the central channel either the helium pressure drop is too large for the specified mass-flow or the mass-flow in the cable is too small.

A large number of measurements performed at SULTAN on model cables have revealed an important and yet unexplained effect. The current-voltage characteristic of the cable is not a simple extrapolation of the current-voltage characteristic of the single strand. Put in a more simple way, if the single strand has a critical current of i_c then one expects, in a cable consisting of N_s strands, a critical current I_c= $N_s i_c$. This is not the case and to establish the reason for this is a key issue in the development of the next generation of CICC.

At a fundamental level there could be two reasons for this effect. First, it was observed that the strands in a real cable do not carry the same current. This non-uniform current distribution is caused by the contact resistance distribution in the joints and by the mutual inductance between the strands. The contact resistances

between the strands also play an important role. ITER coils must withstand AC fields such as those induced by plasma disruption or control actions and the conductors are designed to minimise this effect. This is usually achieved by increasing the contact resistance between the strands using Cr-plated strands and/or wrapping the last stage of the cable with thin, low conducting metal foil. The result is that AC optimised cables have a higher degree of current inhomogeneity.

The second reason is the self-field of the cable itself. At large currents this is not a negligible effect. A typical magnetic field distribution in the cross-section of a CICC is shown in Fig. 2.4.5 and corresponds to a situation with a background field of 5.5T and 100kA in the conductor.

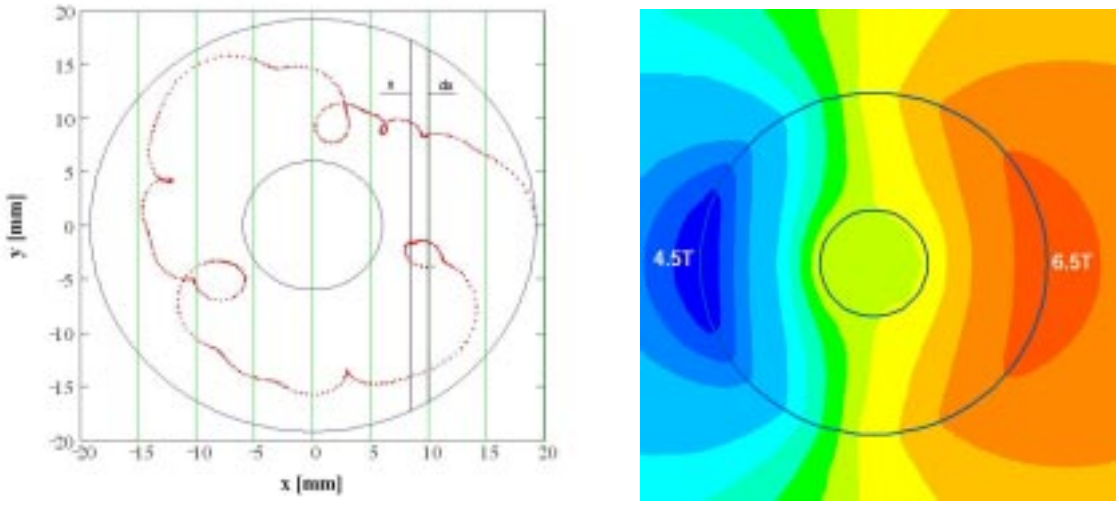

Fig. 2.4.5 A typical strand trajectory over one twist-pitch length and the field distribution over the cross section of a CICC

Figure 2.4.5 also shows the projection of the trajectory of one of the strands on the cross-section of the cable. It is obvious that due to the inhomogeneous field distribution the strand is exposed to different magnetic fields. It is therefore not clear which magnetic field should be considered when the critical current is calculated.

Another difficulty arises when the trajectory points are not uniformly distributed in the cable cross-section. As can be seen in Fig. 2.4.5 there are portions of the trajectory with a higher density, indicating that the strand is immersed in almost the same field over a certain distance and other portions where the density of points is lower indicating a rapid “movement” of the strand which therefore experiences a larger field variation.

We have proposed and developed a theoretical model to describe these effects based on concepts borrowed from stochastic theory. As a first step in the development of the method we considered two simpler cases: a) no current transfer between the strands and b) perfect current transfer between the strands. The basic ingredient of our model is the probability distribution function (PDF) of the representative point of the strand trajectory in the cable cross-section. As shown in Fig. 2.4.5, dividing the cross-section in a large number of stripes of width dx and counting the number of points inside this area one can calculate the PDF by dividing this number by the total number of points. Some results are presented in Fig. 2.4.6 where the strand trajectories for $L=p_5$ and $L=10p_5$ are shown together with the corresponding PDF. For comparison, the PDF for a uniformly distributed strand trajectory is shown. L is

the length of the cable under investigation and p_5 is the length of the twist-pitch for the last stage.

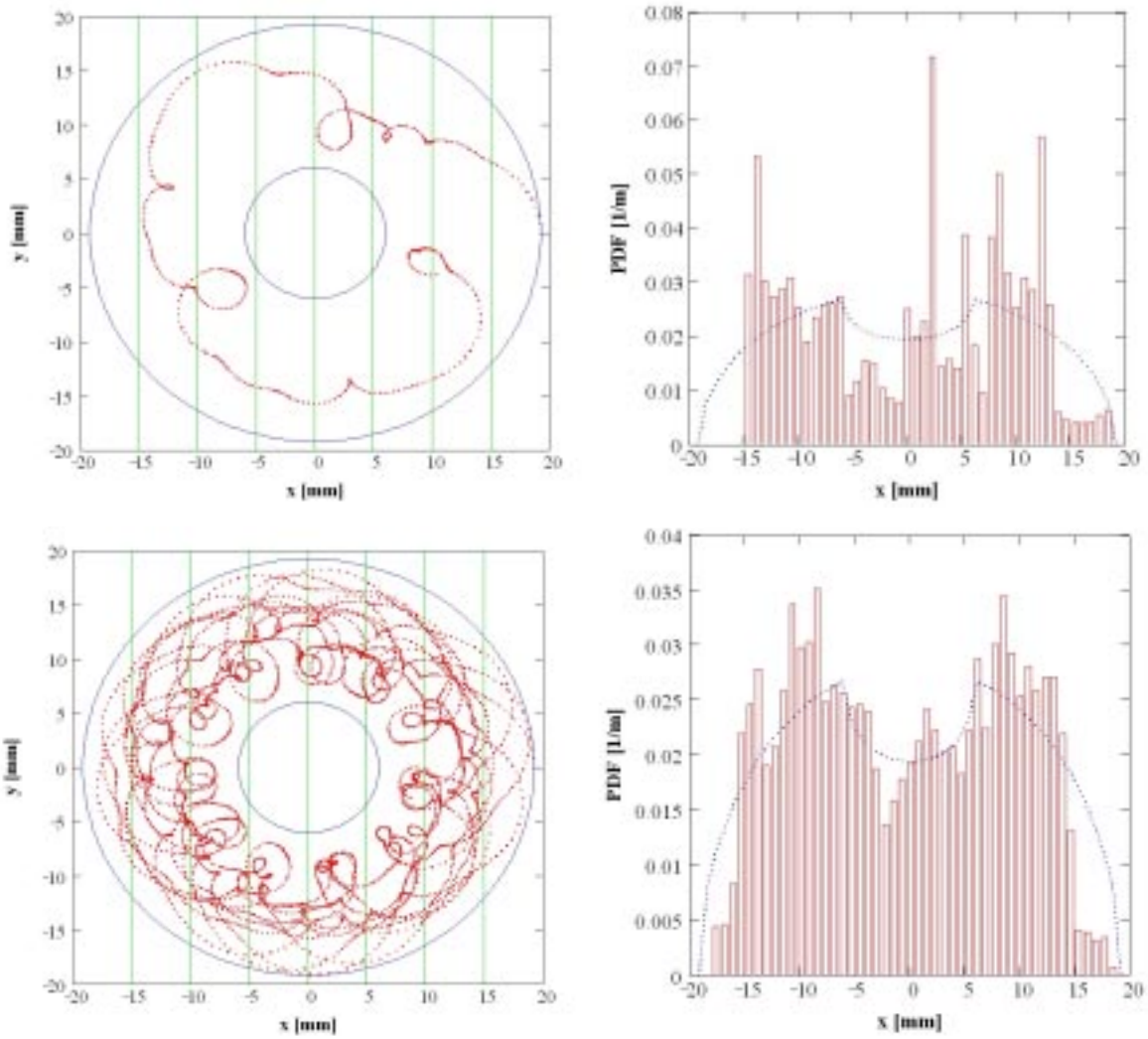

Fig. 2.4.6 The strand trajectories and the PDF calculated for $L=p_5$ (top) and $L=10p_5$ (bottom). The dashed blue line shows the PDF for a uniformly distributed strand.

With increasing L, the real PDF approaches the ideal distribution. This is an important first result indicating that cabling schemes currently used in the ITER conductors quickly approach the ideal distribution. Therefore for calculating the properties of conductors in large coils a uniform PDF can be used. For short lengths we proposed an alternative calculation model based on the Central Limit Theorem (CLT). Each strand in the conductor has its own PDF. The electrical field of each strand is therefore a random variable when it is exposed to the non-uniform magnetic field in the cable cross-section. The total electric field of the cable is the sum of the electric fields of the single strands and then by the CLT its PDF will converge to a normal or Gaussian distribution for large N_s. The Gaussian distribution is centred exactly on the average of the electric field of a single strand calculated with the single strand PDF. This implies that it is not necessary to calculate all the strands trajectories and then integrate the electric field along the strand trajectory for all strands in order to get the electric field in the cable. We demonstrated that it is sufficient to do calculations only once for a generic strand, evaluate the generic PDF and then all cable properties can be obtained. This is an enormous simplification compared with earlier methods.

The PDF of a generic strand is the most important quantity in our model. It allows the calculation of all the cable parameters of interest. For example the critical current of the cable can be calculated using the statistical average of the current-voltage characteristic of one strand and then applying the voltage criterion of 10μV/m. Other quantities of interest are the magnetic field distribution seen by the strands in the cable, the average magnetic field and the distribution of length of strand exposed to a given magnetic field. Using this method different cabling schemes can be analysed and the optimum configuration of twist pitches for a given cable structure can be found.

In order to check the stochastic method, the experimental results obtained during the test of the SS-FSJS conductor were compared with the calculations done with this method and with the calculation based on the peak-field method. The result is shown in Fig. 2.4.7 where the measured average critical current of a stand in the cable is compared with the calculations.

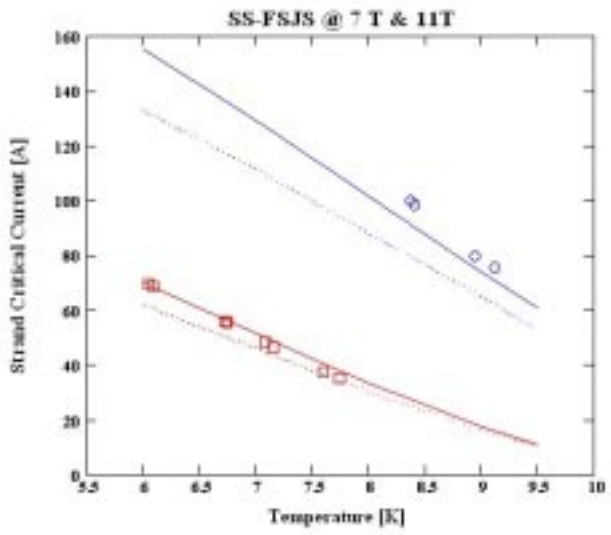

Fig. 2.4.7 Temperature dependence of the strand critical current in the SS-FSJS at 7T (blue) and 11T (red). The symbols represent the measurements, the continuous lines represent the stochastic method and the dotted lines represent the peak-field method.

The main result is that the stochastic method gives better results than the peak-field method. However, at higher fields (11T) the discrepancy between the two calculations is small and this result confirms the earlier observation that the peak-field method is a good approximation at high magnetic fields.

To conclude, a simple method of evaluating the parameters and in particular the critical current of a large CICC under the influence of the self-field effect was developed. The influence of current transfer is considered in the limiting cases of perfect and no current transfer. The method avoids using complicated and time consuming numerical codes to evaluate the strand trajectory of all the strands in the cable (~10^3). It is well suited for cable design or parametric studies. It can be extended to include the temperature effect and the inhomogeneous current distribution. The Lorenz force effect can be accounted by applying a deformation on the strand trajectory proportional to the field and the strand current and calculating the effect on the probability distribution function. We have shows that, for large lengths, cables with standard ITER patterns are ergodic and the average over the strand trajectory can be replaced by a statistical (ensemble) average. For short cable lengths (where the ergodicity does not hold), we show that one can use

the generic strand trajectory and extrapolate the results to the full cable using the Central Limit Theorem.

2.4.1.3 High-T_c Superconductors: A New Class of Materials for Fusion Magnets

Based on the outline design of the International Thermonuclear Experimental Reactor ITER-FEAT and the physical properties of the high-T_c superconductors, the impact of their use on the design of future thermonuclear reactors has been studied. For ITER-FEAT, the next step towards a fusion reactor, high-T_c superconductors have not yet reached the required degree of maturity. However in the longer term, the superior physical properties of high-T_c superconductors may provide significant cost savings and an improved performance of future fusion reactors.

In $Bi_2Sr_2CaCu_2O_8$ (Bi-2212) and $(Bi,Pb)_2Sr_2Ca_2Cu_3O_{10}$ (Bi-2223) tapes with a pronounced grain alignment the severe limitation of the transport critical current due to large-angle grain boundaries can be avoided. In Fig. 2.4.8 the critical current densities of Bi-2212, Bi-2223 and selected low-T_c superconductors are compared. Because of their extraordinarily high upper critical fields of ≈100T, high-T_c superconductors can be operated at higher magnetic fields than Nb_3Sn. The fusion power of self similar tokamaks is proportional to the plasma volume and the fourth power of the toroidal magnetic field. To reach a larger fusion power than in ITER-FEAT the size of the magnet system or the toroidal field has to be enhanced. In both cases the mechanical loads would increase, however, a high field option is expected to cause lower investment costs.

Bi-based superconductors with a AgMg matrix provide a stress tolerance comparable to that of Nb_3Sn. Because of the absence of reversible strain effects, the J_c of Bi-based superconductors is, in contrast to Nb_3Sn, not significantly affected as long as the irreversible strain limit is not exceeded.

Using Bi-2223 high-T_c superconductors an operating temperature of 20K would be feasible for the magnets of a fusion reactor similar to ITER-FEAT (see Fig. 2.4.8 right). The effect of an enhanced operating temperature on the refrigeration operation and investment costs is illustrated in Fig. 2.4.9. Assuming an unchanged heat load the higher refrigerator efficiency related to an operating temperature of 20K would provide savings in the refrigeration operation and investment costs by a factor of ≈5 and ≈3, respectively.

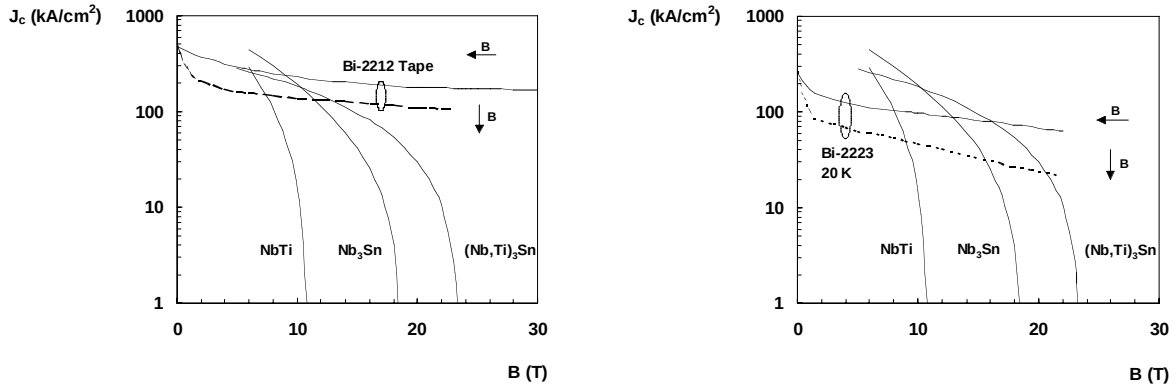

Fig. 2.4.8 Comparison of the critical current densities of Bi-2212 at 4.2K (top) and of Bi-2223 at 20K (bottom) with the J_c values of selected low-T_c superconductors at 4.2K. The J_c values of the two Bi-based superconductors depend on the field direction with respect to the crystallographic ab planes, which are parallel to the broad face of the tapes.

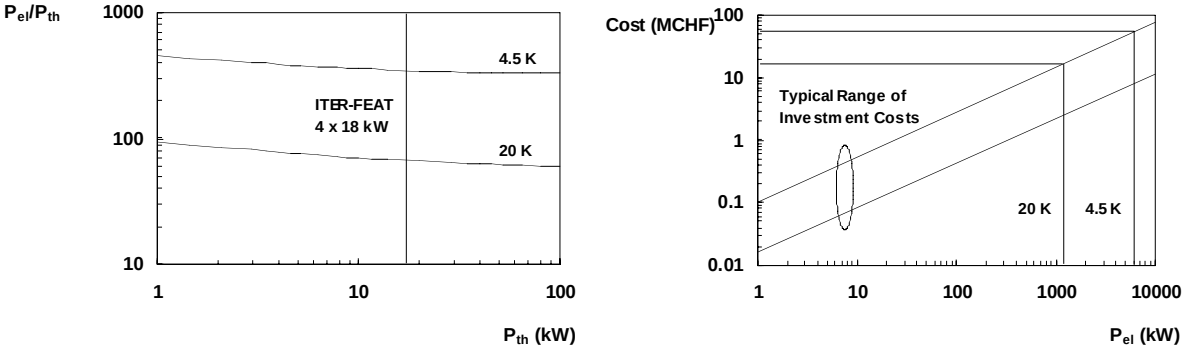

Fig. 2.4.9 Ratios of the electrical input power P_{el} and the removed heat P_{th} versus the thermal load for operating temperatures of 4.5 and 20K (top). The relation between the installed electrical input power and the refrigeration investment costs is shown at the bottom. The lines are based on 18kW modules intended to be used for ITER-FEAT.

For safety reasons, the operating current has to be well below the critical current, so that the onset of the transition to the normal state and the operating temperature are separated by a sufficiently large margin. Figure 2.4.10 shows that for appropriately selected operating conditions the temperature margins of Bi-2212 and Bi-2223 superconductors are considerably larger than those of Nb_3Sn. In the case of high-T_c superconductors, less strict requirements would apply to the coolant inlet temperatures of the individual coils. This advantage may be used to reduce the complexity of the cryogenic system. Furthermore, enhanced margins would allow us to tolerate a larger nuclear heating and higher AC losses at the expense of reduced savings in the refrigeration costs. Because of metal specific heats enhanced by a factor of ≈100 and larger temperature margins, a superior stability would be obtained for high-T_c superconductors operated at 20K. In addition, the larger margins would provide more flexibility in the design of blankets and divertors.

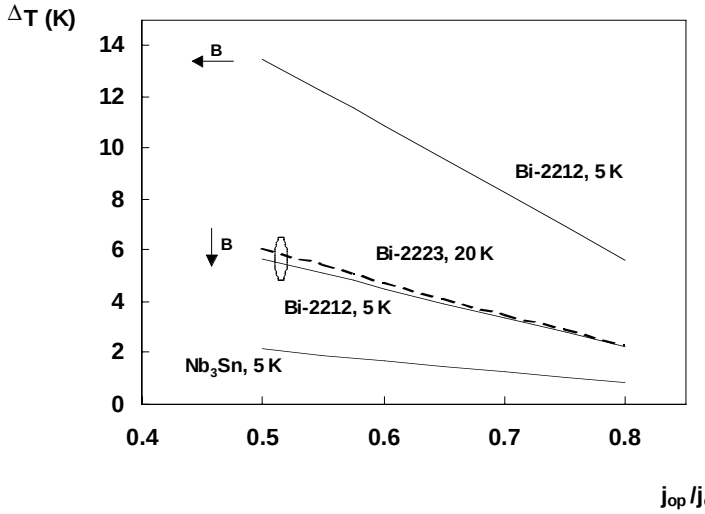

Fig. 2.4.10 Temperature margins of Bi-2212, Bi-2223 and Nb_3Sn versus the ratio of operating and critical current density for a magnetic field of 12T. The temperature margin of Bi-2223 is even for an operating temperature of 20K and the unfavourable field direction (B⊥tape) larger than that of Nb_3Sn at 5K and an intrinsic axial compressive strain of 0.5%.

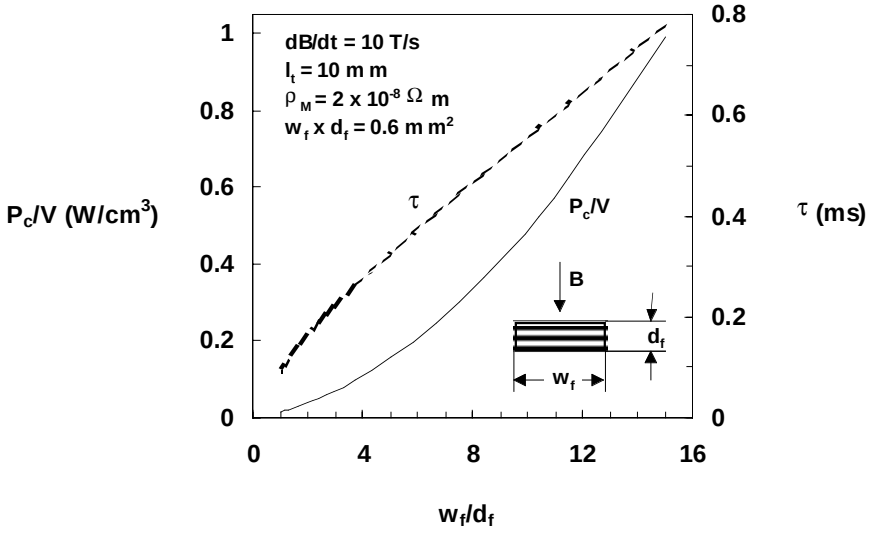

Fig. 2.4.11 Effect of the aspect ratio w_f / d_f of the filament region on the time constant τ for the decay of the coupling currents and the related losses P_c /V per unit volume. The data are based on a twist pitch l_t of 10mm and a transverse matrix resistivity ρ_M of $2\times10^{-8}\Omega$m.

Demagnetisation factors close to 1 are responsible for enhanced coupling losses in tape conductors. Figure 2.4.11 indicates that round wires are more favourable with respect to a reduction of the coupling losses related to induced currents flowing between the filaments across the matrix.

Finally, the effects of high energy neutron irradiation have been considered. The upper critical field and the critical current density of Nb_3Sn are considerably degraded by a neutron fluence of 5×10^{20}neutrons/cm^2. Irradiation of high-T_c superconductors has been found to lead to improved flux pinning but reduced critical temperature. It seems to be unlikely that Bi-based superconductors operated at 20K are more sensitive to irradiation effects than Nb_3Sn.

The results of the present study indicate that an operating temperature of 20K provided by the use of high-T_c superconductors would lead to considerable refrigeration cost savings. In addition, the enhanced temperature margins could be used to enhance the flexibility in the design of blankets and divertors. Higher magnetic fields may allow the enhancement of the power of future fusion reactors.

2.4.2 Pressure drop test for the ITER conductor

For magnets wound as forced flow conductors, it is convenient to make the distance between coolant inlet and outlet ("hydraulic length") as short as possible to reduce the pressure drop and increase the coolant speed. In layer wound coils, the hydraulic inlet/outlet can only be placed at the end of the layers and the electrical connections (joints) are also used as hydraulic inlet/outlet. In the pancake wound coils, the electrical connections between conductor sections may be conveniently placed at the outer radius, where the magnetic field is weaker. The hydraulic inlet is at the pancake transition at the inner radius. The coolant stream splits into the two pancakes and the electrical connections are used as hydraulic outlets. This arrangement, planned for the ITER fusion magnets, offers the advantage of a short hydraulic length (half of the conductor sections) and provides the lowest operating temperature at the highest field. A number of pressure drop measurements have been carried on a 6m long section of ITER conductor, left from the winding of the

second layer of the inner module of the CS Model Coil. Pressurised water at 28C, 10bar is used as the hydraulic medium.

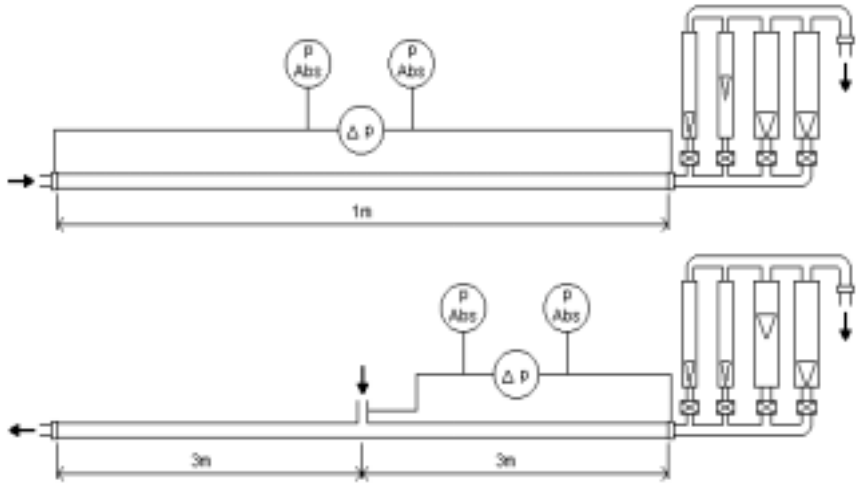

Fig. 2.4.12 Experimental set-up for longitudinal (top) and radial (bottom) pressure drop measurements on an ITER conductor

The longitudinal friction factor is deduced separately for the central hole and the strand bundle area, by blocking the central hole by a rubber pipe and restricting the flow to the bundle area. The test results are discussed in terms of pressure drop per unit length, $\Delta p / l$, and friction factor, λ, according to the basic relation

$$\lambda = \frac{\Delta p}{l} \frac{2 d \rho A^2}{(dm/dt)^2}$$

where d is the hydraulic diameter, A is the coolant cross section, ρ is the coolant density and dm/dt is the mass flow rate. The Reynolds number in the bundle area, $\mathrm{Re}_B = (dm/dt)_B d_B / A_{HeB} \eta$, can be assessed using the average hydraulic diameter in the bundle, d_B, and the Helium area, A_{HeB},. The friction factor, λ_B, in the bundle area, defined according to this equation with index $_B$, and derived from the pressure drop results, $\Delta p_B / l$, is plotted in Fig. 2.4.13 vs. the Reynolds number. The present results for CS1 conductor are well matched by the general correlation proposed by Katheder (see formula in the plot), and retained in the ITER design criteria, with only 5% deviation at the CSMC operating point.

Comparing the pressure drop results with open and blocked central channel, the flow partition α is deduced and hence the friction factor in the central hole, λ_H is otained:

$$\lambda_H = \frac{\Delta p_{ov}}{l} \frac{2 d_{spi} \rho A_{HeH}^2}{((1-\alpha) dm/dt_{ov})^2}$$

The fitted curve of λ_H vs. the Reynolds number in the central hole, $\mathrm{Re}_H = (1-\alpha) dm / dt_{ov} a_{spi} / A_{HeH} \eta$. is $\lambda_H = 0.866\ \mathrm{Re}^{-0.25}$ and differs by a numerical factor from the Blasius correlation for turbulent flow in smooth pipes, $\lambda = 0.3164\ \mathrm{Re}^{-0.25}$. The correction factor N = 0.866/0.3164 = 2.7 is due to the roughness of the spiral, which increases the turbulence compared with a smooth pipe.

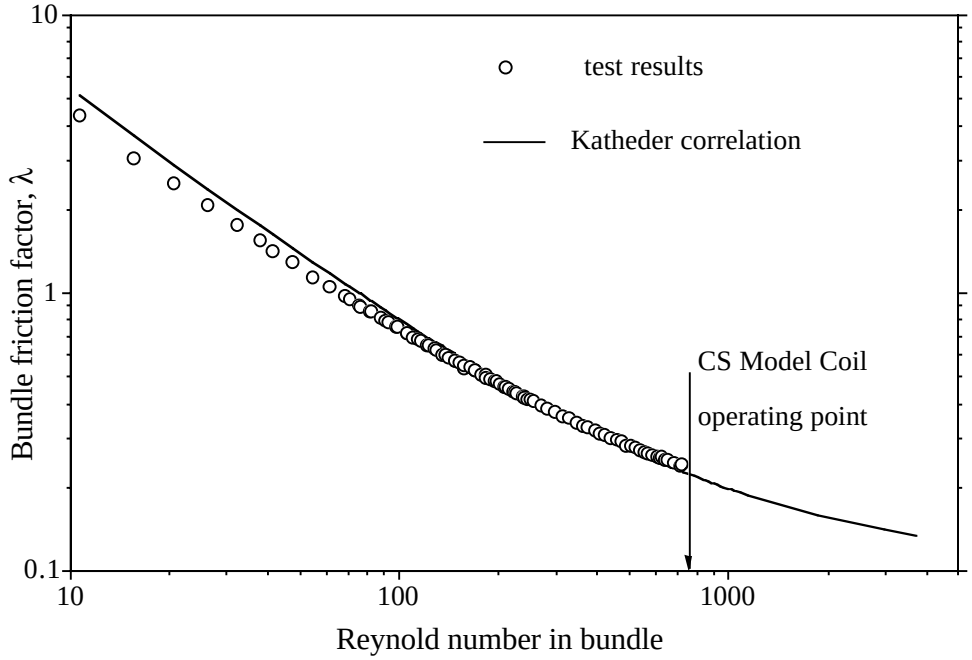

Fig. 2.4.13 Longitudinal friction factor in the strand bundle vs. Reynolds number. The test results are drawn from $\lambda = \frac{\Delta p}{l} \frac{2 d \rho A_{He}^2}{(dm/dt)^2}$. The Katheder correlation is $\lambda = \frac{1}{\upsilon^{0.72}} \left(\frac{19.5}{\mathrm{Re}^{0.88}} + 0.051 \right)$

Two layouts of radial Helium inlets have been investigated and the measured radial pressure drop is assessed in terms of the equivalent conductor length producing the same pressure drop in the axial direction. In one layout, a plain hole, ø=16mm, has been drilled on one side of the jacket. In a second, more sophisticated design, a 200mm long section of jacket is fully removed by a milling machine and replaced by two half shells with machined longitudinal and radial channels to improve the fluid penetration through the strand bundle and avoid stagnant Helium regions.

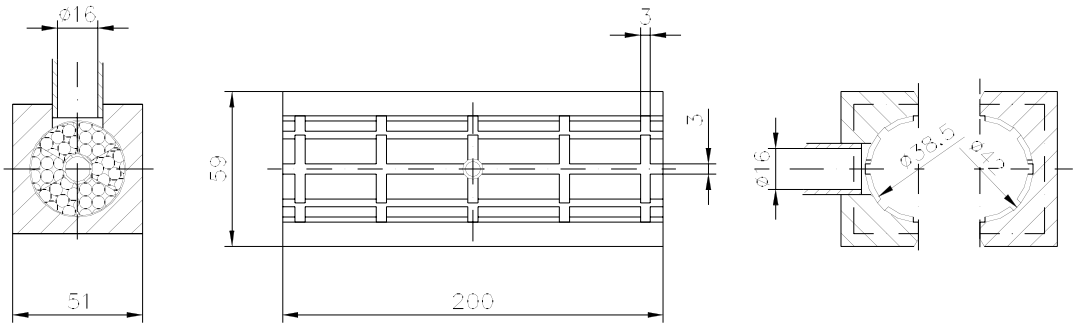

Fig. 2.4.14 Two layouts of radial Helium inlet: a plain hole in the jacket (left) and grooved shells replacing the jacket (right)

The pressure drop results are gathered in Fig. 2.4.15 vs. the mass flow rate. The solid and dotted lines correspond to the longitudinal pressure drop, multiplied by 50 and 10 respectively. The pressure drop with the plain hole in the jacket is equivalent to about 50m axial pressure drop in the conductor. With the machined steel shells, the pressure drop at the inlet decreases by a factor of five, corresponding to about 10m axial pressure drop.

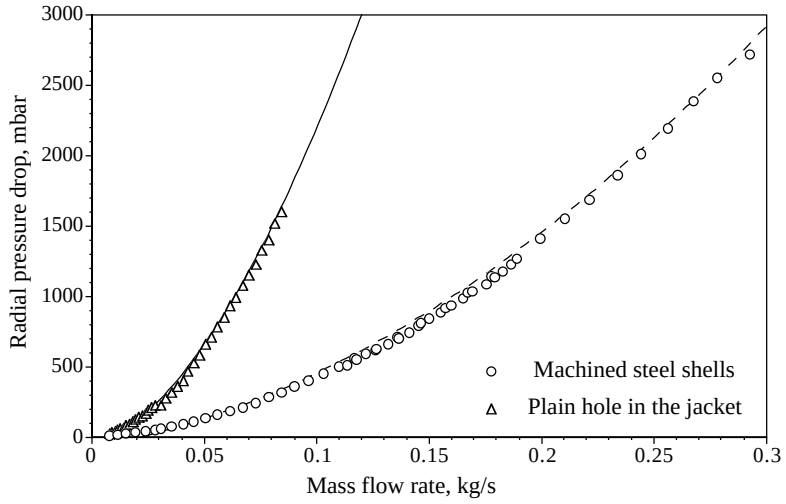

Fig. 2.4.15 Pressure drop results for the radial Helium inlet

In conclusion, the axial friction factor in the strand bundle can be satisfactorily fitted by the general correlation proposed by Katheder and no new correlation is required. A correction factor 2.7 to the Blasius correlation is needed to account for the spiral roughness for the axial friction factor in the central hole. The pressure drop at the radial inlet can be reduced by a factor of 5 using machined steel shells instead of a plain hole in the jacket.

2.4.3 Results of the SeCRETS experiment

Two Nb_3Sn, steel jacketed, cable-in-conduit conductors have been manufactured with identical non-Cu cross sections and the stabiliser either included in the Nb_3Sn composite (conductor A) or partly segregated as copper wires (conductor B). The two conductor sections, each 13m long and 14.5mm diameter, are series connected and wound as a bifilar, single layer solenoid, assembled in the high field bore (11T) of the SULTAN test facility. The operating current is up to 12kA ($400A/mm^2$ non-Cu cross section). A transverse pulsed field is superimposed to the DC field, with ΔB up to 2.7T, field rate of change up to 180T/s and $\int (dB/dt)^2 dt$ up to $530T^2/s$. The investigation of the transient stability under ITER relevant operating conditions and the assessment of the effectiveness of segregated copper as stabiliser are the main objectives of SeCRETS (Segregated Copper Ratio Experiment on Transient Stability).

In the DC test, a good agreement is found between the I_c and the T_{cs} results, both correctly scaling according to the parameters derived from the strand tests. The hoop load on the conductors causes either a compressive or tensile strain in the Nb_3Sn strand, which affects the critical current density. The DC test is carried out in both load directions, see Fig. 2.4.16, and the respective I_c and T_{cs} results are collected as reference points to establish the temperature margin in the stability test. The superconducting transition is smooth, Fig. 2.4.17, and spans a temperature range of about half a degree, with n-value (from fitting to a $V=I^n$ curve) in the range of 15.

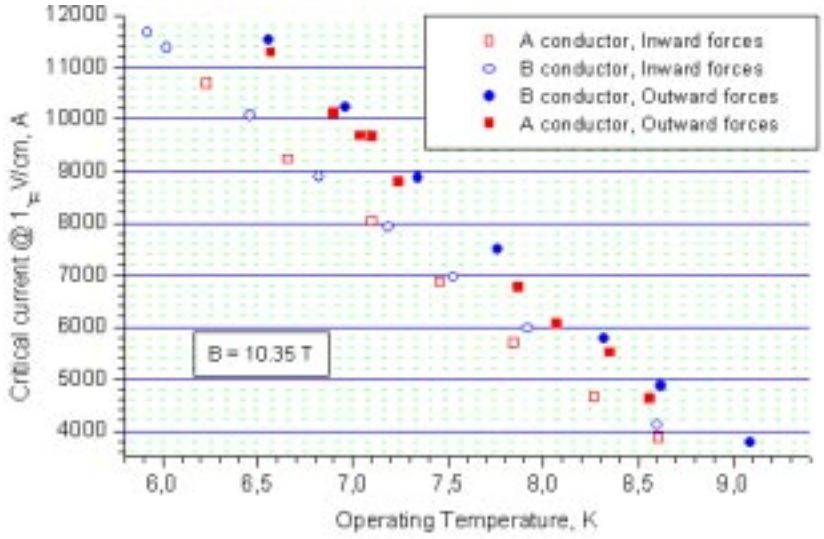

Fig. 2.4.16 Critical current results of the two SeCRETS conductors under both compressive (inward forces) and tensile (outward forces) hoop load

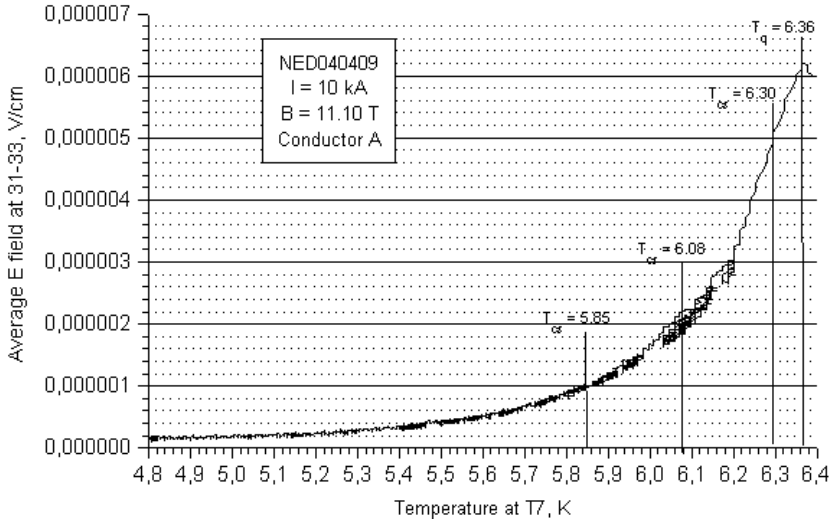

Fig. 2.4.17 Example of a current sharing temperature measurement at high background field. The assessment of T_{cs} is done at different electric fields. The runaway temperature is T_q.

The AC losses results in the range of 2 to 9Hz obtained from gas flow calorimetry indicate that the coupling current constant, $n\tau$, is in the range of 1.5ms at high field, increasing by a factor of 2 with 12kA transport current. A number of loss curves are gathered in Fig. 2.4.18 for both conductors. The conductor with segregated copper has marginally smaller loss. No significant interstrand coupling loss is observed.

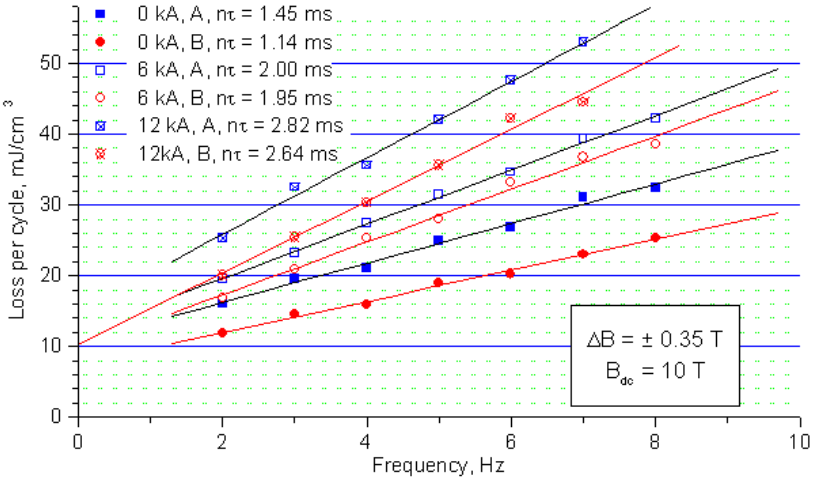

Fig. 2.4.18 AC losses and coupling constant evaluation for both conductors with I_{op} up to 12kA

A comparison of the loss extrapolation to zero frequency with the expected hysteresis loss suggests that the loss curve may be not linear outside the test range, with higher nτ at lower field rate. The calorimetric loss estimation with a fast field transient (f=15Hz) and with I_{op}=12kA indicates nτ≈2ms, i.e. about 30% less than in Fig. 2.4.18

The ITER plasma disruption transients have been reproduced by the pulsed coils. Both conductors, with I_{op}=12kA, are submitted to the plasma disruption transients, reducing the temperature margin. Due to the very low AC losses, no quench could be induced in either conductor even with the temperature margin below 0.2-0.3K.

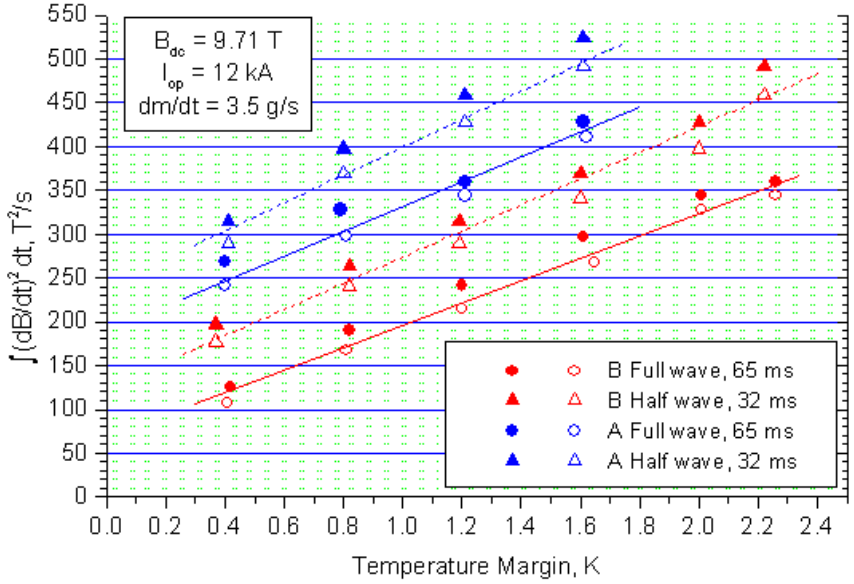

Fig. 2.4.19 Transient stability performance vs. temperature margin for both conductors and two duration of transient

Very large transverse field transients, with $\int (dB/dt)^2 dt > 100 \mathrm{T}^2/\mathrm{s}$, are required to quench the conductors. By way of comparison, an ITER plasma disruption typically

generates $\int (dB/dt)^2 dt < 8 T^2/s$. In that range, the conductor without segregated copper has a superior performance, Fig. 2.4.19. This impressive result is due partly to the low level of coupling loss and partly to the fact that the local temperature is allowed to grow above T_{cs} over a short section without starting a runaway. The most conservative way to extrapolate these results is to consider a coil with very long conductor length in the highest field and a disturbance extended over the whole high field section. In this case the runaway temperature can be approximated to T_{cs}, the available enthalpy is only up to T_{cs} and the stability curve must cross zero. After shifting the experimental stability curves, e.g. $\int (dB/dt)^2 dt$ vs. ΔT in Fig. 2.4.19, to cross zero, the ability to withstand the field transient is still in the range of $15 T^2/s$ for a 0.1K temperature margin. Decreasing the duration of the field transient, by using a half period sinus with 32ms duration, the stability performance improves slightly. No evidence of current re-distribution is observed during the field transients.

The transient stability, measured as a function of the operating current at dm/dt=3.5 g/s, did not show the inflection expected at the limiting current, $I_{\lim} = \sqrt{\frac{A_{cu} p_w h (T_c - T_{op})}{\rho_{cu}}}$, calculated with constant heat transfer coefficient $h=1000 W/m^2K$, see Fig. 2.4.20. The reason is that at the selected operating conditions, the limiting current was higher than the critical current, as the heat transfer coefficient was actually much higher than $1000 W/m^2K$. This apparently trivial finding has important implications for the ITER design, where the conductor layout (the amount of copper to be included in the superconducting strand) is driven by the criterion of $I_{lim} > I_{op}$. We must ask why we should maintain the limiting current criterion with constant $h=1000 W/m^2K$ in the ITER conductor design. On one side the limiting current only plays a role for severe transient disturbances, which do not occur in fusion conductors. On the other hand, the limiting current value is proportional to $\sqrt{h}$, which varies significantly over the range of operating conditions.

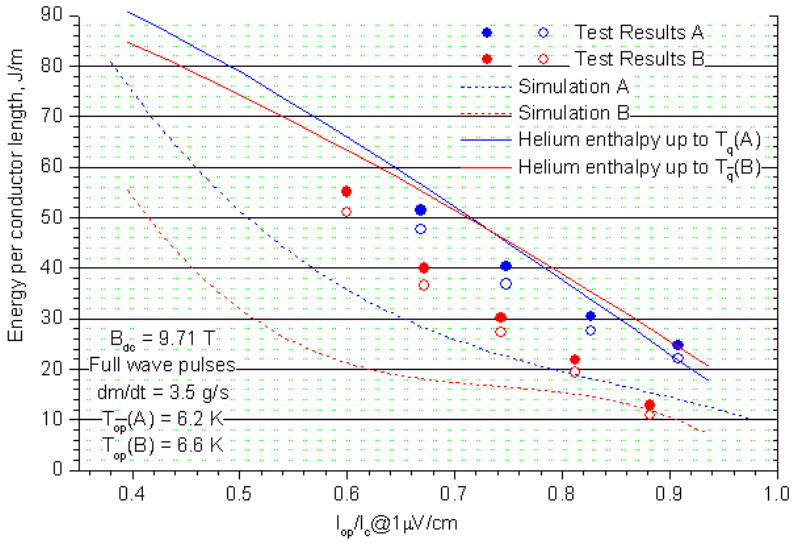

Fig. 2.4.20 Transient stability vs. the fraction of operating to critical current for both conductors. The simulation with the Gandalf code is the dotted line. The energy margin calculated as the Helium enthalpy from the operating temperature to T_{cs} is the solid line.

The stability, the ability to withstand a large transverse field integral with a 65ms time scale, increases linearly with the mass flow rate for both conductors, in the range of coolant speed, 0.3-1.3m/s, investigated. The assumption that the turbulence induced by the heat removal (induced flow) dominates the heat transfer coefficient has not been verified either by the experimental results or the simulations, see Fig. 2.4.21. Whenever the transient stability is an issue (probably not for fusion conductors), the heat transfer coefficient, h, should not be fixed to an arbitrary value.

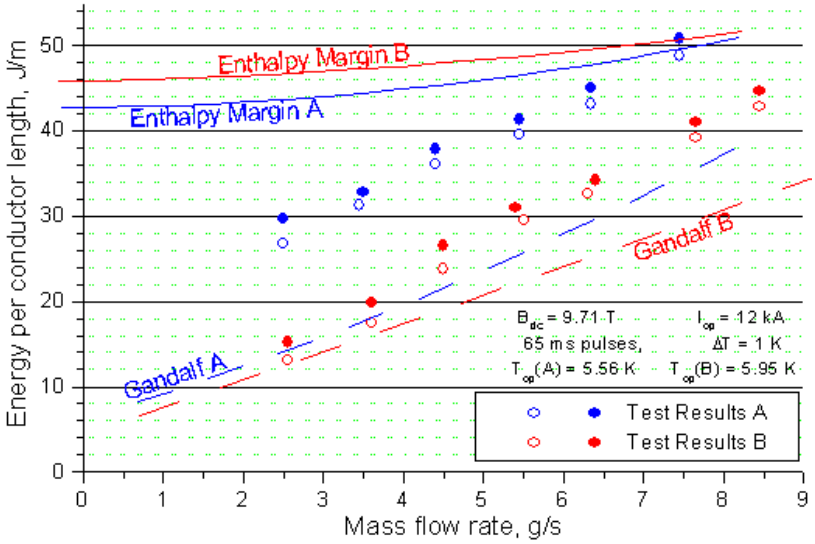

Fig. 2.4.21 Transient stability vs. coolant mass flow rate for both conductors, at constant operating current and temperature. The simulation with the Gandalf code is the dashed line. The energy margin calculated as the Helium enthalpy from the operating temperature to T_{cs} is the solid line.

The use of segregated copper in the Nb_3Sn cable-in-conduit conductors for ITER has been proved to be a viable option. Both DC and transient stability are more than satisfactory for the ITER requirements. The reduction of the Cu:non-Cu ratio down to 1 in the Nb_3Sn strands allows a reduction in the overall need of superconducting strand by keeping constant the non-Cu (i.e. the current carrying) cross section. The corresponding cost saving for the ITER conductor is in the range of 100 M$.

2.4.4 HTS Current Lead

In the frame of the European Fusion Technology Programme, CRPP-FT and the Forschungszentrum Karlsruhe (FZK) started a programme to develop a 60kA HTSC current lead for the toroidal field coil system of ITER in 1997. As the ITER design has since been modified, an upgrade to 70kA has been necessary. Up to now, three of the four sub-stages of the programme were successfully accomplished. In the first stage several 1kA binary current leads using either Bi2212 tubes or Bi2223 tapes with AgAu sheath from American Superconductor Corporation (ASC) have been tested to find the superconducting material best suited for a modular high current application. Based on these results, two 10kA Bi2223 tape modules have been tested. In the third step recently performed a 20kA current lead, composed of the two 10kA modules (ASC), has likewise been successful measured at National Institute for Fusion Science (Japan). In parallel to the third step it was decided to test a 10kA binary current lead composed of a twin set 5kA Bi2212 tube. These

modules are clad with a thin AgAu sheath. During 2000 the test current lead was designed and constructed.

Several different 1kA conductor types have been tested. The AgAu sheathed Bi2223 tape version has been found to be superior with respect to transient effects, compared with the Bi2212 bulk material. The reason is the big difference of the thermal conductivity between the bulk material and the stabilised tape material. This plays an important role in case of a sudden thermal runaway. Such an accident may be caused by a conductor quench for example. It may originate in a sudden stress or a loss of the cooling gas. In addition, stringent requirements are placed on the time scale during which a current lead has to sustain full current after detection of a quench. In the case of ITER the full load can last up to 12 seconds. During the 1kA current lead tests such transient effects have been investigated, showing quite dramatic time differences between the tube and the tape versions. The tape module took about 19 seconds to get from 10mV to 100mV, whereas the bulk module only needed 2 seconds. This indicated that the bulk module is not suitable for high current applications unless some kind of electrical bypass is used. Such a shunt would have to have a rather low thermal conductivity in order not to strongly increase the thermal loads, combined with a rather low resistivity compared with the normal HTS in normal conducting state. Meanwhile Bi2212 bulk tube modules (Nexans formerly Hoechst) with Ag3%Au sheath are available.

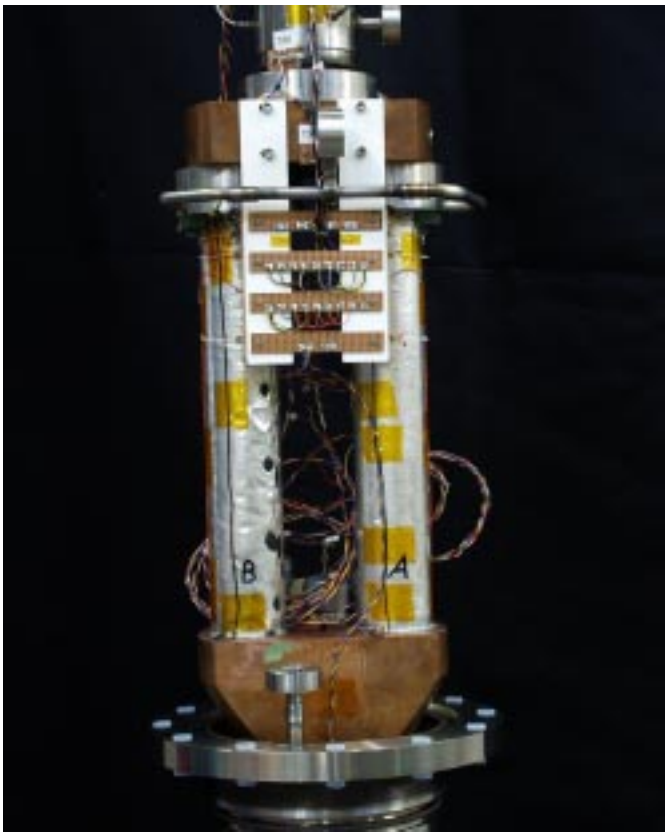

Fig. 2.4.22 Photograph of the fully instrumented 10kA twin lead Bi_{2212} tube current lead. The tubes are covered with an Ag3%Au sheath of 0.2mm thickness.

During 2000 we constructed a 10kA binary current lead consisting of a twin Bi2212 tube configuration (The HTS modules have been provided by FZK and procured by Nexans). Figure 2.4.22 shows a picture of the fully instrumented HTS module part. The upper termination is built by a copper adapter used to connect the HTS module to the normal conducting heat exchanger. The lower one, located in the liquid helium dewar, connects the test lead to the conventional return lead. A special low temperature solder makes the connections. Beside DC and transient experiments calorimetric measurements will also be performed. The latter will give quantitative

information about the conduction as well as the current related heat load into the Helium bath. The tubes are therefore instrumented with a series of temperature sensors to compare the measured temperature profiles to the theoretical calculations. The different contact resistivities and the voltage drop evolution along certain parts of the leads are measured by paired voltage tap configurations. In that frame the contact resistivities of the two modules are of great importance, also giving proof of reproducibility. Large differences will cause current imbalance between the two leads, also affecting the transient behaviour. Several Hall probes are located at the warm ends of the modules to monitor the current distribution at the interface region between HTS and the copper adapter. It is quite clear, that 3D FEM simulations are needed to explain the effective current pattern, and are a basis for an optimised design. Nevertheless Fig. 2.4.23, an example of a 2D FEM simulation, may give a better idea. The current is transferred from the circle in the middle to the two outer ones. Current density is decreasing from red to dark blue. The strong imbalance suggests an optimised design with respect to geometry and contact regions.

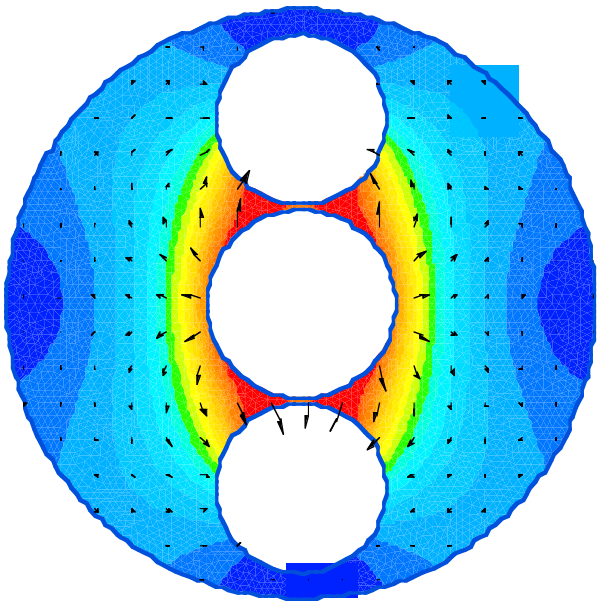

Fig. 2.4.23 2D FEM model for a current transfer. Current is flowing from the inner circle to the neighbourhood ones. Highest current density: red; lowest current density: dark blue

Presently the CRPP and FZK are proposing a development program for a 68kA binary current lead for the ITER-FEAT toroidal field coils, to be started in 2001. It is a significant step towards a deeper understanding of high current binary current lead applications, based on results and experience gained up to now.

2.5 140 GHz gyrotron development*

The test of the 140 GHz first prototype only started in 2000 due to a delay in the delivery of the superconducting magnet. Short pulse operation (150ms) was performed. Due to a misalignment in the internal quasi-optical mode converter the performance of the tubes was reduced and reached 0.65MW (at 40A beam current and 82kV cathode voltage) in pulses of 0.15s duration. The operation of the

* This work was performed in collaboration with the Associations FZK (D), CEA and Thalès (F).

depressed collector was also verified and allowed an increase of the electrical efficiency from 20% (without depressed collector) to 33 % (with the depressed collector). The tube was subsequently sent back to the manufacturer to correct the problem of the misalignment of the quasi-optical converter.

2.6 Industrial process plasmas*

2.6.1 The physics of plasma enhanced CVD for large area coating

Plasma-enhanced Chemical Vapour Deposition (PECVD) of hydrogenated amorphous silicon (a-Si:H) films using reactive gas mixtures of SiH_4, H_2 and small amounts of PH_3, B_2H_6 or $B(CH_3)_3$ for doping, is widely exploited in industry. Uses include the production of the thin-film-transistor (TFT) array in active matrix liquid crystal displays (AMLCD), the production of the p-i-n junction in thin film silicon solar cells, and the production of other opto-electronic devices such as detectors. The substrate usually consists of large glass plates approaching $1m^2$ with a thickness ranging from 0.7mm (AMLCD) to ~4mm (solar cells). The PECVD process temperature is 200-350°C and the pressure lies between 0.1 and 1mbar. The total film thickness to be deposited is typically 500nm and the required uniformity is ±5% for TFT-AMLCD, or ±10% for solar cells, with an allowed substrate edge exclusion ≤10mm. In order to obtain such results at the maximum deposition rate compatible with the desired opto-electronic properties (typically ≤10Å/sec), the PECVD source and reactor must be carefully designed. The constraints on the plasma source uniformity and excitation mode depend on the basic architecture of the industrial system and on the substrate mechanical handling.

The goal of the current CTI project is the design and development of a large area and high throughput coating system for silicon thin film solar cells. For economic production of silicon thin film solar cells it is necessary to coat glass plates of architectural size with a throughput of at least 10 glass substrates per hour. The three partners in this 2 year project are Unaxis (formerly Balzers Process Systems), the IMT (Institut de Microtechnique) of the University of Neuchatel and the CRPP.

Process optimisation includes varying the electrode gap distance and also variation of the plasma excitation frequency. The existing RF reactor at the CRPP, a Unaxis/Balzers KAI-S Plasma-Box reactor (57cm x 47cm) has been modified to allow changes in the electrode gap distance. In addition, excitation frequencies higher than the conventional 13.56MHz are expected to substantially increase the deposition rate without degrading the device quality of the layers.

A significant result is that high deposition rates are observed for narrow electrode gap reactors. For a 13mm electrode gap, which is half of the conventional distance, deposition rates above 10Å/s are easily obtained even with low-to-moderate RF power. Material characterisation performed at IMT Neuchatel shows that the defect density of the resulting amorphous silicon is as good as standard solar material. However, infrared and other analyses suggest that the film is slightly porous, a result subsequently confirmed by ellipsometry at CRPP. A first interpretation is that highly reactive radicals contribute to the deposition before undergoing passivating secondary reactions in the plasma because of the reduced path length to the substrate surface, thereby simultaneously increasing the deposition rate and microvoids in the material. Plasma diagnostic techniques will be used in future to verify this supposition. If correct, this problem could be solved by hydrogen dilution or by other changes to the parameters of the silane plasma.

* The work described under this section was not performed within the frame of the Association Euratom – Confédération Suisse.

Besides physical and chemical problems for the deposition of amorphous silicon, technological problems of large area capacitively coupled plasma reactors have been theoretically and experimentally investigated. A study of the reactor equivalent circuit was undertaken in order to design and construct an efficient impedance matching network for the higher excitation frequencies. Higher frequencies imply increased inhomogeneity of the deposited layer thickness. Consequently, sophisticated RF-coupling to the electrodes has been studied in order to achieve sufficient uniformity for the solar cell applications (<10%). Results of modelling and measurements demonstrate that carefully chosen multi-contact RF can provide the required voltage uniformity. In contrast, theoretical studies of various segmented electrode configurations show only minimal improvements in voltage uniformity (see Fig. 2.6.1). Segmented electrodes would, in any case, create severe practical problems in electrode construction. Practical experience with higher frequencies shows that electrical fringing fields between the electrode edge and surrounding grounded walls causes an intense edge plasma. This is a critical problem for uniform deposition. Two-dimensional plasma simulation using a numerical code has been used to design specially-shaped dielectric walls to reduce fringing fields. Their practical implementation is under consideration.

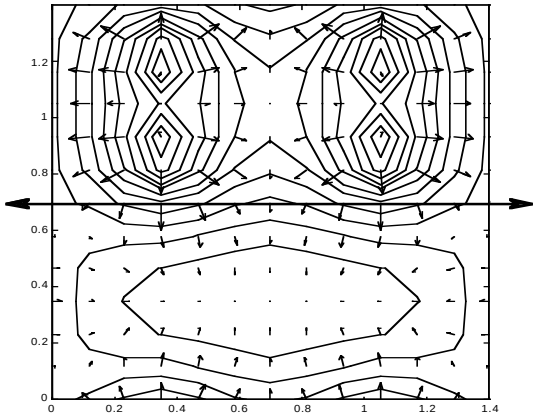

Fig. 2.6.1 Unfolded plot of RF voltage contours (0.5% spacing) at 27MHz for 4 RF contacts on a 1.4x0.7m^2 RF electrode. The plasma facing side corresponds to the lower half of the diagram and the arrows represent the RF current flow.

Gas feeding is also crucial for obtaining homogeneous coatings. At PECVD process pressures in the 0.1 – 1 mbar range, the gas transport is viscous and diffusive, and can be treated with a continuous fluid approximation. The injected reactive gas is consumed by deposition reactions on the substrate and on reactor walls, and one wishes to maximise the gas consumption efficiency for economical reasons. In practice the fraction of the SiH_4 flow dissociated in the reactor should exceed 40% for a-Si:H deposition. Since the atomic hydrogen fraction in a-Si:H film is ~10% this produces a lot of H_2. Consequently the gas composition is expected to vary between injection and exhaust if diffusion cannot compensate the flow velocity. For large area PECVD the most practical answer to this issue is to use a uniform shower-head gas injection along the electrode facing the substrate, while keeping pumping at the reactor edges, as was done in the plasma-box reactor. Indeed, empirical observations, as well as 2D numerical modelling have shown that quite uniform film deposition can be achieved with such a configuration. Nevertheless it is not intuitively clear why this is the case, since the horizontal gas flow velocity increases continuously from the reactor centre (zero gas flow velocity) to the pumping grids. A simplified analytical treatment of the problem demonstrates that the gas composition remains constant along the slab, provided the reactor is isothermal and the pressure variation can be neglected.

As a result of the work carried out in this CTI project and in previous OFEN projects, the collaboration of Unaxis/Balzers, CRPP Lausanne and IMT Neuchâtel aims to design a 1m^2 industrial plasma reactor suitable for industrial production of

photovoltaic solar cells. This would be a significant step in a realistic strategy for creating an industry for photovoltaic power generation in Switzerland.

2.6.2 Plasma spraying

2.6.2.1 Arc root attachment in the Sulzer Metco F4 plasma torch

In spite of its great success, some of the underlying fundamentals of the spraying processes are still poorly understood. A particular example is the behaviour of the arc inside the torch nozzle for which the anodic root position is determined by the complex balance between gas drag and Lorentz forces. The arc column lengthening leads to an increase of the arc voltage and consecutive restrikes or reconnections of the current channel take place across the surrounding cold gas boundary layer. These periodic phenomena result in strong temperature and velocity oscillations of the plasma jet. During plasma spraying this may lead to a non-uniform heating and transport of the injected powder particles and consequently adversely affect the quality and yield of the spray deposits.

Despite experimental studies, the basic understanding of the arc behaviour still requires further investigations. These must be carried out in correlation with advanced modelling and numerical simulations to allow further developments in the direction of improved control, reliability and reproducibility of the existing spraying techniques and for the development of new processes.

In this CTI project, we applied short exposure time, end-on imaging to the plasma torch interior. The exposure period (2µs) for image acquisition has been synchronised with several typical features of the arc voltage signal. This allows visualisation of the anodic arc attachment behaviour throughout the restrike process.

The atmospheric pressure plasma torch investigated is a Sulzer Metco F4 without powder injection equipped with a 6mm diameter atmospheric anode nozzle and a thoriated tungsten cathode fitted with either a straight or a swirl gas injector operated in typical industrial spray conditions. The analysis of the images in correlation with the fluctuating signals and of their power spectra was made for various gas flows, currents and for the two different types of gas injectors. The effect of electrode wear on the position of the anodic arc root was also investigated.

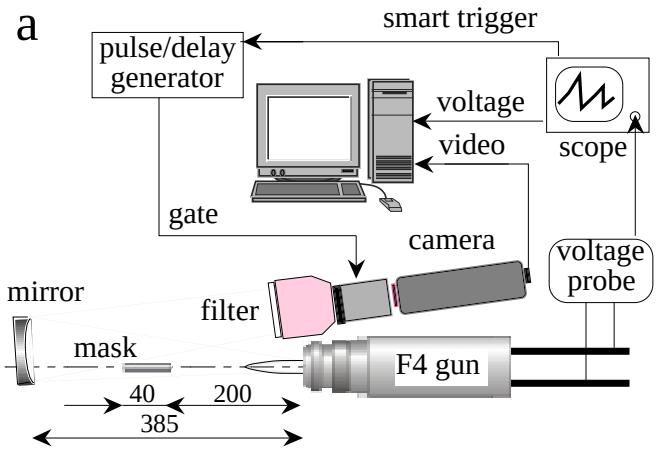

Fig. 2.6.2 Top view of the experimental arrangement with the image synchronization circuit.

The arc voltage was measured directly at the gun electrodes with a differential passive voltage probe. A gated intensified CCD camera is positioned beside the gun for imaging of the nozzle exit via a concave mirror in front of the gun (Fig. 2.6.2). A specially designed mask intercepts the strong light emitted from the arc column on the torch axis. As illustrated in Figure 2.6.2, this device cuts off the brightest emission coming from the hottest plasma region in front of the cathode and allows the camera sensitivity to be increased without saturation, in order to visualise the comparatively weak emission from the anodic arc root at the periphery.

A pulse/delay generator is used to control both the exposure time (0.5 - 5µs) of the camera intensifier and the delay with respect to an external "smart" trigger provided by the digital oscilloscope. This arrangement allows the recording of an image taken at a well defined time with respect to a typical feature of the torch voltage signal, such as a strong voltage drop subsequent to an upstream restrike of the arc.

Previous studies have shown that the fluctuating behavior of a plasma torch can be characterized by different regimes depending on the gas mixture and current: the restrike regime which prevails for Ar/H_2 mixtures is typified by a sawtooth shape of the arc voltage signal as shown in Fig. 2.6.3. The large voltage drops (labeled "1" in Fig. 2.6.3) repeat with a frequency between 3 and 4kHz and have been attributed to "upstream restrikes", for which a breakdown of the arc occurs with a new arc root closer to the cathode. The length of the new arc is strongly reduced, which results in a large drop of the voltage. Between these periodic features there are irregular drops of smaller, amplitude (labeled "2" in Fig. 2.6.3). These have been attributed to "downstream restrikes" for which a breakdown of the arc occurs with a new anodic root farther from the cathode or on the diametrically opposite side of the anode. In this case, the new arc termination does not exhibit an S-shape bending which results in a shorter overall length and leads to a voltage reduction. These small non-periodic voltage drops might also be attributed to short-circuiting of the curved part of the arc at the anode foot.

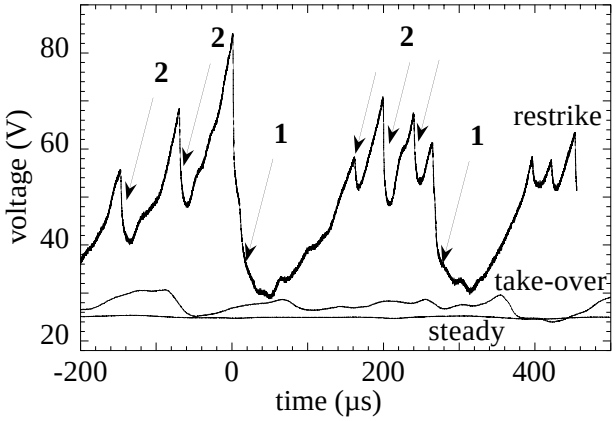

Fig. 2.6.3 Typical voltage traces in the restrike, take-over and steady modes. For the restrike mode, arrows show periodic large voltage drops (labeled "1"), with smaller, irregular voltage drops in between (labeled "2").

In Figure 2.6.4 we present images of the anodic arc root attachment at different times within a restrike cycle using the end-on imaging technique of the nozzle exit. Each sub-figure (A, B, C) corresponds to different acquisition times within a typical restrike cycle and show characteristic features: (A): before a major restrike, (B): after a major restrike, and (C): after a minor restrike. Details of the voltage signals with the exposure time (gate) of the camera (vertical lines) are represented along with the corresponding images of the anodic arc root. Since the camera does not allow for the acquisition of consecutive images within one restrike cycle, the voltage traces are slightly different from one line to the other. However the images and voltage traces shown here are representative of the general features found in a typical restrike cycle such as the one described in Fig. 2.6.3.

In Figure 2.6.4 we have also represented circular intensity profiles taken along the contour indicated with the middle white circle on the image of line C. In the following, this polar representation will help to identify the arc root number and locations. Moreover a general trend in the anodic arc root behavior can be evidenced by averaging a large number of these profiles from a large number of images, which otherwise would be difficult to present.

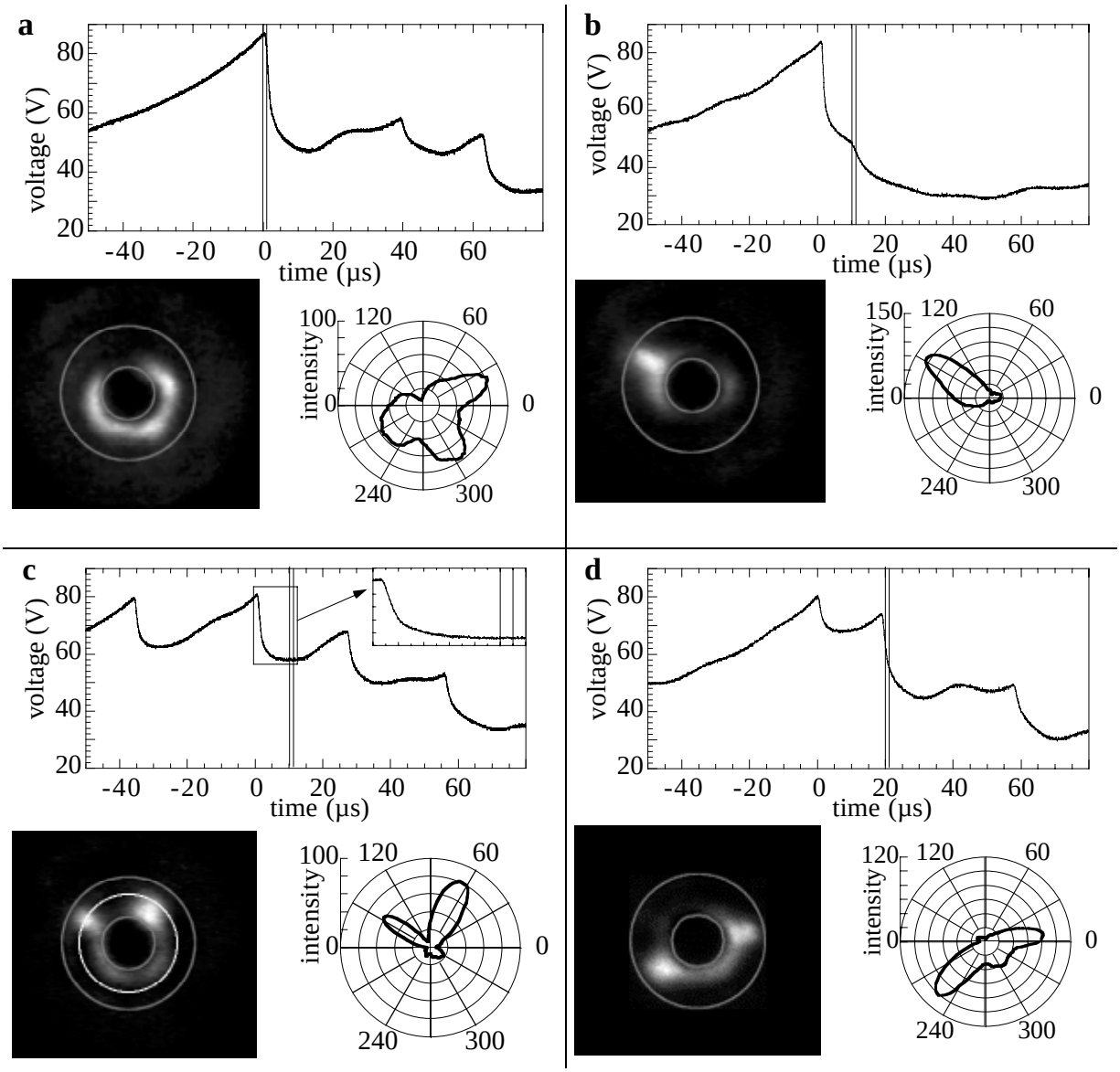

Fig.2.6.4 Voltage signals with exposure time and corresponding end-on images of the nozzle exit for four different characteristic features of the restrike cycle: (a) just before and (b) 10µs after a major restrike, (c) between two minor restrikes, and (d) 15µs after a minor restrike. The polar plots represent circular intensity profiles (taken along the middle white line indicated on image (c). The insert in the voltage graph (c) with magnified time scale (100ns sample interval) does not show any fluctuation during the exposure time. Plasma conditions: 500A, 4/40 SLPM H_2/Ar, straight injector, worn electrodes, exposure time 1µs.

In Figure 2.6.4(A) the image has been acquired just before the large voltage drop corresponding to an "upstream restrike". At this time, the voltage is at its maximum and so is the power dissipated in the arc. There is no clearly defined anodic arc root, which might be because the gas boundary layer temperature is high enough to allow for a diffuse attachment to the anode.

In Figure 2.6.4(B), which corresponds to about 10µs after a major restrike, a single new anodic arc root is clearly visible. This is because the temperature of the cold gas boundary layer has now dropped which leads to a constricted and well-delimited current channel to the anode. We systematically observe a unique arc attachment after major restrikes. This is consistent with the interpretation of upstream restrikes with a new anodic arc attachment closer to the cathode. Moreover, images acquired down to 1µs after the voltage drop edge already show a single sharp attachment which suggests that, in the case of upstream restrikes, the arc current is transferred within less than 1µs from the previous diffuse attachment(s) to the new sharp attachment. This is characteristic of a breakdown phenomenon.

In Figure 2.6.4(C) we present an image taken between two small voltage drops similar to those labelled "2" in Fig. 2.6.3. There are two distinct arc attachments, which coexist for at least the 1µs exposure time of the camera. In these conditions, the gas boundary layer temperature is higher than for Fig. 2.6.4(B), as shown up by the halo with cylindrical symmetry around the mask, and by the fact that the voltage is quite high. However, it seems that the conditions required for an upstream restrike to take place are not fulfilled, even if the peak voltages are of the same order of magnitude for the cases (A) and (C) (around 80V). However, the rate of voltage drop in the present case (less than 1MV/s) is less than in the case of upstream restrikes described above. Note that there is no oscillation on the corresponding voltage signal during the exposure time given the sampling rate (0.2µs per point) and voltage probe bandwidth used here. A transition from one attachment to the other occurring faster than the bandwidth of the voltage measurement is improbable because we systematically observe multiple attachments between minor restrikes, irrespective of the delay after the first voltage drop. Therefore, our interpretation is that there is a creation of a new attachment without the immediate destruction of the previous one. It seems that there is a continuous process of creation/disappearance of anodic attachments. We have observed up to three coexisting attachments. It is not yet clear which mechanisms lead to an upstream restrike with a single new arc root instead of multiple co-existing successive attachments. From the spraying point of view, it might be more favourable if the plasma torch could be operated only in the latter mode which resembles a "take-over" mode. However, in most spraying-relevant operation conditions there is a mixture of both phenomena as shown on the voltage signal in Fig. 2.6.3.

Visualisation of the anodic arc root(s) has been investigated as a function of various operating parameters such as electrode wear, gas flow, gas injector type and current. This study has been performed for the case of pure argon flow, for which the attachment type does not depend on the time within a fluctuation cycle of the take over mode. For worn anodes, the attachment sits preferentially in regions where there is erosion on the anode wall. This has strong consequences for the electrode lifetime, since regions that exhibit wear will be preferentially eroded. However this effect can be attenuated by increasing the gas flow and/or by the use of a swirl gas injector, which both help to randomise the attachment position over the inner anode surface. In addition, increasing the gas flow tends to increase the number of attachments, whereas increasing the current leads to a thinner and hotter gas boundary layer, which favours diffuse attachment (Fig. 2.6.5). At low gas flow and high current the so-called "steady mode" is observed, which is characterised by a single and stable diffuse attachment.

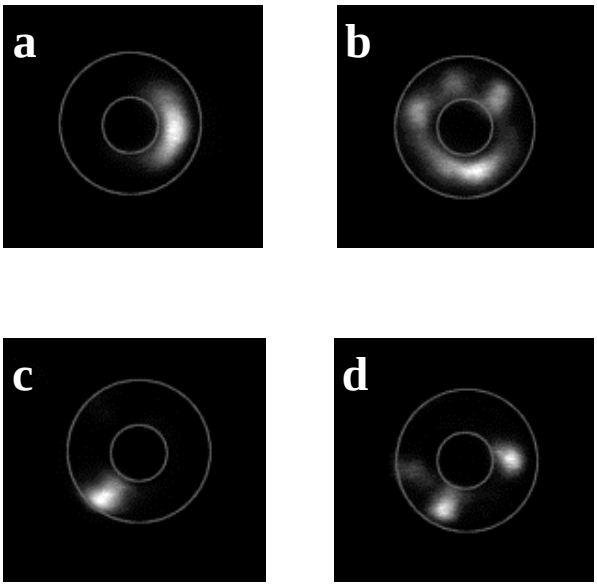

Fig. 2.6.5 Typical end-on images of the torch nozzle illustrating the general trends in the nature of anodic attachment(s) as a function of gas flow and current. Operation parameters: 200A (a and c), 600A (b and d), 20SLPM Ar (c and d), 60SLPM Ar (a and b), straight injector, worn electrodes, exposure time : 1µs (a and b), 2 µs (c and d).

The results presented here reveal the complexity of the nature of the anodic attachment and show, in particular, that any 3D modelling of the arc behaviour inside a DC plasma torch should take into account successive creation and vanishing of multiple attachments that may coexist for a significant time.

2.6.2.2 Low pressure plasma spraying (LPPS)

Thermal spray coating using plasma torches in either ambient or controlled atmosphere is a well-established technology that is successfully applied, particularly in the aeronautics, gas turbine and automotive industries. In these processes, the plasma jet is intrinsically limited in size, which disqualifies them for coating large substrates uniformly in a reasonable time. Recently, a new process (Low Pressure Plasma Spraying-Thin Film) which uses a plasma torch operating at low gas pressure has been developed with the aim of depositing uniform thin layers on large surfaces. Typical applications of this process include deposition of thin layers of metal oxide or other materials on large sheets in a single shot. This new process bridges the gap between conventional CVD/PVD thin film deposition and thick, thermally sprayed deposits. Because of the large pressure difference between the inside and the outside of the plasma gun, the exiting plasma jet experiences unconventional behaviour related to supersonic expansion at the reduced pressure. Moreover at low pressures, the collision rate is strongly decreased and the plasma jet may no longer be in local thermodynamic equilibrium. Therefore its properties, in particular the temperature of the electrons and of the heavy species, the specific enthalpy, the velocity and turbulence remain to be determined.

Previous experimental investigations of the plasma jet from torches used for plasma spraying at reduced pressures were limited to the 100mbar pressure range. The enthalpy probe technique, originally developed in the 1960's, is extensively used for the diagnosis of thermal plasma jets in spraying processes at atmospheric pressure. Its main advantages are the simplicity of the technique and the possibility of obtaining simultaneous measurements of multiple plasma parameters such as enthalpy, temperature, velocity, density and composition, with a reasonable spatial resolution. A modified enthalpy probe system, which allows measurements down to a chamber pressure of 2mbar, has been applied to the new low pressure plasma spraying.

The plasma gun (Fig. 2.6.6) investigated in the frame of the CTI project is a Sulzer Metco O3CP which is operated inside a vacuum vessel for Low Pressure Plasma Spraying. A modified enthalpy probe system, supplied by Tekna Plasma Systems,

was used for the diagnosis of the expanding plasma plume at low operating pressures. The modified enthalpy probe system is based on the common atmospheric probe system with the addition of a roots pump and the enlargment of the probe tip and pumping pipe dimensions in order to achieve the necessary gas sampling throughput at reduced pressure. The probe cooling water flow rate is also increased to account for the higher heat load on the large probe tip (up to 7kW). The probe bulkhead is also larger than the standard one and is equipped with a separate cooling circuit because it is partially immersed in the plasma jet whose length can exceed 2 meters. The system is able to sample sufficient plasma gas to achieve a reliably measurable heat load difference between the "tare" and "sampling" condition for chamber pressure down to 2mbar. Figure 2.6.7 shows the probe inside the plasma jet at 6mbar.

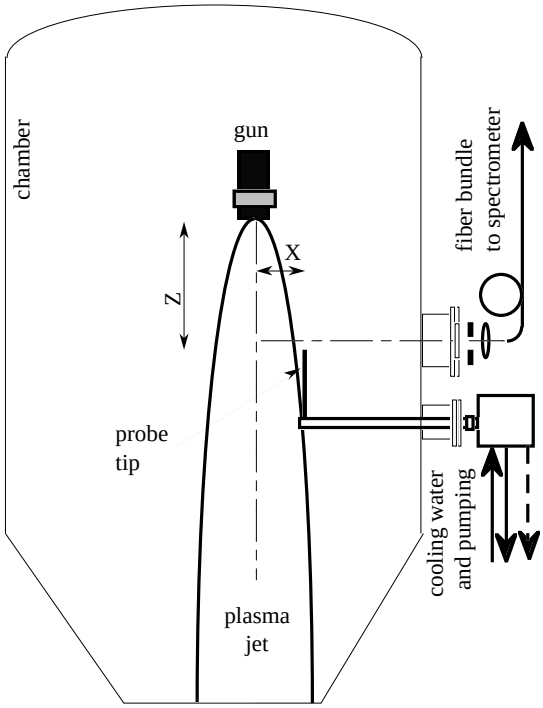

Fig. 2.6.6 Drawing of the experimental arrangement (not to scale), showing the vacuum vessel with the enthalpy probe and the jet light collection for optical emission spectroscopy. X and Z refer to the probe-to-nozzle radial and axial distances, respectively

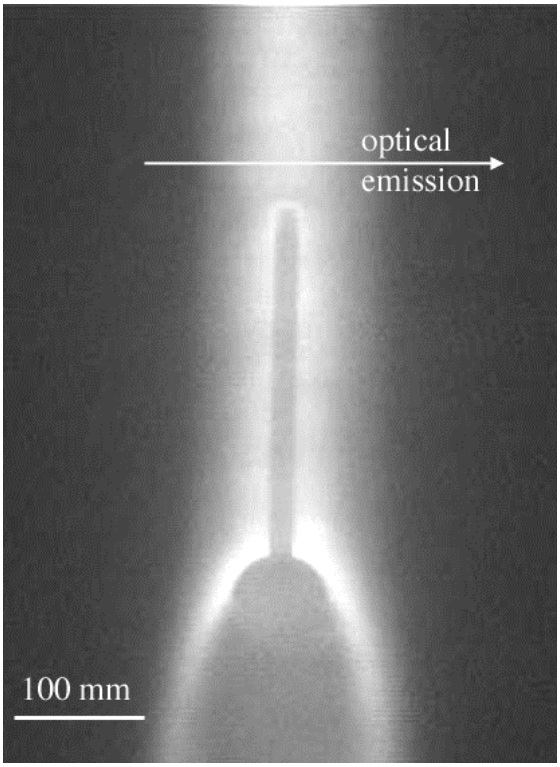

Fig. 2.6.7 Image of the probe on the axis of the plasma jet at Z= 670mm for a 6mbar chamber pressure. The arrow indicates the optical emission collection path.

With this enthalpy probe system axial and radial profiles have been measured in the industrial device at Sulzer Metco in Wohlen. Figure 2.6.8 shows axial profiles along the jet axis of the specific enthalpy and of the local heat flux for three chamber pressures. The heat flux is obtained from the product of the calculated enthalpy, density and velocity. From Fig. 2.6.8(a) one can see that the specific enthalpy is strongly dependent on the operating pressure and that it increases as the pressure decreases. The local heat flux is not monotonic as a function of pressure, and shows a maximum at 6mbar. This is because it depends not only on the enthalpy but also on the density and jet velocity. Moreover, at the axial distance where this measurement is performed, the probe is almost at the end of the 10mbar

plasma jet, whose length is much shorter than for the lower pressure cases. This is shown by the drop in the heat flux on Fig. 2.6.8(b) and the temperature on Fig. 2.6.8(a) as the axial distance is increased. This effect is not observed for the 2 and 6mbar plasmas for which the plasma jet goes much farther than 1m.

To summarize, it is observed that for very low pressure (2mbar) the jet properties are almost constant over a quite large distance from the nozzle exit. This is because the surrounding gas density is very low and interacts only weakly with the jet. Moreover the mean free path is strongly increased and the collision frequency drastically reduced at these low pressures. The flow is laminar (Reynolds number in the range of 100) and the jet is only weakly cooled, or slowed down by the surrounding atmosphere.

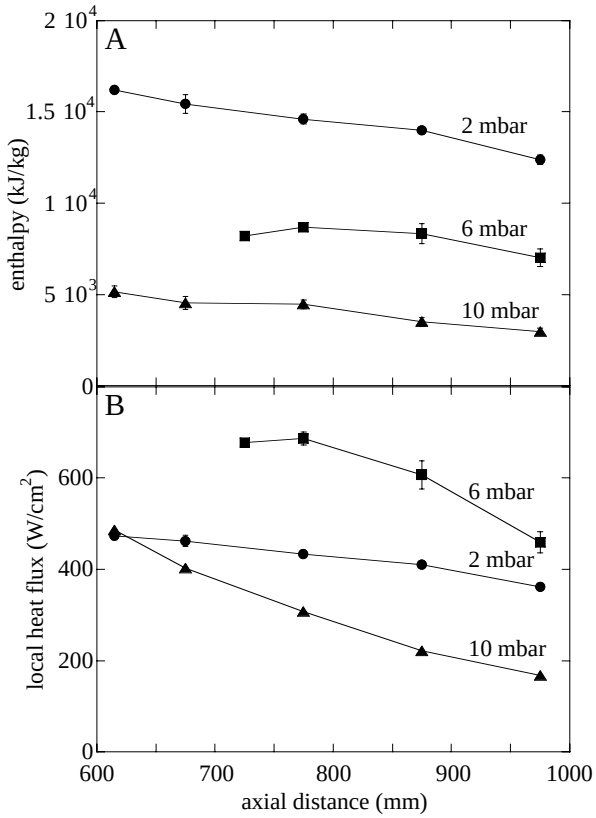

Fig. 2.6.8 Axial profiles on jet axis of the specific enthalpy (a) and of the local heat flux(b) for 3 chamber pressures.

The results show that this new kind of expanding plasma jet is governed by physical mechanisms different from the ones that prevail in atmospheric thermal jets. In particular, the low collision rate between the various plasma species, due to the low density, is reponsible for the large dimensions of the jet, for the spatial uniformity of its properties and for the deviation from local thermodynamic equilibrium. The flow is supersonic over nearly the entire jet volume and the influence of turbulence is weakened. Since these low-pressure jets are no longer in local thermodynamic equilibrium, further work is necessary to account for the low-pressure effect on thermodynamic and transport properties. Moreover other kinds of diagnostics will have to be used, such as laser scattering, in order to validate enthalpy probe measurements.

During the year a new vacuum chamber was designed, constructed and purchased in collaboration with Sulzer Metco a powerful pumping system allowing the extension of the operation range of the F4 plasma torch down to mbar pressure range.

2.6.3 Powder production in reactive plasmas

The study of microcrystalline and hydrogenated amorphous silicon deposition was recently extended to a new material: the so-called polymorphous silicon, which showed enhanced electronic transport properties and interesting material properties for solar cells applications. It was observed that polymorphous silicon contains small ordered structures with a size of about a few manometers.

It was suggested that plasma chemistry could be used to control the structure and the size of these nano-particles incorporated into the amorphous layer. In order to verify the ordered structure of these particles, we studied the particles of pure Silane or Argon-Silane RF plasmas with in-situ infrared absorption spectroscopy, in the region of the plasma where these particles nucleate, agglomerate and grow.

The experiments were performed in a capacitively-coupled RF reactor working at 13.56MHz with 130mm diameter electrodes and a 2.5cm electrode spacing. As principal plasma and particle diagnostics, infrared absorption spectroscopy and cavity ring down spectroscopy have been applied. The infrared absorption spectroscopy was performed using a commercial Bruker FTIR apparatus. The cavity ring-down arrangement consists of a cavity with two high-reflectivity dielectric mirrors. A dye laser pulse is introduced into the cavity and the intensity is measured behind the exit mirror by a photomultiplier. The real time measurements are performed by analyzing the evolution of the ring down decay with time. The presence of absorbing species in the cavity causes a decrease in the decay time from which an extinction coefficient can be determined which depends on the cross-section of the different possible extinction processes such as photodetachment, scattering, absorption.

We observed in-situ that particles which show intense surface-like vibration modes are produced and trapped in the silane-argon plasma. From absorption bands, we calculated a possible content of hydrogen into the powders of 17-30%. We observed a large absorption band centred around 2100cm^{-1} and the band at 2010cm^{-1} provides the signature of amorphous material. Following the interpretations given in the literature this suggests that some part of the powders may contain ordered structures, like nanocrystalline silicon. The modes detected are mostly dihydride R_2SiH_2 surface-like vibration modes and not monohydrides vibrational modes. One vibration mode at 2050cm^{-1} may possibly be attributed to hydrogen platelets which are usually centered round 2035cm^{-1}. After observing the possibility of surface effects in these plasmas, we observed that surface contamination influences the growth of powders in pure silane discharges.

Repetitive experiments were conducted in Argon-Silane RF plasmas at low pressure in order to verify the influence of the reactor contamination on the growth and structure of powders. Changes in size, density and structure of particles up to 200nm diameter were studied in-situ by means of Fourier Transform Infrared Spectroscopy. In particular, we observed large and intense absorption bands centred around 2100cm^{-1} and 660cm^{-1}. These bands are again attributed to a high hydrogen concentration in amorphous silicon particles.

2.6.4 Decorative coatings

In the past the high current DC arc reactor, similar to the commercial Balzers BAI 730 reactor, was used for the development of industrial diamond coating and to investigate the boron nitride deposition. The basics of the high current DC arc reactor (HCDCA) turned out to be very similar to the well-known traditional hot wire reactor. The advantages of the high current DC arc reactor with respect to the hot wire reactor are the much higher gas temperatures, much higher radical density and reduced impurities in particular of metals obtained in this new reactor

type. The radicals necessary for the surface modifications were produced in the hot arc plasma column by a large current (typically 140A) and diffuse out of the plasma. The substrates to be coated were placed in this diffusion region concentrically around the plasma column.

The basic feature of the reactor is a non-self-sustained arc discharge created between an anode and a cathode 40cm apart. Electrons emitted from polarised, hot tungsten filaments sustain a high current DC discharge at a low working pressure with a current up to 340A at a driving voltage of about 50-90V. The typical working pressure is around 1-2mbar. Besides argon, different gases such as hydrogen and nitrogen can be used. Two magnetic field coils in a Helmholtz arrangement (0-250G) confine and stabilise the 5cm diameter arc plasma column. Measurements of the arc plasma show that the electron temperature is around 2eV (23'000K). Electron densities in the range of 10^{12}–$10^{13}cm^{-3}$ have been measured by electrical probes. The plasma produced in the high current DC arc reactor is a typical non-equilibrium plasma. Line broadening measurements and comparison between calculated and measured molecule bands (N_2^+) allowed the determination of the gas temperatures. These temperatures are about 5000K for the most prominent discharge parameters. The substrate located in the diffusion zone is mainly heated due to atomic species recombining on its surface. The deposition temperature, varying from 300 to 900°C according to the films deposited without the use of any external heating or cooling system, is determined by the substrate position, the arc power and the injected gas mixture and flux.

Recently this reactor has been used to modify ceramics for decorative applications. The goals of this work are to nitride ZrO_2 (Y-TZP) ceramics in order to obtain a yellow-gold as well as a wear resistant material for industrial purposes and to understand the process.

Several improvements to the nitriding process of zirconia have been made during the last year and we identified some of the main processes leading to the decorative functionality of the ceramic. Our experiments showed that the nitriding process could be successfully applied if parameters like the ceramic temperature and gas mixture were suitably chosen. In addition the temperature depends on the gas ratio used, i.e. of the nitriding specie(s) impinging on the zirconia surface and is also a function of the exposure time. In our experiments we found that with a nitriding temperature around 750°C we could achieve a good layer, exhibiting a yellow gold colour with good wear resistance.

Material analysis allowed us to form a clearer picture of what happens to the ceramics when nitrided in the arc plasma. At first, a fine ZrN top layer is created and we observed that the tetragonal phase is transformed into a cubic phase during this process. The destabilisation can occur up to several tens of microns into the bulk ceramics. Impurities on the surface have also been detected and it was demonstrated that they slightly modify the colour of the nitrided ceramics.

However, the behaviour of the process plasmas is not well known and different plasma diagnostic methods such as laser induced fluorescence and cavity ringdown spectroscopy are planned to characterise the radical production.

2.6.5 Other collaborations and industrial mandates

Several industrial mandates have been carried out during 2000. These mandates involve essentially basic research and development of new processes or improvement and control of existing plasma processes.

Together with various laboratories of the Material department of the EPFL (Laboratoire de Polymères, Laboratoire de Technologie des Poudres and Laboratoire

de Métallurgie Chimique) the CRPP began activities in the surface modifications of polymer films by plasmas. Plasma treatment has been found to be an extremely attractive way to modify the surface chemistry and morphology of polymeric materials. The plasma modifications may be carried out in the presence of specific gases, such as oxygen, argon, nitrogen and hydrogen. This results in the generation of active species, which activate and modify the material. An interesting aspect of the plasma treatment is that the changes are confined to a depth of a few nanometers at the surface because of the low level of its penetration. This opens up possibilities for producing a wide spectrum of surface chemistries with desired compositions. An additional attractive feature of plasma processing is that by proper control on the exposure conditions, a surface tailored for the desired chemical functionality and morphology may be produced. There are a number of polymeric materials that have excellent physical properties but do not have an active surface for the immobilisation of biomolecules. One of the applications of such polymeric biomaterials is in the form of support structures for tissue growth. Such polymers need selective modifications so that specific functional groups may be imparted to the surface for the binding of biomolecules and culturing of cells.

Plasma treatment of PET films carried out under argon, followed by the exposure to an oxygen atmosphere, cause considerable changes in surface composition and morphology, as demonstrated by contact angle measurements, FTIR-ATR, AFM and XPS. It was found that the surface acquired oxygen containing polar functions as –C=O, -OH, and –OOH, which increased in number as the plasma treatment continued. As revealed by AFM measurements, these changes were accompanied by an increase in roughness in the form of ridges. Using various plasma diagnostics such as mass spectrometry, which allows the measurement of the neutrals, positive / negative ions and their energies, optical emission spectroscopy and different electrical probes (Langmuir and Ion flux probe), an attempt was made to correlate the surface modifications obtained with plasma parameters. In particular, attention was made to measure precisely the type of bombarding species, their energy and the dose applied to the surface which allowed the characterisation of the surface interaction and optimisation of the plasma process.

Plasma processing of SiO_x coatings as apermeation barrier in packaging was the mandate performed for TetraPak R&D Plasma Technology in Romont. Here, as well as basic understanding of the plasma chemistry and physics, process control was of prime interest. These studies were carried out by a PhD student also working at Tetra Pak.

Hexamethyldisiloxane (HMDSO), $Si_2O(CH_3)_6$, plasmas, diluted with oxygen, have been investigated. The complementarity of Fourier transform infrared absorption spectroscopy and mass spectrometry allowed the determination of the most abundant neutral components present in the discharge. The measurements revealed that methyl groups (CH_3), abundantly formed by the dissociation of the HMDSO molecule, are the precursor for the most abundant species which stem from two kinds of reaction. The first kind of reaction is combustion of CH_3 by oxygen, producing formaldehyde (COH_2), formic acid (CO_2H_2), carbon monoxide, carbon dioxide and water. It is shown that high mass carbonated radicals, such as Si-O-CH , first diffuse to the surface and then the carbon is removed by oxygen etching to form carbon dioxide. The second kind of reaction is hydrocarbon chemistry promoted by CH_3, producing mainly hydrogen, methane and acetylene.

The work for Balzers Wear Protection was directed towards novel diamond processing for tribological applications. In the frame of this mandate a diploma work on advance diamond processing has been finished in 2000 in collaboration with the Technical University of Vienna.

It should be added that collaboration with different industries is very stimulating and exciting not only for the research and development, but also for the education of young scientists and future industrial collaborators.

3 TECHNICAL ACHIEVEMENTS OF THE CRPP IN 2000

3.1 TCV tokamak operation

TCV was operated for 9 months in 2000, with a total of 2144 pulses, corresponding to an increase of 12% compared with the previous year. Operational statistics on a monthly basis are shown in figure 3.1.1. Operation was interrupted in October for the installation of the X3 gyrotrons and top launcher and the divertor Thomson scattering system as well as the repair and upgrade of various sub-systems, including the X2 lateral launchers, the Langmuir probes, the Charge Exchange Spectroscopy and the diagnostic and coil cooling systems.

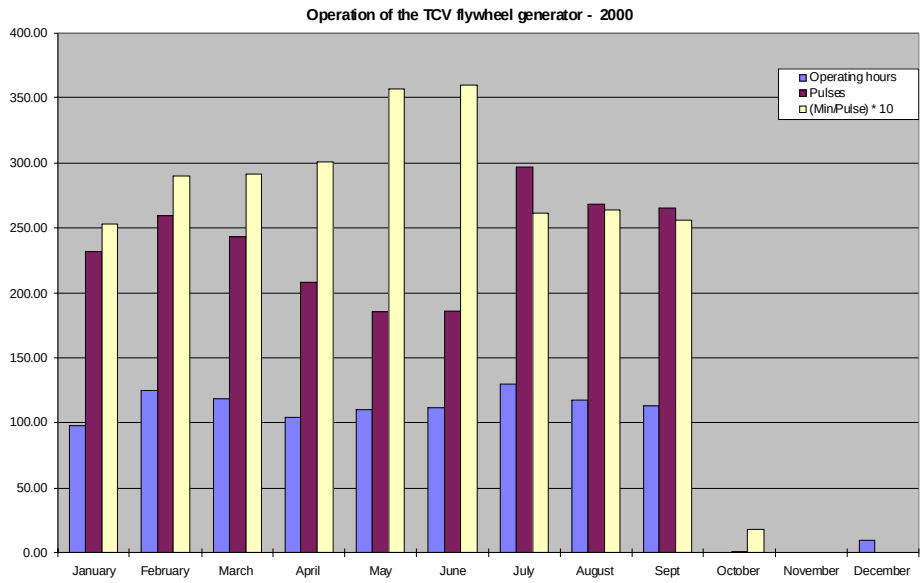

Fig. 3.1.1 TCV operation in 2000 summarised with the number of pulses per month, the hours of operation of the power system and the average time interval between pulses (minutes x 10)

3.2 TCV Diagnostics

Thomson scattering: The current system, which measures the main plasma electron temperature and density, comprises 3 pulsed Nd-Yag laser units forming a cluster of beams which pass through the TCV vessel along the same vertical chord. The three lasers are fired repetitively at 20Hz and can be timed independently so as to provide a 60Hz sampling rate or be fired together to provide better signal-to-noise performance in low density discharges. Implementation of a system to measure the temperature and density in the divertor of lower Single Null discharges was initiated during the 2000/2001 winter shutdown of TCV and is scheduled to be available for the 2001 experimental campaign. This system recycles one of the laser beams after its first passage vertically through the plasma, redirecting it into the vessel for a second passage at a radial position shifted towards the inside, using another port in the same sector. The divertor beam is also slightly displaced in the toroidal direction, allowing the use of the same observation optics as the main system, equipped with an additional set of fibre bundles to transmit the scattered light to filter multichromators optimised for measurements at the low electron temperatures characteristic of divertor plasmas.

In addition, a set of three more powerful lasers have been ordered for improving the signal-to-noise ratio in low-density, high temperature plasmas. Implementation is planned for 2001.

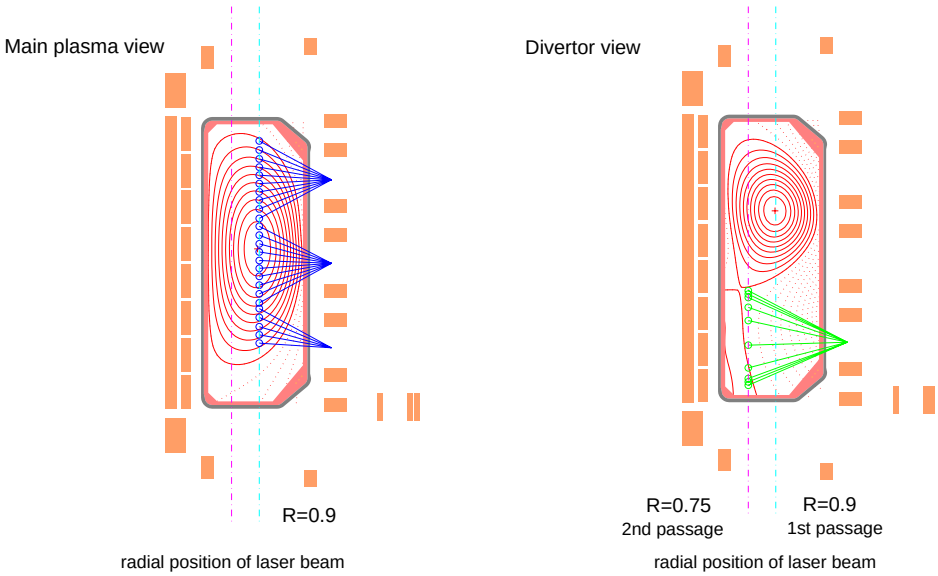

Fig. 3.2.1 Main (left) and divertor (right) Thomson scattering geometries

Fast bolometry: The two prototype bolometer cameras equipped with 16-element AXUV diodes described previously, have been relocated to serve for total power measurements. A third camera, made from spares, has been optimised for divertor measurements (Fig. 3.2.2). At least another two are planned for a full tomographic system. These bolometers have exceptional bandwidth and S/N ratio and are insensitive to low energy neutrals emitted from the plasma edge and to ECH pick-up.

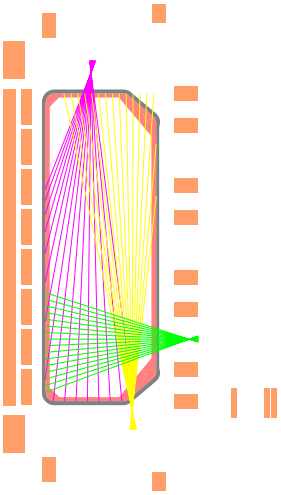

Fig. 3.2.2 Current geometry of the AXUV bolometer cameras on TCV

Edge diagnostics: In addition to the divertor Thomson scattering and AXUV bolometer systems mentioned above, these include tile-embedded Langmuir probes, a reciprocating Langmuir probe, classical metal foil bolometers, tangential visible cameras, infrared cameras and fast pressure gauges. The fast reciprocating Langmuir probe on loan from UCSD, San Diego, was brought into service in 2000 and has been extensively used for detached plasma studies. These studies have also benefited from a triple tangential visible light divertor camera. Using suitable narrow band interference filters, the poloidal distribution of the emission of

Deuterium and selected carbon impurity ionisation stages (CI, CII, CIII) is being routinely measured using CCD cameras during diverted discharges and the resulting images are numerically reconstructed into 2D using an efficient inversion algorithm developed at the CRPP (Fig. 2.1.15).

The installation of two infrared cameras is under way. One of these will monitor inner wall tile temperatures during ECH, while the other will replace an existing, ageing camera used for divertor heat load measurements.

Laser ablation of trace impurities: The CRPP has begun a collaboration with KFKI Budapest on injection of trace impurities into TCV using laser ablation. KFKI has delivered an injection chamber which was mounted onto TCV in October 1998, while CRPP supplied the ruby laser, control systems and diagnostics (Fig. 3.2.3). The evolution the impurity emission, using existing X-ray diagnostics, permits the study of impurity confinement times and local transport coefficients. A fruitful joint campaign in the summer of 2000, during which mainly Si was injected into a variety of plasmas, has revealed unexpected and intriguing dependencies of the ratio of impurity-to-energy confinement time on plasma shape. This research will continue during the 2001 campaign.

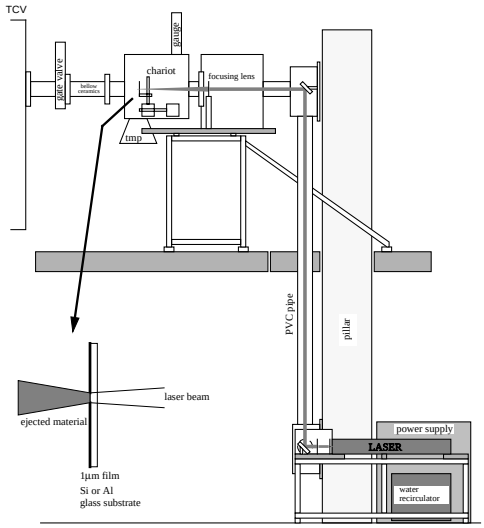

Fig. 3.2.3 Setup of the impurity ablation system on the TCV tokamak.

Active neutral beam diagnostics: Final commissioning of the 2A ion current, 50keV injector, built by the Budker Institute of Nuclear Physics (BINP) in Novosibirsk, was completed by a Russian team in March 2000 (Fig. 3.2.4). The implementation of the control software and integration into the TCV control system, which were also subcontracted to BINP, were finished in May. The system has operated without serious problems up to the end of June, when a liquid Helium shortage enforced priority for the ECH work. This system provides the active source for charge exchange spectroscopy (CXS) for ion temperature measurements on TCV. The light from the beam is gathered by a pair of lenses and relayed to two visible spectrometers using optical fibres (Fig. 3.2.5). One of these spectrometers is equipped with a CCD array for the simultaneous measurement of up to 16 spectra from different positions in the plasma.

Initial measurements allowed the identification of charge exchange lines from the beam volume. These results indicate however that the signal-to-background light

level is not sufficient and improvements of the detection system have been initiated. A combination of a more sensitive, back-illuminated CCD and a higher aperture spectrometer should allow photon counts to be increased by an order of magnitude. Improvements in source brightness are also being considered. These may include operation at somewhat increased current and acceleration voltage, an increased extraction area from the RF plasma source and a more compact injector body design with a beam focal length of 2m, allowing the distance between the extraction grid and TCV to be reduced.

Fig. 3.2.4 Diagnostic Neutral Injector on TCV

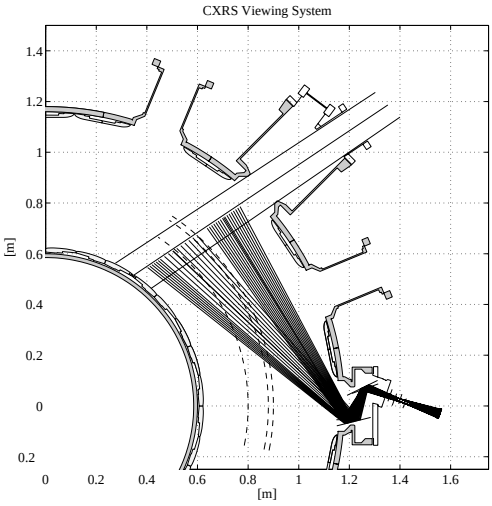

Fig. 3.2.5 Viewing geometry of CXS

SPRED spectrometer: This wide-band VUV-XUV spectrometer which allows a comprehensive monitoring of impurities in TCV has been brought into service at the end of the last campaign. It is equipped with two interchangeable ion etched gratings which disperse the incoming light from 140-10nm and 300-10nm onto a flat image plane where a channel plate detector amplifies the signal and converts the signal to visible photons. The design and construction of a 2048 channel electronic readout system to designed and built at the CRPP has started. This broadband surveillance instrument will be used for long term continuous monitoring of impurity line radiation from essentially any species that may be present in the plasma.

Ultrasoft X-ray spectroscopy: The existing USX spectrometer, produced by IPP Prague has been re-equipped by IPP staff to monitor line ratios of H- and He-like Carbon and Oxygen, which are sensitive to transport near the edge. Further experiments are planned for 2001.

Hard X-ray measurements: A hard X-ray camera was on loan from Tore Supra in 2000 again and will stay on TCV for most of 2001. On TCV, the diagnostic views the

outer half of the plasma cross section vertically through a pinhole and is configured with a spatial resolution of ~2cm over 14 chords; for each chord, measurements are made over 8 energy channels in the range 10-200keV with a resolution of ~7keV (Fig. 3.2.6). The temporal resolution is typically of the order of 2-5ms. The diagnostic measures the spatial and spectral distribution of Bremsstrahlung emission from suprathermal electrons and has yielded valuable information on the fast electron dynamics during ECCD experiments, which generate a substantial suprathermal component in the electron distribution function.

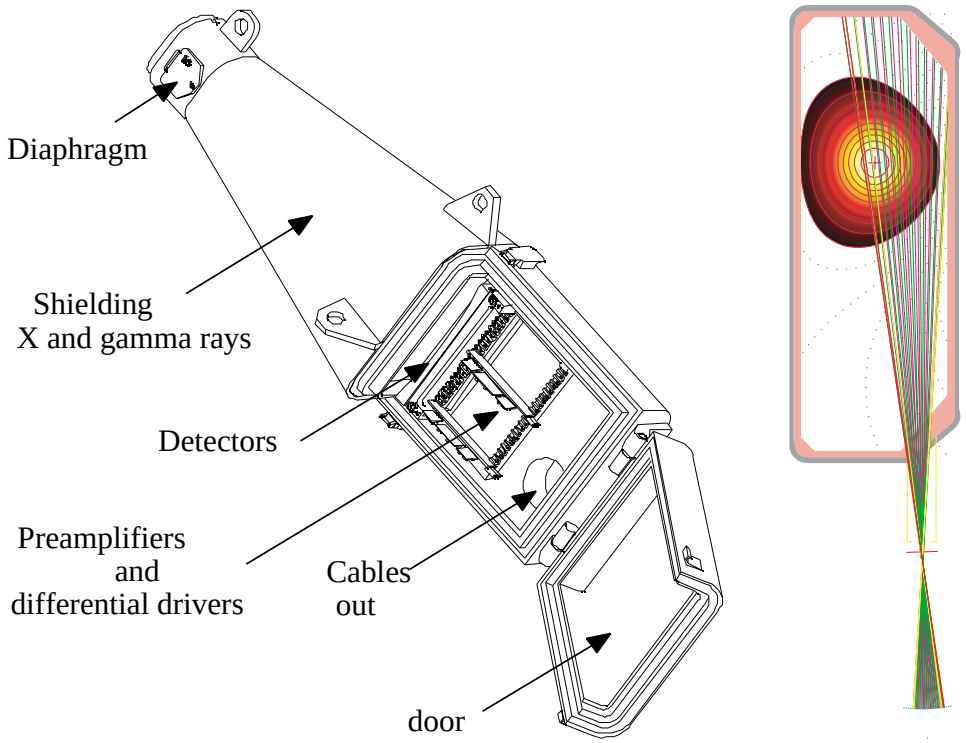

Fig. 3.2.6 Hard X-ray camera (left) and viewing geometry (right)

ECE measurement: The 24-channel ECE radiometer built by the company ELVA-1 (Riga) was finally delivered in April 2000, more than one year behind the original schedule. The frequencies (87-115 GHz) correspond to emission from the high field side of TCV. Two high field side antennae are available for the most common midplane positions on plasmas in TCV (Fig. 3.2.7). Despite initial problems with some of the channels, the system became productive essentially immediately after delivery. Since most of the recent experiments were ECCD discharges, this high field side viewing radiometer so far mainly measured suprathermal emission exceeding the thermal background by far. These measurements are in excellent agreement with those from the hard X-ray system, albeit with higher time resolution. An additional low field side quasi-optical viewing system has also been installed for electron temperature measurements. The purchase of a second system, to allow simultaneous low and high field side measurements is under consideration.

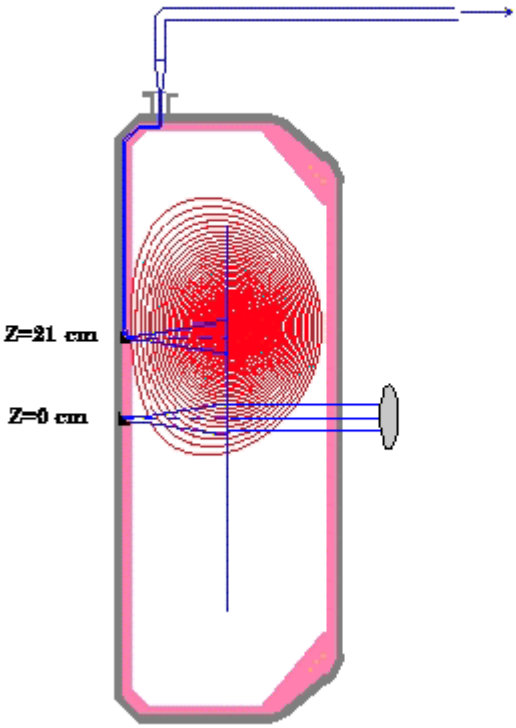

Fig. 3.2.7 ECE antennae on TCV

3.3 X3 System Development

3.3.1 Long pulse gyrotron operation at CEA Cadarache

The pulse length extension beyond 5s on a first series tube for the Tore Supra Tokamak has been carried out in Cadarache with a high voltage power supply compatible with CW operation. After a factory acceptance test performed at reduced pulse length (5s/500kW), the pulse length extension at Cadarache has been at reduced power (350kW) up to 110s. The total energy in the RF pulse of 38MJ is at present the highest value presently achieved world-wide for gyrotrons operating at these frequencies and power levels. Further extension of the pulse length is presently limited by internal gyrotron out-gassing. This enhanced out-gassing might be caused by important RF reflection at the calorimetric load level and a detailed analysis of the possible sources of the out-gassing are presently underway.

3.3.2 TCV series gyrotrons

The last of the three X3 gyrotrons was delivered in November 2000 and is presently being commissioned. A problem on the anode power supply has somewhat delayed the commissioning of this gyrotron. The first of the three gyrotrons was extensively and successfully used in an experimental campaign devoted to absorption measurements of the third harmonic X-mode in presence of second harmonic X-mode pre-heating.

3.3.3 Transmission lines

The mounting of the transmission line system is being completed and will be operational for the next experimental campaign which will begin by May 2001.

3.3.4 Launcher

This launcher is essentially composed of a single mirror onto the surface of which the three RF beams carrying 0.5MW each converge. The combined 1.5MW reflected RF beam is then vertically injected into the plasma. Two degrees of freedom for this mirror allow the independent control of its radial position and the injection angle in the poloidal plane.

A final launcher has been designed and constructed and will be mounted on TCV by the end of April 2001. Figure 3.3.1 shows the X3 antenna for top launch and the three RF beams converging onto the steerable mirror are shown in red.

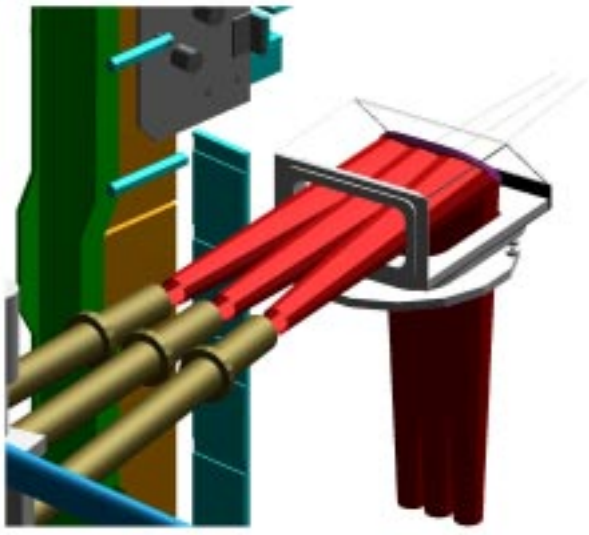

Fig. 3.3.1 X3 top launch antenna

3.4 X2 gyrotrons

During 2000 the full second harmonic system comprising 6 gyrotrons operated on TCV for the first time. The ECH system achieved full power and pulse lengths (2.79MW and 2.0s) into several TCV discharges as well as an extended pulse length regime by staggering the two clusters of 3 gyrotrons in time and achieving >3.4s at 1.4MW.

The second cluster launchers were modified with respect to the initial design installed on TCV. The new launchers removed many of the PEEK pieces, which are susceptible to deformation at high temperatures and to microwave absorption. These pieces were replaced with machinable ceramic. Some of the replacement ceramic pieces were unable to support the stress imposed upon them and resulted in gripping of the launcher. At the end of the 2000 operation on TCV, the launchers were removed and analysed. The ceramic pieces causing the gripping were replaced with PEEK and an additional support was added to reduce stress on these pieces.

As a test of the third harmonic heating a vacuum switch in line number 3 was installed which allowed the sharing of an X2 line and launcher with the first accepted X3 gyrotron. The initial design (1994) of the launcher and line allowed the compatibility of the two systems to test the third harmonic heating of TCV's plasmas.

During the 1999 operating period a gyrotron malfunctioned and was returned to the factory for repairs. The repair work was completed in 2000 and the acceptance test of the gyrotron was performed in November. The tube had an efficiency of >97%, and replaced the second gyrotron (now used as a spare tube) which had the lowest operating reliability. The power supplies providing a DC current in the collector coil magnets were upgraded to a pulsed power supply during the acceptance tests of the repaired tube. The upgrade was performed for the two remaining tubes using the older DC supplies and should increase the reliability of the gyrotrons

3.5 TCV data acquisition and control system

During 2000 the volume of data recorded during each TCV discharge increased by 50% on average, and the number of shots was double that of 1999. The main increase was in the data acquired through the PC-based acquisition modules.

To store these data, two racks of hard disks were installed, with a capacity of 0.5 Tbytes each. This will allow all TCV data to be kept on line (total volume on 31.12.2000: 0.25 Tbytes compressed).

Two computers were brought in operation for data analysis: a 4-processor IBM SP PowerIII2 375MHz and a 2-processor Compaq DS20 at 500MHz. A new centralised backup server now provides archiving and recovery for all the computers on the Lausanne site.

3.6 SULTAN Facility

SULTAN, the unique, high field, large bore test facility, was built as a European contribution to the development program for ITER. The facility has primarily been devoted to the qualification of full-size cable-in-conduit-conductors (CICC) foreseen as potential candidates for use in the Central-Solenoid and the Toroidal-Field Coils of ITER. Fields up to 11T can be imposed to the vertically inserted CICC-Samples. Horizontal insertion of coiled long conductor samples is possible, as demonstrated for the QUELL and for the SeCRETS experiments in the year 2000. Sample currents up to 100kA can be applied by a DC-transformer. Several current sources are available for the pulsed field coils used for AC loss measurements.

The upgrade and unification programme of the SULTAN control system started in 1999 was continued. The major project realised in 2000 was the implementation of the three facility pumping control systems into the Sattline based main facility control system. Concerning the experimental environment, the two race-track shaped pulsed field coils have been replaced by a new pair of saddle shaped pulsed field coils.

3.6.1 Vacuum control system

The SULTAN facility vacuum system can be divided into three different sections. The first one is used for the facility tank itself, housing the split coil magnet system.

The second one is for the test insertion unit where the 100kA transformer and sample are located during normal operation. Separation of both vacuum and cryogenic cycles allows changing the sample without interference to the magnet cooling system. Due to a special sample insertion unit, vertical sample insertion without warming up the whole magnet system is possible. The design cuts down the sample replacement time to a few hours. Including reinsertion, reinstalling of the isolation vacuum and re-cooling, it finally takes about three days until a new mounted sample is ready for measurements. The third vacuum system is used for the He^4 transfer line between refrigerator and facility. The tank vacuum control system, implemented about eight years ago, was based on a DOS running programme written in Pascal, whereas Simatic S5 products controlled the simpler transfer line and the test insertion unit. As a consequence of the good experience with the new control system for both the transformer and magnet cryogenic cycles, and for the unification of the control systems directly related to the facility, the vacuum controls have also been transferred to the Sattline system during 2000. As for the cryogenics, the operator can switch between different modules, representing the three pumping systems. Figure 3.6.1 shows a screenshot of the tank vacuum controlling monitor.

A series of different objects are represented such as: valves (BV, ...) oil diffusion pumps (MHP, ...), rotary pumps (MVP, ...), Pirani sensors for the rough vacuum level (MGH_TPR, MGP, ...) and a Penning sensor (MGH_IKR) for high vacuum level. The active elements are shown in green, whereas the grey symbols represent either closed valves or non-operating pumps. In order to operate the oil diffusion pumps safely, the cooling-water pressure is also monitored. In the case of a sudden pressure increase, the active pumps are immediately switched off, and specified valves are closed in order to prevent the diffusion pump oil from burning. By clicking on most objects new windows are opened, where further actions can be selected. In Figure 3.6.1 a peculiarity of the tank pumping system is shown. It consists of a main pumping station (branch MVP to MHV) and a stand-by one (branch SVP to SHV). The stand-by station is used to save money, when the facility has reached its operation temperature of 4.5K. It is to weak to hold the high vacuum level in transient modes, such as cooling down or warming up, when the cryogenic shields are not fully working. First experience shows the new implementations to Sattline are working very reliably.

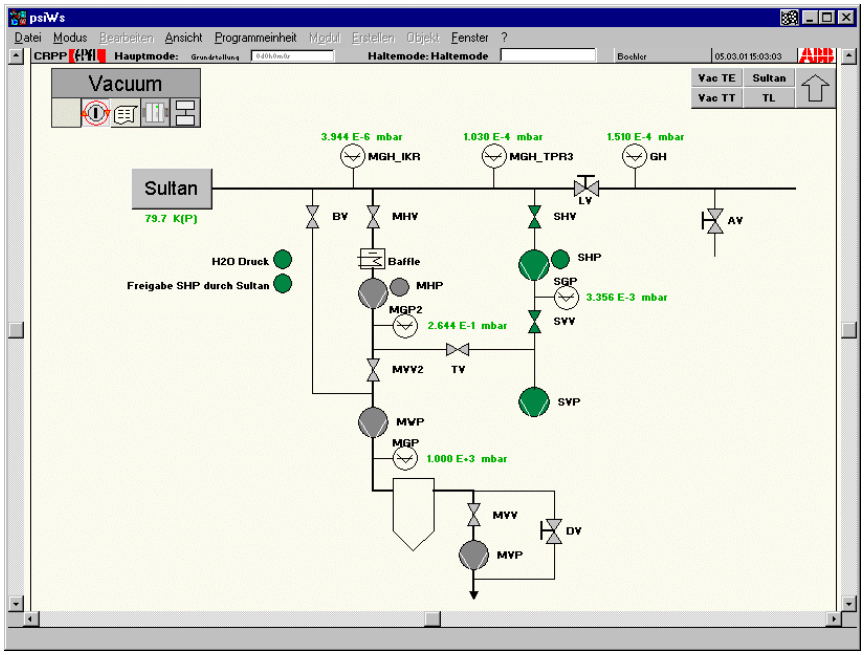

Fig. 3.6.1 Screen shot of the SULTAN facility tank vacuum pumping system control window

3.6.2 Saddle Shaped Pulsed Field Coils

The ITER conductors have to withstand plasma disruptions as well as pulsed operation. The time scale and field change amplitude for normal operation is up to 80 seconds with ΔB between 0.04 and 3T, whereas plasma disruption pulses with amplitudes up to 0.5T may last for more than one second. As a result AC losses due to intra- and inter-strand coupling currents are generated. This directly affects the stability margin of the conductor or joint.

To allow simulation of ITER plasma disruptions, indirect He^4 cooled planar racetrack shaped pulsed field coils were installed into the SULTAN facility in 1997, producing a time varying field perpendicular to both the background field and the conductor sample (see Fig. 3.6.2 for explanation). In order to increase peak field value, repetition rate and active field area, a new pair of saddle shaped pulsed field coils were constructed and built into the facility during 2000. The two series coils are wound with 100 turns each. A copper wire of rectangular shape (4×2mm) and a high Residual Resistivity Ratio of 230 is used (the RRR of the copper stabiliser is defined as the ratio of the electrical resistance of the stabiliser at room temperature to the electrical resistance at the operating temperature and in zero magnetic field. In an external field the magneto-resistance has to be taken into account.). The coils are fully epoxy impregnated. A temperature monitoring system guarantees coil safety. In case of a sinusoidal pulse of ±354A and duration of 40 seconds, the coil temperature is increased from 4.5K to about 50K for example. The resulting re-cooling time of the indirectly helium cooled coils is about 12 minutes, and is about 1/5 of the former waiting time. The peak field value is 0.44T at 500A, and is about twice that of the old racetrack shaped coils. The useful length defined for a field value of 90% B_{max} is 33cm compared to 28cm for the old ones. Compared to the former pulsed field coils, the new arrangement significantly improves the range of pulsed field operation in the SULTAN facility.

Fig. 3.6.2 Schematic view of the saddle shaped pulsed field coils of SULTAN facility (blue shaded). The red-hatched circles indicate the two straight legs of a ITER conductor sample located in the test well (light gray box), separated from SULTAN magnet vacuum system.

3.7 PIREX automation

In collaboration with the ALRO company, the control system of PIREX was partly automated before the beginning of the 2000 irradiation campaign. The new system permanently controls the overall facility and drives some parts of it, such as the LN_2 feeding system. Recording of all the data (temperatures, beam intensity, dose, among others) was redefined and now allows the retrieval of the complete history of an irradiation with a large degree of confidence, since the recording never stops. The main advantage of the new system lies in the fact that the irradiation can be run without personnel on-site and any specific check, in case of stable beam, for about 12 hours. Beam shaping and centring still have to be done on site.

4 INTERNATIONAL AND NATIONAL COLLABORATIONS

4.1 JET

The year 2000 marked an important change in the work and research performed for JET. In the frame of the EFDA structure, the Associations are now directly involved in the scientific operation of the JET tokamak. This is why the CRPP involvement at JET has been significantly increased compared with previous years. The work has focused on two main areas: JET-EFDA 2000 experimental campaigns and JET-EP physics assessment and design work. In addition, the CRPP has detached one person full time at JET to be the Head of the Office of the Associate Leader for JET. One member of the CRPP acted as Leader of the Task Force M specialising in MHD questions.

JET-EFDA 2000 experimental campaigns

The three experimental campaigns at JET in 2000 took place between June and December and were called C1 (June-July), C2 (September-October) and C3 (November-December). Five collaborators from the CRPP participated under "orders" in these campaigns for a total of 221 man-days.

Collaboration with Task Force M (MHD)

The main collaborations related to Task Force M can be grouped in three topics as follows:

A) Sawteeth and NTMs

The fast particles are known to stabilise the sawteeth, in particular those generated by ICRF heating. It is also known that local current drive can strongly influence the sawtooth period. On the other hand the NTMs require a finite size seed island to be destabilised, which is often generated at or near a sawtooth crash. The idea was first to show the direct relation between sawteeth and the NTM, and then to try to destabilise the sawteeth in order to have more frequent smaller crashes and hence smaller seed islands. This program was performed in collaboration with Task Force H. The first experiments showed the possibility of lengthening or shortening the sawtooth period. This was then used to demonstrate the effect on the NTM threshold. The main results are shown in Figs 4.1.1 and 4.1.2. In Fig. 4.1.1 the effect of changing the phase of the RF antennas clearly dramatically changes the sawtooth period. The heating scenario is fundamental H minority heating, at 42MHz, with a plasma current of 2.5MA at 2.5T. The consequent effect on the NTM is important as well, as an NTM is destabilised at the crash after the long sawtooth period, at 16.5s and β_N~1.1, whereas the case with -90° phasing and small regular sawtooth period has no NTMs, even with more than 20MW total heating power.

Another significant contribution from the CRPP to the study of sawteeth is the effect of fast particles from NBI and ICRF, and the effect of plasma shape. Preliminary studies show a similar effect of shape as observed on TCV. The PRETOR transport code has been linked to JET data and has been used to predict the sawtooth period on ITER and is being used to quantitatively simulate the sawtooth periods on TCV and the effect of local ECH and ECCD. However the important part of the sawtooth model in the code, concerning the effects of fast particles has not been tested in detail yet. This is why the comparison with JET is very important. So far, very good

agreement is being found for the NBI cases and we are able to simulate the effects of the fast particle population created by NBI heating on the sawtooth period. This study is being carried out in collaboration with UKAEA Fusion and Princeton Plasma Physics Laboratory.

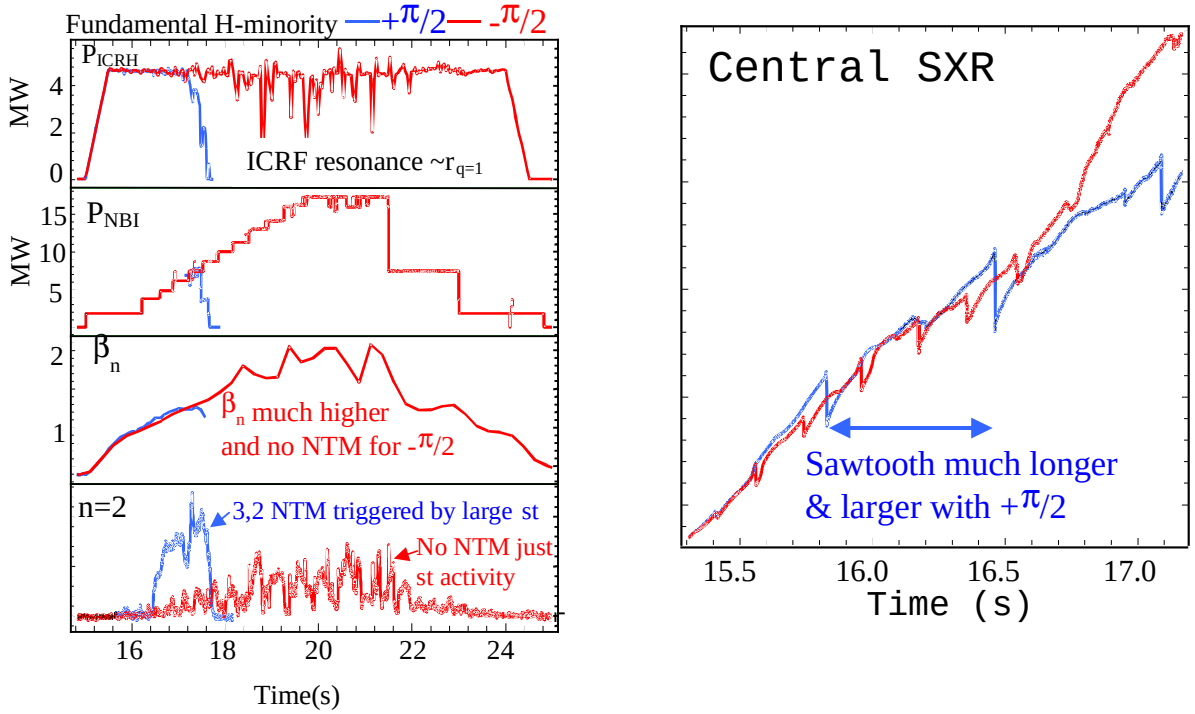

Fig. 4.1.1 Fundamental minority ICRF heating combined with NBI in a 2.5T/2.5MA plasma. The RF resonance is near the HFS inversion radius. Using +90° phasing (or dipole) for the antennas, the central fast particle pressure is increased and the sawtooth period is very long. In this case, a NTM is destabilised at t=16.5 at β_N~1.1 and P_{tot}~9MW (blue case). The NTM disturbs the vertical control system and the plasma is stopped. However with a -90 phasing of the antennas, the fast particles are pushed away from the centre and the sawtooth periods are much shorter. In this case, no NTM is destabilised even at β_N ~2 and P_{tot}~21MW.

B) MHD support for standard and advanced scenarios

In collaboration with other Associations, the CRPP studied MHD activity in these scenarios, contributed to the high speed data analyses of various discharges and have developed tools to analyse the data and to provide an easy interface with the JET data. In particular, the CRPP has contributed to the analysis and to the experimental design of RI-mode, EDA and density peaking experiments, as well as to advanced scenario experiments.

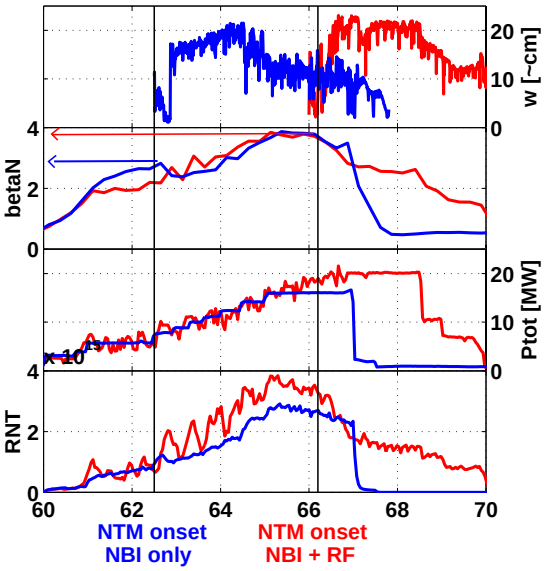

Fig. 4.1.2 NBI only case (in blue) and NBI+ICRH case (in red), for a 1.2T, 1.2MA plasma. With NBI only, an NTM is destabilised with about 7MW of total power, usual for such a low field plasma. Adding 2nd harmonic H minority heating localised just outside the inversion radius, on the HFS, the sawteeth are destabilised and the NTM is destabilised with only 18MW of total power.

C) Effect of ELMs on the plasma vertical control

Another line of research concerned the effect of ELMs on the vertical control system, in particular at high elongation. It has been shown on TCV that the disturbance in the vertical position estimator due to ELMs could be greatly reduced by modifying this estimator, while retaining the correct behaviour when a VDE occurs. The study on JET show that a new estimator can also be constructed for JET and would have these two beneficial properties, as shown in Fig. 4.1.3.

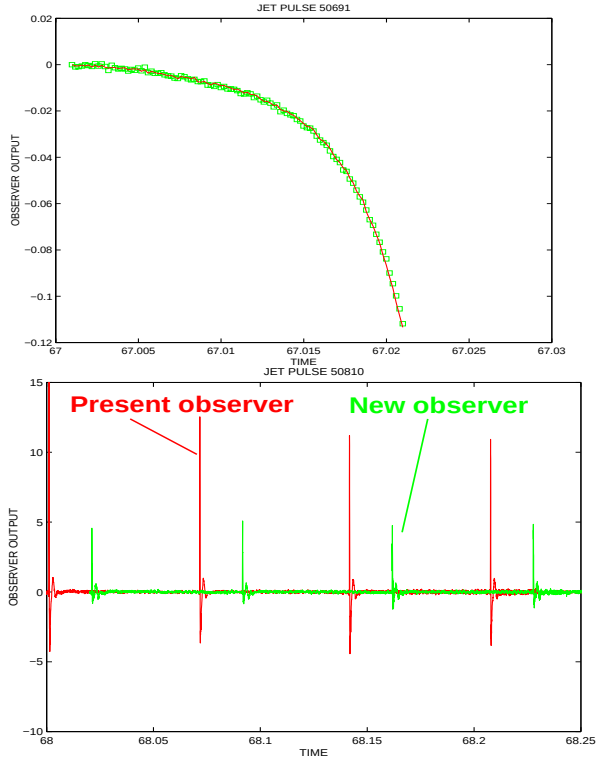

Fig. 4.1.3 New estimator for the vertical position on JET would reduce the disturbances due to ELMs by up to a factor of three, while correctly following the plasma position during a VDE which was onset on purpose for this study.

Collaboration with Task Force E (Exhaust physics)

Participation of CRPP in the activities of the exhaust task force (Task Force E) during 2000 focused on two separate activities:

A. Operation of a retarding field analyser probe head mounted on one of the JET fast reciprocating drives in view of a design study intended to improve the performance of the device under the auspices of a JET Enhancement.

B. Preparation of the scientific programme for the campaign of pure helium discharges planned for 2001.

A) The Retarding Field Analyser (RFA)

A number of attempts have been made over the past few years to successfully operate a retarding field analyser probe head on the JET fast reciprocating probe drive. The RFA is a gridded energy analyser using appropriate bias voltages operating on particles (electrons and ions) entering the device through fine entrance slits of dimensions comparable to the local Debye length in the plasma (typically a few 10's of microns). A suitable choice of swept retarding potential on one grid yields a current on a collector element which is a direct measure of the velocity distribution of the chosen species of particle in a direction parallel to the total magnetic field providing the device is properly aligned. Most often the RFA is used in ion retarding mode, yielding a current-voltage characteristic from which the local parallel ion temperature and sheath potential can be deduced. By nature these devices are rather delicate and difficult to use in the harsh environment of a tokamak with the power of JET.

A number of design iterations at JET led to a device in operation during 1999 but which failed at relatively low power flux densities due to an inappropriate slit design. This was improved slightly by the beginning of 2000, when involvement by CRPP began with some preliminary finite element simulations of RFA slit performance. A number of measurements made with the device over a period of several weeks leading to a series of recommendations for modifications, many of which were implemented throughout the remainder of 2000 ready for testing the in the first experimental campaign planned for early 2001. In parallel, CRPP agreed as part of a JET enhancement project to manufacture a new RFA probe head based on these modifications and to be started following the outcome of tests in 2001 for delivery to JET in late 2001.

B) Preparation of the JET pure helium campaign

In the original planning, only a short time had been allocated to an investigation of pure helium discharges. Towards the end of 2000, a decision was taken to add a fourth experimental campaign and to greatly extend the machine time dedicated to operation in pure helium. This is an important area of study, particularly with regard to plasma-surface interactions and divertor physics, the characters of which change completely in switching from the chemically reactive deuterium fuel to inert helium. CRPP was asked to assume the lead role in the planning and coordination of experiments in pure helium, to be executed in March 2001, and amounting to just over one week of machine time.

Contribution to the JET-EP project

The project of upgrading the JET experiment for 2003-2006 has been supported by the CRPP in many different aspects, the main one being strong involvement in the proposal to install 6MW of ECRH at 113GHz.

The CRPP has also contributed to the physics of JET-EP, in particular to the MHD aspects. In particular, it has been shown that the proposed ECCD system can have a strong effect on the time evolution of the island width of Neoclassical Tearing

Modes. It was also proposed to build a new TAE antenna to couple to higher-n modes, which are deemed to be the most unstable ones in reactor-type tokamaks.

The CRPP has also contributed to the assessment of various diagnostics and has participated in different ad hoc groups responsible of assessing the different JET-EP proposals.

4.2 ITER Tasks and Research & Development

Technology tasks

ITER TASK BL14.2 "Titanium irradiation testing"

An assessment of the tensile, fatigue and fracture toughness performance under irradiation of two titanium alloys for the ITER-FEAT modules is under progress. The two candidate alloys considered are: a classical two-phase Ti6Al4V alloy and a mono-phase alpha alloy Ti5Al2.5Sn alloy. The mono-phase alloy has shown better resistance to irradiation under tensile and fatigue deformation. It has been shown that the difference in behaviour is mainly due to the presence of vanadium in the two-phase alloy. Both alloys have been loaded with different levels of hydrogen at the CRPP and irradiated with neutrons in the test reactor of RISO, Denmark. The synergetic effect of hydrogen combined with irradiation will be studied by measuring the toughness properties. For this purpose a special 3-point bend fixture has been developed. The testing is under progress.

Physics tasks

Neo-classical tearing modes (R&D)

Neo-classical tearing modes (NTM) have been identified in centrally ECH heated low-density discharges on TCV. The island has an m/n=2/1 structure. The modified Rutherford equation for a neo-classical driven mode provides a good description of the evolution at large island width but fails to describe its onset. At the onset two distinct growth phases are observed giving strong evidence for a conventional tearing mode providing the seed island for the neo-classical tearing mode. Therefore, an accurate description requires the reconciliation of conventional and neo-classical tearing modes. The slowly growing conventional seed island allows a precise measurement of the critical island width that is seen to range from 1 to 4cm with the smallest seed islands being observed at the lowest densities.

The effect of plasma shape on sawtooth stability (R&D)

The plasma shape has been found to influence strongly the sawtooth period and amplitude in TCV, an effect emphasised by central ECH power deposition. The pressure profile inside q=1 is found to be essentially determined by Mercier stability, remaining flat at low triangularity and high elongation where the equilibrium is unstable to Mercier and to the ideal internal kink. For these plasma shapes, the increased sawtooth repetition frequency prevents the peaking of the pressure profiles. New measurements at an elongation up to $\kappa=2.8$ show that this flattening persists at these extreme elongation, even though sawtooth activity is below detection level for typically $\kappa>2.5$ and low internal inductance. Plasma shape is therefore one of the ingredients determining sawtooth stability, the sawtooth period and the sawtooth crash size, and could therefore directly influence the generation of a seed-island triggering NTMs.

Other ITER R&D work included the scaling of the sawtooth inversion radius in highly shaped plasmas, H-mode confinement (both reported in Section 2.1) and DINA simulations of TCV equilibria reported in Section 2.1.

4.3 Collaborations with other EURATOM Associations

Y. Peysson, L. Delpech, DRFC, Association EURATOM-CEA, "Temporary installation of an imaging hard-X-ray camera"

W. Treutterer, IPP-Garching, "Modelling the plasma response of ASDEX-UG"

T. Hender, D.C. Robinson, T.N. Todd, UKAEA Fusion, "ST/Sphellamak Hybrid configuration"

B.N. Singh, Riso National Laboratory, DK, "He effects in Fusion Materials and modelling"

4.4 Other International Collaborations

Dr. S.Yu. Medvedev, Keldysh Institute of Applied Mathematics, Academy of Science of Russia, Moscow, "Equilibrium and Stability of 2D and 3D Plasma Configurations" (In collaboration with Drs A.A. Martynov, A.A. Ivanov, Yu.Yu. Poshekhonov, V.D. Shafranov, M. Isaev, A. Subbotin of Kurchatov Institute, Moscow)

K.A. Razumova, V. Andreev, A. Sushkov, Kurchatov Institute, Moscow, “Simulation of ECRH and ECCD in TCV plasmas”

J. Bakos, KFKI, Budapest, "Impurity transport using Laser ablation on TCV"

E. Minardi, Assoc. Euratom CNR, Milano, Italy, "Comparison of predictions of stationary magnetic entropy based theory with TCV data"

A. Sushkov, RRC, Moscow, "Implementation of multiwire proportional X-ray detector for high sensitivity, high speed, high time resolution measurements on TCV"

V. Piffl, IPP Prague, "Collaboration on ultrasoft X-ray spectroscopy"

V.E. Lukash, RRC Kurchatov, Institute of Nuclear Fusion, Moscow, Russia and R.R. Khayrutdinov, TRINITI, Troitsk, Russia, "Simulation of TCV plasma control experiments using the non-linear DINA code"

R. Yoshino, Y. Nakamura, Naka Fusion Research Establishment, JAERI, Japan, D.J.N. Limebeer, J.P. Wainwright, A. Sharma, Imperial College of Science Technology and Medicine, U. London, UK, "Development of a plasma response model for JT-60U"

Y. Nakamura and R. Yoshino, Naka Fusion Research Establishment, JAERI, Japan, "Disruption dynamics in shaped tokamaks"

S. Medvedev, A. Martynov, Y. Poshekhonov, Keldysh Institute, Moscow, M. Isaev, A. Subbotin, M. Mikhailov, V. Shafranov Kurchatov Institute, Moscow, "Equilibrium and Stability of 2D and 3D Plasma Configurations"

D. Monticello, G.Y. Fu, M. Redi, G. Rewoldt, A. Reiman, L.P. Ku, M. Zarnstorff, PPPL, USA, "Design of the NCSX quasi-axisymmetric stellarator"

K. Yamazaki, K.Y. Watanabe, Y. Narushima, H. Yamada, S. Okamura, NIFS, Japan, "LHD and CHS-qa MHD stability analysis"

A. Melnikov, Kurchatov Institute, Moscow, "Heavy Ion Beam probe diagnostic system on the T-10 tokamak"

T. Diaz de la Rubia, B. Wirth, M.J. Caturla, Lawrence Livermore National Laboratory, USA, "Multiscale computer simulations"

R. Odette, G. Lucas, University of California, Santa Barbara, USA, "Small specimen technology and fracture mechanics"

4.5 Collaborations within Switzerland

A. Germond, R. Cherkaoui, Laboratoire de Réseau Electrique, EPFL, "A study of pulsed fusion reactors"

A. Mangili (CSCS), S. Haberhauer (NEC-ESS), Centro Svizzero di Calcolo Scientifico, Manno, "Computation of Stellarator Coils, Equilibrium and Stability"

H. van Swygenhoven, PSI, "The mechanical properties of nanocrystalline metals and computer damage simulations of pulsed irradiation conditions"

F. Groeschel, A. Almazouzi, Group Hot Labo, PSI, "Participation in the European INTERWELD program"

Other collaborations, in the field of plasma processing, are described in detail in Chapter 2.6.

5 THE EDUCATIONAL ROLE OF THE CRPP

The CRPP plays a role in the education of undergraduate and postgraduate students, particularly in the Department of Physics. Advanced education and training in fusion and plasma physics topics is carried out as part of the research activities of the Association. Section 5.1 presents the 7 courses given to physics undergraduates and to engineering undergraduates. In their fourth and final year, physics undergraduates spend time with a research group at the EPFL, typically one day per week for the whole year. During this period, they perform experimental or theoretical studies alongside research staff, discovering the differences between formal laboratory experiments and the “real” world of research. After their final examination at the end of the 4th year, physics students are required to complete a “diploma” work with a research group, typically lasting a full semester. This diploma work is written up and defended in front of external experts. The CRPP plays a role in all of these phases of an undergraduate’s education, detailed in Sections 5.2 and 5.3.

As an academic institution, the CRPP supervises Ph.D. theses, also in the frame of the Department of Physics of the EPFL. Three PhDs were awarded in 2000. At the end of 2000 we had 24 Ph.D. students at the CRPP, mostly in Lausanne but also two in Villigen. Their work is summarised in Section 5.4.

5.1 Undergraduate courses

K. Appert, Chargé de cours – “Plasma physics II”
Option course presented to 4th year Physics students, introducing the theory of hot plasmas via the foundations of kinetic and magnetohydrodynamic theory and using them to describe simple collective phenomena. Coulomb collisions and elementary transport theory are also treated. As a by-product, the student learns to use various theoretical techniques like perturbation theory, complex analysis, integral transforms and solution to differential equations.

N. Baluc, Chargée de cours – “Material Physics”
Basic course on material physics, presented as an option to 4th year Physics students. The course covers the theory of diffusion, dislocation and plasticity as well as the characterisation of materials. Experimental techniques used in materials studies, as well as analysis methods are presented for super-alloys, quasi-crystals, ceramics, composites and polymers.

J.B. Lister, Chargé de cours – “Plasma Physics III”
An introduction to controlled fusion, presented as a one semester option to 4th year Physics students. The course covers the basics of controlled fusion energy research. Inertial confinement is summarily treated and the course concentrates on magnetic confinement from the earliest linear experiments through to tokamaks and stellarators, leading to the open questions related to future large scale fusion experiments.

M.Q. Tran, Professor – “General Mechanics”
Summer semester 2000 (2 hours of lecture and 2 hours of exercises) for the "Microtechnics and Materials" section. The course covers basic Newtonian mechanics of rigid bodies and special relativity.

M.Q. Tran, Professor – “General Mechanics”
Winter semester 2000-2001 (2 hours of lecture and 2 hours of exercises) for the "Communications Systems" section. The course covers kinematics and basic Newtonian mechanics of material points.

M.Q. Tran, Professor – “Plasma Physics I”
An introduction to basic plasma physics, presented as a one semester optional course to 3rd year Physics students. The course treats the fundamental physics of both magnetised and non-magnetised plasmas.

L. Villard, Maître d'Enseignement et Recherche (MER) – “General Physics I-II-III-IV”
An elementary introduction course in physics for engineering students at the EPFL, spanning 4 semesters.

5.2 Undergraduate work performed at the CRPP

EPFL Students

Steve GIRARDIN, "Linked Mirror Stellarator System"

Simon KUENZI, "Diffusivite thermique des electrons"

François MORALES, "Experimental study of DC glow discharges for the deposition of amorphous carbon layers by optical emission spectroscopy and electrical probes"

Exchange students

Raphaël DUQUERROY, ESPEO, Orléans, France, "Analysis of sawtoothing discharges in the TCV tokamak"

Alexei ZABOLOTSKY, Novosibirsk University, Russia. "Assessment of impurity radiation in the TCV tokamak"

Rok DITTRICH, Inst. für Allgemeine Physik, Technische Universität Wien, Austria, "Plasma physics and chemistry of the deposition of nanocrystalline diamond"

Tobias GEMPERLI, ETH-Zürich, "Development of the TCV database software"

Pierre BRIANCEAU, ESPEO, Université d'Orléans, France, "Parametric investigation of powder formation in Hexamethyldisiloxan-Oxygen plasmas"

Damien COSSART, Université Denis Diderot, Paris, France, "Measurement of the transmission and angular variation characteristics of a green interference filter for TCV"

Christophe BONTE, Université Denis Diderot, Paris, France, "Study of the electron cyclotron emission spectra from the TCV tokamak"

5.3 EPFL Diplomas awarded in 2000

Malko Gindrat: “Time-resolved imaging of anodic arc root behavior during fluctuations of a DC plasma spraying torch”. The aim of the diploma work was to study the fluctuations of a Sulzer Metco F4 DC plasma torch used for thermal

spray by time resolved measurements of the arc voltage coupled with end-on imaging of the electrode gap interior using a gated camera. The anodic arc root attachment has been visualized by using a special mask on the optical path to the camera, which cuts off the dominant emission from the arc column. Series of images have been acquired which are synchronized with typical features in the voltage fluctuation signals. For the operation in the restrike mode, three types of attachments have been observed: before major restrikes the arc root is diffuse, just after the major restrike a single, sharp attachment is evidenced and between major restrikes there is a process of creation/vanishing of multiple attachments co-existing during the 1µs exposure time of the camera. In pure argon we showed the effect of various operation parameters such as electrode wear, gas flow, gas injector type and current was evidenced. For worn anodes the attachment sits preferentially in regions where there is erosion on the anode wall, this can be strongly reduced by using a swirl injector. Increasing the gas flow tends to increase the number of simultaneous attachments, whereas increasing the current leads to a thinner and hotter gas boundary layer, which favors diffuse attachment. A so-called “steady mode” was also observed at low gas flows and high current. The results presented in the diploma show the complexity of the nature of the anodic attachment and can be used as new input for numerical modeling.

Lukas STINGELIN: "Discharge phenomena on the PSI high power RF window". A field calculation method is developed using the MAFIA code family to calculate the field distribution at the RF-window as a linear combination of two partial solutions. The size of the problem is reduced considerably this way. A particle tracking code written in Fortran 95 allows the calculation of the electron trajectories in this RF-field. Field filtering is applied at the surface where the electrons start. To improve the accuracy of the trajectories, the program sorts all the necessary information for the search of resonant trajectories and will serve as tool for multipactoring analysis.
In the second part are discharge marks on the ceramic of the RF-window analysed in a SEM with EDX. It is possible to identify the elements Ag and Cu on marks at the air side where an arc must have transported Cu a distance of more than 2cm. No elements could be detected on marks at the vacuum side of the ceramic. A pure chemical analysis showed also there the presence of Ag and Cu. The same methods were applied on thin-film depositions which accumulate in the RF-cavities. The work was carried out in collaboration with Dr. H. Fitze, PSI

5.4 Postgraduate studies

Postgraduate course in the 3^{e} cycle "Physique des plasmas confinés magnétiquement"

This 64-hour course (including exercises) was given during the second semester of the 1999/2000 academic year to 15 students, most of whom were doctoral students at the CRPP. The course consisted of three parts given by different lecturers from the CRPP:

O. Sauter: "*Equilibrium and stability*" (16 hours)
In this introductory part of the course, the derivation and limits of applicability of the Magneto-hydrodynamic fluid equations are discussed, including the two fluid equations and the single fluid model. Toroidal equilibria and their stability are presented, including local criteria and global ideal MHD modes. Resistive and neoclassical effects are treated. The existence of Toroidal Alfven eigenmodes is discussed and finally the properties of stellarators are introduced.

J-M. Moret: "Transport in magnetised plasmas" (20 hours)

This part of the course covered the following subjects: Fusion reactions, requirements on transport; Basic formalism, statistical description of plasma; Coulomb collisions and relaxation processes; Fluid equations of macroscopic quantities; Classical, neoclassical and anomalous transport; Scaling laws, local transport models; Improved confinement regimes; Dynamical approach to confinement.

K. Appert, A. Pochelon, M.Q. Tran, H. Weisen: "Plasma Heating" (16 hours). This part of the course included several different heating methods, but especially Electron Cyclotron Resonance Heating (ECRH) and Current Drive (ECCD) in Toroidal Plasmas, treating the resonance topology and cut-offs in a tokamak to describe accessibility, absorption and refraction. ECCD and ECH are introduced as a tool in tokamaks, and this part of the course finishes with discussions on the future of heating in a reactor.

Doctorate degrees awarded during 2000

Guillaume JOST: "Simulations particulaires d'ondes de dérive dans des configurations magnétiques 3D", EPFL Thesis No. 2174 (2000)
Drift waves are commonly held responsible for anomalous transport in tokamak configurations and in particular for the anomalously high heat loss. The next generation of stellarators on the other hand are hoped to be characterised by a much smaller neo-classical transport and by particle confinement close to that of tokamaks. There is nevertheless a strong interest in the stellarator community to study the properties of drift waves in 3D magnetic configurations. To serve this interest we have developed the first global gyrokinetic code, EUTERPE, aimed at the investigation of linear drift wave stability in general toroidal geometry. The complete 3D model has been successfully validated in toroidal axisymmetric and straight helical geometries and has permitted the first simulation of unstable global ITG driven modes in non-axisymmetric toroidal configurations. As a first application, two configurations have been studied, the Quasi-Axially symmetric Stellarator with three fields periods (QAS3) currently one system under consideration at the Princeton Plasma Physics Laboratory and the Helically Symmetric eXperiment (HSX) which has recently started operation at the University of Wisconsin. QAS3 is characterised by a tokamak-like field in the outer part of the torus. In this structure the drift waves are mainly affected by the magnetic shear and barely by the shape of the plasma. Also, the results are very close to those obtained for a tokamak. On the other hand, results for the HSX configuration, which is characterised by a dominant helical magnetic field, show a clear 3D effect, namely a strong toroidal variation of the drift wave mode structure. However, first results show that the growth rate of the ITG driven mode is largely unaffected by this effect.

Matteo MACCIO: "Effect of ExB flows on global linear microinstabilities", EPFL Thesis No. 2219 (2000)
In the context of theories for anomalous transport in magnetically confined plasmas, there has been recently a great interest on the essential role played by the presence of radial electric fields. It is widely admitted now that microinstabilities are underlying the turbulence that generates the observed transport levels. This work dealt precisely with the effect of radial electric fields on microinstabilities of the Ion Temperature Gradient (ITG) type.
The studies have been performed with a global spectral gyro-kinetic code in tokamak configurations. The results show that radial electric fields have a strong stabilising effect. The mechanism which had been previously identified, namely through a shearing of the mode structure, has been confirmed. Moreover, another new mechanism has been found, in which the stabilisation occurs even for shearless profiles of radial electric field: in this case the mode structure is not sheared, but the position of maximum

mode amplitude is shifted away from the unfavourable (i.e. destabilising) region of the plasma. We have also studied the effect of radial electric field shear in combination with the magnetic shear, including shear-reversed profiles.
Finally, a comparison has been made with the experimental results obtained on the ASDEX-Upgrade tokamak of the IPP Garching, Germany. The results of the global numerical simulation are compatible with the experiment, and we were able to identify, in addition to the stabilising role of radial electric fields, two other physical effects that are of importance (in that they must be included in the theoretical model in order to get agreement with the experiment): the large ion to electron temperature ratio is stabilising, whereas the dynamics of trapped electrons is destabilising.

Pedro Miguel RODRIGUES DE ALMEIDA: "The Order-Disorder Transformation and Microstructure Evolution in Nickel-Aluminium Intermetallics after Heavy-Ion Irradiation", EPFL Thesis No. 2281 (2000)
Nickel-aluminium intermetallics constitute interesting systems for the study of irradiation-induced phase transformations and production of defects. Irradiation of ordered intermetallics may induce disorder or amorphisation depending on the projectile characteristics, irradiation conditions, and chemical and physical properties of the target. The present research was aimed at performing a comparative study of the behaviour of NiAl and Ni_3Al ordered intermetallics under heavy-ion irradiation by combining molecular dynamics calculations of cascade damage with transmission electron microscopy (TEM) observations of irradiation-induced defects (types, densities, sizes). Note that TEM observations have been complemented with image simulations. Polycrystalline thin films of NiAl (or Ni_3Al) deposited on a substrate made of single crystalline nickel have been studied, as well as bulk single crystals. Molecular dynamics calculations showed that NiAl (but not Ni_3Al) should undergo a crystalline-to-amorphous transformation upon a 15keV nickel recoil, but such a transformation was not observed experimentally. This result indicates that the mechanism for crystalline-to-amorphous transformation is driven by accumulation of defects and not by quenching of the cascade itself.

Ph.D. Theses underway at the end of 2000

Clemente ANGIONI: "Tokamak 1D transport modelling: experimental and theoretical basis".
The PRETOR transport code has been modified to simulate the highly flexible ECH system of TCV and interfaced with the TORAY ray tracing code, used to determine the power deposition profile in TCV on a regular basis. This allows to perform time evolution simulations of full EC heated discharges with an automatic, user-friendly procedure. Several transport simulations have been performed in order to explore the effects of ECH and current drive on plasma current profile tailoring, analysing several results obtained in recent TCV experimental campaigns. In particular local effects of current profile modifications close to the $q = 1$ surface have strong influence on the sawtooth period. Detailed analysis of some representative discharges have allowed a convincing validation of a sawtooth period model, and a theoretical understanding of the experimental capability of controlling the sawtooth period with ECH. When current profile modifications are performed involving a broader plasma cross section, the global plasma performance can be changed, and scenarios with improved energy confinement can be obtained. Applying the local Rebut-Lallia-Watkins transport model, discharges with a global confinement exceeding by a factor up to 3.5 the global RLW scaling have been successfully simulated in a majority of cases: this has been explained by the superimposition of two effects, namely the heating power localisation in the low transport central plasma region, created by an off-axis preheating phase, and the current profile tailoring, obtained by an amount of counter current drive which exceeds half of the total plasma current, and which can imply, in the simulations, reversed safety factor profiles.

Juliette BALLUTAUD: "Study of high deposition rate amorphous silicon in Plasma Enhanced Chemical Vapour Deposition (PECVD) reactor for silicon thin-film solar cells".
We used 1D and 2D Radio-Frequency plasma simulations to study the effect of the reactor electrode gap on the deposition rate of amorphous silicon. From these simulations, we have decided to reduce the gap between reactor electrodes from 2.4 cm to 1.3 cm. For the same process conditions of pressure, power and gas flux, the deposition rate increased from 3 _.s-1, in the 2.4cm gap reactor, to 8 4 _.s-1, in the 1.3 cm gap reactor. Samples of amorphous silicon, on wafer substrates and Corning substrates, have been sent to IMT, at Neuchâtel, for material analysis. The amorphous silicon material deposited in our small gap reactor has a good defect density, equal to the defect density of IMT a-Si standard material. But, I.R. analysis has revealed that our material is porous. This porosity is an indication that the plasma chemistry may be modified in the small gap reactor, compared to the one in the 2.4cm gap reactor. New experiments are underway to distinguish between different plasma chemistries, according to plasma parameters and reactor design. At the same time, we are using a computer simulation of the plasma chemistry, with an exact treatment of the diffusion, to help our understanding.

Patrick BLANCHARD: "Study of the suprathermal emission in TCV with electron cyclotron heating"
The Electron Cyclotron Emission (ECE) system on TCV has antennas on the High Field Side (HFS) of the torus that allow us to observe and analyse the EC emission of the plasma coming from the HFS radius. If suprathermal electrons are created, we observed that the EC radiation from the HFS is composed by a thermal part and by a suprathermal part, whose fractions depend of the corresponding optical thicknesses, temperatures and densities. Suprathermal electrons are produced in many experimental conditions, in particular with X2 ECCD and X3 ECH with X2 preheating. We focused this work on the understanding of this radiation from an experimental and a theoretical point of view. In Ohmic plasmas or in pure ECH plasmas, the EC emission comes from the thermal bulk and is proportional to the electron temperature. In ECCD plasmas, the EC emission is no more proportional to the bulk temperature. Experimental evidences show a strong correlation between the EC emission and the angle of toroidal X2 injection i.e. the density and temperature of the superthermal electrons. Current work is aimed at modelling the radiation taking into account a velocity distribution function of the electrons either bi-Maxwellian or as a solution of the Fokker-Plank equation.

Paolo BOSSHARD: “Charge exchange spectroscopy measurements of ion temperature and impurity ion density”
A Charge eXchange Recombination Spectroscopy (CXRS) diagnostic has been installed on TCV for measuring the temperature and the density of the plasma ions. The measurement is based on the spectral analysis of the plasma impurities (mainly carbon) line emission due to the CXR reactions with the high energy neutrals injected into the plasma by a radial diagnostic hydrogen neutral beam injector (50kV of extraction voltage and 0.8A of equivalent current). Initial experiments showed that 20% of the measured signal was due to the CXR reactions between the plasma impurities and the beam neutrals at an average plasma density of $2.10^{19}m^{-3}$, falling to a few percent at $5.10^{19}m^{-3}$.The background CXR emissivity is ascribed to the CXR reactions with the thermal plasma neutrals. The measurements of the background emissivity radial profile showed that it is concentrated in outer quarter of normalised radius and over 20x less in the plasma centre. The S/N ratio for the active CXR signal is of the order of 2-3. The CXRS diagnostic is being equipped with an high aperture monochromator (f/5 instead of f/9) and a back illuminated CCD (quantum efficiency ~80%) for increasing the efficiency of the system and to reduce the photon noise.

Alberto BOTTINO: “Modelling of magnetically confined plasmas”
During the past years, the CRPP theory group has developed several Particle In cell (PIC) codes in 2D and 3D configurations in order to study low frequency electrostatic micro-instabilities. All those codes contain finite Larmor radius (FLR) effects only to second order. A more sophisticated quasi-neutrality equation has been implemented in order to include higher order FLR effects. This was done using a Pade' approximation instead of the second order Taylor expansion in the polarisation density. The new algorithm has been implemented in the linear PIC code L-ORB5. The code was successfully benchmarked against a spectral code. Pade' approximation has been applied also to a version of L-ORB5 containing trapped electron dynamics developed by Dr. T.M. Tran and myself. Here the electrons are modelled using drift kinetic equations, so no finite electron Larmor radius effects are retained. This code has been used to study the transition from Ion Temperature Gradient (ITG) modes to Trapped Electrons Modes (TEM) in the presence of a small wavelength perturbation. The second step of this work was the introduction of an external radial electric field in order to induce a (sheared) ExB flow in the plasma. This seems to play a crucial role in improving the confinement in a localised region of the plasma. The final version of this code will hopefully be a powerful tool for studying the interplay between the sheared ExB flow and the magnetic shear in stabilising drift-waves.

Florian DALLA TORRE: "Mechanical properties of nano-crystalline metals in relation to their microstructure"

The goal of this PhD work is the synthesis of several nano-crystalline fcc type metals, their micro-structural characterisation and the determination of their mechanical properties. As synthesis methods we use Inert Gas Condensation (IGC) and Electrodeposition (ED) both available in our lab. Further we investigate samples produced by Severe Plastic Deformation (SPD). Since nowadays synthesis techniques still don't allow to produce large amounts of homogenous material we built for this purpose a miniaturised tensile testing machine for measuring small 3 mm long specimens. In general, nano-crystalline metals with a typical grain size of 20 nm exhibit much higher yield strength at room temperature and less plasticity compared to their coarse grained counterparts. Intense research on nano-crystalline Nickel made by IGC and ED showed differences in initial microstructure at room temperature as well as a different grain growth behaviour in annealing experiments. While electroplated Ni behaves superplastic with abnormal grain growth when tested in tension at about 300°C, IGC samples still behaves in a brittle manner with normal grain growth. Both materials exhibit an increase in flow stress with increasing strain rate.
More work is planed on electro-deposited Nickel to investigate the relation between grain growth and plastic deformation. Further we are about to investigate the different mechanical behaviour of equilibrium and non-equilibrium grain boundaries of SPD Cu.

Thierry DELACHAUX: ”Study of carbiding and nitriding plasmas in a high current arc reactor, with application to zirconium coating”
We performed wear tests on the coatings obtained last year which showed we had achieved a stable nitriding process. Indeed, our samples could resist to shocks (ceramics vs ceramics) and their yellow gold colour was not alternate during a simulation of a twenty year lifetime in a salt steam atmosphere. This positively concluded the first part of our project which was to investigate the possibilities of treating ceramics in a nitrogen-hydrogen plasma in order to obtain functional surfaces.
From the plasma point of view, experiments showed that the use of hydrogen is crucial to achieve the surface treatment. However, we don’t know the mechanism involved by its presence. It can be important for either the gas phase (chemical reaction between hydrogen and nitrogen, leading to reactive species like NH, for instance) or the surface interaction (« activation » by reacting with the oxygen from

the ceramic leading to vacancies which enhance nitrogen adsorption). To gain more understanding on the role of atomic hydrogen and in order to better characterise our discharge, we began a 1-D chemical modelling of our high current DC discharge in collaboration with the department of physics in Lisbon (Portugal). In the same idea and to test our model we will do measurements by laser induced fluorescence (LIF) on atomic hydrogen and atomic nitrogen during this year.

Christian DESCHENAUX: "Dust Growth mechanisms in reactive plasmas"
We verified the influence of applied power and residence time of hydrocarbon gases on the growth of powders in RF capacitive plasmas. Homogeneous and heterogeneous phases were isolated and characterised by Cavity Ring-Down spectroscopy, Mass Spectrometry, Optical Spectroscopy and Infrared absorption.
We extended our study to reactive plasmas of silane, argon and hydrogen, used to produce polycrystalline layers. We showed the possibility to obtain in-situ information on structure, composition, size and density of powders with adapted deconvolution of infrared absorption spectra. In-situ Photoluminescence and Raman diffusion experiments are underway to confirm the amorphous or crystalline structure of powders.

Gloria FALCHETTO: "Electromagnetic effects on microinstabilities in tokamak plasmas"
The study of electromagnetic effects on ion temperature gradient (ITG) driven instabilities, by means of the electromagnetic extension of the global gyro-kinetic spectral code, GLOGYSTO, has been carried on. Electron dynamics has been taken into account with the drift-kinetic approximation and trapped electrons have also been included. Results show that electromagnetic effects are strongly stabilising ITG modes even taking into account trapped electrons. The study has been also extended to trapped electrons modes (TEM), which are drift waves propagating in the electron diamagnetic direction, showing that finite beta effects have just a little influence, which is not astonishing given the electrostatic character of these instabilities. Finally different magnetic shear profiles have been analysed to study the combined effect of beta and magnetic shear, eventually negative. Results are in good agreement with the electrostatic cases: negative magnetic shear cannot account for a complete stabilisation of ITG modes in presence of trapped electrons, while it does damp TEM.

Jean-Yves FAVEZ: "Non-linear control of a tokamak plasma"
All present-day tokamaks routinely use PID controllers, designed on crude assumptions and tuned by experience. Thus, as a result, the control performance is rather limited. Recently, considerable attention has focused on optimal controllers with enhanced robustness like LQG and H∞(infinity). Although these linear controllers have shown valid results, they usually fail to maintain control in the presence of large disturbances (ELMs). This weakness is due to the saturation of the actuators and can cause considerable damages to the plant. The future work aims at the investigation of non-linear methods, which could avoid this problem by maintaining the tokamak into a stable and save operational domain even if large disturbances occur. A further goal in tokamak control research is to find a way to reduce the power consumption and the ac-losses while maintaining a fast response time. This work is targeted at the TCV, JET and ITER tokamaks. Work has so far concentrated on understanding the modelling of the tokamak and on studying the controllability regions of SISO (single input, single output) systems with a saturated input. This project is carried out in collaboration with the Institut d'Automatique (IA) at the EPFL

Olivier FISCHER: "The behaviour of magnetic field lines and drifts in 3D configurations"
The study of neoclassical transport and α-particle confinement are analysed in 3D reactor designs like the QAS3, the ST/sphellamak hybrid and the sphellamak. We have observed that neither the QAS3 nor the ST/sphellamak are quasi-

axisymmetric configurations. Thus the transport are governed by the helical deformation of the magnetic field strength and these configurations do not confine the trapped α-particles. On the other hand, the sphellamak is a nearly isodynamic structure in the plasma core which leads to good α-particle confinement and the neoclassical transport is very similar to that obtained in a 2D equivalent tokamak.

Ivo FURNO: “Transient transport events in TCV”
During the last year, the major effort has been devoted to understanding the particle transport in the plasma core in the presence of strong Electron Cyclotron Heating (ECH) and Electron Cyclotron Current Drive (ECCD). These methods are used to inject auxiliary power and to drive non-inductive current in magnetically confined plasmas and they are at the origin of the electron density "pump-out". This phenomenon consists in the particle depletion from the plasma core with centrally deposited ECH/ECCD and it may be important for fusion plasmas. In stellarators, the density pump-out is qualitatively explained by neoclassical thermodiffusion arising from the presence of locally trapped particles due to the modulation of the magnetic field in the plasma core. Since in axisymmetrical tokamaks the magnetic field ripple is very small on the magnetic axis with no locally trapped particles in the plasma core, the origin of the density pump-out through neoclassical thermodiffusion has appeared unlikely in this case. In the context of the thesis, we have proposed that the neoclassical processes involving locally trapped particles may account for the density pump-out in tokamaks as well. The presence of a saturated magnetic island, observed in TCV in moderate triangularity discharges, causes the plasma core to be helically displaced. This results in a field modulation along the central magnetic field lines and consequently in the formation of locally trapped particles on the axis which may give rise to a coupled heat and particle transport in tokamaks as well as in stellarators.

Malko GINDRAT: “Experimental study of the behavior of a DC plasma spraying torch operated at low pressure”
This thesis will continue the work on the DC plasma spraying reported as a Diploma project in this section.

Laurent KLINGER: “3D numerical simulation of a plasma torch using a finite volume method”
In order to obtain a 3D numerical simulation of a stationary electrical arc inside a plasma torch, we use a fluid model assuming local thermodynamical equilibrium. So, we consider the full Navier-Stokes equations, supplemented by an equation for the electrical potential and magnetic field calculation using Biot-Savart law. Ohmic heating, j x B and the temperature dependence of the electrical conductivity link the fluid and electrical part. These equations are solved using the fluid mechanics code NSMB, which was further developed to suit our needs. It implements a finite volumes method, and runs on parallel computers, which is required for the large computations demanded. We tested our code on fully 3D flows for which the stream direction is perpendicular to the arc column. Arc core temperatures, voltages and displacements due to the flow were consistent with published experimental work. Nevertheless, the arc shape first obtained was incorrect due to a numerical effect enhanced by the strong non-linearity of the system.

David MAGNI: “The chemistry in a hexamethyldisiloxane (HMDSO) plasma and consequences for the deposition of silicon oxide”
The complementarity of in situ infrared absorption spectroscopy and mass spectrometry allows a clear description of the most abundant neutral species produced in oxygen diluted hexamethyldisiloxane (HMDSO) rf plasmas. In oxygen dilution conditions, the infrared spectra reveal the presence of oxidation steps of the methyl-groups: formaldehyde (COH2), formic acid (CO2H2), CO and CO2 and water as combustion products. The presence of methane (CH4) and acetylene (C2H2) indicates the presence of hydrocarbon chemistry. The methyl radical (CH3) is shown to be the most important precursor for the formation of the species

mentioned above. Infrared spectra clearly show that all the species produced under different dilution conditions (O2/HMDSO), except CO2, are mainly the result of homogeneous reactions between oxygen and CHx for $1 \leq x \leq 3$. It is shown that CO2 also comes from the reaction between oxygen and the carbon present on the surface of the reactor (heterogeneous reaction). This effect dominates at high dilution conditions (flow ratio [O2]/[HMDSO]>>10). The partial fragmentation of the HMDSO molecule and the heterogeneous contribution of the CO2 in the plasma imply that carbonated radicals contribute to the growing film and confirms that oxygen concentration strongly influences the carbon concentration in the deposit.

Adriano MANINI: “Dynamic response of plasma temperature to additional heating”
During the year 2000, the work aimed to develop a robust method to experimentally determine the ECH power deposition focused on the analysis of the plasma response during modulated ECH, using a DiaMagnetic Loop (DML), and at the ECH shut off, using soft X-ray measurements. The analysis of the soft X-ray emissivity at the ECH shut off allowed the development of an approximate but fast method to rapidly determine the deposition location. The method has still to be tested on electron temperature measurements. The analysis of the DML data allowed the determination of the absorbed ECH power in the frame of the first third harmonic X-mode (X3) heating in TCV. These measurements showed that full absorption was achieved for the 470kW of injected X3 with as little as 350kW of X2-CO-ECCD preheating. This high absorption exceeded the TORAY predictions by a factor higher than 2. The sensitivity of the newly installed ECE system to fast electrons limited the use of this diagnostic for the plasma dynamic response analysis. A collaboration with ASDEX-Upgrade has been planed for the beginning of the year 2001 in order verify the diagnostic possibilities for the future work on TCV.

Andrei MARTYNOV: “MHD activity of tokamak plasmas”
The dependence of internal kink growth rate on tokamak plasma current and shape parameters has been studied. The numerical equilibrium code CHEASE and the ideal MHD stability code KINX were used. The stabilising effect of triangularity on the ideal internal kink mode has been demonstrated. It has been shown that in the high aspect ratio limit the high triangularity (both positive and negative) can lead to stabilisation of the internal kink mode destabilised by high elongation (kappa > 1.8). This effect is less pronounced in the case of real aspect ratios, but at lower elongations (kappa ~ 1.5) it can be studied experimentally on TCV. The appoximative scaling of the dependence of ideal kink growth rate on plasma shape and current profile parameters has been proposed.

Petri NIKKOLA: “Simulations of electron cyclotron wave propagation in TCV”
A study of electron cyclotron driven current in plasmas with a small or vanishing toroidal electric field, E, has been made. The current drive efficiency [A/W] was evaluated for different toroidal launching angles using both experimental and theoretical methods. Also, a comparison between a linear model for the EC current calculation (code TORAY) and values obtained from the loop voltage, corrected by the bulk plasma temperature to compensate different plasma conductivities, was performed. It was found that the theoretical values are close to the experimental values with small and moderate launching angles but with large parallel wave numbers the code underestimates the efficiency. This is most probably due to the interplay between the toroidal electric field and the hot electron tail created by the EC waves because, in the case of vanishing E, the results were consistent even with a large toroidal launching angle, 35 degrees The neoclassical plasma conductivity was also found to be smaller than the experimental value, the difference most probably being due to the hot plasma conductivity.

Pavel POPOVITCH: “Electromagnetic waves propagation in 3D plasma configurations”
The subject of this research is the study of the electromagnetic wave propagation in three-dimensional plasma configurations. One of the possible applications of this

work is the optimisation of low-frequency plasma heating systems in stellarators. The aim is to develop a 3D code that will allow for the calculation of perturbed electromagnetic potentials, fields, and energy deposition in a plasma at low frequencies (Alfvén, ion-cyclotron frequency) when the wavelength becomes comparable to the plasma dimensions. At these frequencies, a homogeneous plasma approximation is not applicable, so a solution of a full wave equation, with an inhomogeneous dielectric tensor, is necessary. The equation is to be solved numerically, applying Fourier decomposition in the poloidal and toroidal angles and finite elements discretisation in the radial direction. We are presently expanding the equations in a Boozer magnetic coordinate frame applying the transformation algorithms employed in the TERPSICHORE code to treat 3D equilibria produced with the VMEC code. We have tested this procedure for large aspect ratio tokamak configurations.

Holger REIMERDES: "MHD stability limits in TCV plasmas"
In the course of this thesis several MHD stability limits are investigated in TCV. Recent work focused on the onset of neoclassical tearing modes, which are believed to impose the most restrictive pressure limit in a future fusion reactor such as ITER. Neoclassical tearing modes were identified by the characteristic beta dependence of their saturated island width. Measurements with the magnetic probes as well as the soft X-ray diodes has revealed a m/n=2/1 island structure. A detailed analysis of the island evolution at the onset of the mode shows two growth phases, which is consistent with a conventional tearing mode triggering the neoclassical growth, providing the first experimental evidence for such a trigger mechanism. The slowly growing seed island also allows an accurate measurement of the critical island width, which range from 1 to 4 cm increasing with increasing density. All discharges had a similar ion Larmor radius and no beta dependence was observed.

Edgar SCAVINO: “Impurity transport measurements using laser ablation of impurities”
The study of impurity transport in TCV plasmas is carried on. A fully operational laser ablation system produces short puffs of known, non recycling impurities whose e.-m. emissions are collected by other existing diagnostics, above all the soft X-ray tomography. The decay of the raw line integrated signals provides the value of the global confinement time for impurities, whose behaviour is evaluated for different plasma geometries. Scans of density, elongation, and triangularity have been made and the global confinement time has been compared to the electron energy confinement time. Remarkably this parameter decreases in highly elongated plasmas, as well as the ratio tau_imp/tau_e, whose low values are important from a reactor point of view. In order to quantify the transport parameters (namely the radial profile of diffusion coefficient and velocity drift) of the impurities, the particle transport code STRAHL is systematically being used. The simulation of the fast influx phase and of the decay of the impurities density and the calculation of the corresponding X-ray emission is done. The transport parameters are sought in order to reproduce the actual signals measured in actual impurity injections.

Marco WISCHMEIER: "Modelling of the TCV divertor region"
For some time, simulation of TCV diverted configurations have been performed using the fluid-Monte Carlo code package, B2-Eirene under the auspices of a collaboration between B2-Eirene and A. Loarte of EFDA-CSU Garching. The success of this work led naturally to a requirement that the code be installed at CRPP and this, together with transfer of the detailed knowledge required to run the code, was accomplished during a four week visit to IPP Garching in August-September of 2000. The code currently exists in two versions, SOLPS4.0 and SOLPS5.0, both of which are now installed on the CRPP's IBM 9000. The previous simulations run by Dr. Loarte on TCV detachment shots have been successfully reproduced at CRPP and work is now beginning on refinements to these runs, in particular including the effects of molecular ions. In parallel, effort is now being devoted to participating in

the European B2-Eirene modelling effort in support of divertor physics experiments on the EFDA-JET facilities. This is expected to constitute a large part of the thesis research. Experimentally, the two TCV ASDEX-type in-vessel fast pressure gauge feed-throughs have been redesigned and the gauges successfully installed on the machine ready for operation during the next experimental campaign. Thanks to a second set of power supply and control electronics on loan from JET, both gauges will for the first time be able to be operated simultaneously.

Zhongwen YAO: "Mechanical properties and microstructure of irradiated metals"
In the present work, the following model metals are considered: Nickel, for its still unexplained peculiar microstructural behaviour under irradiation, as well as Copper and Palladium, which radiation induced microstructure is well clarified and allow for the exploration of the dislocation interaction with radiation induced damage. Irradiation of pure Nickel single crystal has been performed to 0.1dpa at room temperature. Tensile tests of un-irradiated Nickel were done for future comparison with tensile tests of irradiated Nickel. The shear stress-shear strain curves show a critical yield shear stress in agreement with values found in the literature. TEM observations of deformed specimens revealed typical dislocation cells. Average cell diameter was measured. Un-irradiated copper single crystal has been strained in situ in the TEM after a careful design of the specimen crystallographic geometry. It shows clearly how dislocation interactions take place. TEM image simulations of split dislocations in copper were performed in order to explore the limits in identifying and resolving small crystal defects. It appears that for a TEM observation using weak a convergence angle of 5mrad or more drastically improves the visibility of partial dislocations. Copper single crystal specimens with TEM in-situ geometry were prepared for irradiation to 0.001dpa at room temperature.

Alexei ZABOLOTSKY: "Particle transport in TCV"
The goal of this work is to understand the particle transport phenomena in both Ohmic and electron cyclotron heating plasma conditions. Using the technique of impurity injection and one-dimensional transport modelling with the STRAHL code the radial dependence of transport parameters were obtained for Ohmic plasmas. The next step includes the investigations of the behaviour of electron density profiles in a variety of on-axis and off-axis ECH and ECCD discharges in order to understand the phenomenon referred to as 'density pumpout', when the electron density profile becomes strongly hollow, allowing explanations in terms of changes to the diffusion coefficient to be excluded.

6 PUBLIC AWARENESS OF FUSION RESEARCH

Public awareness of fusion research is becoming increasingly important in a democratic society where a strong dialog between citizen and researcher is mandatory in fields which will have strong impacts on the society. The CRPP has played a leading role in one aspect. During 1999-2000, we produced a 3D virtual model (a film made from computerised animated pictures called "The Starmakers"), in which we could see the infrastructure of a type of reactor, based on today's understanding of a fusion reactor. This film gives an excellent idea of the dimension of such a device by walking into the heart of the reactor vessel, by visiting the different areas, such as the cryogenic circuit of the superconductor-magnets, the auxiliary systems, the computer centre, the fuel storage area and the remote handling systems to change or repair components in situ.

This movie, romantically named "The Starmakers", was totally produced by a computer and is a 3D real virtuality, where the audience is transported into the heart of a fusion reactor. It was produced by the CRPP, with the support of the European Commission, Direction de la Recherche. The images were computerised by Digital Studio SA (Paris) based on the ITER CAD integrated design produced in the Catia system, with the assistance of the ITER team. It was shown in 3D at the Hannover Universal Fair from June to November 2000, which attracted 250'000 to 300'000 visitors. The movie was sited alongside some experimental hardware from IPP Garching, in the Theme Park for energy.

"The Starmakers" was selected for the first International Scientific Film Festival in Beijing (Oct-Nov. 2000) in relation to the impact of virtual reality on the popularising of science, as well as for the Québec Festival of Scientific Film (Nov. 2000). The movie was screened in 3D at the "Journée sur la Fusion" at the EPFL in June 2000 and also in 3D at the IAEA International Conference in Sorrento in October 2000, together with the Fusion Expo produced in 1998 by the CRPP and the ITER animated model produced by the CRPP in 1999. It was screened in 2D at the SOFT conference in Madrid (September 2000).

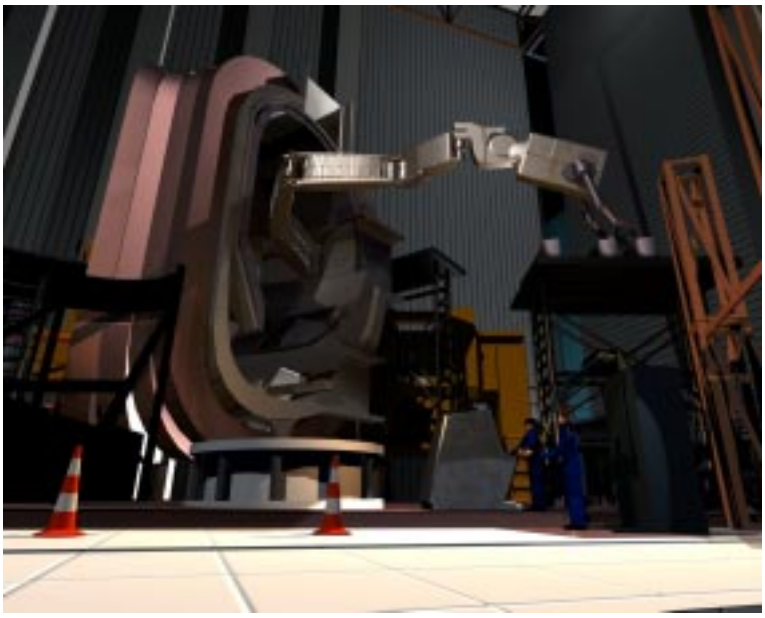

Fig. 6.1 A view of the ITER assembly hall, taken from "The Starmakers"

Although simple pictures of the movie cannot replace the impact of the 3D viewing, Figures 6.1 and 6.2 show typical views taken from the tour around the ITER device.

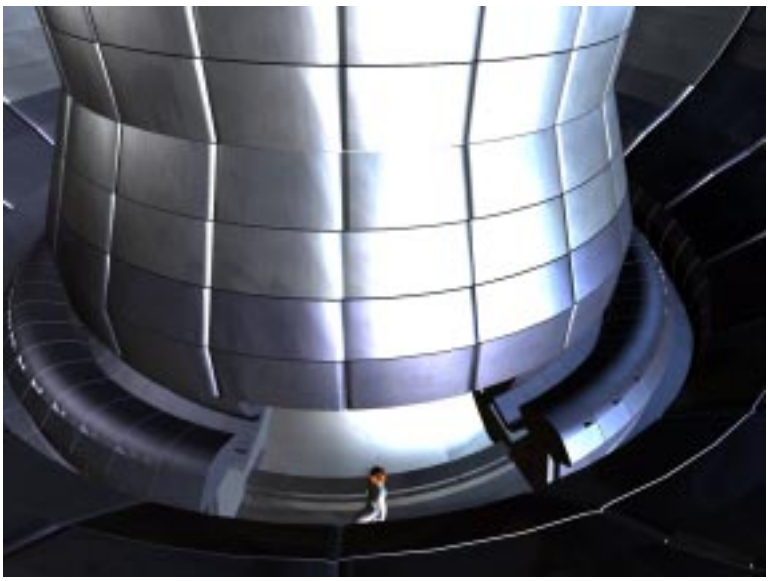

Fig. 6.2 A view of the inside of the reactor vessel, from the film "The Starmakers"

A special invitation at the APS conference in Québec for the APS Division of Plasma Physics Science Teachers' Day workshop "Harnessing the Energy of the Stars" allowed us to introduce a new CD-ROM. This was developed at the CRPP in 1999 in collaboration with the Trilateral Euregio Cluster and released in June 2000, for individual and classroom use. The CD-ROM has now been produced in English, German, French, Spanish, Italian and Portuguese. In addition "The Starmakers" movie of a fusion research experimental reactor, made entirely on virtual animation basis, was shown in VHS video projection).

As well as these large scale public relations exercises, a large number of visitors were welcomed to the CRPP as every year, about 800 visitors during 2000. They are guided throughout the experimental areas, principally in visits dedicated to the TCV tokamak as well as to the industrial plasma processing facilities. These visits range from school classes, through technical college classes, groups visiting the EPFL for other meetings and visits from specialists from industry and research in our specific fields of interest. All of these activities are designed to improve and enhance the communication of the motivation and progress in our field to the public at large.

APPENDIX A Articles Published in Scientific Reviews During 2000

Anghel A., Jakob B., Pasztor G., Wesche R., Vecsey G., Bieri H., Baumann H., Hansen F.X., "Design, construction and operatio of a neon refrigeration system for a HTS power transmission prototype cable", To be published in Proceeding of the International Cryogenic Materials Conference, Montréal, Canada, July 1999, Advances in Cryogenic Engineering, 45, Kluver Academic, 2000

Anghel A., Jakob B., Pasztor G. Wesche R., Fuchs A., Vécsey G., "Design, construction and operation of a neon regrigeration system for a HTS power transmission cable", Advances in Cryogenic Engineering, 45, Plenum Press, 2000

Angioni C., Sauter O., "Neoclassical transport coefficients for general axisymmetric equilibria in the banana regime", Phys. of Plasmas 7(4), 1224 - 1234 (2000), Errata 7(7), 3122 (2000)

Bailat C., AlMazouzi A., Baluc N., Schäublin R., Gröschel F., Victoria M., "The effects of irradiation and testing temperature on tensile behaviour of stainless steels", J. Nucl. Mater., 283-287, 731 – 735 (2000)

Baluc N., Schäublin R., Bailat C., Paschoud F., Victoria M., "The mechanical properties and microstructure of the OPTIMAX series of low activation ferritic-martensitic steels", J. Nucl. Mater., 283-287, 731 – 735 (2000)

Bottura L., Marinucci C., "Two-channel analysis of QUELL experimental results", IEEE Trans. Appl. Supercond., 10, 1:1106-1109 (2000)

Brazis R., Raguotis R., Moreau Ph., Siegrist M.R., "Enhanced third-order nonlinearity in semiconductors giving rise to 1 THz radiation", Int. J. of Infrared & Millimeter Waves 21(4), 593-602 (2000)

Bruzzone P., Fuchs A.M., Vecsey G., Zapretilina E., "Test results for the high field conductor of the ITER central solenoid model coil", Adv. Cryog. Eng. 45, 729-739 (2000)

Bruzzone P., "Manufacture and performance results of an improved joint for the ITER conductors", Adv. Cryog. Eng. 45, 737-744 (2000)

Bruzzone P., "Stability under transverse field pulse of the Nb3Sn ITER cable-in-conduit conductor", IEEE Trans. Appl. Supercond. 10, 1062-1065 (2000)

Bruzzone P., "Hysteresis and coupling losses in superconductors", Wiley Encyclopedia of Electrical and Electronic Engineering, Suppl. 1, 233-248 (2000)

Bruzzone P., "Superconductors, forced flow conductor manufacture", Wiley Encyclopedia of Electrical and Electronic Engineering, Suppl. 1, 643-665 (2000)

Bruzzone P., Shikov A., Vorobieva A., Specking W., Nijhuis A., "Characterization tests of the Nb3Sn cable-in-conduit conductors for Se.C.R.E.T.S.", IEEE, ASC 10, 1086-1089 (2000)

Bruzzone P., Vecsey G., Shikov A., Pantsyrny V., Sytnikov V, Oswald B., Strasser H., Nijhuis A., Nordmann N., "Se.C.R.e.T.S. A stability experiment on the role of segregated copper in Nb3Sn cable-in-conduit conductors", IEEE, ASC 10, 1082-1085 (2000)

Buttery R.J., Gunter S., Giruzzi G. et al., Sauter O., "Neoclassical tearing modes", 27th EPS Conference on Controlled Fusion and Plasma Physics, Budapest, Hungary, June 2000, Plasma Physics and Controlled Fusion 42, Suppl. 12B, B61-73, 2000, ISSN 0741-3335

Charles C., Degeling A.W., Sheridan T.E., Harris J.H., Lieberman M.A., Boswell R.W., "Absolute measurements and modelling of radio frequency electric fields using a retarding field energy analyser", Phys. Plasmas 7, 5232 (2000)

Coda S., Porkolab M., Burrell K.H., "Decorrelation of edge turbulence at the transition from low- to high-confinement mode in the DIII-D tokamak", MIT Report PSFC/JA-99-27, Phys. Lett. A 273, 125-131 (2000)

Coda S. and TCV Team, Peysson Y (CEA Cadarache), Sushkov A. (Kurchatov Institute, Moscow), "High power ECH and fully non-inductive operation with ECCD in the TCV tokamak", Invited paper presented at, 27th EPS Conference on Controlled Fusion and Plasma Physics, Budapest, Hungary, June 2000, Plasma Physics and Controlled Fusion 42, Suppl. 12B, B311-B321, 2000, ISSN 0741-3335

Cooper W.A. with Groups from, PPPL, IPP Greifswald, Oak Ridge, Columbia University, Texas University, NIFS Nagoya, ANU-PRL Canberra and, Kurchatov Institute, presented by A .Reiman, "Physics Design of a high b quasi-axisymmetric stellarator", Special issue: Invited papers from the 26th EPS Conference on Controlled Fusion and Plasma Physics, Maastricht, The Netherlands, June 1999, B273-B283, 41, Suppl. 12B, December 1999, ISSN 0741-3335, and, Proc. on EPS Website (http://epsppd.epfl.ch/),

Cooper W.A., "Stability of a compact three-period stellarator with quasiaxial symmetry features", Physics of Plasmas 7(6), 2546 - 2553 (2000)

Cooper W.A., "Local three-dimensional MHD stability in equilibrium optimized coordinates", Plasma Physics Reports 26(8), 641 - 645 (2000)

Cooper W.A., Todd T.N., Allfrey S., Hender T.C., Robinson D.C., "Effect of helical coils on the magnetic field and the stability of a compact toroidal plasma", Plasma Phys. and Contr. Fusion 42, 1105 – 1121 (2000)

Cooper W.A., Fischer O., "Stability and a-particle confinement in the sphellamak reactor concept", EPFL Supercomputing Review 12, 22 – 28 (2000)

Coutlis A., Limebeer D.J.N., Wainwright J.P., Lister J.B., Vyas P., "Frequency response identification of the dynamics of a tokamak plasma", IEEE Transactions on Control Systems Technology 8, 646 (2000)

Cuenat A., Schäublin R., Hessler-Wyser A., Gotthard R., "Structural analysis of Ni implanted Al: amorphous zones and short range order", Ultramicroscopy, 83, 179 – 191 (2000)

deAlmeida P., Schäublin R., Almazouzi A., Victoria M., Lévy F., "Microstructure and growth modes of stoichiometric NiAl and Ni3Al thin films deposited by rf-magnetron sputtering", Thin Solid Films Journal, 368, 26 – 34 (2000)

DeAlmeida P., Schäublin R., AlMazouzi A., Victoria M., "Quantitative long-range-order measurement and disordering efficiency estimation in ion-irradiated bulk Ni3Al using cross-sectional conventional transmission electron microscopy", Appl. Phys. Lett., 77, 2680 – 2682 (2000)

Diaz de la Rubia T., Zhib H.M., Kraishi T.A., Wirth B.D., Victoria M., Caturla M.-J., "Plastic flow localization in irradiated materials: A multiscale modeling approach", Nature 406, 871 (2000)

Falchetto G.L., Vaclavik J., Maccio M., Brunner S., Villard L., "Applicability of the ballooning transform to trapped ion modes", Physics of Plasmas 7(4), 1196 -1203 (2000)

Fischer O., Cooper W.A., Villard L., "Magnetic topology and guiding centre drift orbits in a reversed shear tokamak", Nucl. Fusion, 40(8), 1453 – 1462 (2000)

Franz D., Hollenstein M., Hollenstein Ch., "Diborane nitrogen/ammonia plasma chemistry investigated by infrared absorption spectroscopy", Thin Solid Films 379, 37 (2000)

Fu G.Y., Ku L.I., Cooper W.A., Hirshman S.H. Monticello D.A., Redi M.H. Reinman A. Sanchez R., Spong D.A., "MHD stability of compact stellarators", 41st Annual Meeting, APS Division of Plasma Physics, Seattle, Washington, USA, November 1999, Phys. of Plasmas 7(5), 1809 – 1815 (2000)

Giacometti E., Baluc N., Bonneville J., "Creep behavior of icosahedral Al-Cu-Fe", Mat. Sci. & Eng. A, 294-296, 777 – 780 (2000)

Gupta B., Hilborn J., Hollenstein C., et al., "Surface modification of polyester films by RF plasmas", J. Appl. Polym. Sci., 78(5), 1083 – 1091 (2000)

Hofmann F., Favre A., Isoz P.-F., Martin Y., Moret J.-M., Nieswand C., "Vertical position control in TCV: Comparison of model predictions with experimental results", Nuclear Fusion 40(4), 767 - 774 (2000)

Hollenstein Ch., "The physics of dusty plasmas", Plasma Phys. & Contr. Fusion 42, R93 (2000)

Jaun A., Fasoli A., Vaclavik J., Villard L., "Stability of Alfvén Eigenmodes in optimized tokamaks", (Invited talk at the 6th IAEA Technical Committee Meeting on Energetic Particles in Magnetic Confinement Systems in Naka, Japan, October 1999), Nucl. Fusion 40(8), 1343 (2000)

Lister J.B., Bruzzone P.L., Costley A.E., Fukuda T., Gribov Y., Mertens V., Moreau D., Oikawa T., Pitts R.A., Portone A., Vayakis G., Wesley J., Yoshino R., "Technical issues associated with the control of steady-state tokamaks", 2nd IAEA Technical Committee Meeting on Steady-State Operation of Magnetic Fusion Devices, Fukuoka, Japan, October 1999, Nuclear Fusion 40(6), 1167 - 1181 (2000)

Luppo M.I., Bailat C., Schäublin R., Victoria M., "Tensile properties and microstructure of 590 MeV proton irradiated pure Fe and Fe-Cr alloys", J. Nucl. Mater., 283-287, 483 – 487 (2000)

Magni D., Deschenaux Ch., Hollenstein Ch., Creatore A., Fayet P., "Oxygen diluted hexamethyldisiloxane plasmas investigated by means of in situ infrared absorption spectroscopy and mass spectrometry", J. Phys. D: Appl. Phys. 34, 87 (2000)

Marmy P., Leguey T., Belianov I., Victoria M., "Tensile and fatigue properties of two titanium alloys as candidate materials for fusion reactors", J. Nucl. Mater., 283-287, 602 – 606 (2000)

Neilson G.H., Reiman A.H., Zarnstorff M.C., et al., Cooper W.A., "Physics issues in the design of high-beta, low-aspect-ratio stellarator experiments", 41st Annual

Meeting, APS Division of Plasma Physics, Seattle, Washington, USA, November 1999, Phys. Plasmas 7(5), 1911-1918 (2000)

Perrin J., Schmitt J., Hollenstein Ch., Howling A.A., Sansonnens L., "The physics of plasma-enhanced CVD for large area coating: industrial application to flat panel display and solar cells", Invited paper at the 27th European Physical Society Conf. on Contr. Fusion and Plasma Phys., Budapest, Hungary, 12-16 June 2000, Plasma Phys. & Contr. Fusion 42, B353 (2000)

Peysson Y., Coda S., Imbeaux F., "Hard X-ray CdTe tomography of tokamak fusion plasmas", Nucl. Instrum. & Methods in Phys. Res. A., 458, 269 (2000)

Pietrzyk Z.A., Angioni C., Behn R., Coda S., Goodman T.P., Hofmann F., Henderson M.A., Hogge J.-P., Moret J.-M., Pochelon A., Reimerdes H., Sauter O., Weisen H., "Central electron temperature enhancements due to sawtooth stabilization during counter ECCD in TCV", Phys. of Plasmas 7(7), 2909-2914 (2000)

Porcelli F., Angioni C., Behn R. , Furno I., Goodman T., Henderson M.A., Pietrzyk Z.A., Pochelon A., Reimerdes H., Rossi E., Sauter O., "Model for humpback relaxation oscillations", Nuclear Fusion 40(10), 1691 - 1695 (2000)

Redi M.H., Diallo A., Cooper W.A., Fu G.Y., Johnson J.L., Nührenberg C., Pomprehy N., Reiman A.H., White R.B., Zarnstorff M.C., "Robustness and flexibility in compact quasiaxial stellarators: global ideal MHD stability and energetic particle transport", Physics of Plasma 7(6), 2508 - 2516 (2000)

Reimerdes H., Pochelon A., Sauter O., Goodman T.P., Henderson M., Martynov An., "Effect of triangular and elongated plasma shape on the sawtooth stability", Plasma Phys. & Contr. Fusion 42, 629 - 639 (2000)

Rewoldt G., Ku L.P., Tang W.M., et al., Cooper W.A., "Drift mode calculations for the Large Helical Device", Phys. of Plasmas 7(12), 4942 - 4947 (2000)

Sansonnens L., Howling A.A., Hollenstein Ch., "A gas flow uniformity study in large-area showerhead reactors for RF plasma deposition", Plasma Sources Sci. Technol. 9, 205-209 (2000)

Sauter O., Martin Y., "Considerations on energy confinement time scalings using present tokamak databases and prediction for ITER size experiments", Nuclear Fusion 40(5), 955 - 964 (2000)

Sauter O., Henderson M.A., Hofmann F., Goodman T., et al., "Steady-state fully noninductive current driven by electron cyclotron waves in a magnetically confined plasma", Physical Review Letters 84(15), 3322 - 3325 (2000)

Schäublin R., DeAlmeida P., AlMazouzi A., Victoria M., "Quantitative analysis of CTEM images of small dislocation loops in Al and stacking fault tetrahedra in Cu generated by molecular dynamics simulation", J. Nucl. Mater. 276(1-3), 251-257 (2000)

Schäublin R., Victoria M., "Differences in the microstructure of the F82H ferritic/martensitic steel after proton and neutron irradiation", J. Nucl. Mater., 283-287, 339 – 343 (2000)

Schäublin R., DeAlmeida P., AlMazouzi A., Victoria M., "Quantitative correlation of TEM images with irradiation induced damage", J. Nucl. Mater. 283–287, 205 – 209 (2000)

Schäublin R., Meng X., Stobbs W.M., "Weak beam under convergent beam illumination", Ultramicroscopy, 83, 145 – 157 (2000)

Song S.-H., Faulkner R.G., Flewitt P.E.J., Smith R.F., Marmy P., "Temper embrittlement of a CrMo low-alloy steel evaluated by means of small punch testing", Mater. Sci. & Eng. A, 281, 75 – 81 (2000)

Spätig P., Odette G.R., Donahue E., Lucas G.E., "Constitutive behavior and fracture properties of the F82H ferritic/martensitic steel", J. Nucl. Mater., 283-287, 721 – 726 (2000)

Victoria M., Baluc N., Bailat C., Dai Y., Luppo M.I., Schäublin R., Sing B.N., "The microstructure and associated tensile properties of irradiated FCC and BCC metals", J. Nucl. Mater. 276, 114 – 122 (2000)

Zanino R., Marinucci C., Santagati P., Savoldi L., "Joint and conductor thermal-hydraulic model validation on the Full Size Joint Sample Experiment", IEEE Trans. Appl. Supercond., 10, 1:1110-1113 (2000)

Zou X.L., Geraud A., Gomez P., et al., "Edge cooling experiments and non-local transport phenomena in Tore Supra", Plasma Phys. & Contr. Fusion 42, 1067-1076 (2000)

APPENDIX B Conferences and Seminars

B.1 Conference proceedings published in 2000

Alberti S., Tran M.Q. et al., "European high-power CW gyrotron development for ECRH systems", Proceedings of the IAEA Technical Committee Meeting on "ECRH Physics and Technology for Fusion Devices and the 11th Joint Workshop on Electron Cyclotron Resonance Heating (EC-11), Oh-Arai, Japan, October 1999, JAERI-memo 12-041, 446 - 455 (March 2000)

Almazouzi A., Spaczer M., Alurralde M., Victoria M., "Amorphisation and order-dirsorder in Ni-Al system under High energy ion-Irradiation: A computer simulation study", To be published in Proceeding of the Int. Conference on Solid-Solid Phase Transformations, Kyoto, Japan, May 1999,

Angioni C., Goodman T.P., Pietrzyk Z.A., Sauter O., "Simulations of improved confinement discharges and sawtooth period with electron cyclotron heating and current drive in TCV", Invited paper, Proc. Joint Varenna-Lausanne International Workshop "Theory of Fusion Plasmas", Varenna, Italy, 28 August - 1 September 2000, ISPP-19, ISBN88-7794-248-7, 73 – 86 (2000)

Ariola M., Lister J.B., Pironti A., "Design and experimental testing of robust MIMO controllers on TCV", Proc. 2000 IEEE Int. Conf. On Control Applications Anchorage, Alaska, USA, September 25-27 September 2000, Paper TA3-6 / 11:10, 419 – 424 (2000)

Bailat C., Almazouzi a., Baluc N., Schäublin R., Groschel F., Victoria M., "The effects of irradiation and testing temperature on the tensile behavior of stainless steels", Proc. 9th Int. Conference on Fusion Reactor Materials, Colorado Springs, USA, October 1999 (2000)

Baluc N., Schäublin R., Bailat C., Paschoud F., Victoria M., "The mechanical properties and microsctructre of the OPTIMAX series of low activation ferritic-martensitic steels", Proc. 9th Int. Conference on Fusion Reactor Materials, Colorado Springs, USA, October 1999 (2000)

Blau B., "NbTi conductor with ITER CSMC geometry", To be published in Proceeding of the Workshop on Short Sample Conductor Test Results, Villigen, Switzerland, June 1999

Bottino A., Tran T.M., Sauter O., Vaclavik J., Villard L., "Linear gyrokinetic simulations using particles for small perpendicular wavelength perturbations", Proc. Joint Varenna-Lausanne International Workshop "Theory of Fusion Plasmas", Varenna, Italy, 28 August - 1 September 2000, ISPP-19, ISBN88-7794-248-7, 327 – 333 (2000)

Carreña-Morelli E., Cheng B.L., Demura M., Schaller R., Baluc N., Bonneville J., "Mechanical loss associated with stress anomaly in Ni3Al and Ni3(Al,TA) single crystals", Proc. Materials Research Society Symp. On Multiscale Phenomena in Materials: Experiments and modeling, Ed. by I.M. Robertson, D.H. Lassila, B. Devincre and R. Philipps, 578, 181 – 186 (2000)

Dammertz G., Alberti S., Arnold A., Giguet E., LeGoff Y., Thumm M., "Cold test measurements on components of the 1 MW 140 GHz, CW gyrotron for the Stellarator Wendelstein 7-X", Proceedings of the IAEA Technical Committee Meeting on "ECRH Physics and Technology for Fusion Devices and the 11th Joint Workshop on

Electron Cyclotron Resonance Heating (EC-11), Oh-Arai, Japan, October 1999, JAERI-memo 12-041, 644 - 653 (March 2000)
Proceeding

Deschenaux Ch., Affolter A., Magni D., Hollenstein Ch., "Investigations of CH4, C2H2 and C2H4 dusty RF plasmas", Société Suisse de Physique, Printemps 2000, Montreux,, Bull. SPG/SSP 17, 30 (2000)

Diaz de la Rubia T., Caturla M.J., Alonso E., Wirth B., Zbib H., Kraishi T., Victoria M., "Multiscale modeling of defect production, damage accumulation and mechanical properties changes in irradiated metals", Invited talk, Proc. 9th Int. Conference on Fusion Reactor Materials, Colorado Springs, USA, October 1999 (2000)

Duchateau J.L., Fillunger H., Fink S., et al, Marinucci C., "Test program preparations of the ITER toroidal field model coil (TFMC)", to appear in Proc. SOFT 2000

Falchetto G.L., Vaclavik J., "Effects of finite β on the linear stability of ion temperature gradient (ITG) driven modes", Proc. Joint Varenna-Lausanne International Workshop "Theory of Fusion Plasmas", Varenna, Italy, 28 August - 1 September 2000, ISPP-19, ISBN88-7794-248-7, 321 326 (2000)

Fischer O., Cooper W.A., Isaev M. Yu., Villard L., "Confinement study of a compact quasiaxisymmetric toroidal system", Proc. Joint Varenna-Lausanne International Workshop "Theory of Fusion Plasmas", Varenna, Italy, 28 August - 1 September 2000, ISPP-19, ISBN88-7794-248-7, 401 – 406 (2000)

Grandgirard V., Agullo O., Benkadda S., Biehler B., Garbet X., Ghendrih P., Sarazin Y., "Impurity transport in flux-driven models of edge turbulence", Proc. Joint Varenna-Lausanne International Workshop "Theory of Fusion Plasmas", Varenna, Italy, 28 August - 1 September 2000, ISPP-19, ISBN88-7794-248-7, 427 – 432 (2000)

Hatzky R., Tran T.M., Könies A., Kleiber R., "Energy conservation for a nonlinear simulation code for ion-temperature-gradient-driven (ITG) modes for the theta-pinch", Proc. Joint Varenna-Lausanne International Workshop "Theory of Fusion Plasmas", Varenna, Italy, 28 August - 1 September 2000, ISPP-19, ISBN88-7794-248-7, 407 – 412 (2000)

Henderson M.A. , Goodman T., Hogge J.-P., Pietrzyk Z.A., Pochelon A., Sauter O., "Poloidally asymmetric plasma response with ECH deposition near q=1 in TCV", Proceedings of the IAEA Technical Committee Meeting on "ECRH Physics and Technology for Fusion Devices and the 11th Joint Workshop on Electron Cyclotron Resonance Heating (EC-11), Oh-Arai, Japan, October 1999, JAERI-memo 12-041, 275 - 281 (March 2000)

Henderson M.A., Goodman T.P., Behn R., Coda S., Hogge J.-P., Martin Y., Peysoon Y., Pietrzyk Z.A., Pochelon A., Sauter O., Tran M.Q., TCV Team, "Initial ECCD and current profile modification experiments on TCV", Proceeding of the 4th Int. Workshop on Strong Microwaves in Plasmas, Nizhny Novogord, Russia, August 1999 (Invited paper), Vol. 1, 114 - 133 (2000)

Hollenstein Ch., "Technological plasmas", Invited paper, Société Suisse de Physique, Printemps 2000, Montreux, Bull. SPG/SSP 17, 28 (2000)

Jost G., Tran T.M., Appert K., Cooper W.A., Villard L., "Global linear gyrokinetic PIC simulations in 3D magnetic configurations", Proc. Joint Varenna-Lausanne

International Workshop "Theory of Fusion Plasmas", Varenna, Italy, 28 August 1 September 2000, ISPP-19, ISBN88-7794-248-7, 143 - 156 (2000)

Kruml T., Spätig P., Martin J.L., "Dislocation core geometry and mechanical strength in Ni3Al compounds", Proc. 12th European Congress on electron Microscopy (EUREM 12), edited by L. Frank and F. Ciampor, Czechoslovak Society for Electron Microscopy, Brno, 65 – 68 (2000)

Kurishita H., Zinkle S.J. , Abe K., Victoria M., Stamm H., Davis J.W., "Technology and radiation effects critique of high temperature refractory alloys", Invited talk at, Proc. 9th Int. Conference on Fusion Reactor Materials, Colorado Springs, USA, October 1999 (2000)

Klinger L., Vos J.B., Appert K., "3D numerical simulation of a plasma torch using a finite volume method", Société Suisse de Physique, Printemps 2000, Montreux, Bull. SPG/SSP 17, 29(2000)

Lister J.B., Martin Y., Fukuda T., Yoshino R., Mertens V., "Control of modern tokamaks, Proceeding 7th Int. Conference on Accelarator and Large Experimental Physics Control Systems", Trieste, Italy, October 1999, ICALEPCS 99, ISBN: 88-87992-00-2, 235 - 239 (2000)

Lister J.B., Bruzzone P.L., Costley A.E., Fukuda T., Gribov Y., Mertens V., Moreau D., Oikawa T., Pitts R.A., Portone A., Vayakis G., Wesley J., Yoshino R., "The technical issues associated with the control of steady-state tokamaks", Proceedings 2nd IAEA Technical Committee Meeting on Steady-State Operation of Magnetic Fusion Devices - Plasma Control and Plasma Facing Components -, Fukuoka, Japan, October 1999, FURKU Report 99-04(65), Vol. 1, 210 - 220 (1999) ISBN 4-87780-007-7

Luppo M.I., Bailat C., Schäublin R., Victoria M., "Tensile properties and microstructure of 590 MeV proton irradiated pure Fe and Fe-Cr alloys", Proc. 9th Int. Conference on Fusion Reactor Materials, Colorado Springs, USA, October 1999 (2000)

Magni D., , "Insitu gas phase and particle diagnostics of hexamethyldisiloxane rf plasmas", Société Suisse de Physique, Printemps 2000, Montreux, Bull. SPG/SSP 17, 30 (2000)

Marinucci C., Bottura L., "Predictive quench initiation analysis of the ITER TF model coil", Proc. ICEC-18, ISBN 81-7319-395-9, 173-178 (2000)

Marmy P., Leguey T., Victoria M., "Tensile and fatigue properties of two titanium alloys as candidate materials for fusion reactors", Proc. 9th Int. Conference on Fusion Reactor Materials, Colorado Springs, USA, October 1999 (2000)

Martynov An., Sauter O., "Dependence of internal kink growth rate on tokamak plasma current and shape parameters", Proc. Joint Varenna-Lausanne International Workshop "Theory of Fusion Plasmas", Varenna, Italy, 28 August - 1 September 2000, ISPP-19, ISBN88-7794-248-7, 387 – 392 (2000)

Nikkola P., Sauter O., "Numerical and experimental studies of electron cyclotron current drive efficiency in plasmas with nearly zero ohmic current", Proc. Joint Varenna-Lausanne International Workshop "Theory of Fusion Plasmas", Varenna, Italy, 28 August - 1 September 2000, ISPP-19, ISBN88-7794-248-7, 345 – 350 (2000)

Pasztor G., Anghel A., Fuchs A.M., Jakob B., Trajkovic D., Vecsey G., Wesche R., Schindler R., "Manufacture and testing of a neon gas-cooled HTS prototype cable

for power transmission", Proc. EUCAS 1999, Inst. Phys. Conf. Ser. No. 167, 1119 (2000)

Sauter O., Goodman T.P., Coda S., Henderson M., Hofmann F., Hogge J.-P., Peysson Y., Pietrzyk Z.A., Pitts R., Reimerdes H., Weisen H., "Sustained fully non-inductive scenarios using pressure and current profile control with ECCD", Proceedings of the IAEA Technical Committee Meeting on "ECRH Physics and Technology for Fusion Devices and the 11th Joint Workshop on Electron Cyclotron Resonance Heating (EC-11), Oh-Arai, Japan, October 1999, JAERI-memo 12-041, 338 - 349 (March 2000)

Schäublin R., DeAlmeida P., Almazouzi A., Victoria M., "Quantitative correlation of TEM images with irradiation induced damage", Proc. 9th Int. Conference on Fusion Reactor Materials, Colorado Springs, USA, October 1999 (2000)

Schäublin R., Victoria M., "Differences in the microstructure of the F82H ferritic/martensitic steel after proton and neutron irradiation", Proc. 9th Int. Conference on Fusion Reactor Materials, Colorado Springs, USA, October 1999 (2000)

Svandrlik M., Pasotti C., Marchand P., Bosland P., Anghel A., "The SUPER-3HC project: An idle superconducting harmonic cavity for bunch length manipulation", EPAC 2000

Vecsey G., "High current conductors for superconducting fusion magnets", Invited paper, Société Suisse de Physique, Printemps 2000, Montreux,, Bull. SPG/SSP 17, 27 (2000)

Victoria M., "The development of structural materials for future fusion reactors", invited paper at, Société Suisse de Physique, Printemps 2000, Montreux,, Bull. SPG/SSP 17, 28 (2000)

Victoria M., "Microstructure and tensile properties of irradiated materials", Invited talk, Proc. 9th Int. Conference on Fusion Reactor Materials, Colorado Springs, USA, October 1999 (2000)

Victoria M., Baluc N., Spätig Ph., "Structural materials for fusion reactors", Proc. 18th IAEA Fusion Energy Conf., Sorrento, Italy, 61 – 65 (2000)

Wesche R., Anghel A., Fuchs A.M., Pasztor G., Vecsey G., "High current applications of high-temperature superconductors", Invited paper, Société Suisse de Physique, Printemps 2000, Montreux, Bull. SPG/SSP 17, 27 (2000)

Zanino R., Marinucci C., Santagati P., Savoldi L., "Joint+conductor thermal-hydraulic model validation on the full size joint sample experiment", To be published in Proceedings of the 16th Int. Conference on Magnet Technology, Ponte Vedra Beach, Florida, USA, Sept./Oct. 1999

B.2 Seminars presented at the CRPP in 2000

Dr. R.A. Pitts, CRPP-EPFL, "Divertor detachment in TCV ohmic discharges"

G. Jost, CRPP-EPFL, "Simulations particulaires d'ondes de dérives dans des configurations magnétiques tri-dimensionnelles"

M. Wischmeier, Inst. für Laser- und Plasmaphysik, Heinrich Heine Univ. Düsseldorf, Germany, "Numerical simulation and emission spectroscopy of a large volume ECR discharge"

Dr. W.A. Cooper, CRPP-EPFL, "A survey of alternate post-TCV confinement concepts and relevant physics issues"

Dr. S. Brunner, Princeton Plasma Physics Laboratory, PPPL, Princeton, USA, "Scheme with evolving background for nonlocal transport simulations"

Dr. J. Stober, IPP-Garching, Germany, "Variation of triangularity of H-modes on ASDEX Upgrade"

Dr. V. Lukash, Kurchatov Inst., Moscow, Russia, "The DINA simulations of TCV discharges"

Dr. L. Sansonnens, CRPP-EPFL, "Modélisation des arcs plasma à pression atmosphérique"

Dr. L. Scibile, CERN, Geneva, Switzerland, "Non-linear control of the plasma vertical position in a tokamak"

Dr. K.A. Razumova, RRC Kurchatov Inst., Nuclear Fusion Inst., Moscow, Russia, "Investigation of the mechanism of internal thermal barrier formation"

Dr. K. Takahashi, RF Heating Lab., RF Facility Div. & JT-60 Team, JAERI, Japan, "Development of ECRF system and initial results of ECRF experiments in JT-60U"

Ch. Perez von Thun, Univ. Heidelberg, Germany, "Influence of trapped particles on the neutron rates of rotating tokamak plasmas"

Dr. X. Litaudon, DRFC-CEA, Cadarache, France, "Rôle du profil courant dans les régimes à barrière interne de transport dans les tokamaks"

Dr. C. Darbos, DRFC-CEA, Cadarache, France, "Présentation du système FCE en cours d'implémentation sur Tore Supra"

Prof. Dr. G. Wolf, Member of the Economic & Social Committee, CE, "Considerations on research and development in Europe – Towards a European Research area"

Dr. B. Blau, Lab. für Hochenergiephysik, ETH-Zürich, Switzerland, "Stability and Quench of Dual cooling channel cable-in-conduct superconductors"

Dr. P. Bak, JAERI Naka Research Establishment, Japan, "The importance of unstable periodic orbits to edge localised mode dynamics"

Dr. A.V. Sushkov, RRC Kurchatov Inst., Nuclear Fusion Inst., Moscow, Russia, "Reconstruction of the ECRH power deposition and electron heat conductivity from SXR intensity evolution after ECRH shut-off in TCV"

Dr. M. Victoria, CRPP/TF-EPFL, "The relation of the mechanical properties to the defect microstructure in irradiated metals"

Dr. V. Piffl, Inst. of Plasma Physics, Ac. of Sciences, Praha, Czech Rep., "Spatially resolved measurements of He- and H-like Carbon line emission on TCV using modified USX spectrometer"

Prof. J. Li, Director, Inst. of Plasma Phys. Ac. Sinica in Hefei, P.R. China, "Recent progress on HT-7 superconducting tokamak and present state of HT-7U project"

Dr. R. Dux, IPP-Garching, Germany, "Measurements of impurity transport coefficients in the confined plasma of ASDEX Upgrade"

Dr. R. Wesche, CRPP/TF-EPFL, "High-current applications of high-T_c superconductors"

Dr. P. Barabaschi, ITER-JCT, Garching, Germany, "An overview of the design of the proposed ITER-FEAT tokamak"

Dr. K. Lackner, EFDA Physics Leader, Garching, Germany, "Transport barriers in electron and ion transport dominated regimes"

A. Zabolotski, CRPP-EPFL, "Analysis of impurity transport in TCV ohmic discharges"

I. Klimanov, Kurchatov Inst., Moscow, Russia, "Small-scale modes in T-10 tokamak"

J. Horacek, Inst. of Plasma Phys. Ac. of Science, Praha, Czech Rep., "Langmuir probe measurements of turbulent structures in CASTOR and divertor target plasmas in TCV"

Dr. E. Bésuelle, CEA-Bruyère-le-Châtel, France, "Use of whistler wave propagation as a diagnostic for strong magnetic fields in very dense plasmas"

Dr. R. Prakash, Inst. for Plasma Research, Bhat, Gandhinagar, India, "SST-1 Update"

S. Ferrando i Margalet, Dept. of Mathematics, Kings Kollege, London, UK, "Geometric aspects of quantum theory"

A. Scarabosio, PSFC, MIT, Boston, USA, "Magnetic field profile measurements for the magnetic reconnection experiment at the Versatile Toroidal Facility"

Dr. N. Lisi, ENEA-Casaccia, Roma, Italy, "High charged ions from laser produced plasmas"

Dr. D. Meade, Princeton Plasma Physics Laboratory, PPPL, Princeton, USA, "FIRE, a next step option for magnetic fusion"

N. Ramasubramanian, Inst. for Plasma Research, Bhat, Gandhinagar, India, "On the influence of an insulator surface in the evolution of a Spark discharge"

Dr. N. Lopes Cardozo, FOM Inst. voor plasmafysica, Rijnhuizen, The Netherlands, "Magnetic turbulence in a tokamak probe with 30 MeV electrons"

M. Hole, School of Electrical & Information Engineering, Univ. of Sydney, Australia, "Plasma phenomena of a vacuum arc centrifuge"

C. Bonté, Univ. Denis Diderot, Paris, France, "Radiomètrie ECE et température électronique"

Dr. A. Degeling, CRPP-EPFL, "Unstable periodic orbits in ELM time series"

Dr. P. Gomez, CRPP-EPFL, "Approche théorique de la synergie ECX2-ECX3"

Dr. M. Tournianski, UKAEA, Culham Science Centre, Abingdon, UK, "Experimental investigation of ion behaviour in spherical tokamaks"

B.3 Seminars presented externally in 2000

Appert K., AVES (Aktion für vernünftige Energiepolitik Schweiz), Winterthur, Schweiz, April 2000, "Stand der Fusionsforschung in der Schweiz und international"

Baluc N., Université de Poitiers, France, January 2000, "Mechanical properties and applications of quasicrystals"

Coda S., General Atomics, San Diego, CA, USA, June/July 2000, "Recent experiments with ECH and non-inductive operation with ECCD in TCV"

Coda S., Physics Department, Univeristy of Madison, WI, USA, June/July 2000, "Recent experiments with ECH and non-inductive operation with ECCD in TCV"

Coda S., Plasma Science and Fusion Center, MIT, Cambridge, MA, USA, July 2000, "Recent experiments with ECH and fully non-inductive operation with ECCD in TCV"

Coda S., University of Milano, Milan, Italy, November 2000, "Esperimenti di ECH nel tokamak TCV con funzionamento non induttivo mediante ECCD"

Falchetto G., Risö National Laboratory, Roskilde, Denmark, December 2000, "Global modelling of tokamak microinstabilities using pyrokinetic equations"

Furno I., Massachusetts Institute of Technology, Boston, MA, USA, "Sawtooth activity modification in ECH/ECCD experiments on TCV"

Furno I., General Atomics, San Diego, USA, November 2000, "Understanding sawteeth in TCV"

Furno I., Los Alamos National Laboratory, Los Alamos, USA, January 2001, "Sawtooth activity modification in ECH/ECCD experiments on TCV"

Gomez P., CEA, Cadarache, France, January 2000, "Etude et influence des électrons rapides diagnostiquées par le rayonnement cyclotronique électronique (ECE) dans le Tokamak Tore Supra"

Paris P.J., 2000 Beijing International Scientific Film Festival, Beijing, China, November 2000, "On the impact of immersive virtuality in the outreaching mission"

Paris P.J., Dans le cadre de.... Action Démoncratique pour l'Energie, Novembre 2000, Genève, "La fusion thermonucléaire: un espoir pour une énergie illimitée"

Pitts R., KFKI, Budapest, Hungary, January 2000, "Divertor detachment in TCV"

Pitts R., University of California at San Diego, San Diego, USA, November 2000, "Divertor Detachment on TCV"

Pitts R., Lawrence Livermore National Laboratory, Livermore, USA, November 2000, "Recent results from TCV and overview of divertor detachment studies at CRPP"

Reimerdes H., ASDEX-Upgrade Seminar, IPP Garching, Germany, 11 October 2000, "MHD stability of shaped TCV plasmas"

Reimerdes H., General Atomics, San Diego, USA, November 2000, "Understanding sawteeth in TCV"

Reimerdes H., UKAEA, Culham Science Centre, UK, 30 November 2000, "Shape dependence of sawteeth and onset of neoclassical tearing modes in TCV"

Sauter O., Naka, Japan, January 2000, "Prediction of NTM island evolution in ITER-FEAT"

Sauter O. & Hender T., Naka, Japan, January 2000, "The New structure of the JET facility and the 2000 Work Programme related to the MHD Task Force"

Schäublin R., Pacific Northwestern National Laboratory, USA, November 2000, "Relating molecular dynamics simulations to transmission"

Schäublin R., Hahn-Meitner-Institut Berlin, Germany, November 2000, "Transmission electron microscopy of small crystal defects"

Victoria M., Internal Workshop at LLNL, Livermore, USA, February 2000, "The mechanical properties resulting from the primary damage microstructure"

Victoria M., EFDA JET-CSU, Abingdon, England, March 2000, "...."

Villard L., Max-Planck-Institut für Plasmaphysik, Garching, Germany, November 2000, "Global gyrokinetic simulations in tokamaks and stellarators"

Weisen H., CEA-Cadarache, France, November 2000, "Expériences ECH et ECCD dans le tokamak TCV"

B.4 Conferences and meetings organised by the CRPP

"JET Enhancement Meetings", January 12th, February 8th and 9th, and April7th, Lausanne.
During this series of meetings the Electron Cyclotron Wave Co-ordinating Group, under the Chairmanship of Prof. M.Q. Tran, discussed and prepared the Phase II proposal concerning the Electron Wave System of the JET-EP project. About 13 participants attended these meetings.

"Ad-hoc Group of the Fusion Physics Committee on Code Development", 12th-13th January, Lausanne.
This meeting, under the chairmanship of L. Villard, reviewed the major numerical codes developed and in use in the EURATOM Fusion Programme in the fields of transport, turbulence, heating, current drive, fast particle physics, Fokker-Planck and MHD. The primary aim was to identify possible overlaps and to issue recommendations on further code developments.

"Fusion: Energy for the 21st century", June 20th, Lausanne.
The objective of this one day meeting was to show that fusion is a potential candidate for electricity production. A series of lectures was given by high visibility speakers from Switzerland and from Europe. We took the opportunity to invite Prof.

P. Aebischer, in his new role of president of the EPFL, to give a welcome talk to an assembly of about two hundred people. An introduction allowed the audience to enter into the field of fusion research. Swiss and European policies were underlined, with enthusiasm.
The results obtained on JET with D-T plasmas discharges illustrated impressive and major progress in controlled fusion. The international project ITER, in its new version known as ITER-FEAT, gives an idea of the importance and of the dimension of this research. ITER was also illustrated in the 3-D movie " The Starmakers".
Finally the developments in materials technology and in the design of a fusion reactor were presented. This approach is essential for keeping fusion energy on the line of sustainable development and for becoming acceptable to the general public, and gave a true idea of the path we have to follow to render fusion, feasible, reliable, environmentally friendly and economically acceptable.
The speakers at this meeting were: Prof. P. Aebischer (EPFL), Prof. M.Q. Tran,(CRPP-EPFL) Dr E. Kiener (OFEN), Dr J.-P. Rager (CE), Dr J. Paméla (EFDA-JET), P.J. Paris (CRPP-EPFL), Dr R. Aymar (ITER), Dr R. Andreani (EFDA-Technology),Dr G. Marbach (CEA).

"Third EU-Japan Workshop on RF Heating Antennas and Related Technology", September 7th and 8th, Lausanne. This two day meeting was hosted by the CRPP for about 21 experts in this field, from several European countries and from Japan. 20 presentations covered the 3 ranges of heating frequencies: Ion cyclotron (IC), Lower Hybrid (LH) and Electron Cyclotron (EC). Future possibilities of collaboration between EU and Japan in the area of RF heating were also discussed together with a list of potential subjects of interest.

"Theory of Fusion Plasmas, Joint Varenna-Lausann International Workshop", August 28th - September 1st, Varenna, Italy.
This international meeting for 48 participants included 21 invited papers and 32 contributed papers and was organised by the CRPP, the International School of Plasma Physics "Piero Caldirola". The workshop proceedings have been published as a separate volume.

"SeCRETS workshop", September 25th to 28th, Morschach.
This workshop was held to present and discuss the results of the transient stability experiment with segregated copper conductors (SeCRETS) carried out in SULTAN during 2000. The discussion focussed on the transient stability results and their implications for the ITER conductor design criteria.
The participants came from Switzerland (9), Russia (4), ITER (3), Italy (3), Holland(2), EFDA, Germany, France, China, and USA.

"Optimum Location of Hall sensors for current distribution measurements", December7th, Villigen.
A one day specialist meeting was held for 10 participants from Switzerland (4), Holland (2), Italy (3), France.

"European Fusion Physics Workshop", December 13th to 15th, Leysin. This 3 day annual meeting was hosted by the CRPP and held in Leysin for about 100 European fusion physicists to present and discuss the most important issues in magnetic confinement. A series of satellite meetings was organised at the same time.

APPENDIX C External activities of CRPP Staff during 2000

C.1 National and international committees and ad-hoc groups

MEMBERSHIP

K. Appert	EFDA* JET Sub-Committee
J.B. Lister	ITER MHD, Disruption and Control Expert Group
M.Q. Tran	ITER-JCT meeting as Task Area Leader regarding development programme of an EC antenna for ITER Consultative Committee for the Euratom Specific Research and Training Programme in the field of Nuclear Energy, Fusion (CCE-FU) Fusion Physics Committee EFDA* Steering Committee EFDA* Technology Sub-Committee
F. Troyon	Chairman of the JET-Council
L. Villard	Fusion Physics Committee Member of the "Conseil Scientifique du Département de Recherche sur la Fusion Contrôlée" – CEA - France
H. Weisen	Member of the International Advisory Board of the IPP Prague, Czech Republic

PARTICIPATION

K. Appert	Fusion Evaluation Board
R. Behn	Meeting on High Spatial Resolution Thomson Scattering System, June 5 – 6, 2000 Working group on Thomson Scattering, EFDA-JET
B. Duval	Remote Participation Users Group, EFDA-JET
J.B. Lister	EU Domestic Assessment ad hoc group of ITER-FEAT Ad hoc group for FTU-D
Y.R. Martin	ITER Confinement Database and Modelling Expert Group
O. Sauter	ITER Physics Expert Group on MHD, Disruption and Control
M.Q. Tran	Fusion Evaluation Board Chairman of the Technical Evaluation Group for the field of Plasma Engineering in view of the Qualification of European Industries within Technologies relating to controlled thermonuclear fusion
H. Weisen	Edge and Pedestal Physics Expert Group

* EFDA: European Fusion Development Agreement

C.2 Editorial and society boards

S. Alberti	Member of the Committee of the SSP (Swiss Physical Society) Responsible for Applied Physics
Ch. Hollenstein	Vice President of the Swiss Vacuum Society Member of the Committee URSI (Union Radio-Scientifique Internationale) Member of the Editorial Board of Plasma Chemistry and Plasma Processing
J.B. Lister	Member of the Editorial Board of Plasma Physics and Controlled Fusion Vice President of the European Physical Society Plasma Physics Division Board and representative of this board at the APS
Y.R. Martin	Chairman of the AVCP (Association Vaudoise des Chercheurs en Physique)
P.J. Paris	Project Manager : Interactive Model of ITER and start of Fusion Power Plant Virtual Reality Member of the Fusion Expo Consortium Committee Member of the EFDA Information Network
M.Q. Tran	Member of the Board of Editors of Nuclear Fusion

C.3 EPFL committees and commissions

Ch. Hollenstein H. Weisen	Commission de Recherche du Département de Physique, EPFL
X. Llobet	Commission Technique d'Informatique
K. Appert	Commission d'Informatique

APPENDIX D

D.1 Lausanne Reports (LRP)

Benz A., Bruhns H., Vandenplas P.E.M., Weisse J. Margaud Ph. Marbach G., Hollenstein Ch., Paris P.J., Tran M.Q., "Plasmas: des étoiles ... au quotidien – Fusion: ... énergie du 21ème siècle", Journée CRETE - FUSION, énergie du 21e siècle
LRP 666/00

Brazis R., Raguotis R., Moreau Ph., Siegrist M.R., "Enhanced third-order nonlinearity in semiconductors giving rise to 1 THz radiation"
LRP 658/00

Cooper W.A., "Stability of a compact three-period stellarator with quasiaxial symmetry features"
LRP 674/00

Cooper W.A., Todd T.N., Allfrey S., Hender T.C., Robinson D.C., "Effect of helical coils on the magnetic field and the stability of a compact toroidal plasma"
LRP 675/00

Cooper W.A., Fischer O., "Stability and a-particle confinement in the sphellamak reactor concept"
LRP 679/00

Coutlis A., Limebeer D.J.N., Wainwright J.P., Lister J.B., Vyas P., "Frequency response identification of the dynamics of a tokamak plasma"
LRP 667/00

deAlmeida P., Schäublin R., Almazouzi A., Victoria M., Lévy F., "Microstructure and growth modes of stoichiometric NiAl and Ni3Al thin films deposited by rf-magnetron sputtering"
LRP 661/00

Diaz de la Rubia T., Zhib H.M., Kraishi T.A., Wirth B.D., Victoria M., Caturla M.-J., "Plastic flow localization in irradiated materials: A multiscale modeling approach"
LRP 672/00

Dorier J.-L., Gindrat M., Hollenstein Ch., Salito A., Loch M., Barbezat G., "Time-resolved imaging of anodic arc root behavior during fluctuations of a DC plasma spraying torch"
LRP 681/00

EPS participants, Papers presented at the, 27th EPS Conference on Controlled Fusion and Plasma Physics, Budapest, Hungary, June 12 - 16, 2000
LRP 671/00

Furno I., Angioni C., Porcelli F., Weisen H., Behn R., Goodman T.P., Henderson M.A., Pietrzyk Z.A., Pochelon A., Reimerdes H., "Understanding sawtooth activity during intense electron cyclotron heating experiments on TCV"
LRP 665/00

IAEA Participants, Papers presented at the, 18th IAEA Fusion Energy Conference, Sorrento, Italy,, October 4 - 10, 2000
LRP 684/00

Jost G., Tran T.M., Cooper W.A., Villard L., Appert K., "Global Linear Gyrokinetic Simulations in Quasi-Symmetric Configurations"
LRP 687/00

Jost G., "Simulations particulaires d'ondes de dérive dans des configurations magnétiques 3D", (Thèse EPFL 2000)
LRP 670/00

Khayrutdinov R.R., Lister J.B., Lukash V.E., Wainwright J.P., "Comparing DINA code simulations with TCV experimental plasma equilibrium responses"
LRP 673/00

Lister J.B., Sharma A., Limebeer D.J.N., Nakamura Y., Wainwright J.P., Yoshino R., "Plasma equilibrium response modelling and validation on JT-60U"
LRP 680/00

Maccio M., "Effect of E x B flows on global linear microinstabilities", (thèse EPFL 2000)
LRP 676/00

Maccio M., Vaclavik J., Villard L.
Effect of E x B flows on global linear ion temperature gradient modes
LRP 677/00

Magni D., Deschenaux Ch., Hollenstein Ch., Creatore A., Fayet P., "Oxygen diluted hexamethyldisiloxane plasmas investigated by means of in situ infrared absorption spectroscopy and mass spectrometry"
LRP 686/00

Manini A., Moret J.-M., Furno I., Goodman T.P., Henderson M.A., "Analysis of the dynamic response of the plasma in the presence of sawteeth on TCV"
LRP 664/00

Minardi E., Weisen H., "Stationary magnetic entropy in ohmic tokamak plasmas: experimental evidence from the TCV device"
LRP 669/00

Müller H., Howling A.A., Hollenstein Ch., "Power laws for the spatial dependence of electrical parameters in the high voltage, capacitive RF sheath"
LRP 659/00

Müller H., Howling A.A., Hollenstein Ch., "Charge screening in the high voltage, capacitive rf sheath"
LRP 662/00

Participants in SOFT, Papers presented at the, 21st Symposium on Fusion Technology, Madrid, Spain, September 11 - 15, 2000
LRP 683/00

Pietrzyk Z.A., Angioni C., Behn R., Coda S., Goodman T.P., Hofmann F., Henderson M.A., Hogge J.-P., Moret J.-M., Pochelon A., Reimerdes H., Sauter O., Weisen H., "Central electron temperature enhancements due to sawtooth stabilizing during counter ECCD in TCV"
LRP 660/00

Pietrzyk Z.A., et al., "Quasi-steady-state improved central confinement in the TCV Tokamak" ... voir avec Elisabeth
LRP 678/00

Pitts R.A., Duval B.P., Loarte A., Moret J.-M., Boedo J.-A., Coster D., Furno I., Horacek J., Kukushkin A.S., Reiter D., Rommers J., and TCV Team, "Divertor geometry effects on detachment in TCV", Presented at, 14th Int. Conference on Plasma Surface Interactions in Controlled Fusion Devices, Rosenheim, Germany, May 2000
LRP 668/00

Reimerdes H., Pochelon A., Sauter O., Goodman T.P., Henderson M., "Effect of triangular and elongated plasma shape on the sawtooth stability"
LRP 657/00

Sauter O., Henderson M.A., Hofmann F., Goodman T. , et al., "Steady-state fully non-inductive current driven by electron cyclotron waves in a magnetically confined plasma"
LRP 663/00

Sauter O., "Steady-state fully non-inductive operation with ECCD and current profile control in the TCV tokamak", Invited paper at the 42nd Annual Meeting, APS Division of Plasma Physics, Quebec, Canada, October 2000,
LRP 688/00

Theory Group, Papers presented at the Joint Varenna - Lausanne International Workshop on Theory of Fusion Plasmas, Varenna, Italy, August 28 - September 1, 2000
LRP 682/00

D.2 Internal Reports (INT)

Luppo M.I., Paris P.J., Victoria M., "Hydrogen loading equipment sieverts' type"
INT 200/00

Marlétaz B., "Electronique du diagnostique spred"
INT 198/00

Zabolotsky A., Weisen H., "Analysis of impurity transport in TCV ohmic discharges"
INT 199/00

APPENDIX E The basis of controlled fusion

E.1 Fusion as a sustainable energy source

Research into controlled fusion aims to demonstrate that it is a valid option for generating power in the long term future in an environmentally, politically and economically acceptable way. Controlled fusion is a process in which light nuclei fuse together to form heavier ones: during this process a very large amount of energy is released. For a fusion reactor it is planned to use the two isotopes of hydrogen: deuterium (D) and tritium (T), which fuse together much more readily than any other combination of light nuclei according to the following reaction:

$$D^2 + T^3 \rightarrow He^4 + n + 17.6MeV$$

The end products are helium and neutrons (n). The total energy liberated by fusing one gram of a 50:50% mixture of deuterium and tritium is 94000kWh, which is 10 million times more than from the same mass of oil. 80% of this energy is carried by the neutrons with an energy of 14MeV while the remaining 20% is carried by the helium nucleus. All this energy eventually becomes heat to be stored or converted by conventional means into electricity.

The temperature at which fusion reactions start to become significant are above a few tens of millions of degrees. For the D-T reaction, the optimal temperature is of the order of 70-200 million degrees. At such temperatures the D-T fuel is in the plasma state.

Deuterium is very abundant on the earth and can be extracted from water (0.034g/l). Tritium does not occur naturally, since its half-life is only 12.3 years, but it can be regenerated from lithium using the neutrons produced by the D-T fusion reactions. The two isotopes of natural lithium contribute to this breeding of tritium according to the reactions:

$$Li^6 + n \rightarrow He^4 + T^3 + 4.8MeV$$

$$Li^7 + n \rightarrow He^4 + T^3 + n - 2.5MeV$$

The relative abundance of the two lithium isotopes Li^6 and Li^7 are 7.4% and 92.6%, respectively. The known geological resources of lithium in the earth are large enough to provide energy for several thousand years without counting the lithium present in sea water.

E.2 Attractiveness of fusion as an energy source

The inherent advantages of fusion as an energy source are:

- The fuels are plentiful and their costs are negligible because of the enormous energy yield of the reaction;
- The end product of the reaction is helium, an inert gas;
- No chain reaction is possible; at any time only a very small amount of fuel is in the reacting chamber and any malfunction would cause an immediate drop of temperature and the reaction would stop;
- No after-heat problem can lead to thermal runaway;
- None of the materials required by a fusion power plant are subject to the provisions of the non-proliferation treaties.

Its further potential advantages are:

- Radioactivity of the reactor structure, caused by neutrons, can be minimised by careful selection of low-activation materials resulting in a manageable quantity of long lived radioactive waste;
- The release of tritium in normal operation can be kept to a very low level. The inventory of tritium in the breeding section of the reactor and on the site can be sufficiently small so that the worst possible accident could not lead to a harmful release to the environment requiring evacuation of the nearby population.

APPENDIX F Glossary

The following is a general purpose glossary for the field of controlled fusion and plasma physics.

Additional heating: Usually with reference to a plasma which is initially heated by a toroidal current induced in the plasma (ohmic heating), additional heating designates other means of heating a plasma (absorption of electromagnetic waves or of injected fast neutral particles).

Advanced Tokamak Scenarios: Tokamaks normally generate natural profiles of plasma current and plasma pressure. Using external non-inductive current drive and local control of the current and pressure profiles can allow access to enhanced regimes and even steady state operation, generally referred to as Advanced Tokamak Scenarios.

ALCATOR C-MOD: High field, high density tokamak at MIT (USA) with an elongated, diverted plasma.

Alfvén gap modes: The toroidal nature of tokamak plasmas produces gaps in the otherwise continuous spectrum of Alfvén waves, populated by discrete, weakly damped Alfvén gap modes. Under certain conditions these modes can be destabilised by resonant energy transfer from energetic particles, e.g. α-particles from fusion reactions.

Alfvén waves: A fundamental plasma wave, which is primarily magneto-hydrodynamic in character with an oscillation of the magnetic field and, in some cases, plasma pressure. In tokamaks, these waves are typically strongly damped. See also fast Alfvén wave.

Alfvén velocity: The velocity of propagation of Alfvén waves in the direction of the magnetic field; it is proportional to the magnetic field strength, and inversely proportional to the square root of the mass density.

alpha particle, or α-particle He^4: The nucleus of the helium atom, composed of two protons and two neutrons, is one of the two products of the DT fusion reaction (the other one is a neutron). The α-particles, being electrically charged, are trapped by the magnetic confinement field and therefore can release their energy to the plasma contrary to the neutrons which escape from the plasma and transfer their energy in the blanket surrounding the plasma core. The plasma heating which is provided by these α-particles as they slow down due to collisions is essential for achieving ignition.

Alternative lines: Magnetic confinement development other than the tokamak.

Analytic/Computational modelling: Analytic: algebraic solution of basic equations. Computational: numerical solution of basic equations.

Anomalous transport: Measured heat and particle loss is anomalously large compared with collisional theory of heat transport in toroidal plasmas.

ASDEX-Upgrade: Medium-sized Tokamak at Garching (Association Euratom-IPP, Germany) with an elongated, diverted plasma.

Aspect ratio: The ratio between the large radius and the small radius of a torus.

Auxiliary heating: See additional heating.

Ballooning instability: A local instability which can develop in the tokamak when the plasma pressure exceeds a critical value; it therefore constrains the maximum β that can be achieved. It is analogous to the unstable bulge which develops on an over-inflated tyre.

Beta (β): Ratio of plasma pressure to magnetic field pressure. One of the figures of merit for magnetic confinement: the magnitude of the magnetic field pressure determine the cost of the field coil that generates it; since fusion reactivity increases with the square of the plasma pressure, a high value of ß indicates good performance. The highest values achieved in tokamaks reach 40% (START).

Beta-normalised (β_N): The ratio of plasma current (in MA) to the product of minor radius (in m) and magnetic field (in T) characterises the limit to the achievable β imposed by ideal MHD. Beta-normalised is the ratio of β (as a percentage) to the above ideal MHD parameter. Generally $\beta_N \sim 3$ should be achievable, but techniques for obtaining higher values have been observed experimentally.

Blanket: A structure containing lithium or lithium compounds surrounding the

plasma core of a fusion reactor. Its functions are to breed tritium, via lithium-neutron reactions, and to absorb most of the fusion energy to be used for electricity generation.

Bootstrap current: Theory developed in 1970 predicted that a toroidal electric current will flow in a tokamak which is fuelled by energy and particle sources that replace diffusive losses. This diffusion driven "Bootstrap current", which is proportional to β and flows even in the absence of an applied voltage, could be used to provide the poloidal magnetic field: hence the concept of a Bootstrap tokamak, which has no toroidal voltage. A Bootstrap current consistent with theory was observed many years later on JET and TFTR; it now plays a role in optimising advanced tokamaks.

Breakeven: The fusion performance of a power plant is denoted by Q, which is the ratio of the power released by fusion reactions to that used to heat the plasma. As a convention, scientific breakeven corresponds to Q=1 and ignition to Q=infinity. A fusion power plant would operate at Q~50.

Breeding ratio: The number of tritium atoms produced in the blanket of a fusion power station per tritium nucleus burned in the fusion plasma.

Burn: The fusion process of consuming DT fuel in a reactor, releasing energy.

CCE-FU: The Consultative Committee for the Euratom Specific Research and Training Programme in the field of Nuclear Energy, Fusion. Formerly the CCFP.

CCFP: Consultative Committee for the Fusion Programme. Advisory body to the Commission (in French CCPF, in German BAPF). Renamed under the 5th Framework Programme as the CCE-FU (q.v.).

CEA: Commissariat à l'Energie Atomique, France. Partner in the Association EURATOM-CEA which operates the TORE SUPRA tokamak.

CFI: Committee on Fusion-Industry.

CFP: Community Fusion Programme. Renamed under the 5th Framework Programme as the "Key Action Fusion".

Charge exchange measurement: Measures the plasma ion temperature. Neutral atoms in the plasma (for example from a neutral beam) donate electrons to hot plasma ions, which are thereby neutralised. These hot atoms are no longer confined by the magnetic field and leave the plasma. Their energy is measured by a neutral particle analyser.

CIEMAT: Centro de Investigaciones Energéticas Medioambientales y Tecnológicas, Spain. Partner in the Association EURATOM-CIEMAT. Operates the flexible heliac stellarator TJ-II.

Classical transport: Collisions between the individual particles of a plasma allow them to move across the magnetic field. Theories which describe this mechanism are called "classical" (or "neo-classical" when additional effects due to the toroidal geometry are included). The measured heat and particle transport is usually higher than predicted by these theories.

Collisionality: Non-dimensional parameter, which is the inverse ratio of the mean free path of plasma particles between collisions to a characteristic length of the magnetic field configuration.

Compact torus: Class of closed magnetic configurations in which no material elements (coils, conductors or walls) need to link through the bore of the plasma torus. Thus the vessel of compact tori can be spherical or cylindrical.

COMPASS: COMPact ASSembly, a tokamak for studies of plasma stability, at Culham, UK (Association EURATOM-UKAEA). Originally with circular vessel (COMPASS-C), now with D-shaped vessel (COMPASS-D).

Confinement time: In a fusion plasma neither particles nor energy are perfectly confined. Particle confinement time is the time during which the particles, on average, stay confined. The energy confinement time, which is usually shorter than the particle confinement time, is defined in steady state as the ratio of the plasma energy content to the total power input to the plasma and is a measure of how fast a plasma would cool if there were no heating.

CRPP: Centre de Recherches en Physique des Plasmas. Fusion laboratories of the Association EURATOM-Swiss Confederation at the Ecole Polytechnique Fédérale de Lausanne and the Paul-Scherrer Institute, Villigen (CRPP-Fusion Technology).

Current drive (non-inductive): In a tokamak, plasma current can be driven inductively, with the toroidal plasma acting as a secondary winding of a transformer whose primary coil is at the central column of the device. Continuous current cannot

be driven by transformer action. 'Non-inductive' current drive methods are applied either by injecting particles with directed momentum into the plasma or by accelerating electrons by electromagnetic waves so that they carry the current. Also being applied to control instabilities and to optimise confinement by modifying the current profile. The bootstrap effect also drives current.

Current profile (current distribution): The distribution of current density across the minor radius of the plasma.

Current ramp-up (down): The increase (decrease) of plasma current either at the start of operation or during operation.

Cyclotron frequency: Charged particles in a magnetic field have a natural frequency of gyration in the plane perpendicular to the magnetic field - the cyclotron frequency. For electrons in a tokamak, the cyclotron frequency is typically a few tens of GHz (28 GHz per Tesla), and for ions, a few tens of MHz (7.5 MHz per Tesla for deuterium).

Cylindrical approximation: An approximation to the true tokamak geometry in which the torus is straightened, so that the toroidal direction becomes the cylinder axis. There are two directions of symmetry: along the axis (the 'toroidal' direction) and about the axis (the 'poloidal' direction).

DCU: Dublin City University, Ireland. Partner in the Association EURATOM-DCU.

DEMO: Demonstration Reactor (the first device in the European fusion strategy intended to produce significant amounts of electricity).

Deuterium: A stable isotope of hydrogen, whose nucleus contains one proton and one neutron. In heavy water, normal hydrogen is replaced by deuterium. Sea water contains, on average, 34g deuterium per m^3. Deuterium plasmas are used routinely in present-day experiments; in a fusion power plant the plasma will consist of a mixture of deuterium and tritium which fuse more readily then two deuterium nuclei.

DG Research (DG RTD): The Directorate-General of the European Commission, Brussels, responsible for Research and Development. Formerly DG XII.

Diagnostic: Apparatus used for measuring one or more plasma quantities (temperature, density, current, etc.).

Diffusion, thermal (or particle): The random flow of heat (or particles) in the presence of a thermal (or density) gradient.

DIII-D: The largest operating US tokamak, run by General Atomics, San Diego. It has a flexible configuration and studies core and divertor physics with intense additional heating.

D-He^3: Deuterium-^{3}Helium: A potential fuel for fusion with low release of neutrons, but which would require a much higher fusion triple product ($nT\tau$) than DT to reach ignition. ^{3}Helium is an isotope of helium which is not available in appreciable quantities on Earth.

Disruption, Disruptive instability: A complex phenomenon involving MHD instability which results in a rapid release of energy to the wall and strong electromechanical forces in a tokamak. Plasma control may be lost, triggering a VDE (q.v.). This phenomenon places a limit on the maximum density, pressure and current in a tokamak.

Distribution function: Describes both the space and velocity distribution of plasma particles.

Divertor: A magnetic field configuration with a separatrix, affecting the edge of the confinement region, designed to remove heat and particles from the plasma, i.e. divert impurities and helium ash to divertor plates in a target chamber. Alternative to using a limiter to define the plasma edge.

Double null: See Single/double null divertors.

Drift kinetic theory: Kinetic theory which describes plasma processes which have spatial scales much greater than the particle Larmor radii.

Drift orbits: Particle motion is tied to straight magnetic field lines. However, electric fields and gradients of the magnetic field give an additional drift perpendicular to the magnetic field creating drift surfaces displaced from the magnetic surfaces.

Driven current: Plasma current produced by a means external to the plasma, inductively or non-inductively.

Driver: In inertial confinement fusion, the laser or particle beam system used to compress a target pellet.

DTE: The deuterium-tritium experiment at JET which in 1997 set new records for fusion power production. Followed the Preliminary Tritium Experiment of 1991.

ECCD: Electron Cyclotron Current Drive. Non-inductive current drive technique using directed electron cyclotron resonance waves.

ECE: Electron Cyclotron Emission. Radiation emitted by electrons as a result of their cyclotron motion around magnetic field lines. Used to measure electron temperature.

ECH: Electron-Cyclotron Heating. Radio wave heating near the resonance frequency (or its multiple) of the electron gyration in a magnetic field. In present and future machines ECH is at typically 60-170 GHz, depending on the magnetic field strength in a machine.

EFDA: European Fusion Development Agreement. The new organisational framework of the EU fusion activities on the exploitation of the JET Facilities, international collaboration (including ITER) and supporting technology. EFDA replaces the NET agreement.

EFET: European Fusion Engineering & Technology: a fusion technology oriented European Economic Interest Grouping.

Electron temperature: A measure of electron thermal energy in units of degrees or electron volts (1 eV ~ 10^4 degrees Kelvin).

ELM: Edge localised mode. An instability which occurs in short periodic bursts during the H-mode in divertor tokamaks. It modulates and enhances the energy and particle transport at the plasma edge. These transient heat and particle losses could be damaging in a reactor.

ENEA: Ente per le Nuove Tecnologie, l'Energia e l'Ambiente, Italy. Partner in the Association EURATOM-ENEA.

Energetic particle: In terms of energy, the particles in a plasma can be divided into two classes. The more numerous thermal particles are characterised by a temperature typically in the range 1-30 keV for modern tokamaks. The less numerous class of energetic particles has significantly higher energy up to several MeV. Energetic particles can be created by electric fields, fusion reactions, neutral beam injection or RF heating.

Error fields: The magnetic coils of a tokamak are designed to give the desired magnetic field configuration. The finite number of coils and imperfections in their construction lead to unwanted deviations from this configuration known as error fields. These could lead to disruptions and are of particular concern for larger tokamaks.

EXTRAP T-II: External Trap II, a medium-sized reversed field pinch (RFP) at the Royal Institute of Technology, Stockholm (Association EURATOM-NFR), built for RFP transport and shell stabilisation studies in support of RFX.

EURATOM: European Atomic Energy Community.

Faraday rotation: The rotation of the plane of polarisation of light passing through a magnetised plasma.

Fast Alfvén wave: The fast Alfvén wave exists over a broad frequency spectrum, from the ion cyclotron range of frequencies (ICRF) where its character is electromagnetic, down to magnetohydrodynamic frequencies. Its velocity is comparable to the Alfvén velocity. The fast Alfvén wave is used routinely for high-power (~20MW) ICRF heating on JET, as it is efficiently absorbed in the plasma by the mechanism of ion cyclotron resonance. Although usually stable in tokamaks, the wave can be excited by energetic ion populations.

Fast wave current drive: Current drive produced by a fast wave. The wave can penetrate the plasma more easily than a lower hybrid wave.

Feedback: Use of measurements of plasma parameters to control the parameters, shape or profiles of the plasma to obtain desired conditions.

Field lines, Flux surfaces: Imaginary lines marking the direction of a force field. In a tokamak these define a set of nested toroidal surfaces, to which particles are approximately constrained, known as flux surfaces.

Field reversed configuration: A compact torus with a strongly elongated plasma. The plasma is contained in a cylindrical vessel inside a straight solenoid. The confining magnetic field usually has only a poloidal component. Not to be confused with reversed field pinch.

FIR: Far infra-red (e.g. wavelength ~ 0.2 to 1mm). FIR lasers are used to measure the magnetic field and plasma density.

"Fishbones": Rapid bursts of MHD activity sometimes observed when neutral beam heating is used in tokamaks (fishbone refers to the shape of the bursts in oscillating magnetic field when plotted as a function of time).

First wall: The first material boundary that surrounds the plasma. Today, the first wall in all machines is protected by low-Z materials (such as carbon tiles, boron or beryllium coating).

Flat-top current: Constant current during quasi-stationary operating conditions.

Fokker-Planck Code: A computer code to calculate the velocity distribution of plasma particles allowing for collisional relaxation and plasma heating. Calculates distribution functions (q.v.).

FOM: Stichting voor Fundamenteel Onderzoek der Materie (Foundation for basic investigations of matter), The Netherlands. Partner in the Association EURATOM-FOM.

FPC: The Fusion Physics Committee, a sub-committee of the CCE-FU which reports to it principally on the physics aspects of the programme. Formerly the Programme Committee (PC).

FTC: The Fusion Technology Committee, a sub-committee of the CCE-FU which reports to it principally on technology activities and contributions to international collaborations. Formerly the Fusion Technology Steering Committee (FTSC).

FTU: Frascati Tokamak Upgrade, a high density, high current tokamak at Frascati, Italy (Association EURATOM-ENEA).

Fusion triple product: Product of (ion) density, (ion) temperature and energy confinement time. A measure of the proximity to break-even and ignition.

Fusion product: The product of a fusion reaction, for example an α-particle or neutron in a deuterium-tritium plasma.

Fusion reactivity: Fusion reaction rate. For present typical tokamak conditions, it increases with the square of the density and the ion temperature of the plasma.

Full wave theory: Wave theory which includes complete accounting of wave energy (transmitted, reflected and absorbed, including energy transferred to other waves) for studying RF heating.

FZK: Forschungszentrum Karlsruhe, Germany. Partner in the Association EURATOM-FZK, active in fusion technology and, with the development of gyrotrons, in plasma engineering.

FZJ: Forschungszentrum Jülich GmbH, Germany. Partner in the Association EURATOM-FZJ, operating the tokamak TEXTOR.

GSI: Gesellschaft für Schwerionenforschung, Darmstadt, Germany. Studying heavy-ion physics, and driver physics with possible application for inertial confinement fusion.

Gyro-kinetic theory: Version of kinetic theory in which the Larmor radius is not assumed to be small. An essential theory for investigating fine-scale instabilities which might be responsible for driving turbulence, which may in turn be responsible for anomalous transport.

Gyrotron: Device used for generating high power microwaves in the electron cyclotron range of frequencies (50 - 200 GHz). This UHF wave is mostly used to heat the plasma at the electron cyclotron resonance frequency. It also could be used to diagnose the plasma.

Heliac: Stellarator configuration with a central toroidal coil around which the plasma column is wound helically. Because of its high capability of investigating a wide range of stellarator configurations, it is used for TJ-II.

Helias: Optimised stellarator configuration, used with modular coils for Wendelstein VII-X (Germany) and SHEILA (Australia).

H-mode: A High confinement regime that has been observed in tokamak plasmas. It develops when a tokamak plasma is heated above a characteristic power threshold, which increases with density, magnetic field and machine size. It is characterised by a sharp temperature gradient near the edge (resulting in an edge “temperature pedestal”), ELMs and typically a doubling of the energy confinement time compared to the normal “L” regime. Today, a variety of high confinement modes have been identified in divertor and in limiter configurations (e.g. the I-mode), which, in part, have been obtained by special tailoring of the radial plasma current profile.

H-transition (or L-to-H transition): Transition into the H-regime from the L-regime, usually quite sudden, at a certain threshold power of additional heating and specific plasma parameters.

Halo currents: See Vertical Displacement Event.

Helicity injection: The helicity of a toroidal plasma is related to a linkage of

toroidal and poloidal magnetic fluxes, and is approximately conserved throughout a discharge. If additional helicity can be injected, the plasma current could be sustained or even increased.

Helium ash: Fusion reactions in a deuterium-tritium plasma produce energetic α-particles (helium nuclei), which heat the plasma as they slow down. Once this has happened, the α-particles have no further use: they constitute helium ash, which dilutes the fuel and must be removed to maintain a burning plasma.

High beta (β): Condition in which the plasma energy is a significant fraction of the energy in the magnetic field. An alternative measure is the ratio between the plasma energy and the energy in the poloidal magnetic field, the poloidal β.

High field ECH launch: Electron cyclotron waves can be launched from the inside of the plasma torus. This allows higher density plasma to be heated.

Hydrogen: The lightest element; the nucleus consists of only one proton, the atomic shell of one electron. Isotopes of hydrogen, with one or two additional neutrons in the nucleus, are deuterium and tritium respectively.

IAEA: International Atomic Energy Agency (of the United Nations), Vienna, Austria. The ITER-EDA is undertaken under the auspices of the IAEA.

ICE: Ion Cyclotron Emission. Observed in JET and TFTR as a suprathermal signal, apparently driven by collective instability of energetic ion populations such as fusion products and injected beam ions.

ICF: Inertial Confinement Fusion. Intense beams of laser light or light or heavy ion beams are used to compress very rapidly and heat tiny target pellets of fusion fuel to initiate fusion burn in the centre. Sufficient fusion reactions must occur in the very short time before the fuel expands under its own pressure. The inertia of the pellet's own mass determines the time scale during which fusion reactions occur, hence the name inertial confinement.

ICRH: Ion Cyclotron Resonance Heating by launching waves into the plasma in the range of the ion cyclotron frequency (radio frequency, typically at several tens of MHz).

ICRF: Ion Cyclotron Resonance Frequencies.

Ideal: In the context of MHD, 'ideal' implies that the magnetic field and the plasma always move together. For this to occur, the electrical resistivity of the plasma must be negligible.

Ideal internal kink modes: An MHD instability of the central region of a tokamak. This, or its close relative the resistive internal kink mode, may be involved in the Sawtooth disruptions which occur in most Tokamaks.

IEA: International Energy Agency (of the OECD), Paris, France. Implementing agreements for international collaboration on specific topics in fusion have been set up in the frame of the IEA.

Ignition condition: Condition for self-sustaining fusion reactions: heat provided by fusion α-particles replaces the total heat losses. External sources of plasma heating are no longer necessary and the fusion reaction is self-sustaining. Ignition is not required for energy gain in a power station. Retaining a level of external heating or current drive will be required to control the plasma pressure and current profiles, to optimise the performance, leading to a so-called "driven burn".

Impurities: Ions, other than the basic plasma ion species, which are unwanted as they lose energy by radiation and dilute the plasma.

Impurity screening: The prevention of impurities from entering the plasma.

Internal kink: A type of MHD instability that can occur within the central region of the plasma (where $q < 1$) reducing the peak temperature and density.

Internal Reconnection Event (IRE): An instability which breaks magnetic field lines and reconnects them with a different topology to reduce the system to a lower energy state - associated with the operating limits of spherical tokamaks.

Ion Bernstein wave: A wave which only exists in a hot plasma and is supported by the ions. It propagates at right angles to the magnetic field, when it is undamped, at harmonics of the ion cyclotron frequency. There is also an electron Bernstein wave which propagates at harmonics of the electron cyclotron frequency.

Ion Cyclotron Current Drive (ICCD): Non-inductive current drive using ICRH.

Ion Cyclotron Resonance Heating (ICRH) / Ion Cyclotron Resonance Frequencies (ICRF): Additional heating method using

RF waves at frequencies (~ 20-50 MHz) matching the frequency at which ions gyrate around the magnetic field lines.

IPP: Max-Planck-Institut für Plasmaphysik, Garching, Germany. Partner in the Association EURATOM-IPP, operating the tokamak ASDEX-Upgrade and the stellarator Wendelstein VII-AS. Also has sites in Berlin and in Greifswald, where the construction of the large superconducting stellarator Wendelstein VII-X is in progress.

IR: Infra Red part of the electromagnetic spectrum.

IRE: Internal Reconnection Event.

IST: Instituto Superior Técnico, Portugal. Partner in the Association EURATOM-IST.

ISTTOK: Small tokamak, for study of non-inductive current drive, at the Instituto Superior Técnico (IST), Lisbon, Portugal.

ITER: International Thermonuclear Experimental Reactor (the next step as a collaboration between EURATOM, Japan, the Russian Federation and originally the USA, under the auspices of the IAEA). After a conceptual design phase - CDA (1988-1990), now under engineering design activities (ITER-EDA, 1992-2001). TAC, Technical Advisory Committee. See also Next Step.

JAEC: Japan Atomic Energy Commission, Tokyo, Japan.

JAERI: Japan Atomic Energy Research Institute. Headquarters in Tokyo, Japan.

JET: Joint European Torus. The largest tokamak in the world, sited at Abingdon, UK. Operated as a Joint Undertaking (JET Joint Undertaking), until the end of 1999. The scientific exploitation of the JET facilities is now guaranteed by the Euratom fusion Associations within the EFDA framework. The operation of the facility is the responsibility of the Association Euratom-UKAEA.

JT-60U: Japanese tokamak at Naka. The largest Japanese tokamak and second largest operating experiment after JET, but not designed for use with D-T fuel.

keV: Kilo-electronvolt. Energy which an electron acquires passing a voltage difference of 1000 volts. Also used to measure the temperature of a plasma (1 keV corresponds to 11.8 million degrees Kelvin).

Kinetic instability: Oscillation which is unstable as a result of the energy distribution of ions or electrons.

Kinetic theory: A detailed mathematical model of a plasma in which trajectories of electrons and ions are described. More complex than fluid and two-fluid theories, it is necessary in the study of RF heating and some instabilities, particularly when energetic particles are involved.

L-H transition: Change from L regime to H regime (usually quite sudden).

L-mode: As opposed to the H mode. Regime with degradation of confinement, in additionally heated plasmas, with respect to plasmas heated ohmically by the plasma current.

Langmuir probe: Electrical probe inserted into the edge of a plasma for measurements of density, temperature and electric potential.

Larmor radius: Radius of the gyratory motion of particles around magnetic field lines.

Large scale ideal modes: A large scale mode has a wavelength which is a significant fraction of the plasma dimensions and assumes ideal MHD.

Laser ablation: Use of lasers to produce a sudden influx of impurities into the plasma from a solid surface.

Last closed flux surface: The boundary separating those magnetic field lines that intersect the wall (open lines) from the magnetic field lines that never intersect the wall (closed lines).

Lawson criterion: The value of the confinement time multiplied by the ion density (at the required temperature) which must be exceeded in a fusion reactor to reach ignition.

Limiter: A material surface within the tokamak vessel which defines the edge of the plasma and thus avoids contact between the plasma and the vessel. A pumped limiter can also be used to remove heat and particles and is an alternative exhaust system to the divertor.

LLNL: Lawrence Livermore National Laboratory, Livermore, USA.

Locked modes: MHD modes that cease rotating (though they can still grow).

Low-activation materials: Materials which do not develop high, long-lived radioactivity under neutron irradiation.

Low aspect ratio: Low ratio of major to minor radius of the torus.

Lower hybrid current drive (LHCD): Non-inductive current drive using lower hybrid waves.

Lower hybrid heating (LHRH): Plasma heating by radio frequency waves at the "lower hybrid" resonance frequency in the plasma. Typical frequencies are a few GHz.

Lower hybrid (LH) wave: A plasma wave of frequency between the ion and electron cyclotron frequencies. It has a component of electric field parallel to the magnetic field, so it can accelerate electrons moving along the field lines.

Magnetic axis: The magnetic surfaces of a tokamak form a series of nested tori. The central 'torus' defines the magnetic axis.

Magnetic Confinement Fusion (MCF): Confinement and thermal insulation of a plasma within the reactor core volume by the action of magnetic fields. In toroidal magnetic confinement, usually both toroidal and poloidal components of the magnetic field are needed (the field lines are threaded like the filaments of a cable which is bent into a ring).

Magnetic islands: Islands in the magnetic field structure caused either by externally applied fields or internally by unstable current or pressure gradients. See tearing magnetic islands.

Magnetic surfaces (flux surfaces): In toroidal magnetic confinement, the magnetic field lines lie on nested toroidal surfaces. The plasma pressure, but not the amplitude of the magnetic field, is a constant on each magnetic surface.

Magneto-acoustic cyclotron instability: This instability results from an exchange of energy between the fast Alfvén wave (or magneto-acoustic wave) and an ion Bernstein wave which has a source of free energy through the presence of a population of energetic (non-thermal) ions, e.g. fusion products. The instability occurs for propagation perpendicular to the equilibrium magnetic field.

Major radius: The distance from the tokamak symmetry axis to the plasma centre.

Marfe: A localised and radiating thermal instability sometimes observed near the edge of tokamak plasmas.

Marginal Stability: Close to the transition from stability to instability.

MAST: Mega Amp Spherical Tokamak at Culham (Association EURATOM-UKAEA), twice as big as START. Began operation in 1999.

MeV: Mega-electronvolt, unit for nuclear energies. Energy which an electron acquires passing a voltage difference of 1 million volts.

MHD (Magnetohydrodynamics): A mathematical description of the plasma and magnetic field, which treats the plasma as an electrically conducting fluid. Often used to describe the bulk, relatively large-scale, properties of a plasma.

MHD instabilities: Unstable distortions of the shape of the plasma/magnetic field system.

Microinstabilities: Instabilities with characteristic wave-lengths similar to the ion Larmor radii, rather than to the tokamak dimensions. These are thought to be responsible for the fine scale turbulence in tokamaks, and hence anomalous transport.

Minor radius: Half the small diameter of the tyre-shaped toroid.

Mirnov coils: Pick-up coils at the edge of the plasma for measuring the time variation of magnetic fields arising from instabilities.

Mirror: A linear magnetic confinement concept with a weaker magnetic field in a central region and with strong fields at both ends which reflect contained particles by the mirror effect. Some variants exist to increase the magnetic field in all directions from the centre or to improve the closure of the bottlenecks. The Tandem Mirror confinement concept also involves electrostatic fields.

MIT: Massachusetts Institute of Technology, Boston, USA. Operates the high-field divertor tokamak ALCATOR C-MOD.

Mode: A resonant wave or oscillation in a plasma. Also used as a synonym for an operating regime.

Mode number: Characterises the wavelength of a mode.

Monte Carlo code: A statistical technique used in numerical calculations where events may occur many times, each with a certain probability.

Motional Start Effect (MSE): The measurement of shifts and splitting of spectral lines emitted from particles moving in a local electric field. This can be interpreted to give the local magnetic field inside the tokamak if the particle velocity is known, and is a major diagnostic on some tokamaks to deduce the current profile.

MPQ: Max-Planck-Institut für Quantenoptik, Garching, Germany. Active, within its programme, in ICF (laser fusion) related physics. Partially supported by Euratom, for a “keep in touch activity” in ICF.

Negative ion beam: To produce neutral beams, negative ions (obtained by the addition of electrons to neutral atoms) are accelerated and then neutralised before entering the plasma. The efficiency of creating neutral beams from positive ions is too low at the beam energy required for a fusion power station, of the order of 1 MeV.

Neo-classical theory: Classical collisional plasma transport theory, corrected for toroidal effects. The neoclassical theory predicts the existence of the bootstrap current.

Neo-classical tearing mode: The magnetic island produced by a tearing mode perturbs the bootstrap current which further amplifies the island and degrades confinement or leads to a disruption.

NET: Next European Torus, a design for the Next Step which had been prepared by the NET team (located at the Association EURATOM- IPP in Garching) and which has largely influenced the ITER design. The European ITER contributions in physics and technology were organised by the NET team, until its replacement by EFDA in 1999.

Neural network: A computer algorithm that uses incoming data to derive plasma parameters, having previously been "trained" on a series of examples of a non-linear input-output mapping.

Neutrons: Neutral particles in the nucleus. Products of Deuterium-Tritium and other fusion reactions.

Neutral beams: Since charged particles cannot easily penetrate the magnetic confinement fields of the plasma, high energy beams of neutral atoms are injected into the plasma for fuelling, heating and current drive. Within the plasma, the atoms of the beam are ionized and are then confined.

Neutron multiplier: The fusion of deuterium and tritium consumes one tritium nucleus per reaction, producing one neutron. Since in the blanket of a power station not every neutron reacts with lithium to produce a new tritium atom, a neutron multiplying element may be used in the blanket to enhance the tritium production so as to make the power station self-sufficient in tritium supply.

Next Step: The next experimental device in the strategy of the European Fusion Programme. Presently pursued via the ITER EDA, with a European activity as a fall-back option. The generic name for an experimental reactor with a long pulse burning plasma at high fusion gain.

NFR: Naturvetenskapliga Forskningsrädet (Natural Science Council), Sweden. Partner in the Association EURATOM-NFR.

NIFS: National Institute for Fusion Science, Nagoya, Japan.

NRIM: National Research Institute for Metals, Sakura-mura, Japan.

Non-inductive heating and current drive: See additional heating and current drive.

NSTX: Spherical tokamak at Princeton, USA. A similar size to MAST, but of different design. Started operation in 1999.

Ohmic heating (OH): The resistive heating resulting from a current flowing within the plasma corresponding to the heating of a wire by a current flowing through it. Ohmic heating in a tokamak is insufficient to reach thermonuclear temperatures since, contrary to a wire, the resistance of a plasma decreases strongly with increasing temperature, thus making Ohmic heating weak at high temperatures.

ORNL: Oak Ridge National Laboratory, USA.

Operating limits: See tokamak operating boundaries.

Optimised shear: Adjusting the current profile to optimise tokamak.

PbLi: Eutectic lithium-lead alloy considered for use as blanket breeding material.

Peeling mode: An edge MHD instability which exists when the current density at the plasma edge is non-zero. It may be associated with ELMs.

Pellet: In inertial confinement concepts, the fuel is contained in tiny spheres, called

pellets, which are compressed by laser or particle beams. In magnetic fusion, pellets of frozen hydrogen, deuterium, tritium, accelerated up to several kilometres per second, are used to refuel the plasma and to obtain very high densities.

PIREX: Proton Irradiation Experiment, material test facility (Association Euratom-Switzerland, CRPP-FT, PSI, Villigen, CH).

Plasma: State of matter above a few thousand degrees where atoms are broken into their constituents, ions and electrons, thereby creating an electrically conducting medium. Plasmas can therefore interact strongly with electric and magnetic fields.

Plasma confinement: Retention of plasma energy or particles within a given region, including the heat and particle losses from the plasma.

Plasma parameters: Physical quantities which characterise the plasma and which must be measured experimentally, such as current, density, temperature, confinement time, beta.

Plasma pressure: Proportional to the product of plasma density and temperature. There is an electron and an ion pressure and the plasma pressure is the sum of the two. In magnetic confinement devices, this pressure is counterbalanced by magnetic pressure.

Plasma shape: Describes the plasma vertical cross-section, circular, elongated, D-shape, diverted, single null, double null.

Polarimetry: Measurement of the rotation of the plane of polarisation of light passing through a magnetically confined plasma; used to measure the local magnetic field and thus the safety factor (see Faraday rotation).

Poloidal field: Component of the magnetic field perpendicular to the toroidal direction and the major radius. The poloidal field is essential for confinement and is generated in a tokamak by the plasma current and the external coils.

Power threshold: The L-H transition and improved performance regimes related to reversed shear occur when the power exceeds a certain threshold value - the power threshold.

PPPL: Princeton Plasma Physics Laboratory, New Jersey, USA.

Preliminary Tritium Experiment (PTE): Three plasma discharges on JET, November 1991, into which a significant amount of tritium was injected for the first time in a tokamak. The power liberated from fusion reactions (~ 2MW for ~ 2 seconds) was in accordance with expectations. Followed by the more ambitious DTE in 1997.

Profile: Variation of plasma parameters with minor radius.

Profile control: Controlling the profiles of pressure, density or current, in order to control instabilities.

PSI: Paul-Scherrer-Institut, Villigen, Switzerland, active, in muon physics among others fields. The Association EURATOM-Swiss Confederation has their fusion technology activities working in superconductor and materials technology located at Villigen.

Pumped divertor: Divertor field lines directed into a pumped chamber surrounding the target plate.

q, q_{95}: See Safety factor.

Q: Ratio of fusion power to total additional heating power. At $Q=\infty$, no external power is required and the plasma is said to be ignited. A power station should operate with Q~50 to be economical.

Radial electric field: Arises when there is a charge imbalance in the plasma.

Radio frequency (RF) heating: Heating with waves in the radiofrequency range at resonance frequencies of the plasma (see ECH, ICRH, LHH).

Reflectometry: Use of reflected microwaves to measure plasma density.

Relaxation: The evolution of a plasma to a lower energy state.

Resistive ballooning modes: A class of ballooning mode which would be stable in the absence of resistivity, but can be unstable in its presence. Related to tearing modes, but topologically different.

Resistive instability: Instability due to diffusion and rearrangement of magnetic field lines. When the plasma resistivity is small, these instabilities have a slow growth rate.

Resistivity: The tendency to resist the flow of electric current, thereby dissipating energy. Plasmas are very good conductors of electric current, so that their resistivity can often be neglected. In this case, 'ideal' magnetohydrodynamics may be applied.

Resonant ions/electrons: Resonance occurs when one of the characteristic frequencies of particle motion in the plasma (for example, the cyclotron frequency) matches the frequency of some applied perturbation (for example, an RF wave).

Resonant magnetic perturbation (RMP): An externally applied magnetic perturbation matched to the spatial structure and optionally the frequency and phase of an instability.

Reverse Field Pinch (RFP): A toroidal magnetic confinement device, similar to a tokamak, in which the poloidal and toroidal fields are of comparable magnitude. Capable of higher plasma current and pressure for a given external magnetic field. They require a conducting shell close to the plasma for stabilisation.

Reverse (magnetic) shear: In a tokamak the current density is usually greatest at the magnetic axis, in which case the safety factor increases from the centre to the edge of the plasma. Using non-inductive current drive and/or the bootstrap current the current density can be made to increase away from the centre. In this "reverse shear" case, the safety factor has a minimum away from the plasma centre. Using reverse or low shear ("optimised shear") some tokamaks, notably DIII-D and TFTR in the US and more recently JT-60U in Japan and JET, have shown greatly improved plasma performance. Reverse shear is an attractive option for advanced tokamak scenarios.

RF: Radio-Frequency.

RFX: Reversed Field pinch Experiment at CNR-Padova, Italy (Association EURATOM-ENEA).

RISØ: Forskningscenter Risø, Denmark. Partner in the Association EURATOM-RISØ.

Rotational transform: Measure of the ratio of poloidal to toroidal flux defining the pitch of the helical field lines. The q-value of the tokamak is proportional to the reciprocal of the rotational transform.

RTP: Rijnhuizen Tokamak PETULA, for study of transport in a plasma, at Nieuwegein (Rijnhuizen), the Netherlands (Association EURATOM-FOM). Ceased operation in 1998, the activities of the Association being transferred to TEXTOR, as part of the Tri-lateral Euregio Cluster.

Runaway electron: An electron with a very high energy has a decreasing probability of colliding with another charged particle and of losing its energy. Such a particle then gains more and more energy in the electric field of a tokamak, reaching 10's of MeV.

Safety factor: Number of turns the helical magnetic field lines in a tokamak make round the major circumference for each turn round the minor circumference, denoted q. Has no connection with the ordinary sense of "safety" other than q=1 surfaces are ideally unstable. For diverted plasmas q goes to infinity at the separatrix, so instead q_{95} is used to describe the safety factor near the edge, which is the safety factor of the plasma surface which contains 95% of the poloidal flux.

Sawtooth: A cyclically recurring instability which causes an energy loss from the central region of tokamak discharges. The temperature periodically falls abruptly, then slowly recovers. The jagged trace produced by plotting temperature against time gives the instability its name.

Sawtooth crash: The rapid collapse of the central temperature in a tokamak during a sawtooth cycle.

Scaling laws: Empirical or theoretical expressions for how various plasma phenomena (eg confinement, power threshold, etc) vary with tokamak parameters. They are particularly used for predicting the performance of future tokamaks.

Scrape-off-layer (SOL): The residual plasma between the "edge" of the plasma (defined by the limiter radius or the separatrix) and the tokamak vessel wall.

Semi-empirical: A theoretical approach in which the behaviour of some key quantities is deduced from experiment, rather than a priori.

SEAFP: The Safety and Environmental Assessment of Fusion Power is an extensive study conducted by several teams in the associated laboratories, NET, industry and the JRC, published in June 1995.

SEAL: The Safety and Environmental Assessment of Fusion Power Long-term is a programme, launched in 1995, being undertaken for the European Commission in the framework of the Fusion Programme.

Separatrix: Magnetic surface at which the rotational transform vanishes and the safety factor becomes infinite.

Shear: The safety factor usually varies from magnetic surface to magnetic surface across the plasma cross-section; this variation is measured by the non-dimensional quantity called “shear”. Also refers to the variation of plasma flow (flow shear). If the type of shear is not specified, it usually means magnetic shear.

Single/double null: Points of zero poloidal magnetic field where the separatrix crosses itself are the X-points or nulls. Usually sited above and/or below the plasma. Tokamak divertor configurations have either one or two nulls.

Single fluid model: The set of equations which represent a plasma as a magnetised, electrically conducting fluid with the usual fluid properties of viscosity, thermal conductivity, etc. The possibility of distinct behaviour of electrons and ions (i.e. 2 “fluids”) is excluded.

Small aspect ratio: Same as Low aspect ratio.

Spectroscopy: The detection and analysis of the spectrum of radiation emitted by a plasma. This can yield information about temperatures, impurities, rotation, using different parts of the electromagnetic spectrum (IR, visible, VUV, XUV, etc.)

Spherical tokamak (ST): A very low aspect ratio tokamak - it appears almost spherical, though topologically it remains a torus with a centre column. The spherical tokamak is being further investigated, with a larger experiment, MAST.

Spheromak: A spherical plasma in which comparable toroidal and poloidal currents flow. The toroidal current is not driven by transformer action.

Stability theory: The theory of how small perturbations to a system evolve in time. Spontaneous growth is due to instability. Instabilities can saturate at some small amplitude, in which case they may degrade confinement, or grow uncontrollably, in which case the equilibrium is lost leading to a disruption.

START: Small Tight Aspect Ratio Tokamak, a “spherical” tokamak with a very small aspect ratio at the Association EURATOM-UKAEA (Culham). This very fat ring-shaped configuration showed experimentally a lesser tendency to disruptions and is efficient in its use of magnetic energy. Ceased operation in 1998, replaced by MAST.

Start-up assist: Assisting plasma formation to cross a range of plasma temperature at which impurities radiate strongly, with the aim of minimising the start-up delay and transformer requirements, usually using ECH.

STC: Scientific and Technical Committee, advisory committee set up by the EURATOM Treaty, competent for nuclear programmes.

Steady state power plant: A continuously (as opposed to cyclically) operated power plant.

Stellarator: Closed configuration having the shape of a three-dimensionally distorted ring in which the plasma is confined principally by an externally generated magnetic field (produced by non-planar coils outside the plasma vessel). The coils can be arranged in a modular fashion. Stellarators do not need a transformer; they need an additional heating system for the plasma start-up. Due to the fact that no toroidal plasma current is needed to maintain the confinement configuration, they naturally provide steady state operation.

SULTAN: Supra Leiter Test ANlage. Large Superconductor Test Facility, CRPP at PSI Villigen, Switzerland (Association EURATOM-Swiss Confederation).

Super Alfvénic velocity: A velocity greater than the Alfvén velocity. In a tokamak, only energetic particles have super Alfvénic velocities; because they satisfy this condition, they may resonantly transfer their energy to magnetohydrodynamic modes, which may grow as a result (eg TAE modes).

Superthermal radiation: Electromagnetic radiation produced by energetic particles, as opposed to thermal particles.

Survey spectrometer: An instrument which gives information concerning the radiated spectrum over a large range of frequencies.

TAE modes: Toroidal Alfvén Eigenmodes. One class of Alfvén gap modes.

Target plates: See Divertor.

TCV: ”Tokamak à Configuration Variable”, for study of elongated and strongly shaped plasmas, at Lausanne, Switzerland (Association EURATOM-Swiss Confédération).

TEKES: Technology Centre Finland. Partner in the Association EURATOM-TEKES.

Tearing magnetic islands: The disturbance caused by a tearing mode which alters the topology of the confining magnetic field and causes transfer of heat across the affected region.

Tearing mode: A class of resistive MHD instability which has been predicted theoretically in tokamaks and positively identified in experiments.

Temperature pedestal: In an H-mode discharge there is a region of steep temperature gradient at the plasma edge. The temperature at the top of this steep gradient region is the temperature pedestal.

Tesla: Unit of magnetic field strength (more exactly the magnetic induction). $1T = 1Vs/m^2 = 10{,}000Gauss$.

TEXTOR: Torus Experiment for Technology Oriented Research. Tokamak at Jülich, Germany (Association EURATOM-FZJ). Refurbished and upgraded, in 1994, as TEXTOR-94.

TFTR: "Tokamak Fusion Test Reactor" at Princeton, the largest US device with a major campaign using deuterium-tritium fuel from 1993 - 1997. Ceased operation in March 1997.

Thermal cycling: Successive heating and cooling of materials can lead to cracks or rupture, particularly at boundaries between materials that expand at different rates.

Thermal particles: As a result of collisional energy exchange, the energy of most plasma particles falls within a Maxwellian distribution which is described by a single temperature (typically 1-30keV for tokamaks). These are the thermal particles, as distinct from energetic particles which lie outside the thermal distribution.

Thomson scattering diagnostic: Diagnostic to measure temperature and density by detecting laser light scattered and Doppler shifted by the thermal plasma electrons.

Tight aspect ratio: Same as Low aspect ratio.

TJ-II: A heliac stellarator at Madrid, Spain (Association EURATOM-CIEMAT). (TJ-IU was a torsatron at CIEMAT, built and operated in preparation for TJ-II).

Tokamak: Magnetic configuration with the shape of a torus. The plasma is stabilised by a strong toroidal magnetic field. The poloidal component of the magnetic field is produced by an electrical current flowing toroidally in the plasma. This current is induced via transformer action and, for steady state, must be maintained by non-inductive current drive and by self-generation of bootstrap current inside the plasma.

Tokamak operating boundaries: The set of plasma parameters, beyond which it is impossible to operate a tokamak. Careful choice of plasma cross-sectional shapes and current and pressure profiles can increase the operating regime.

TORE SUPRA: Large tokamak with superconducting toroidal magnetic field coils and a circular plasma cross-section at the Association EURATOM-CEA in Cadarache, France.

Toroidal Alfvén Eigenmodes: See TAE modes.

Toroidal field: The component of the magnetic field along the major circumference of the torus. The largest magnetic field component in a tokamak.

Toroidal stability: Stability analysis taking account of effects due to the toroidal geometry. These are sometimes neglected to identify possible instabilities, but must usually be included for accurate predictions of stability boundaries.

Toroidal turbulence code: A turbulence code which includes effects due to the toroidal geometry.

TOSKA: Large facility testing for superconductors (Association EURATOM-FZK, Karlsruhe, Germany).

Transformer drive: The use of a transformer action to produce plasma current.

Transport: The processes by which particles and energy move across magnetic surfaces.

Transport barrier: In certain operational scenarios (e.g. the H-mode or ITB-mode) a region of low transport exists giving rise to a steep local pressure gradient. Such a region is referred to as a transport barrier.

Transport scaling: The magnitude of heat transport may be expressed, empirically or theoretically, in terms of a simple functional dependence on a few plasma parameters. This allows us to model how the heat transport varies (scales) in

response to changes in the value of these parameters.

Trapped particles: The outside (large major radius) of a tokamak plasma has a lower magnetic field than the inside. Particles with low velocity parallel to the magnetic field compared with the velocity perpendicular to the magnetic field may not enter the higher field (inside) region and become trapped on the outside. They are not free to circulate toroidally but instead bounce back and forth, performing so-called banana orbits.

Tri-lateral Euregio Cluster (TEC): A collaboration between the Associations Euratom-FZJ, -FOM and –Etat Belge, to exploit the TEXTOR tokamak at FZJ, Julich, Germany.

Tritium: An isotope of hydrogen, whose nucleus consists of one proton and two neutrons. Tritium does not occur naturally, because it is unstable to radioactive decay with a half-life of 12.3 years. Due to its rapid decay, tritium is almost absent on earth. For a fusion reactor, tritium will be produced in the breeding blanket surrounding the core of a fusion power station. Special tritium-handling technology is required whenever the use of deuterium-tritium plasmas is contemplated and has been developed on TFTR and JET.

Tritium inventory: The amount of tritium contained in a fusion power station or in a specified part of it.

Turbulence: Randomly fluctuating, as opposed to coherent, wave action. For example, the turbulent water beneath a waterfall can only be described in terms of its averaged properties, such as the scale and duration of fluctuations; whereas a more systematic description can be given to waves on the surface of a still pond.

Turbulent transport: Anomalous heat transport associated with plasma turbulence.

Two-fluid model and multi-fluid model: The extended set of equations which represent a plasma as interpenetrating and interacting fluids of electrons and ions, impurity ions etc.

UKAEA: United Kingdom Atomic Energy Authority. Partner in the Association EURATOM-UKAEA which operates the tokamak COMPASS-D and the spherical tokamak MAST. Also charged with the operation of the JET facilities under EFDA.

Vertical Displacement Event (VDE): An event which arises when control of the plasma is lost and the plasma moves vertically. It can lead to a “halo current” in components which surround the plasma resulting in large, potentially damaging, forces on these components. The forces are much larger in larger tokamaks and are therefore a particular concern for JET and ITER.

VUV: The “Vacuum Ultra Violet” range of the electromagnetic spectrum.

Warm plasma refuelling: Fuelling of plasma using medium energy particles or particle clusters.

WEC: World Energy Council.

WENDELSTEIN VII-AS: Advanced stellarator, in operation at Garching, Germany (Association EURATOM-IPP).

WENDELSTEIN VII-X: Large advanced stellarator, optimised to produce a reactor-relevant plasma configuration, designed at Garching. Construction in progress at Greifswald, Germany (Association EURATOM-IPP) with first operation scheduled for 2006.

X-point: See single/double null.

XUV: The “Extreme Ultra Violet” range of the electromagnetic spectrum. Shorter wavelengths than VUV.

Acknowledgement: This glossary was adapted from the “Glossary of fusion terms” by UKAEA Culham, UK, and from the glossary of “Fusion programme evaluation”, 1996, EUR 17521, European Commission

APPENDIX G Sources of Financial Support

The work carried out at the CRPP and presented in this annual report was financed from several sources. The major long-term financial support is derived from the Ecole Polytechnique Fédérale de Lausanne (EPFL), EURATOM, the Paul Scherrer Institute (PSI) and the Swiss National Science Foundation. Other public and private organisations which contributed funding for our research in 2000 include, in alphabetical order: ASULAB, Balzers, Balzers Tribology and Balzers Process Systems, Brite Euram, the Commission pour la Technologie et l'innovation (CTI), the Conseil des Ecoles Polytechniques Fédérales - Materials Priority Program (CEPF-PPM), the Office Fédéral de l'Education et de la Science (OFES), the Office Fédéral de l'Energie (OFEN), Sulzer Metco AG and Tetra Pak SA.